UNIVERSITY OF LONDON THESIS

Degree PHD Year 2008 Name of Author BRADBURN, JODY, NIKL.

The Integration of City Models and GNSS for the Simulation and Modelling of Multipath and Availability: Paving the Way for New Applications

Thesis submitted for the degree of Doctor of Philosophy (PhD)
UCL

Jody Neil Bradbury

Department of Civil, Environmental and Geomatic Engineering
University College London
September 2008

ProQuest LLC
789 East Eisenhower Parkway
P.O. Box 1346
Ann Arbor, MI 48106-1346

STATEMENT OF AUTHORSHIP

I, Jody Neil Bradbury, confirm that the work presented in this thesis is my own. Where information has been derived from other sources, I confirm that this has been indicated in the thesis.

Signed.....

Date.....

ACKNOWLEDGEMENTS

This research was undertaken at the UCL Department of Civil, Environmental and Geomatic Engineering. I would like to acknowledge all those in the department who have helped me in so many ways over the years. In particular I wish to offer my deepest thanks to my two supervisors. Dr. Marek Ziebart, for your considerable guidance, encouragement, honesty and patience, it has truly been a privilege to be your student. Professor Paul Cross, for your wisdom, depth of knowledge and vast experience in our field, and also for your support – thank you.

I am extremely grateful for the support and expertise provided by SPIRENT Communications. I would particularly like to thank those directly involved in this project at SPIRENT Communications in Paignton, Devon; Peter Boulton, Arnie Read and Martin Foulger.

Special thanks to the best of friends and companions - those who's enduring belief and optimism has made this happen. Matt, Gemma, Will and Martin you all contributed more than you realised. Yasmin, without you this would not have been possible. Thanks are definitely due to my fellow PhD students, Andrew, Tip, Pete and Madge you brightened up the experience when things got tough – seriously! Also, thanks to my friends in Devon, Heidi, Tom and Vivek. Sara, your timing was perfect and your interest, patience and understanding has been invaluable.

To my parents Ernest and Jacqueline and my brother Michael and sister Jacqui – to all of whom I offer my most heartfelt thanks. This thesis is dedicated to them.

ABSTRACT

Positioning in the urban environment, using Global Navigation Satellite Systems (GNSS), is hampered by poor satellite availability due to signal obstruction and disruption caused by both manmade and natural features of the urban environment. In addition, range measurement to satellites for positioning and for navigation, is severely degraded by the presence of reflected and diffracted signals. The arrival and continuous enhancement of computerised geometric environment models, makes it possible to tackle these problems through mathematical modelling.

Environment models have been used by architects and town planners for around thirty years. Within the last decade city model quality in terms of coverage, level of detail and geometric accuracy, has increased. Consequently, the number of applications for such models is continuously increasing and this ensures their continued availability and future usage.

Currently, accurate prediction of satellite availability, particularly in cities, is extremely problematic. This thesis presents research undertaken into the use of environment models for the accurate prediction of satellite availability. A software simulator has been developed in order to accurately predict satellite availability, taking as input any environment model. Line of sight (LOS), Fresnel zone, diffracted propagation and reflected signal propagation models have been implemented in the simulator.

Validation of each signal propagation model has been performed by comparison of observed data with corresponding simulated outputs. Successful validation of the Fresnel and diffracted propagation models, presented in this thesis, clearly indicate an enhancement over the use of conventional LOS propagation models alone. The reflected propagation model provides a potentially significant enhancement to the area of multipath modelling. It is certain that this work is of importance for mobile positioning devices. With the arrival of greater computational resources inside GNSS receivers, this research is likely to provide a means of reducing positioning errors due to multipath.

CONTENTS

LIST OF FIGURES

LIST OF TABLES

ACRONYMS AND ABBREVIATIONS

BDW	Bandwidth
BE	Broadcast Ephemeris
BPSK	Binary Phase Shift Keying
C/A	Coarse Acquisition
CAD	Computer Aided Design
CM	City Model
DEM	Digital Elevation Model
DLL	Delay Lock Loop
DOP	Dilution of Precision
ECEF	Earth Centred Earth Fixed
EGNOS	European Geostationary Navigation Overlay System
ENU	East, North, Up
ESA	European Space Agency
ETRF89	European Terrestrial Reference Frame 1989
ETRS89	European Terrestrial Reference System 1989
EM	Electromagnetic
GDOP	Geometric Dilution of Precision
GNSS	Global Navigation Satellite Systems
GPST	Global Positioning System Time
GTD	Geometric Theory of Diffraction
HDOP	Horizontal Dilution of Precision
INS	Inertial Navigation System
ITRF	International Terrestrial Reference Frame
ITRS	International Terrestrial Reference System
ITU	International Telecommunications Union
LBS	Location Based Services
LHCP	Left Hand Circularly Polarised
LIDAR	Light Distance and Ranging
LOS	Line of Sight
MCIR	Multipath Channel Impulse Response
P	Precise
PC	Personal Computer

PDA	Personal Digital Assistant
PDF	Power Distribution Function
PDOP	Position Dilution of Precision
PE	Parabolic Equation
PLL	Phase Locked Loop
PR	Pseudorange
PRN	Pseudo Random Noise
PVT	Position Velocity and Time
RAM	Random Access Memory
RF	Radio Frequency
RHCP	Right Hand Circularly Polarised
RINEX	Receiver INdependent Exchange
RX	Receiver
SNR	Signal to Noise Ratio
SPC	Spacing
SW	Software
TDOP	Time Diltion of Precision
TOF	Time Of Flight
TRF	Terrestrial Reference Frame
TRS	Terrestrial Reference System
TX	Transmitter
UTD	Uniform Theory of Diffraction
UCL	University College London
VDOP	Vertical Diltution of Precision
VPL	Vertical Plane Launch
VRML	Virtual Reality Markup Language / Virtual Reality Modelling Language
WGS-84	World Geodetic System 1984

1 INTRODUCTION AND OVERVIEW

1.1 Introduction

Global Navigation Satellite Systems (GNSS) receiver performance is, to a certain extent, a function of the environment surrounding the receiver. Signal obstruction or disruption of the quality of a GNSS observable due to objects present in the local area can disrupt the range measurement process or even render the signal completely unusable. For GNSS users operating in urban environments the effect of signal obstruction and disruption is of great consequence.

It is predicted [SiRF, 2007] that by 2010 there will be as many as two billion positioning enabled devices in use worldwide. With high concentrations of these devices operating in the more densely populated areas of the world, it is inevitable that problems of positioning in urban areas will become a serious issue that may even act as a barrier to the uptake of GNSS technologies. It is likely that such problems will act as motivation for the development of new GNSS related technologies aimed at resolving such issues. For urban applications in particular, the mitigation of signal obstruction and disruption problems is not necessarily enabled by the increase in satellite availability that will arise following the arrival of additional GNSS constellations such as Galileo (predicted to be fully operational by 2013 [Council of the European Union, 2007]). Although extra satellites will present more available signals [Rizos et al., 2005], and receivers will be afforded greater flexibility in the choice of signals to use in, or to reject from, position, velocity and time (PVT) solutions, signals presented to an antenna will still have modified attributes following their propagation in challenging environments. Complex geometries and varied material types are characteristics of obstacles that can be expected in urban environments. Manmade structures, from buildings to street furniture, combine with naturally occurring features, such as terrain and trees, to hamper the reception of incoming signals. With no current way of fully compensating for these factors and an increasing dependence on accurate and reliable positioning, it is imperative that our understanding of signal propagation in difficult environments is enhanced.

To expand upon these issues, it is first necessary to distinguish satellite visibility from satellite availability. Satellite visibility implies that there exists an unobstructed transmission path (occupying zero volume) between satellite and receiver. This is also referred to as a *clear line of sight* (LOS). The satellite is only 'visible' when the LOS is unobstructed. This is distinct from satellite availability, which describes any condition whereby a receiver is able to make a range measurement (or range measurements) to a satellite. This includes LOS (provided the LOS signal is not subject to heavy interference) and also conditions whereby a range measurement is made despite the LOS being obstructed. This can occur due to complex signal propagation modes such as diffraction and reflection (both discussed at length during this thesis).

The development of new GNSS hardware can be greatly enhanced by performance testing using GNSS signal simulators. Such equipment generates radio frequency (RF) signals that replicate those that would be presented to the antenna of a receiver. In this way, many complex adjustments to signal properties have to be made, in order to emulate a specific user environment and conditions without the need for costly field trials and repeated testing. The performance of receiver hardware and software under development can therefore be assessed under many typical signal conditions. Such technology forms an important, and increasingly relied upon, aid to furthering the cababilities of GNSS positioning and navigation equipment. At present, such signal simulators lack the ability to emulate signals that would be present within a defined environment. One major enhancement to such a system would be the addition of specific built environment data, in order that a defined location could be used for testing. For the purposes of this research, the term *built environment* is used to refer to an environment that is present around a receiver. The word built is appropriate as many computerised models are being developed of envrironments populated by manmade structures. This does not preclude the application of models describing naturally occurring environments, e.g. terrain models. The arrival and continuous improvement of highly accurate computerised environment models (also referred to as city models throughout this work) could provide such data to enhance signal simulation techniques. Computerised models of physical environments have been in existence for a number of years. Initially used as visualisation tools for architects and town planners, applications for structural environment models have increased in number and diversity. Consequently, the quality and coverage of environment models is increasing all the time. It is considered feasible that such environment models could be integrated with

GNSS signal propagation models to predict the signals, together with their associated attributes, that would be observed by a receiver in a particular environment and under particular conditions, however, little research has been carried out in this area.

This thesis presents work that has been performed at University college London (UCL), in collaboration with SPIRENT Communications, in order to further our ability to predict the behaviour of radio frequency (RF) signals transmitted by GNSS satellites. The possibility of introducing environment model data to the problem is explored.

1.2 Objectives and Scope

A logical first step towards the correction of effects relating to the user environment on PVT solutions is successful modelling of the signal propagation. In order to successfully determine the number and quality of signals that will be present at an antenna, a vast amount of specific detail concerning the user environment is required, such as the geometrical detail of structures surrounding the receiver. An increase in applications has fuelled the development of computer aided design (CAD) models of built environments. Sophisticated and continuously improving data collection and processing techniques used for the construction of such models have resulted in finished model products of very high quality, in terms of level of accuracy and level of detail. This makes them ideal sources of reliable user environment data. A trade-off exists between the model quality and the size of model files, and so efficient data processing problems are also to be addressed.

There are two fundamental questions that this research seeks to answer:

By using computerised models of environments surrounding a receiver, is it possible to predict the observations that will be made, given that not all observations will originate from simple LOS propagation? If it is possible, then the achievable accuracy of such predictions should be examined. Further to this, to what extent can the contribution of unwanted signal propagation paths to the main LOS mode be characterised?

The aim of this work is to characterise satellite availability and signal degradation, due to a variety of signal propagation modes, by using computerised models of complex environments. This aim can be expanded to give the following objectives:

1. The development of techniques for the reliable prediction of satellite availability using computerised models of urban environments. Beneficiaries of this technology are likely to include low resource devices, and so it is essential that the computation of any such prediction is performed via data processing algorithms that minimise computational burden in terms of memory usage and time.

2. The consideration of satellite availability predictions using a range of signal propagation modes, including LOS, diffraction and reflection. This objective accounts for the complex nature of signal propagation and all results from this consideration are of importance in understanding signal behaviour. The results of this objective are also pertinent to the refinement of existing methods to model satellite signal propagation.

3. To use a structural environment model to predict the presence and characteristics of reflected signals arriving alone or in combination with the LOS signal. Reception of reflected signals in combination with the direct signal or as a reflected-only signal is a proven phenomenon. Predicting reflection occurrences and even specific attributes of signals originating by such a mechanism is a major enhancement towards full mitigation of the effects of the reception of reflected only signals.

4. Promote understanding of the effects that degraded signals (and combinations of degraded signals) have on the ability of a GNSS receiver to perform a PVT solution, leading to the ability to characterise signal degradation. Treatment of degraded signals is dependent upon the specification and design of an idividual receiver architecture. It is therefore the intention that this work focuses on a generalised receiver model and attempts to characterise position degradation. Reflected only signals can be received following propagation over paths that are tens of meters greater than the LOS path.

5. The impact of structural environment model quality on the simulated satellite availability and signal degradation results is to be considered. Characterising the effect of environment model quality on the simulation and prediction of signal propagation is important for future research as well as the development of any technologies resulting from this research. Model quality can be evaluated using parameters such as position accuracy and level of detail.

6. The consideration of the current state of the art, future form and availability of structural environment models. This work is not concerned with techniques for urban model data collection or construction techniques. Questions surrounding the current state and future of such models are, however, of importance when considering future uses of this research.

7. Develop data processing techniques for the prediction of satellite availability and signal degradation using widely available computer hardware and software. It is desirable that techniques produced during this research should be completely independent of dedicated graphics processing hardware and software. Although great gains can be made by utilising such elements, it is considered important that we maintain a full control over all algorithms employed to process geometry data. This has two main benefits. Firstly, it allows a better understanding of the problems associated with signal propagation, as we can interrogate all parts of the process as opposed to being restricted to working with third party software, that might present restricted access. Secondly, ground-up development provides an understanding of the issues that would be of relevance for the possible implementation of algorithms and techniques onto low resource devices.

1.3 Thesis Outline

The following chapters are contained within this thesis. A short description of the contents of each chapter is given. Note that analysis and discussion of results is included within several of the topic specific chapters, rather than having all analysis concatenated within one chapter.

Chapter 2 – *Positioning and Navigation in the Urban Environment*

Problems resulting in poor quality navigation and positioning in difficult environments are introduced in this chapter. Future GNSS developments are discussed. The motivation for undertaking the research is identified.

Chapter 3 – *Background*

The physical properties of signal propagation under different modes are examined in this section, together with an explanation of the mechanics of code multipath. City models are described and discussed. For all the topics in this chapter a full description is given of the state of the art. Precursors to this work, existing literature and sources of current knowledge are detailed.

Chapter 4 – *Methodology*

A description of the simulator developed during this research is provided. Detailed description of the Virtual Reality Markup Language (VRML) processing algorithms developed is also given. The mathematical models implemented to predict signal propagation modes including LOS, diffraction and reflection are explained in depth.

Chapter 5 – *Simulator Verification*

The definition of verification in the context of this work is given at the start of this chapter. A full account of the methods employed to test all elements of the simulator is provided. In particular the use of numerical and graphical data output from the simulation process is described.

Chapter 6 –*Model Datasets Used in this Research*

An overview of the environment models used during this work is presented. For the work presented in this thesis, two urban models are focussed on. This chapter describes the environment models that are used for validation of the propagation models and for generation of the results presented in this thesis. One of the two model datasets has been the subject of a validation exercise (separate to the work presented in this thesis) to quantify aspects of model quality. The results of this validation, and their impact upon the accuracy of simulator results, are presented and assessed.

Chapter 7 – *Propagation Model Validation*

The definition of validation in the context of this work is given at the start of this chapter. Real world data collected during field work is used as a truth model to validate the signal propagation models implemented within the simulator. Description is provided of the methods used and comparison of simulated data with the truth is made.

Chapter 8 – *Spatial and Temporal Variation for Satellite Availability Prediction*

Description is given of satellite availability prediction across an entire area described by an environment model. A map of satellite availability, averaged over a defined time period, can then be generated.

Chapter 9 – *Spatial and Temporal Sensitivity to Multipath*

In this chapter, it is shown that a model of the receiver code correlator can be used to determine estimates of range measurement error due to multipath. Predicted range measurement errors are generated at defined points in space, within an area described by an environment model. For each position, results are averaged over time. A map of signal degradation due to the presence of reflected signals, over a chosen area and time period, is then presented.

Chapter 10 – *Simulator Performance*

Computing resources consumed by the simulator are first presented in this chapter. Subsequently, an example set of tests are performed for varying configurations of environment models. The results of these resource useage tests are then presented.

Chapter 11 – *Summary, Conclusions and Discussion*

Within this chapter, a summary of the work presented within this thesis is provided. The research objectives are revisited and the extent to which they have been met is stated. Conclusions that have emerged during this research are stated. During the discussion, the context of developments made throughout this research is examined. Future uses of this research and the expected impact of this work on GNSS technologies are also provided.

2 POSITIONING AND NAVIGATION IN THE URBAN ENVIRONMENT

In this chapter problems facing static and dynamic positioning devices operating in urban environments, are introduced. Effects of the urban environment on signal propagation are detailed. Firstly, satellite signal availability in urban environments is considered. Secondly, the disruption to range measurements that occur due to the interaction of incoming signals with objects present in the urban environment is considered. Finally, future GNSS developments are discussed along with their impact on this work.

2.1 Satellite Signal Propagation in the Urban Environment

For a receiver (RX) and transmitter (TX) pair, the first approximation for radio frequency propagation is that of the volumeless straight line of sight (LOS). By studying the signals tracked by a receiver during a static GNSS survey, it becomes apparent that more complex propagation modes must be considered. This is particularly evident when observing a signal originating from a satellite that is setting over the top of a building. Elevation and azimuth readings, from the receiver, provide a means by which to estimate the signal origin with respect to the receiver position and also to the top of the structure over which the signal is setting. Often the signal is tracked by the receiver for a considerable period of time after the LOS between satellite and receiver is obstructed.

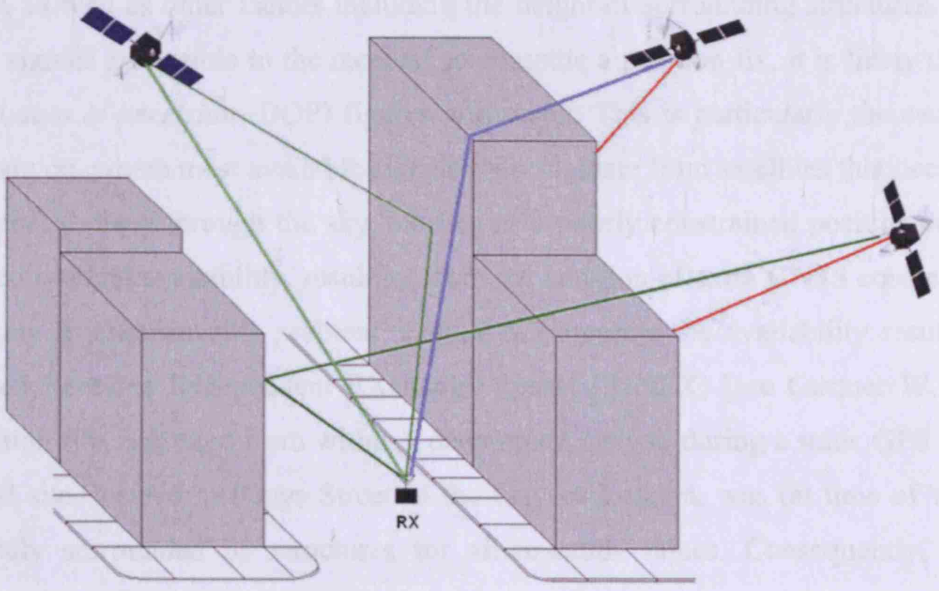

Figure 2-1: Simplified overview of signal propagation in urban environments

The signal behaviour highlighted by this crude experiment is more rigorously explained in section 3.1.3, but this serves as an indication of the requirement for more complex propagation models. Similar crude tests, where signals that can only have originated from reflection by nearby surfaces are tracked by a receiver, provide further evidence for the complex nature of signal propagation. A dense concentration of objects surrounding a receiver causes signal obstruction. This effect is worse for receivers near ground level. Structures in urban environments, on the whole, consist of large surfaces, e.g. walls, windows, roofs and floors. The interaction of transmitted signals and these smooth surfaces can result in the reflection of a satellite signal, thus making it possible for a signal to be received via multiple paths. In a similar fashion, the interaction of a satellite signal at building edges gives rise to signal refraction. In this case, the resultant propagation mode is diffraction, whereby an apparent bending of the signal occurs and thus the signal occupies an area in which LOS is obscured. The above effects are caused by interactions between satellite signals and objects present in the environment local to the receiver. An illustration of these modes is provided in Figure 2-1.

2.2 Static Positioning Problems in the Urban Environment

The quality of results obtained from many surveying and location based applications is dependent upon accurate position determination using GNSS receivers. A lack of available signals, particularly in urban canyons, means that position determination in certain locations is impossible during certain periods throughout each day [Taylor et al. 2005]. In general this effect is related to the density of the built environment around the receiver, as well as other factors including the height of surrounding structures. Where enough signals are visible to the receiver to compute a position fix, it is likely that that poor *dilution of precision* (DOP) figures will result. This is particularly the case in an urban canyon, where most available signals will originate from satellites that occupy the same vertical plane through the sky, leading to a poorly constrained position solution. Increased satellite availability, resulting from the addition of extra GNSS constellations is unlikely to alleviate this problem. Figure 2-3 presents the availability results of a processed Receiver INdependent EXchange format (RINEX) [see Gurtner W., 2001] observation file, collected from within a deep urban canyon during a static GPS survey. This test site, located in Pepys Street in the City of London, was (at time of writing) completely surrounded by structures for all azimuth values. Consequently, only a limited section of sky was unobstructed.

Figure 2-2: Pepys Street (London, EC3) - Example of location with poor satellite availability

A map and a photograph of the location are provided in Figure 2-2. In this example an available satellite is defined as one for which code and carrier measurements can be made on both L1 (1575.42 MHz) and L2 (1227.60 MHz) frequencies [ICD-GPS-200, 1995]. The issue of defining satellite availability with respect to GNSS observables is discussed in section 2.4. As shown in the current example (Pepys Street), very few range measurements can be made to satellites throughout this dataset, a section of which is included in APPENDIX A. In Figure 2-3, the number of available satellites is shown with respect to number of epochs collected at an update rate of one second. Unacceptable DOP values, cycle slips and complete loss of lock are symptoms of positioning in difficult environments and will often result in no measurements being recorded. The figure indicates epochs where the receiver has been unable to record any measurements as a zero.

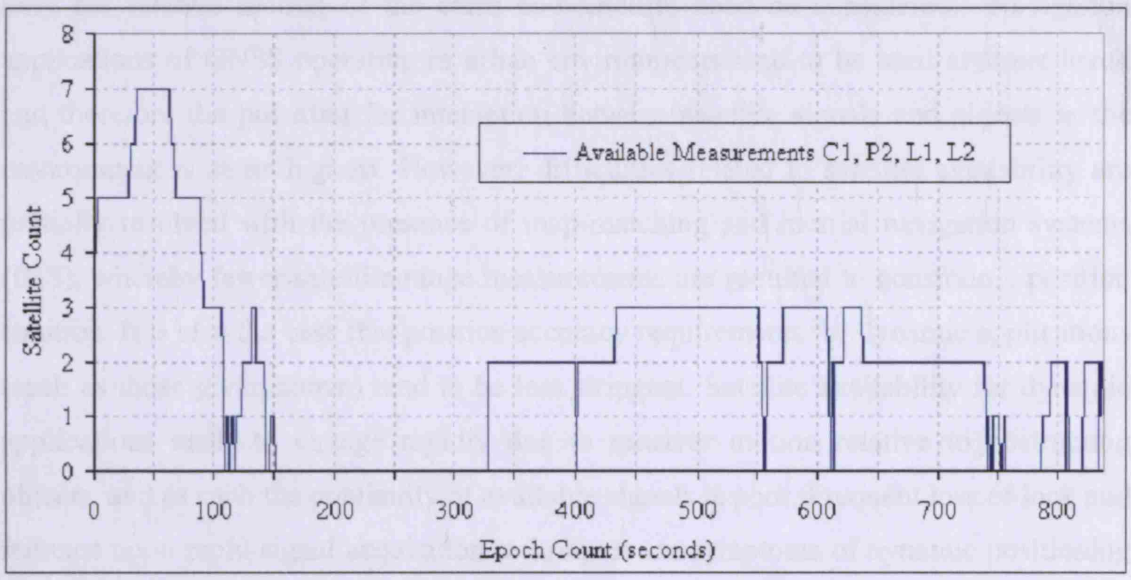

Figure 2-3: Typical satellite availability for urban canyon static positioning

In addition, ranging signals that can be made in such a situation will not necessarily have been made upon the LOS signal alone. It is more likely that measurements will have been contaminated with reflected and diffracted signals, leading to multipath, or even be made upon diffracted or reflected signals without the presence of the LOS signal. The reception of signals that have arrived via propagation paths other than LOS only, results in incorrect position determination that can be of the order of tens of metres [Yang et al., 2004] depending on the type of receiver used. The ability to identify, in advance, locations that will exhibit high signal degradation and/or low satellite availability could feature in the decision making process when surveys are performed using GNSS. It is conceivable that the use of such information could lead to shorter occupation times when, for example, laying down control points during a GNSS survey. In addition to selecting more favourable locations for GNSS surveying, the user would be able to plan survey times based upon the predicted availability and signal quality.

2.3 Dynamic Positioning Problems in the Urban Environment

Dynamic positioning in urban environments is subject to the same signal propagation problems associated with static positioning. For the purposes of this work, examples of dynamic applications include mobile equipment with integrated GNSS receivers, e.g. car navigation systems and personal digital assistants (PDAs) with built in navigation. It is likely that the magnitude of multipath present on a range measurement will vary more rapidly when positioning a mobile object, due to the effect of receiver motion relative to static objects in the environment surrounding the receiver. For the static case, only the relative motion of the earth and satellite need be considered. Navigation applications of GNSS operating in urban environments tend to be used at street level, and therefore the potential for interaction between satellite signals and objects in the environment is at its highest. However, difficulties related to satellite availability are partially resolved with the presence of map-matching and inertial navigation systems (INS), whereby fewer satellite range measurements are required to constrain a position solution. It is also the case that position accuracy requirements for dynamic applications (such as those given above) tend to be less stringent. Satellite availability for dynamic applications tends to change rapidly due to receiver motion relative to obstructing objects, and as such the continuity of available signals is poor. Frequent loss of lock and reliance upon rapid signal acquisition techniques are symptoms of dynamic positioning in urban environments. These factors all impact upon signal integrity. Prediction of

satellite availability becomes a powerful asset in route planning, especially when applied to safety critical activities such as those undertaken by emergency services. In certain situations a route planning application will identify more than one route with similar associated properties (journey time, distance, traffic conditions and other factors). Routes with higher GNSS signal degradation and/or lower satellite availability may be avoided and a higher precedence given to other routes.

2.4 Satellite Availability

As described in the previous sections, satellite signals arrive at an antenna through a variety of different propagation modes. The interaction of signals with objects surrounding the antenna introduces changes in signal attributes. Reflected and diffracted signals typically exhibit reduced signal power amplitude, changes in signal polarization and changes in carrier phase as well as an increased time of flight [Novatel, 2000]. The ability to track signals with these characteristics depends upon the sensitivity and specification of the receiver. Similarly the collection of measurements that can be made on each frequency under certain conditions is also dependent upon the design of a receiver. Receivers are all designed to accept GPS signals as specified in [ICD-GPS-200, 1995]. However, individual receiver designs will have different tolerances to deviations from the original signal specification and therefore different receivers will detect signals with different characteristics. As demonstrated by Melgard [Melgard et al., 1994], in urban environments, the difference in satellites tracked by different receivers over time can be as large as 60% due to differences in signal tracking performance. Prediction of signals that will be present at an antenna involves modelling the transmission path, or all conceivable transmission paths, that a signal will take from a satellite to a receiver. Often, in difficult environments, code measurements will be made on L1 and not on L2. This is due to the slightly weaker transmission power of the L2 carrier. Performing a signal power budget reveals that the minimum received power for the P-Code on L1 is around -163.0dBW and for the P-Code on L2 is around -166.0dBW [ICD-GPS-200, 1995]. Consequently, the L2 P-Code measurement is easily lost when obscured by tree foliage etc. The definition of satellite availability is therefore raised. It is important to note that different equipment will have different definitions for availability. For example, if the C/A code is observed, then for a single frequency user a satellite is available. As both code measurements are used in linear combination to extract ionospheric errors, one approach, particularly for dual frequency users, might be

to deem a satellite as being available only when code and carrier measurements can be made on both frequencies. This approach is only applicable for dual frequency equipment with the ability to make measurements on the P-code. The signal available condition is only met when measurements are made on both frequencies. This respects the slightly weaker L2 signal strength, by effectively meaning that a satellite is deemed unavailable during periods when range measurement on the L2 signal is not possible. This is considered a valid satellite availability definition for a dual frequency user. Another valid approach to satellite availability is a statistical assessment of periods throughout which the HDOP value is below a specific threshold [Melgard et al., 1994].

This section has addressed the definition of satellite availability. The notion that a different definition of availability exists for users with different equipment, has been asserted. For the reasons presented within this section, later work within this thesis involving data collected with a dual frequency receiver, will use the afore presented definition of satellite availability, whereby a satellite is only available when code measurements can be made on both frequencies.

2.5 Pseudorange Measurement Disruption

Interaction of GNSS signals with objects near to a receiver is proven to result in incorrect determination of signal time of flight (TOF) [Hoper et al, 2001]. Several factors affect this error. Firstly, receiver performance varies according to the number of reflected and diffracted signals. Secondly, the geometry of the reflected or diffracted signal paths determines the delay for each signal. Thirdly, the attributes of a surface causing a reflection or diffraction dictate the attenuation, polarisation and phase of the signal. Finally, correlator design and susceptibility to signals exhibiting specific characteristics defines the time of flight range measurement error. For code measurements it is suggested that the maximum range measurement error due to code multipath, for a receiver with a standard correlator, is given as follows [Kaplan, 1996].

$$P \leq 1 + \frac{\tau}{2} \qquad \text{(eqn. 2-1)}$$

For C/A code: $$R = P \times ChipLength(C/A) \qquad \text{(eqn. 2-2)}$$

For P code: $$R = P \times ChipLength(Pcode) \qquad \text{(eqn. 2-3)}$$

P = Difference between direct and reflected signal path lengths (chips).

τ = Correlator Spacing, generally 1 for Standard, 0.1 for Narrow (chips).

R = Range measurement error (m).

In a similar fashion to the modelling of error sources associated with making GNSS range measurements, such as atmospheric and clock errors, this work seeks to model those range errors that occur following interaction with the environment surrounding the receiver. It is anticipated that the magnitude of such range errors will be a function of a number of parameters that will encompass the disruption of the received signal/(s) and also the specification of the receiver correlator. It is expected that such range errors will be positive (extra path length) or negative depending upon distortion effects within the receiver correlator that are particular to the scenario under consideration. When any comparison of modelled errors (due to the surrounding environment) with observed data is made, it will be important to note the effect of residual errors from other error sources that will have been removed, and their potential to interfere with analysis. This is unlikely to be a problem as only disruption to code measurements will be assessed by this work. It is therefore the case that residual errors, following the removal of other modelled errors are likely to be small in comparison to any predicted code measurement error (the output of this research).

In the same way as modelled errors for atmosphere or clock are subsequently removed from the position solution, successful achievement of the objectives of this work would also make it possible to remove errors due to reflection, multipath, and diffraction. The aim throughout the research presented in this thesis is to achieve a high correlation between simulated signal degradation and observed signal degradation. It is anticipated that such an outcome would logically lead to real time implementation of such simulations which could be adopted as on-chip technology in future GNSS receivers.

2.6 Consideration of Future GNSS Developments

At the time of this research, GPS is the only fully operational GNSS. A program to modernise GPS is already under way. The existing Russian GNSS (GLONASS) is entering a stage of revitalisation and a brand new European GNSS (Galileo) is expected to reach full operating capability within the next five years. It is important to establish the impact that these developments will have on positioning and navigation in the urban environment.

The introduction of an improved civilian signal, referred to as L2C is intended to provide GPS civilian users with less susceptibility to multipath and more immunity to interference. A third frequency, L5, will be introduced for safety critical applications. A full description of the GPS modernisation process, including satellite Block numbers and planned launch schedules, is given by Rizos [Rizos et al., 2005]. It is expected that full GPS modernisation with a constellation of 30 GPS-III satellites will be completed around 2018. GLONASS-M satellites which broadcast in the L1 and L2 signal bands are currently being launched, and GLONASS-K satellites which also contain a civilian L3 signal are also planned. Galileo, which aims for interoperability with GPS (although some elements are not compatible) will broadcast signals in frequency bands L1 and E5 (E5a and E5b) that are compatible with the L1 and L5 GPS signals. Also, signals on a third frequency (not compatible with GPS) named E6 will be transmitted. Further detail regarding GNSS signals and structures, can be found in Rizos [Rizos et al., 2005].

The result of such developments will be that by around the middle of the next decade (2015) there will be somewhere in the region of 80 satellites for GNSS based positioning and navigation purposes. This figure is increased further if regional satellite system signals are also considered. This means that with respect to a GPS only system, when considering a system of GPS, GLONASS and Galileo, there will be a 350% increase in satellite availability and that this is accompanied by significantly reduced overall DOP values [Rizos et al., 2005]. On first inspection this means that satellite based positioning will be less influenced by satellite geometry and current availability issues. However, for the cases highlighted in this chapter, where positioning in deep urban canyons, problems of poor availability and geometry still exist. It is, however, true to say that the additional satellites will allow better continuity. It is the case that positioning is sometimes possible in the deep urban canyon. Enough satellites with an

acceptable geometry are sometimes available, however, this tends to be for very short time periods. More satellites will allieviate this effect. However, for other scenarios, it matters not how many satellites are available in the area of sky that is unobstructed, the geometry will always be too poor. An area in which definite improvement will result, following the planned GNSS developments is that of indoor positioning. High sensitivity receivers can track extremely weak signals that have penetrated through building walls, and also those that have often reached the receiver by reflected propagation paths. Such positioning is reliant upon the reception of signals through these unconventional propagation paths. A greater number of transmitted signals is of real benefit to such a receiver. The availability of a greater number of signals on which to make range measurements, again with reference to deep urban canyon positioning, means greater scope for a receiver to reject signals based upon suspicion of interference or multipath. Additionally, the availability problem in deep urban canyons could likely be relieved if the reflected signals reaching the receiver could be determined, and their attributes (e.g. extra path travelled due to reflected propagation) could be reliably established.

3 BACKGROUND PRINCIPLES AND LITERATURE REVIEW

Throughout this section a full appraisal is given of the background material that is directly applicable to this research. Four distinct subject areas exist; city models, signal propagation modes, code multipath and GNSS signal simulators. As each of these sections comprises a large body of research, the following sections of this chapter are not intended to give a comprehensive description of each of the four individual subject areas, only the pertinent detail for each is provided. As far as possible, existing work in each of the areas is identified and reviewed.

3.1 GNSS Signal Propagation Modes

The interaction of electromagnetic signals with manmade and naturally occurring surfaces of different material types is a vast and well studied topic [e.g. Felsen et al. 1994]. The reaction of signals at specific frequencies encountering objects of different shapes and dimensions is well understood, and is characterised by a set of established mathematical relationships and equations. Maxwell's equations, describing the relationship between electric fields, magnetic fields, electric charge and electric current, are the fundamentals from which the mathematics of electromagnetic signal propagation originate. A brief introduction to the electromagnetic signal propagation models that are considered within this research is given. The reader is asked to appreciate that the subject of computational electromagnetics is a large topic and to present any aspect in depth would be impractical.

3.1.1 LOS

Line of Sight is the simplest and least effective signal propagation model. This model relies upon the assumption that a volumeless transmission zone exists between receiver and transmitter. It also assumes that no interaction occurs between the incoming signal and any object that does not directly obstruct the satellite to receiver vector. LOS results are therefore obtained by simply testing a point to point vector for obstruction. The implementation of such a model is shown via two popular methods; vector testing as shown in Figure 3-1, and shadow testing as shown in Figure 3-2.

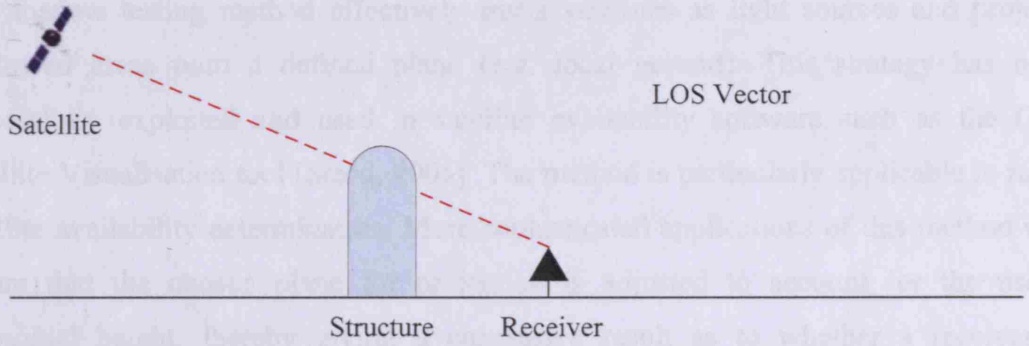

Figure 3-1: Vector testing for LOS propagation model (2D representation)

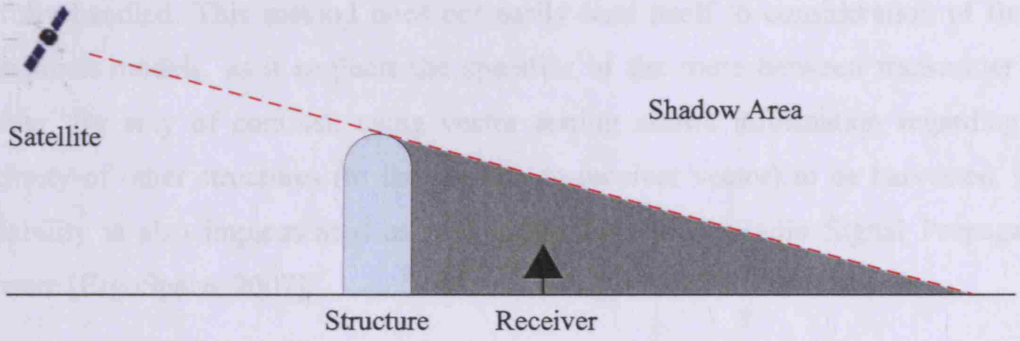

Figure 3-2: Shadow testing for LOS propagation model (2D representation)

Satellite and receiver positions (if known) can be used to determine a receiver to satellite vector. This vector can be tested against all planar surfaces within a dataset to determine whether an interaction will occur. Vector test approaches employ a well known set of mathematical principles to assess geometric arrangements of surfaces. Problems associated with such methods are assumed to include the definition of a search space and strategies for efficient computation over an entire dataset. Vector test methods lend themselves to applications where a user can define objects in the environment surrounding a receiver. An example of such an application is the Trimble Office Planning software [Trimble Navigation Ltd, 2002]. The technique of vector testing is useful for determining the relationship between the transmission channel and surrounding objects. Knowledge of, for example, the proximity of nearby objects to the vector can be used when applying more sophisticated propagation models.

The shadow testing method effectively treats satellites as light sources and projects shadowed areas onto a defined plane (e.g. local ground). This strategy has been successfully exploited and used in satellite availability software such as the GPS Satellite Visualisation tool [Steed, 2005]. The method is particularly applicable to rapid satellite availability determination. More sophisticated applications of this method will ensure that the chosen plane for projection is adjusted to account for the user's ellipsoidal height, thereby giving a conclusive result as to whether a receiver is shadowed or not. An advantage of this method is that an entire dataset area can be assessed for satellite availability at a single epoch, without the need to specify a receiver location. However, this can only be done providing issues with the projection plane are carefully handled. This method does not easily lend itself to consideration of further propagation models, as it neglects the specifics of the route between transmitter and receiver. By way of contrast, using vector testing allows information regarding the proximity of other structures (to the satellite to receiver vector) to be harvested. LOS availability is also implemented as part of the ErgoSpace Radio Signal Propagation Software [ErgoSpace, 2007].

Evidence is provided for the complex nature of signal propagation in texts such as [Felsen et al., 1994], however one of the most compelling indications that consideration of LOS propagation only is insufficient can be found by examination of receiver observables. When situated in a difficult environment, the collected data will often reveal that signals have been tracked to satellites that are evidently obscured by objects surrounding the receiver. This effect has been noted and studied by numerous projects e.g [Ercek et al., 2006]. Hence to simulate GNSS signal propagation thoroughly, LOS must be used in conjunction with more sophisticated models of signal propagation.

3.1.2 Fresnel Zone Analysis

It can be convenient to consider the propagation of electromagnetic waves as following a straight line between transmitter and receiver. In reality, wave propagation is a collective phenomenon in which particle motion is organised over a finite region of space [Spetzler and Snieder, 2004]. Wave propagation, between a transmitter receiver pair, can be modelled by describing a collection of concentric volumes, defined by prolate spheroids, each with the direction of signal propagation (LOS vector) acting as their major axis. In this way a set of regions, known as Fresnel zones, surround the LOS vector as shown in Figure 3-3.

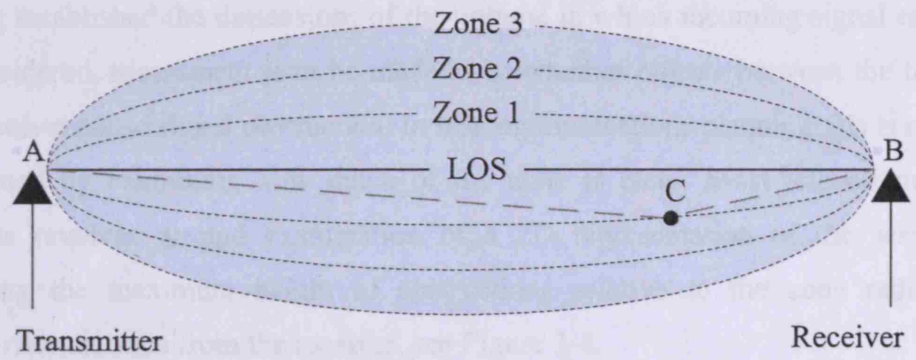

Figure 3-3: Prolate spheroids describing signal propagation volumes (Fresnel zones)

The following, with reference to Figure 3-3, presents the relationship that defines the dimensions of each volume.

$$AC + CB = AB + n*(\lambda/2) \quad (3\text{-}1)$$

Where:

n = Fresnel zone number (integer).

λ = Wavelength (m).

Signal energy originating from any point within the first Fresnel zone (n=1) will contribute to the signal arriving at the receiver antenna by virtue of constructive interference [Spetzler and Snieder, 2004]. This is only true where the extra path length travelled by the disrupted signal is small in comparison to the signal wavelength. In addition, any diffraction event that occurs within this zone can, if geometrically appropriate, add to the received signal energy, provided enough of the zone is free from obstruction. Spetzler and Snieder [Spetzler and Snieder, 2004] provide analytical evidence for the first Fresnel zone being defined by signals that travel an extra path length (w.r.t LOS) of not more than $\lambda/2$, where n=1 in (3-1), for 3D situations. Signal energy originating from odd numbered Fresnel zones apply constructive interference and even zones 2,4,6… apply destructive interference. However, the higher order zones make less of a contribution to the overall received signal [Spetzler and Snieder, 2004] and so only the first zone need be considered in signal propagation models. This first Fresnel zone is often simply referred to as the Fresnel zone or even as the 'physical ray' [Hubral et al, 1993].

Having established the dimensions of the volume in which incoming signal energy will be considered, assessment is to be made as to whether objects between the transmitter and receiver cause signal obstruction. In telecommunications planning this is most often performed by examining how much of the zone is clear. Most telecommunications analysis revolves around examination of a 2D representation of the scenario and assessing the maximum height of obstructions relative to the zone radius at the appropriate distance from the receiver, see Figure 3-4.

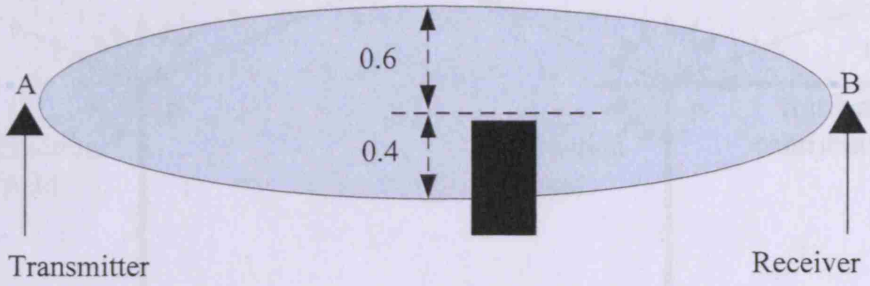

Figure 3-4: 2D analysis of Fresnel zone obstruction

Some obstruction of the zone is tolerable, however, there is little evidence for the existence of a certain obstruction value, beyond which the signal will no longer be received. A rule of thumb among telecommunication planners for siting of antennas and transmitters is to ensure that at no point in the propagation path is the cross section area of the first Fresnel zone obscured by more than 60%. A more ideal analysis than that of the above is shown in Figure 3-5. A 3D analysis of Fresnel zone obstruction yields the maximum obstruction that occurs in the zone, taking account of non-uniform obstruction shapes.

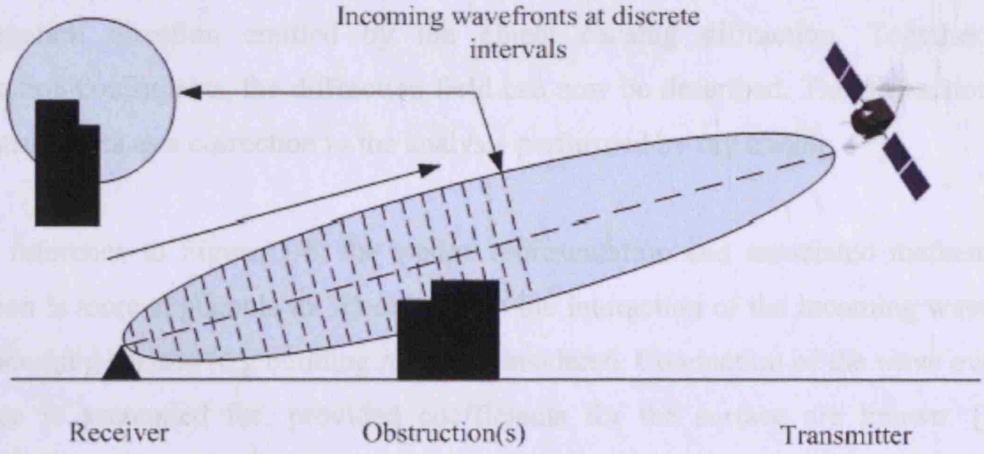

Figure 3-5: 3D analysis of Fresnel zone obstruction

3.1.3 Diffracted Propagation

When passing objects or apertures, all waves are disrupted in some way. Diffraction refers to the bending, scattering or interference that follows such an interaction. Neglecting the use of geometric primitives, which have unique solutions, and considering electromagnetic wave diffraction over a straight edge only, there exist two classes of the diffracting object; the knife-edge and the wedge.

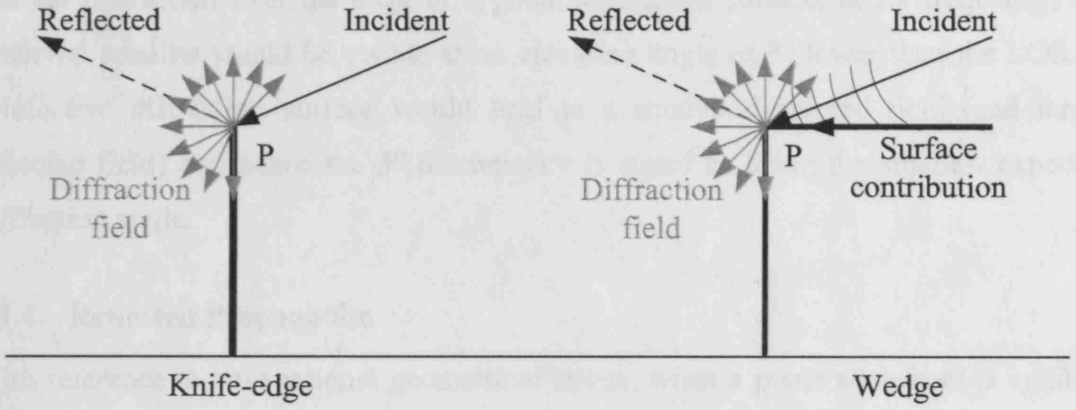

Figure 3-6: Simple signal diffraction by two representations of building edges

The aim of the diffraction model, with reference to the above, is to determine the nature of the signal radiated by the interaction of the straight edge with the incoming signal wavefront. The contribution of the diffraction field for an object placed at P is sought. It is possible to combine elements of geometrical optics with signal characteristics and knowledge of surface attributes to successfully describe the diffracted field. The solution of electromagnetic scattering problems, using this information, is generally performed using a discipline of numerical analysis known as the Geometric Theory of Diffraction (GTD) [James, 1986]. The field strength and phase is calculated for each propagation direction emitted by the object causing diffraction. Together with diffraction coefficients, the diffraction field can now be described. The diffraction field essentially acts as a correction to the analysis performed by ray tracing.

With reference to Figure 3-6, the wedge representation and associated mathematical solution is more applicable to 3D objects, as the interaction of the incoming wave with the incoming surface (e.g building roof) is considered. Conduction of the wave over this surface is accounted for, provided coefficients for the surface are known. [James (chapter 5), 1986].

With reference to the diffraction of GPS signals, a method involving solution of the Parabolic Equation (PE), an alternative to GTD, has been used to assess the effect of diffraction for signal propagation in 2D [Walker and Kubik, 1996]. The method involves a numerical solution to the PE which provides a direct solution to Maxwell's wave equations. Signal attenuation resulting from a variety of test scenarios can be determined using this method. This research involved a comparison of experimental observations and theoretical calculations to assess diffraction. Results of this work noted that for diffraction over the edge of a good conducting surface, at L1 frequency, the observed satellite would be visible at an elevation angle of 3° lower than the LOS. A conductive diffraction surface would lead to a smaller diffracted field (and larger reflected field) and hence the 3° discrepancy is stated as being the smallest expected diffraction angle.

3.1.4 Reflected Propagation

With reference to conventional geometrical optics, when a plane wavefront is incident upon a planar interface between two slightly lossy homogeneous media there exists a reflected and a refracted field. The mathematical solution for such a problem yields the reflected signal power in a specified direction, given transmission coefficients of the two media, incoming power and incident angle. The solution can be found in [James (chapter 4), 1986]. A representation is provided in Figure 3-7, below.

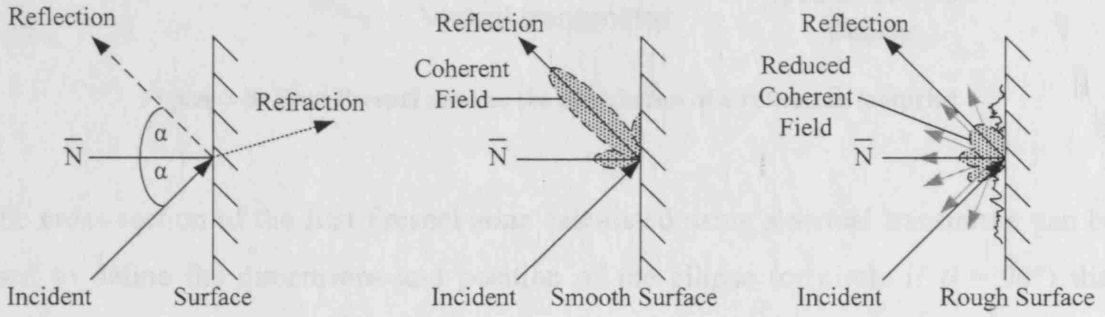

Figure 3-7: Geometrical optics – demonstrating reflection

As with diffraction, mathematical solutions exist to describe the field of interest (in this case the reflection field), following some numerical analysis. The simplest model is that of specular reflection, whereby it is assumed that the reflector is a perfect mirror and all reflected energy propagates only in one path from the reflector. This path follows the law of reflection, whereby the angle of incidence is equal to the angle of reflection, measured from the normal to the surface. Specular reflection is in contrast to diffuse

reflection, in which the reflected energy is deemed to radiate in a number of directions, see Figure 3-7. Diffuse reflection is more commonly associated with rough surfaces e.g concrete, where the magnitude of variation in surface pattern is a substantial fraction of the signal wavelength.

In order to re-radiate enough energy from an incident signal, to induce a current in a receiver antenna, a reflector must possess a surface area of sufficient size. Reflected energy from within a defined area of a reflector will contribute to the received signal by means of constructive interference. This is in the same manner as the diffracted signal from within the first Fresnel zone. Received energy resulting from this interaction will yield a coherent signal.

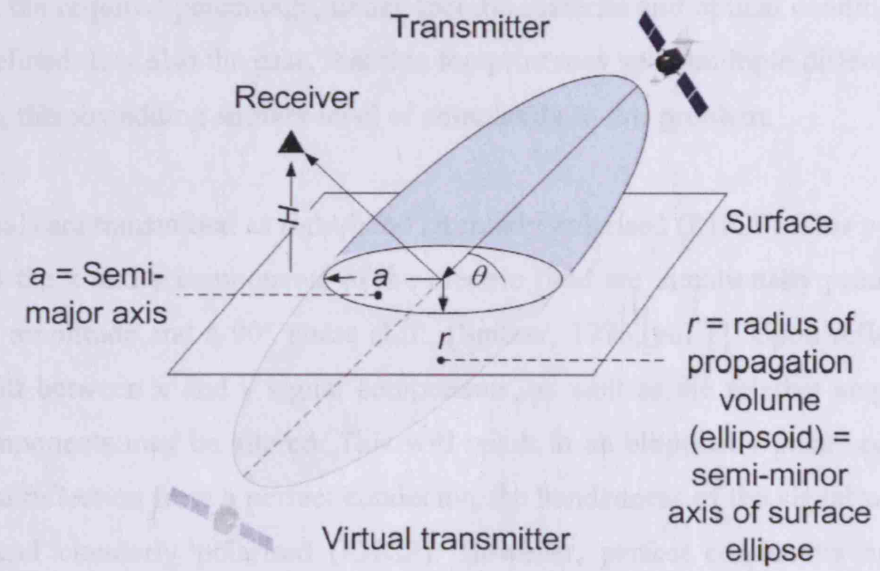

Figure 3-8: First Fresnel zone as the calculation of a reflection footprint

The cross-section of the first Fresnel zone calculated using a virtual transmitter can be used to define the dimensions and position of the ellipse (or circle if $\theta = 90°$) that defines the re-radiation footprint, as shown in Figure 3-8. It can be shown (see APPENDIX B) that the equations for the semi-major axis (a) and the semi-minor axis (r) of such a footprint are:

$$r = \sqrt{\lambda \frac{H}{\sin\theta}} \qquad \text{(eqn. 3-2)}$$

$$a = \frac{r}{\sin\theta} \qquad \text{(eqn. 3-3)}$$

Where:

H	=	Perpendicular distance from surface (m).
A	=	Semi-major axis of ellipse formed on reflecting surface (m).
R	=	Semi-minor axis of ellipse formed on reflecting surface (m). This is equal to the radius of the propagation volume (ellipsoid).
θ	=	Angle of incidence (radians).
λ	=	L1 or L2 wavelength.

Electromagnetic energy re-radiated from any part of the defined footprint will add to the signal strength at the receiver. For a reflection to be successfully received, a significant percentage of this footprint must be available. However, as with the Fresnel obscuration problem, the required percentage, under specific material and optical conditions etc, is poorly defined. It is also the case, that this footprint may span multiple different surface materials, thereby adding another level of complexity to this problem.

GPS signals are transmitted as right-hand circularly polarised (RHCP). This polarisation occurs as the x and y components of the electric field are intentionally produced with the same amplitude and a 90° phase shift, [Spilker, 1996, vol 1]. Upon reflection, the phase shift between x and y signal components, as well as the relative amplitudes of these components may be altered. This will result in an elliptically polarised reflected ray. Upon reflection from a perfect conductor, the handedness of the signal will change to left-hand circularly polarised (LHCP). However, perfect conductors are seldom found, particularly in urban environments. On the whole, antennas have different gain patterns for RHCP and LHCP patterns and a reflected signal generally consists of components of both RHCP and of LHCP. Therefore in reality, total rejection of LHCP is not obtained [Spilker, 1996, vol 1, p.559, paragraph 2]. The degree of polarisation change is a function of the relative permittivity of the reflector material and the incident angle. The polarisation factor F is an indicator of the degree of match between the polarisation of an incoming signal and the polarisation of the receiver antenna. A polarisation factor (F) of an incoming signal is 100% for an appropriately polarised antenna setup, denoting that the x and y components of the transmitted signal (and the received LOS signal) are of the same amplitude and are phase shifted by 90°. As the polarisation becomes more elliptical, the polarisation efficiency falls. This polarisation efficiency is reduced upon reflection (with a non-perfect conductor) and the resulting polarisation efficiency is given by Mott [Mott, 1992]:

$$F = \frac{(AR_1 AR_2 - 1)^2 + (AR_1 - AR_2)^2 + (AR_1^2 - 1)(AR_2^2 - 1)\cos 2(\tau_1 + \tau_2)}{2(AR_1^2 + 1)(AR_2^2 + 1)} \qquad \text{(eqn. 3-4)}$$

Where:

AR_1	=	Axial ratio of the incident signal (LOS or reflected).
AR_2	=	Axial ratio of the receiving antenna.
τ_1	=	Tilt angle of incident reflected signal.
τ_2	=	Tilt angle of receiving antenna.

In the case of signal reflection, F is an indicator of the degree of match between the reflected signal and the receiver antenna. As F is relative to the polarisation state of the antenna, it provides a good indicator of the match. Different GPS receiver equipment will have different tolerances to the polarisation efficiency.

In addition to an extended path length, reflected signals can exhibit a phase shift [Jones et al., 2004]. If this phase shift is between 90 and 270°, then a modulated signal can be inverted.

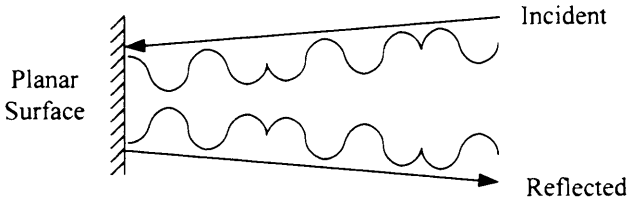

Figure 3-9: Phase shifted reflection resulting in inversion of a modulated signal

The precise nature of phase shifting, as a function of signal wavelength and material properties is poorly undersood, for pratical cases (e.g. non perfect reflecting surfaces).

3.2 Disrupted Signal Measurement and Code Multipath

GNSS receivers are required to track signals with power levels that are below the noise band of the local spectrum. This requires highly sensitive RF front end components which include signal amplification as well as band pass filtering. The use of such sensitive hardware inevitably leads to a receiver's susceptibility to reception and processing of signals that arrive via disrupted propagation paths. Reflection and scattering of signals (described in section 3.1), by objects surrounding the receiver, can result in one of, or a combination of, the following scenarios:

a. Interference to the electromagnetic wave of the direct LOS signal (occurs before current is induced in the antenna).

b. Range measurement made using a disrupted signal where LOS is unavailable (reflected-only).

c. Reception of the reflected signal/(s) in addition to reception of the LOS signal copies (multipath).

The following subsections provide a review of published material offering evidence for the existence of the reflection-only range measurement, and describing the causes and effects of code multipath. Firstly it is beneficial to provide a brief explanation of the code correlation process in order to describe how a disrupted signal leads to erroneous range measurement.

3.2.1 Range Measurement by Code Correlation

GPS is a spread spectrum Code Division Multiple Access (CDMA)[1] system. Pseudorandom binary codes modulated onto two carrier frequencies are processed by the receiver to establish apparent signal TOF, which is subsequently converted into range measurements between receiver and transmitter. Coarse acquisition (C/A) and precise (P) codes are modulated onto the appropriate carrier waveforms, according to the GPS signal structure [ICD-GPS-200, 1995]. A binary phase shift keying (BPSK) modulation scheme is used and a navigation message is modulated onto both carrier signals at a data rate of 50 bits per second (bps) in phase quadrature to the PRN codes [Leick, 1995]. For the PRN codes, the rate at which modulation occurs is 1.023Mbps for C/A and 10.23Mbps for P. A PRN bit is also known as a chip, and as such, the modulation rate is also referred to as the chipping rate [Spilker, 1996, vol 1, p.550]. A spread spectrum system is desirable for such a system in order to mitigate interference and jamming as well as to provide a means for all satellites to transmit on the same frequency.

[1] A full description of the spread spectrum communication technique and CDMA modulation can be found in [Viterbi, 1995].

Neglecting the intricacies of the spread spectrum system and the complexity of the GPS signal, in terms of its modulation by more than one PRN code together with a navigation message, it is convenient to consider the process of range measurement at its simplest level. Measurement involves comparison of a received code with a locally generated replica. The transmitted code will arrive at the receiver with a time delay (relative to transmission time) which is equal to the TOF of the signal. The internally generated replica code, inside the receiver, must be time shifted by an appropriate amount until the received and generated codes are aligned, thereby establishing the signal TOF which is later converted to a range.

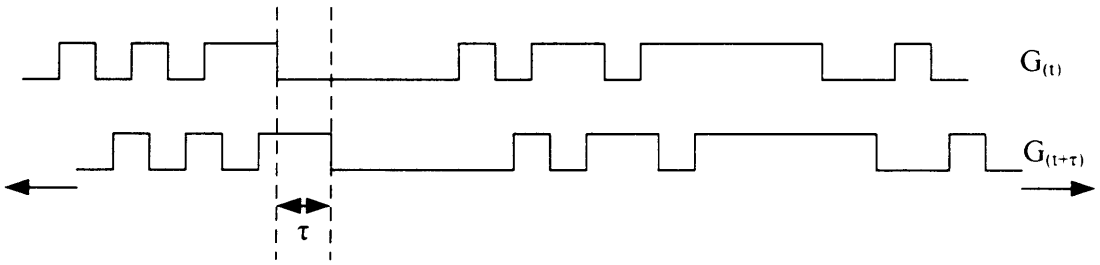

Figure 3-10: Determining signal TOF using code measurements

A code correlation value describes the number of bits between two code sequences that agree for a single phase offset. The term autocorrelation is used to describe the situation whereby a code is correlated with a time shifted version of itself. For each time shift in the internally generated replica, a correlation value with the received signal is calculated. This is essentially the sum of all samples with agreeing binary values minus the sum of all disagreeing samples across the whole code sequence [Misra and Enge, 2004, p.269]. The highest correlation value will result when the two codes are exactly aligned. For the C/A code, with reference to Figure 3-10, the corresponding normalised peak function is given [Spilker, 1996]:

$$R_{G(\tau)} = \frac{1}{1023T_{C/A}} \int_{0}^{1023} G_i(t)G_i(t+\tau)dt \qquad \text{(eqn. 3-5)}$$

Where:

$T_{C/A}$ = Chipping period for C/A code (seconds).

t = Time.

τ = Offset between received and internally generated signal (seconds).

As can be seen from (3-5), the autocorrelation process involves multiplying the received code with a time-shifted replica of itself to form a product that is subsequently integrated. If $Gi(t)$ resembles $Gi(t+\tau)$ then $R_{G(t)}$ will be large [Misra and Enge, 2004,

p.268]. Although the maximum correlation value is achieved at the appropriate code phase shift, non-zero correlation values will result at other code phase shifts. This provides the autocorrelation function, which is a measure of the correspondence between the two identical codes at particular phase shift values. Figure 3-11 provides a representation of an autocorrelation function for a PRN code. The correlation value has not been normalised in this representation.

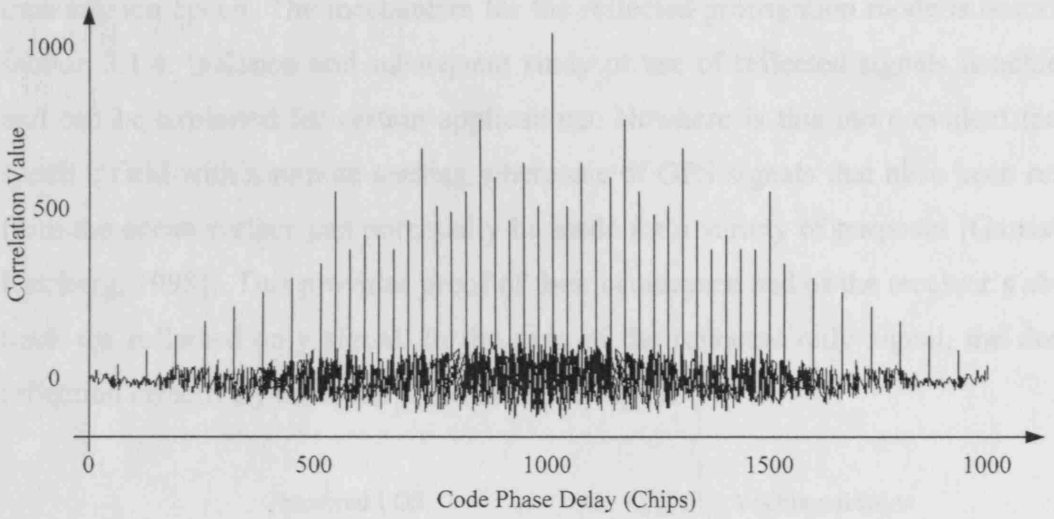

Figure 3-11: Autocorrelation function

Multiple transmitters are required in order to solve for a position velocity time (PVT) solution, and therefore the codes originating from each transmitter must be uniquely identifiable. In the case of the C/A code, modulated onto the L1 frequency, this is achieved using Gold codes. Gold codes are generated using two linear feedback shift registers with two specific polynomials. Cross correlation describes the comparison of one code with a different code of the same length.

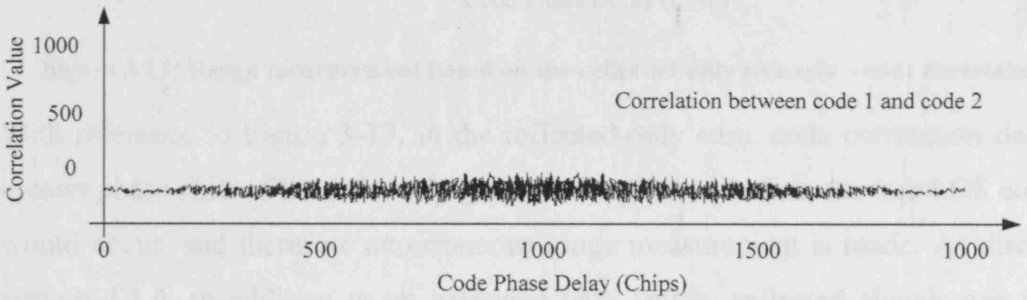

Figure 3-12: Cross correlation

Gold codes exhibit very low cross correlation, meaning that the comparison of one code with another will yield extremely low cross correlation values. Hence each code is uniquely distinguishable and will not interfere with codes originating from different transmitters, despite being modulated onto the same frequency.

3.2.2 Reflected Signal Range Measurement

Firstly, we consider the scenario whereby a reflected signal is visible to the receiver, and the direct (LOS) signal is obstructed. This case is referred to as the reflected-only propagation mode and differs from that of the multipath case only with regard to the absence of a LOS signal. Signals that have travelled via indirect paths always arrive later in time than direct signals originating from the same source at the same transmission epoch. The mechanism for the reflected propagation mode is described in section 3.1.4. Isolation and subsequent study or use of reflected signals is achievable, and can be exploited for certain applications. Nowhere is this more evident than in a specific field within remote sensing where use of GPS signals that have been reflected from the ocean surface can potentially be made for a variety of purposes [Garrison and Katzberg, 1998]. This provides proof of their occurrence and of the receiver's ability to track the reflected only signal. In the case of the reflected only signal, the dominant reflection effectively takes the place of a LOS signal.

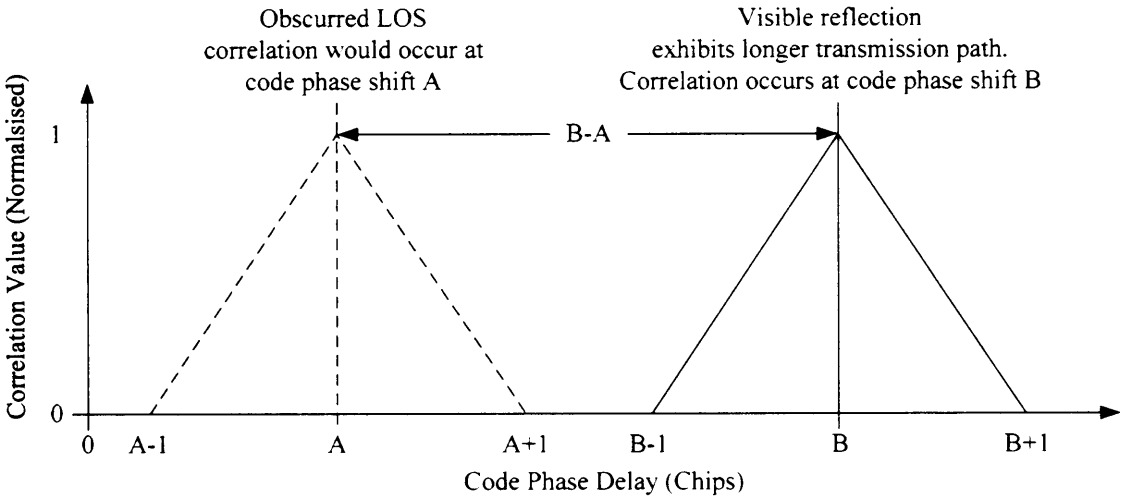

Figure 3-13: Range measurement based on the reflected-only scenario – code correlator view

With reference to Figure 3-13, in the reflected-only case, code correlation occurs at a greater phase shift of the internally generated replica code than the true LOS correlation would occur, and therefore an erroneous range measurement is made. As discussed in section 3.1.4, in addition to an extended path length, reflected signals can exhibit a phase shift [Jones et al, 2004]. If this phase shift is between 90° and 270°, then the received code can be an inverse of the original. In this case the correlation value will be at its most negative and a negative correlation peak will result. However, as the absolute correlation value is used to determine the correlation power function, this inversion is irrelevant [Schwartz, 2001].

3.2.3 Code Multipath

The antenna of a GPS receiver is a natural receptor of multipath generated copies of the GPS signal [Kunysz, 1998]. Reflected and diffracted propagation modes are responsible for presenting the antenna with copies of the original signal. The case under consideration in this section, occurs where both LOS and one or several signal copies enter the receiver. Signal copies are also referred to as disrupted signals, owing to the fact that an indirect path is taken from satellite to receiver. As described by Kaplan [Kaplan, 1996], the reception of multipath signals leads to distortion of the PRN code and navigation data modulated onto the carrier, and also disrupts the phase of the carrier itself. The way in which this disruption occurs, and the impact it has upon the range measurement process will now be considered.

3.2.3.1 Code Correlation

The impact of the multipath signal(s) upon the range measurement process is dependent upon the following [Misra and Enge, 2004]:

a. The amplitude of disrupted signal(s) relative to the LOS signal.
b. The delay of the reflected signal relative to the LOS signal.
c. The phase of the reflected signal relative to the LOS signal.
d. The rate of change of the relative phase.

The combination of the direct (LOS) signal with the multipath signal(s) results in the formation of a composite spread spectrum signal [Kaplan, 1996, p.548]. An expression for the composite signal can be given as follows:

$$x(t) = \sum_{i=0}^{M} a_i(t)\,p(t-\tau_i(t))\cos[\omega t + \theta_i(t)] \qquad \text{(eqn. 3-6)}$$

Where i denotes the signal number with the LOS signal at i=0 and:

$x(t)$ = Time dependent spread spectrum signal level.
M = Number of multipath signals.
$p(t)$ = The PRN code (-1 or +1).
ω = Angular frequency of the line of sight signal (carrier plus Doppler) in rads/sec.
$a_i(t)$ = Time dependent amplitude of the ith signal relative to that of the LOS signal.
$\tau_i(t)$ = Time dependent delay of the ith signal relative to the LOS signal.
$\theta_i(t)$ = Time dependent phase of the ith signal relative to that of the LOS signal.

From equation (3-6) it can be seen that depending upon the value of $\theta_i(t)$, disrupted signals can arrive in-phase or out-of-phase with the LOS signal. The reception of an in-phase signal produces constructive interference and this strengthens the direct signal. Out-of-phase disrupted signals cause destructive interference, referred to as fade [Misra and Enge, 2004, p.308]. Equation (3-6) describes the disruption to the signal upon which phase measurement will subsequently be made. With regard to pseudorange measurement, the output of the correlation process is the sum of all RF samples for each satellite, multiplied by a locally generated PRN code replica, operating at a specific code phase delay [Fenton and Jones, 2005]. Consequently, the presence of reflected signals causes the occurrence of unwanted correlation peaks, appropriately time delayed and attenuated with respect to the position and amplitude of the LOS signal. If the interference (from the disrupted signal) is constructive, then the instantaneous correlation values of the disrupted signal are added to those of the LOS signal. If the interference is destructive, then the correlation values are subtracted [Misra and Enge, 2004]. Disruption to the correlation process, and the formation of a composite correlator peak is illustrated in Figure 3-14.

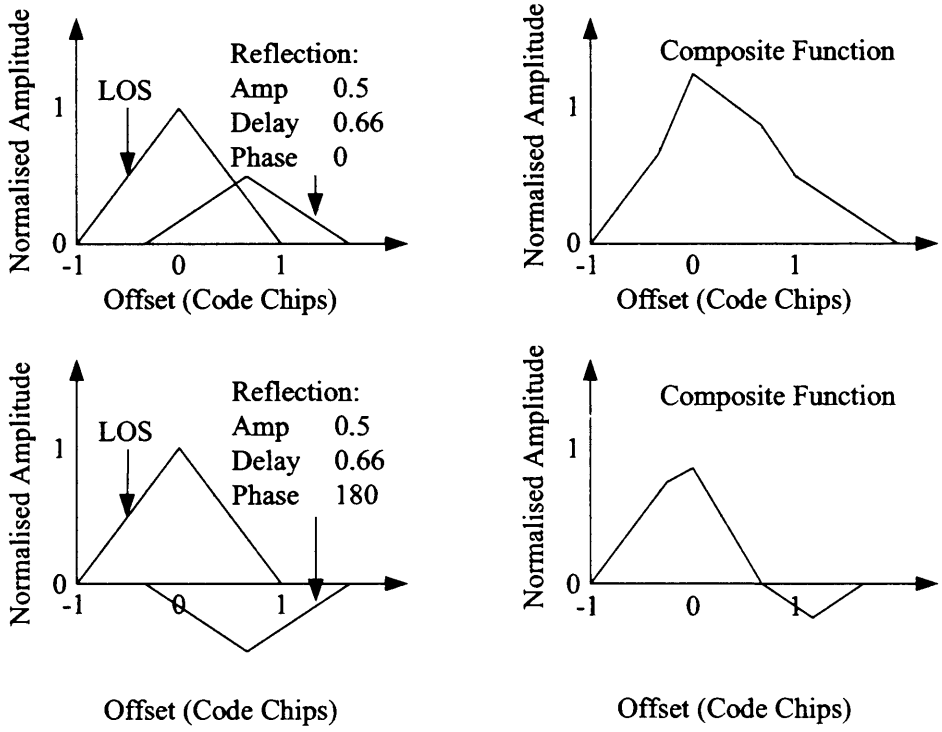

Figure 3-14: Correlator peak distortion due to in-phase and out of phase code multipath

The delayed multipath signal(s) are likely to exhibit reduced amplitudes relative to that of the LOS signal [Jones et al., 2004] due to attenuation during reflection. As with all RF signals, antenna response is a function of the antenna gain pattern at the frequency,

elevation and azimuth of the incoming signal. Peak distortion is therefore a function of reflected signal delay, phase and amplitude all relative to the LOS signal [Sleewaegen and Boon, 2001]. A Delay Lock Loop (DLL) tracks the signals from each GPS satellite. The DLL is responsible for correlating the received signal with slightly early and slightly late replicas of the signal. An early correlator samples the peak on the rising edge of the correlation function when locked to the received signal, and a late correlator samples the falling edge of the peak [Misra and Enge, 2004, p.299]. The fixed time period (in chips) between the correlators is referred to as the correlator spacing and is typically 1.0 chip for a standard correlator and 0.1 chips for a narrow correlator. A prompt correlator is then applied to sample the correlation function in between the early and late positions. The prompt correlator is effectively monitoring the peak of the correlation function. Sampling of the correlator peak in the manner described performs correctly for well formed correlator peaks. Distortion of the peak, caused due to the presence of multipath signals leads to erroneous TOF measurement as shown in Figure 3-15. On the left of Figure 3-15, a correlator peak has been distorted by in-phase reflection and on the right a correlator peak has been distorted by an out of phase reflection. In the given illustration, the phase shift error is positive for the in-phase case and negative for the out of phase case, although this rule does not apply in all cases as peak distortion is also a function of delay and amplitude of reflected signals.

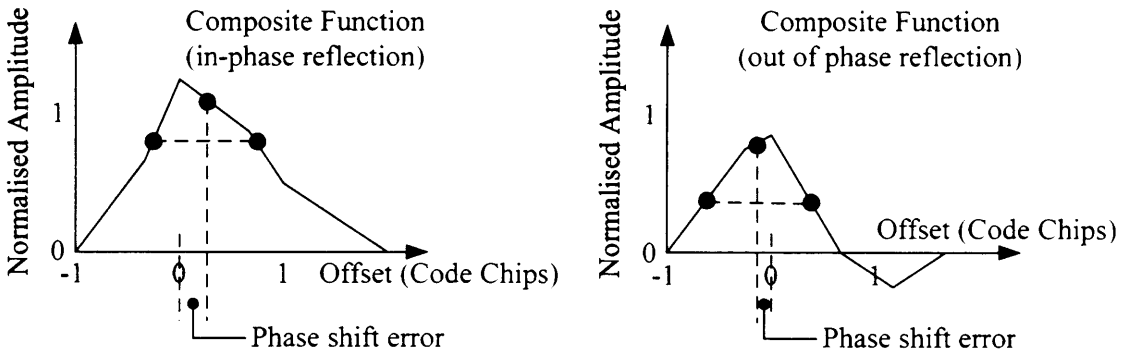

Figure 3-15: Erroneous TOF determination due to distorted correlator peak

Correlator spacing has a dramatic effect on the susceptibility of a receiver to the presence of multipath signals. One of the reasons for this will now be described with reference to Figure 3-16.

$$delay(chips) < (1 + \frac{cs}{2}) \qquad \text{(eqn. 3-5)}$$

$$delay(m) < T_{(CA/P)}(1 + \frac{cs}{2}) \qquad \text{(eqn. 3-6)}$$

Where:

delay	=	Delay of disrupted signal.
cs	=	Correlator spacing (chips).
T	=	Chip length (meters) for C/A or P code.

Disrupted signals delayed by more than *delay* in equations (3-6 and 3-7) above will result in distortion that is outside of the receiver correlator window and as such will result in little or no error [Kaplan, 1996, p.258] and also [Braasch,1995 (see Spilker., 1996, vol 2)]. In addition to consideration of the correlator window, defined by the correlator spacing, the phase shift error (of the internally generated replica code) under multipath conditions is, under most circumstances reduced when a narrow correlator spacing is applied. This is illustrated by Figure 3-16 in which a standard correlator is applied to a distorted correlator function on the left and a narrow correlator is applied to the same distorted function on the right of the figure. The spacing between early and late correlator (E-L spacing) can be seen to be different for the two correlator types. The correlators are applied to detect the peak of the function. Under conditions whereby the correlator function is distorted it can be seen that a better peak detection, and therefore lower signal time of flight measurement error, is achieved with a narrow correlator.

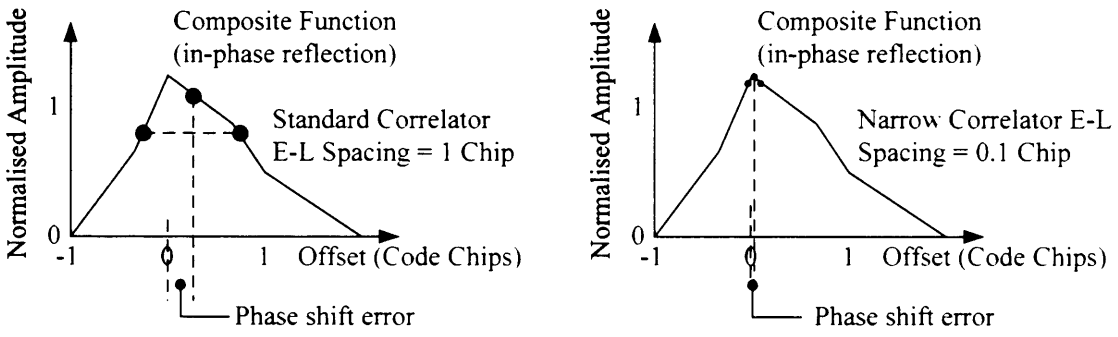

Figure 3-16: Reduction of multipath error by using a narrow correlator

Jones [Jones et al., 2004] suggests that for a standard correlator, the most significant C/A code multipath bias occurs at around 0.75 chips and at around 0.1 chips for a

receiver with narrow correlator technology. Distortion of the correlation function near its peak due to multipath is less severe than at regions away from the peak [Van Dierendonck et al., 1992]. This is shown in Figure 3-17. This response is exploited by the use of correlator technologies such as the narrow correlator, whereby the spacing between the early and late correlator is reduced, Figure 3-16. For more information on correlator behaviour see Cannon [Cannon et al., 1994].

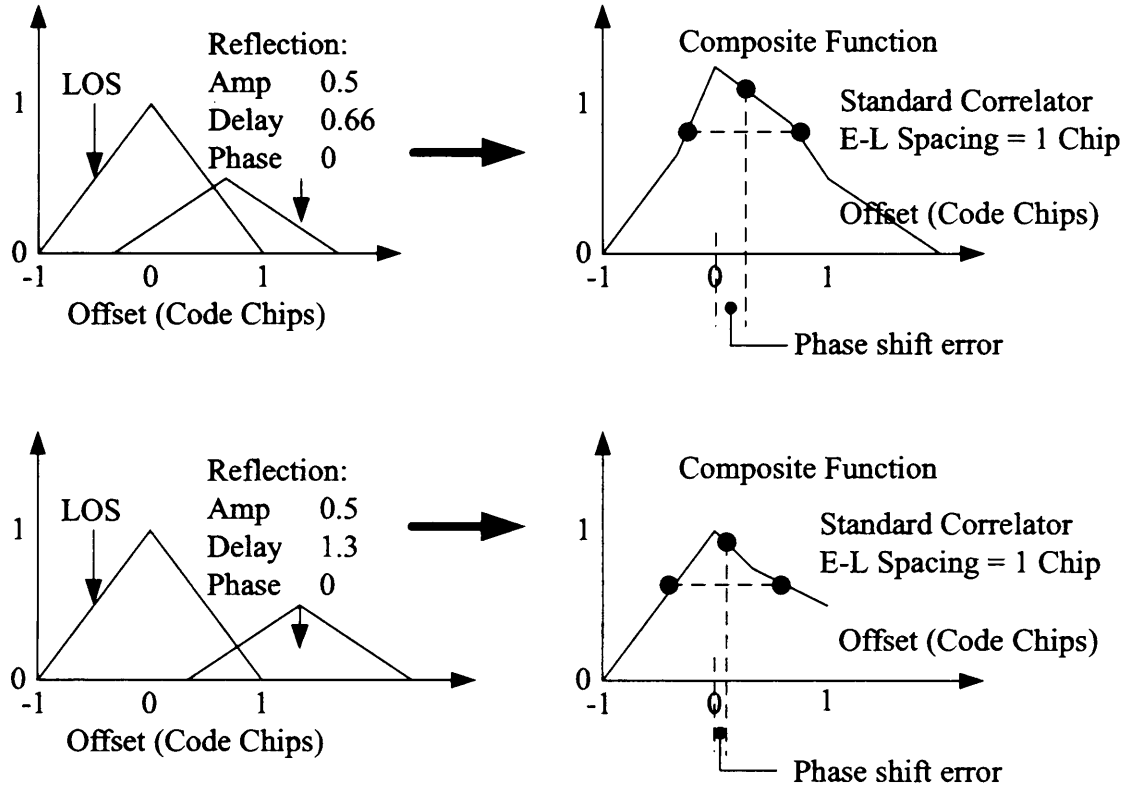

Figure 3-17: Correlator function distortion near to and far from correlation peak

3.2.4 Pseudorange Error

Distortion of the code correlation peak occurs following the reception of disrupted GPS signals in combination with the LOS signal. Subsequently, erroneous TOF measurements are calculated, following application of the code correlators, and these translate into a range error. Jones [Jones et al., 2004], suggests that the error on a code range measurement using a standard correlator can be up to 80m and up to 10m for a receiver with narrow correlator technology.

3.2.5 Algorithms and Hardware Enhancement for Multipath Mitigation

Multipath remains one of the last sources of error to be successfully removed by detection or modelling. The detection of multipath signals in real time, and its subsequent removal from range measurement is generally performed through the use of

novel receiver technologies such as adaptive antenna and multipath mitigating correlator configurations. A method of adaptive filtering is described by Nelson [Nelson et al., 1997]. An adaptive noise-cancelling algorithm accommodates changes in the user environment and detects code delay and multipath in GPS signals. Kunysz [Kunysz, 1998] discusses the effect of antenna performance on GPS signal accuracy, concluding that poor axial ratios of antenna patterns cause significant phase/amplitude errors in high multipath environments. The role of the correlation process in reducing the receiver response to multipath is most notably addressed by the narrow correlator [Fenton et al., 2005], Multipath Elimination Technology (MET) [Townsend et al., 1995] and the Multipath Estimating Delay Lock Loop (MEDLL) [Townsend et al., 1995] among others. Adaptive multipath mitigation techniques such as that described by Rlinami [Rlinami, 2000] typically aim to predict multipath within the receiver, create a multipath profile, and then subtract the multipath effects from the measured autocorrelation value of the GPS signal.

The characteristics of an environment surrounding a receiver will determine the attributes of the signals present at the antenna. That is to say, that the density, material types, proximity, size, shapes and configuration of structures that surround a receiver will determine the number of reflected and diffracted signals visible to an antenna. These factors will also determine the associated extra path lengths, phase shifts and attenuations of the received reflected and diffracted signals. Receiver response to disrupted signals is a function of the receiver design including the performance of any mitigation technologies (such as those discussed above) that are employed. The effect of the surrounding environment on code based range measurements is profound (as described in section 3.2.4). Urban environments are particularly problematic for code based range measurement. For code measurement, time delayed copies of the GNSS signal (resulting from reflection and diffraction events) will interfere with range measurements from substantial distances (see eqn 2-1 section 2.5).

For high accuracy applications, carrier phase multipath presents a significant problem. Reception of reflected signals disrupts the phase of the carrier [Kaplan, 1996]. The carrier is tracked in a Phase Locked Loop (PLL) [Ray and Cannon, 1999], and as the phase of a composite signal (in the prescence of multipath) is rarely the same as that of a direct signal, a tracking error within this loop is introduced [Townsend et al., 1995]. Depending upon the receiver specification, the maximum range measurement error of

5cm on L1 [Cannon et al. 2000] is highly likely in urban environments, given the high level prescence of nearby reflecting objects.

Enhanced algorithms and hardware have undoubtedly progressed far in reducing receiver errors caused by multipath. However, the techniques identified above are integral to the receiver design and take no account of the environment in which the receiver is operating. The complex behaviour of electromagnetic signals in difficult environments and the requirement for receivers to track signals with low signal to noise (SNR) ratios leave receiver technology susceptible to reception and processing of unwanted signals. For this reason, much current thinking, and in particular the aim of this project, revolve around approaches that afford a receiver better knowledge of the local signal disruption conditions (for example [Weiss et al., 2006]). As such, consideration of the environment in which the receiver is operating could result in the generation of corrections for the signal disruption. Such work will undoubtedly prove useful where reflected and multipath signals are desirable, for example with high-sensitivity receivers. Such technology typically uses heavy amounts of digital signal processing to seach for GPS signals that have been attenuated, often by transition through thin building walls or following reflection. The above mentioned generation of range corrections for signals that have arrived through disrupted signal propagation paths, could be applied to positive effect.

3.3 Urban Models

In this section, computerised models of physical environments are defined. Data collection and model production techniques are presented as background information. Formats and standards for encapsulation of model data are introduced. Model useage, quality and availability are discussed. An introduction to the Virtual Reality Markup Language (VRML) is given before the conclusions of the urban models section are stated.

3.3.1 Computerised Models of Physical Environments

Techniques including Light Distance and Ranging (LIDAR) provide vast amounts of coordinate and material attribute data, relating to physical objects. When logically organised and encapsulated in well defined file formats, this data can be processed for a range of applications. Modern computing provides ever increasing storage capacity and

faster processing times. Combination of the above factors, make feasible the idea of accurately describing entire environments in high levels of detail.

It should be noted that it is not within the scope of this research to assess the numerous methods for acquiring urban environment data, or the technologies used to construct urban models. No work within the study has been undertaken to collect, or produce any model data. This work focuses purely on the use of existing data, with some comment on the future of the topic.

3.3.1.1 Definition of a Model

With reference to the description of physical objects, as data that is retained and processed by computers, the following must be considered.

- Despite rigorous efforts to eliminate and mitigate measurement error, this error will always be present at some level in any type of data collected by any spatial data acquisition technique.

- For raw data assembled into a dataset, methods can be employed to achieve results with lower residual errors across the entire dataset. Examples of such techniques include least-squares fitting and bundle adjustments for coordinate point datasets. The distribution of original errors is therefore changed.

- Storage and manipulation of numerical data is subject to machine introduced errors originating from rounding, floating point, and numerical instability.

- The capture of continuous data is impossible. Data is collected at discrete points and there is, therefore, a practical resolution at which detail is captured. At some level inference or interpolation is required to describe the regions between data points.

Consequently, the description of a physical object encapsulated in a computerised format is essentially a modelling task, and the output is a model of the physical object. Thus we often refer to a dataset as a model. A collection of modelled objects consistently scaled and appropriately positioned in an absolute sense (and therefore also in a relative sense), constitutes a model environment.

3.3.1.2 Data Acquisition, Production and Processing Techniques

Sources of data for the production of city models include, but are not limited to, the following:

- Topographic maps.
- Aerial photographs.
- LIDAR data.
- Building survey data.

All or a combination the above sources can be employed depending upon the technique used. Sadek [Sadek et al., 2007] describes the conventional steps toward generation of a 3D city model using topographic map data together with aerial photographs. In such a method, topographic map data is used to provide geographical reference points for urban objects and natural features. The coordinate information for 2D footprints of individual structures and naturally occurring objects are then found by combining topographic map reference data with orthophoto image data derived from a stero pair of aerial photographs. Stereo photogrammetry presents an appropriate method for this task [Gruen, 1997]. The combination of topographic map data and stero photography also allows the production of a digital elevation map (DEM), whereby heights of objects within the area of interest can be determined. Finally, textures derived from photographs, taken at ground level, can be draped over the geometric model. In the case of this work described by Sadek [Sadek et al., 2007], the word texture is used to describe photographic information relating to the visual appearance of the surface of an object within the 3D city model.

The current driver of research into the production of such models is in the automatic generation of 3D environments. A system for the production of 3D city models using laser profiler data, 2D digital maps and aerial photogrammetry is described by Takase [Takase et al., 2004]. Novel approaches to enhance the production, in terms of quality, speed and automation are constantly being developed. The rapid generation of 3D models by using two inexpensive fast laser scanners as opposed to the conventional use of one high quality scanner, is described by Fruh and Zakhor [Fruh and Zakhor, 2001]. The complexity of natural scenes and current inadequecies in the performance of image understanding algorithms leads to a semi-automated approach. Such an approach for the generation of 3D models from image data is implemented within the CyberCity Modeler

software as described by Gruen [Gruen and Wang, 1999]. Different techniques exhibit different strengths and weaknesses. The automated extraction of roof morphology remains a limitation in the development of automated techniques [Batty et al., 2000]. It should be considered that model data must be recollected at regular intervals in order to increase model quality and crucially to keep the models current. Together with a desire to collect data at high resolution and over large geographical areas, the development of high quality automated data collection and model production techniques is of key importance.

3.3.1.3 Model Data Formats

The primary function of a format is to define a standard for the expression of data. A list of model formats that can be used for the encapsulation of city mode data is provided in APPENDIX C. The name of the format is provided together with the accompanying acronym. This list was compiled in 2004 to identify a shortlist of candidate formats that could be used within the simulator developed during this study.

3.3.1.4 City Model - Current Useage

There are four defined categories of use for city models, as described by Shiode [Shiode, 2001]. The defined categories are, planning and design, infrastructure and facility services, commercial sector and marketing, and promotion and learning of information on cities. A more extensive list is provided by Batty [Batty et al., 2000] in which 12 categories of use are defined:

Emergency services	Property analysis.
Urban planning	Tourism and entertainment.
Telecommunications	E-commerce.
Architecture	Environment.
Facilities and utilities management	Education and learning.
Marketing and economic development	City portals.

Within each of these categories new applications are emerging rapidly. Interest in these applications creates a continuous demand for better quality models in terms of accuracy, level of detail and resolution. Combined with the amount of work being undertaken around the world in research and development into further techniques and possibilities for modelling the urban environment, there is little doubt that the future of such models,

and more importantly the creation and development of future models, can be relied upon. Current applications for city models range from the presentation of spatial data for architecture to simulators for navigation during warfare.

3.3.1.5 State of the Art

Ever increasing levels of detail are being achieved within computerised models of physical environments. The maximum level of detail in terms of number of objects within a specified area is potentially limitless, but for manual model creation techniques, detail is a function of the resources (time and labour) spent extracting object detail from source material such as stereo photographs. It is not uncommon to find models of urban environments that contain levels of detail including doors, windows and even air conditioning units. Models of more densely populated areas tend to be more detailed, as a greater demand for models of these areas is experienced. Capture and representation of artifacts such as window ledges is currently only observed in very high quality models, the likes of which cover only very small physical areas. A trade-off between model size and the level of detail exists, such that a reduction in the level of detail allows more physical area to be modelled. Levels of accuracy for current models is generally at decimetre level, again, a trade-off exists between the effort expended to produce a model and the resulting quality. Demand for a dataset generally drives the amount of resources employed to produce the model. An assessment of a large model dataset is presented in chapter 6. With reference to the data contained within computerised physical environment models, much emphasis is placed upon the storage of data-rich models, and many data compression techniques have been developed in order to achieve practical file sizes. It is important that such techniques retain the initial geometric fidelity as realised in the original data. Such issues are addressed by Yan [Yan et al, 2001].

3.3.1.6 Future Availability

The use of well established efficient data formats facilitates the distribution of city models over the internet. The use of a format allows a product from different originators to be used by a variety of computer aided design (CAD) software, as opposed to requiring dedicated proprietary tools. As previously stated, the rise in applications for model datasets is fuelling the creation of models, and acts as a driver for increased quality, in turn increasing the number of applications. Consequently more models appear over time, and the development of more efficient production techniques should act as a catalyst for this process. It is therefore predicted that model availability in the

future is guaranteed. The distribution of models over telecommunications systems is also likely, thereby allowing the consideration of their use in mobile devices. A list of models available over the internet was compiled as part of this study in 2004. The list is presented in APPENDIX D. It should be noted that the supplied list was compiled to indicate model availability and popularity. The list is correct as at 2004, and is growing rapidly.

3.3.1.7 Computerised Model Characteristics with Respect to this Research

In order to analyse the environment surrounding a receiver and to determine accurate predictions of satellite availability, using multiple sophisticated propagation models as performed during this research, environment models must exhibit certain characteristics. The ideal environment model will be highly accurate with respect to the position accuracy of all objects (and each artefact of each object) contained within the model. Ideally, an extremely high level of detail in terms of the artefacts within a model should be achieved. An example of this is the capture of small detail on structures such as window frames. In addition, a model must be as complete as possible with a consistent level of data capture throughout the area of interest. Ideally, the level of accuracy, level of detail and level of completeness, will apply consistently throughout the model. Section 6 provides quantitative assessment of the quality of a state of the art urban model.

It is also worthy of note, that research is being undertaken to derive material attributes of objects within environment models. This is of importance to this work, as it would provide the means with which to determine the attenuation of signals upon their interaction with objects surrounding a receiver. Currently, however, such material attribute data is not available. The idea of capturing and assigning such information to an existing model for the purposes of this research is impractical, as the data could not be collected to a sufficient level of completeness over a wide enough area without some sort of automated collection process. Additionally, the use of such attributes falls outside the scope of this thesis, however, as it is likely that models in the future will contain such data this does provide a logical direction for some further work.

3.3.2 Virtual Reality Markup Language

3.3.2.1 Description

The preferred format for the visualisation of 3D objects and spaces (at time of study) amongst the computing and 3D world visualisation community is that of the Virtual Reality Markup Language (VRML). In addition to providing a format for the exchange of 3D model data, VRML effectively defines a standard. Essentially, as a format, VRML permits the encapsulation of geometric, aesthetic, sound, animation and other data for the interpretation and visualisation of 3D spaces and/or objects. As a standard, it encourages the adoption of a set of well established conventions for the compilation and organisation of spatial and visual data. The aim of the standard is to provide a means for the exchange of virtual reality data, thereby escaping the sole use of proprietary standards and associated software. The standard is defined by the Web3D Consortium [Web3D, 2007] and is based upon SGI's platform independent OpenInventor format.

3.3.2.2 Typical Useage

Visualisation is achieved by interpretation of a VRML file by specific software packages or plugins and extensions to existing software e.g Cortona plugin for Internet Explorer [Parallel Graphics, 2007]. As VRML is open source, there is no shortage of available interpretation and authoring software. Open source code for integration of interpreters into software that might be under development is also available. Interaction is possible in VRML worlds. However, the most popular use is conveyance of spatial data through visualisation. When immersed within a VRML world, the user is able to perform a set of movements such as flying, walking, spinning, zooming panning etc according to the functionality of the visualisation software. Applications involving communication of information regarding specific objects, often favour VRML. A CAD object, perhaps produced in a specific piece of software, can often be converted into the VRML format. This permits the distribution of the object to a wider audience. Individual objects can be manipulated and studied as is possible with traditional CAD software.

3.3.2.3 Future

Products such as Cortona Pocket [Parallel Graphics, 2007], are emerging to enable the use of VRML models on mobile platforms. Specifically aimed at use on low resource devices, including mobile communications equipment (PDAs etc), there is little doubt

that use of the standard for mobile computing on a wide scale is feasible. A successor to the standard looks likely to arrive in the form of X3D. A new specification is being designed and implemented by The 3D Graphics Working Group [Web3D, 2007]. This new standard seeks to achieve the same objectives as VRML. Effectively X3D will be an extension of the geometry and behaviour capabilities contained within VRML via an extensible markup language [Pomaska, 2003].

3.3.2.4 Technical Description

As a fully established standard, a formal technical specification for VRML exists, and is available for both VRML1.0 and VRML2.0 [Bell et al., 1995]. A full insight into the creation of VRML worlds is given by Ames et al [Ames et al., 1997].

VRML consists of objects referred to as nodes. A total of 54 nodes can be grouped into the following main categories [Pomaska, 2003]:

- Geometric Primitives.
- Light Sources.
- Appearance nodes.
- Sound.
- Definitions and prototypes.
- Sensors.
- Scripting nodes.

Use of the planar polygon geometric primitive permits the construction of 3D triangular mesh objects. Favoured for the construction of complex shapes, the triangular mesh is the subject for many data compression techniques, see Li and Kuo [Li and Kuo, 1998]. The reduction of bandwidth requirements for transmission and storage of VRML is addressed by Taubin [Taubin et al., 1998].

3.3.3 Conclusions Regarding the use of Urban Models for this Research

The motivation for using computerised models of the environment surrounding a receiver, in order to further enhance our understanding of the behaviour of GNSS observables in urban environments, has been made in the opening chapters of this thesis. The applicability of such models for predicting satellite visibility is well accepted, and this is evident in the adoption of early environment models by others

(section 3.1.1 and section 3.4.1). Production of 3D urban models has been introduced as background information in this section, although such techniques remain outside of the scope of this research. However, research into 3D models has revealed the following critical outcomes that are of relevance to the work detailed in this thesis:

1. Many urban environment models are available. The future availability of such models is guaranteed, in part due to the number of applications for them.
2. New techniques are being developed for data capture and model production. Such techniques increase model quality in terms of the level of accuracy and the level of detail.
3. Applications for such models are becoming more diverse, and this acts as a driver to further increase model quality.
4. A variety of proprietary and non-proprietary data formats and standards for the encapsulation of environment model data already exist. Many of these are freely available.
5. A mature, well adhered to and well adopted standard for the encapsulation of environment data exists in the form of VRML. This standard is considered highly suitable for this work.

The quality of models can be assessed in a variety of ways and varies widely from model to model. Quality is dependent upon the methods used during creation and the resources applied to the production of the model (e.g. man-hours for processes requiring manual work). For this reason, a full assessment of a model used for this work is provided in section 6.

3.4 GNSS Signal Simulators

In this section, a review of existing GNSS signal simulator work is given. Software simulators are focussed upon, however, it should be realised that software simulators can be used to simulate signal characteristics and attributes, in order to feed information to hardware that is in turn capable of producing the corresponding radio frequency response.

3.4.1 GNSS Signal Simulation as an Enhancement to Receiver Technology

The ability to predict the individual signals arriving at an antenna (or lack thereof), as well as their associated properties, would benefit the GPS user segment in a number of ways. The possibility of making range measurement corrections based upon predicted signal propagation information, or to characterise the signal environment and provide a quality figure to the user, would both be a substantial improvement to the current situation. The author is aware of projects aimed towards the improvement of positioning accuracy for use on railways, for example the EGNOS (European Geostationary Navigation Overlay System) Controlled Railway equipment project by ESA (European Space Agency), which is entitled ECORAIL. Such safety critical activities would benefit greatly from the ability to predict availability and signal quality in real time or in advance, local to the user, or via some central processing facility.

Advancement of positioning and navigation is by no means the only motivation for GNSS signal simulation. Vrhovski [Vrhovski, 2003] demonstrated the use of satellite simulation in urban environments for road user charging. This work involved the use of a crude GIS model of the receiver local area. Application of a LOS only signal model together with a poor quality city model resulted in a poor correlation between the simulated and real world data. 3D-GIS models of environments is also used to good effect by Lee [Lee et al., 2006]. In this research, a probability based approach is taken to identify satellites with high likelihood of multipath error. Satellites with expected high levels of multipath are then excluded from or down-weighted in the position solution. The identification of multipath 'hotspots', forms the basis of this statistical approach. Although reasonable experimental results were obtained, the rejection of satellites employed by such a system places greater importance upon the addition of GNSS constellations and assured interoperability. There is also an issue with the effect of satellite geometry when rejecting observations. Also, it is apparent that a more sophisticated 'hotspot' identification algorithm is required. Rakkolainen [Rakkolainen et al., 2001] demonstrates the applicability of VRML in describing the area surrounding a receiver. The paper describes the use of such a model to determine satellite availability and reflected signals, with the aim of enhancing location based services (LBS) and GPS accuracy. An initially accurate model had to be simplified for runtime issues and only 5100 polygons were contained with the whole dataset. Being a user orientated piece of work, the implemented tool aimed to provide the user with rendering details as well as geometry. A very simple LOS propagation model was assumed, and

specular reflection was considered about a single point with no determination of available surface for signal re-radiation. No model of receiver performance is applied to the simulation results, and validation of availability and multipath for this tool could not be found in the published literature. No diffraction modelling was implemented, and no rigorous attempt to predict the arrival of signals via paths other than LOS or simple reflection was made. The work proved to be a successful application of city models for such a task, but its orientation seems to be towards LBS useage rather than improvement of positioning and navigation accuracy. The importance of predicting reflected signals present at Geodetic GNSS installations is addressed by Weiss [Weiss, 2006]. A ray tracing tool is used to predict reflected signals. For this application, where multipath generally occurs following ground reflection, the performance of different terrain models is assessed. No surrounding objects or structures are considered. Use of a LIDAR modelled terrain is found to be of sufficient quality to yield simulation results that compare well with observations. LIDAR data is combined with photogrammetry in research undertaken by Taylor [Taylor et al., 2005]. The development of a real time simulator for satellite availability based upon a simple LOS only propagation model is presented. The best result achieved in the study, using a LIDAR dataset, displayed a mean error (expressed as a percentage) of 8%, for the variation of modelled versus true number of visible satellites for multiple epochs at 767 positions. This error is stated in the literature as originating from poor modelling of the surrounding structures, however, it is considered by the author of this thesis that the propagation models used may not have been suitable. Suh [Suh et al., 2004], uses GIS data as a model of the environment surrounding the receiver, and ray tracing for simple LOS, reflected and diffracted propagation modes. Shu et al note that ideally a numerical solution of the wave equation according to finite element analysis for diffracted propagation (numerical analysis) would be applied. However, it is considered impractical to use of such a tool for dense geometric areas such as cities. Results show a good correlation to the observed results for availability, although no account is made for the inability of the approach to predict all modes of propagation, with respect to the observations. Also, no account is made of the reflected-only signal case, and LOS is modelled as a volumeless transmission. With regard to multipath, the use of a single reflection, specular model is successfully validated against real world data. No assessment of the quality of the specific model datasets used in the experimental data has been found in the published literature, although general quality figures are quoted for the data contained within the GIS system used. Byun [Byun et al., 2002] introduce a GPS multipath simulator that establishes

reflected signals and diffracted signals based upon the principle of ray tracing. The primary application of such a simulator was to establish, in the early phases of experimentation on RF elements of GPS equipment, if the proposed test site would exhibit hazardous levels of multipath. A General Theory of Diffraction (GTD) approach enables calculation of the expected received signal power, assuming attributes of the surfaces surrounding the receiver are known. The effect of the phase and range errors induced by the reflected and diffracted signals is translated into an estimate of the effect that would be experienced by the delay lock loop within a receiver. As with many GNSS signal propagation models, this approach can potentially yield extremely high quality estimates of the received signals and their attributes. However, the quality of the resulting estimates is heavily dependent upon the geometric accuracy of objects surrounding the receiver, and also detailed knowledge of the material types of these objects. The techniques used within the approach are also only practically applicable to very small localized areas.

Signal propagation simulators have been developed specifically for GNSS signals that rely upon numerical analysis of electromagnetic propagation. These include use of the parabolic equation (PE) technique demonstrated by Hannah [Hannah et al., 1999]. In this work, parameters associated with multipath, including relative signal delay, relative amplitude and reflection phase are brought together to form the Multipath Channel Impulse Response (MCIR). A PE propagation model and Fourier time-synthesis are employed to determine the MCIR for certain environments. Reflection and diffraction are both considered, and the approach yields results comparable with observations. However, the technique is not applicable to environments containing high levels of geometrical data or areas with very complex 3D geometries, as the technique is based upon use of an environment profile. Use of the PE model was also made by [Walker and Kubik, 1996]. Again, multipath and diffracted signal propagations were simulated and only 2D signal propagation could be considered. This study noted that a satellite becomes visible 3° earlier than expected due to diffraction at the straight edge of the top of structures. This was performed for a good conductor, and as the diffraction field is stronger for less conductive materials, this represents the lowest expected diffraction. Simulation time is an issue for this approach even when considering advances in computing since this research was undertaken. The work concluded that diffraction errors can be significant for elevation angles near the LOS obstruction angle. Fisher [Fisher et al., 2002] describes the application of computational electromagnetics for

urban canyon operation using GALILEO signals. A simple block model of an urban canyon is used in this study. The importance of using models with detailed material attribute information when performing EM numerical analysis is highlighted in this research. Also discussed is the requirement for highly accurate geometric representations of the user environment. The effect of poorly defined surfaces and inaccurate geometrical representations is shown to highly influence the predicted received power levels. An International Telecommunications Union (ITU) propagation model utilizing a combination of geometrical (deterministic) and empirical elements is used by Gouldsworthy [Gouldsworthy et al., 2002] in the development of a model of EM propagation originating from GPS jamming equipment. A great deal of research on EM simulation originates from defence related applications. This work seeks to simulate the performance of GPS receivers operating under conditions where signal jamming is experienced.

As well as numerical analysis, attempts have been made at statistical modelling of signal propagation in specific environments. Ma [Ma et al., 2001] presents an urban three state model, in which signals are divided into three categories, clear LOS, shadowed, and blocked signals. With reference to these three classifications, the fading distribution of GPS signals is determined and the result is a description of the signal composition. The fading distribution for clear LOS signals is expressed by a Ricean power distribution function (PDF). The assumption is made that obscured satellites only result in multipath signals, and the fading distribution for this case is that of a Rayleigh PDF. In tests use of a well located reference and a mobile receiver permitted the extraction of most errors through differencing. Comparison of signal to noise ratio (SNR) of the two receivers yielded differences that were assumed to be due to signal fading including masking. Although this approach differs from that of simulation based upon knowledge of the local environment, conclusions were drawn that impact upon the modelling of GNSS signal propagation from any technique. Most significantly, the study found that roadside trees cause signal fading, but on the whole, satellites could still be tracked. Lachapelle [Lachapelle et al., 1994] addressed the masking effects of tree foliage on GPS signal availability and accuracy for vehicular navigation. This research concluded that GPS signals are still available on the whole, but availability is reduced. Multipath was found have an increased effect in the presence of tree foliage, as the LOS signal can be attenuated. The use of a receiver with a Narrow correlator was found to alleviate the resulting position inaccuracies. Steingass et al. [Steingass et al.,

2003 and 2004], undertook a study for measurement of the multipath channel particularly for pedestrian navigation applications. This was performed using a simulated satellite, and evaluation of signal reflection was undertaken in urban, suburban and rural environments. Again, received signal power was analysed to allow a statistical analysis of the multipath channel. The work proves the dependency of this channel on satellite elevation angle. Ultimately it is hoped that this approach will be used to produce an *a priori* probability function for use by a receiver.

Ray-tracing techniques have been employed in the prediction of reflected and diffracted signals. Ercek [Ercek et al., 2006] describes a ray tracing approach combined with the uniform theory of diffraction (UTD). In this work, only simple models of urban canyons are used, rendering the approach unsuitable for availability analysis and incapable of detecting the high frequency multipath occurring from distant reflectors. However, received signal power could be estimated, essentially due to the numerical modelling of EM propagation. Also, the contribution from multiple signal reflections, were modelled in this work. It was assumed that only the nearest diffraction point to the receiver produced a detectable diffraction field. Pseudorange (PR) error distributions were produced by two methods, firstly by considering expected signal attenuation, and secondly by estimating the true PR error using a receiver model with an early late correlator strategy. Of most significance, this work concluded that the single reflected ray and the single diffracted ray provide the main contribution in the PR error distribution, where single reflected and single diffracted rays denote that only one interaction of the a signal with an object has occurred. Liang [Liang et al., 1998] highlights poor performance of statistical models for the prediction of signal propagation in areas with mixed building sizes. The use of ray tracing methods for prediction of the dominant propagation paths is considered by this work as a better approach in difficult environments. During this work, a vertical plane launch (VPL) method is described. As the name suggests, VPL involves consideration of the propagation of a signal in vertical planes originating from a source. This approximation is less intensive than the traditional 3D ray tracing approaches, and can model multiple diffraction and reflection events. Interactions that undergo multiple forward diffraction at horizontal edges, or double diffraction events at vertical edges are accounted for. Reflections from vertical building walls are also considered. Combined with UTD for the prediction of received signal power, favourable comparison of simulated and observed results were achieved. However, the approach uses models comprised of

vertical and horizontal surfaces only. It therefore neglects interactions resulting from non horizontal or vertical surfaces. This solution offers a method by which rigorous numerical analysis of electromagnetic signal propagation can be undertaken over areas described by large geometric models. This is of value as a real barrier to adopting rigorous numerical electromagnetic analysis over large model areas, is the computational overhead. No indication of resource useage with this technique could be found. Also, it is unsuitable for modelling signal propagation originating from above objects present within the geometrical model, as with GNSS.

4 METHODOLOGY

4.1 Introduction

This chapter presents a software simulator written specifically for this research. Firstly, the objectives of the simulator are stated. The motivation behind the chosen form of the simulator is examined, and a high level description is given. Individual sections of the simulator are then described in detail by partitioning the high level description into logical elements, and then decomposing the high level description of each element.

4.2 Simulator Objectives

Research presented in this thesis concerns the use of computerised models of built environments surrounding a GNSS receiver. The overall objective of the simulator is to take such a model, and predict the signals that will be available, based upon location and time. The arrival of signals originating from disrupted (non-LOS) signal paths is also to be considered, and the level of signal disruption due to these signals is sought. A simplified illustration of the simulator, represented as a system, is provided in Figure 4-1. The objectives of the simulator are now stated:

- To take as input a computerised model of a dense urban environment, in a standardised format, and harvest the relevant geometric data efficiently.
- To store and maintain model data in novel data structures, defined during this research. This data is to be retained and manipulated, in both Random Access Memory (RAM) and external files, so as to maximize efficiency in terms of time and memory useage.
- To consider the reception of GNSS signals via LOS, diffracted and reflected propagation modes. Assess the disruption caused by non-LOS signals.
- To describe the LOS and non-LOS signals present at an antenna so as to characterise the signal environment in which the receiver is operating.

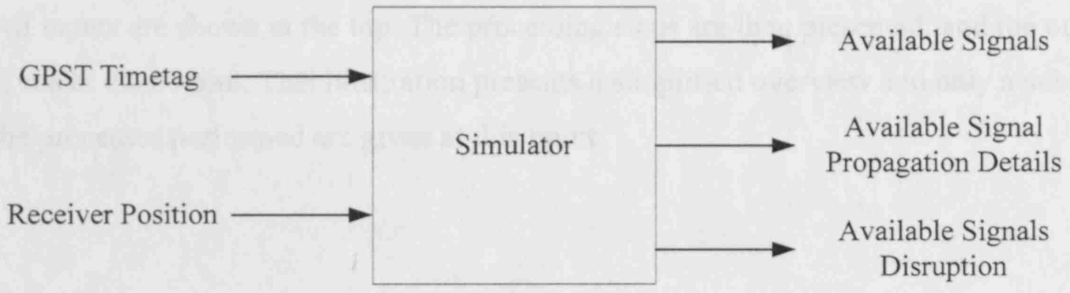

Figure 4-1: Simple system illustration of simulator

It is important to note, that this research is applicable to GNSS as whole and not specifically one satellite system. However, in order to fulfill the objectives listed above, and for the assessment of the performance of the simulator using collected observation data, the work presented in this thesis focuses on GPS signals only. It is an additional objective of this simulator that only small software modifications need be made in order that it can be applied to other GNSS. It is appropriate that this is further discussed following a full description of the simulator, and this is presented in section 4.10.

4.3 Simulator Description

4.3.1 Simulator Form

To establish answers to the questions posed at the start of this research, it has been necessary to develop a software toolkit. The software toolkit is comprised of individual elements that collectively comprise a simulator. All code used in the simulator has been designed, written, and developed from the ground up. No external code from any external source is included in this work. By developing all simulator code, and not adopting code from external sources, understanding and experience in all underlying algorithms and data sources has been gained. It is also the case that (at the time of writing) no software exists to perform the exact set of functions required for this work. In addition, this approach allows for the test of all components of the simulator even at the most detailed of levels, something that could not be achieved if external code was integrated into the simulator. For flexibility, and an anticipated requirement for future interoperability with other software, it was decided at the outset, that all code would be written in C++. Visual Studio V6 and 2005 [Microsoft, 1998, 2005] tools have been used for the development of all software.

4.3.2 Simulator Architecture

Figure 4-2 expands upon the high level system representation provided in Figure 4-1. All inputs are shown at the top. The processing steps are then presented, and the outputs given at the bottom. This illustration presents a simplified overview and only a subset of the processes performed are given at this point.

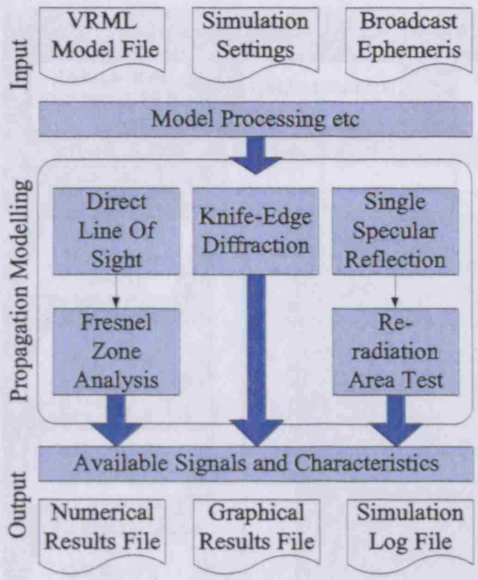

For all simulator illustrations throughout this thesis, the following conventions are adopted:

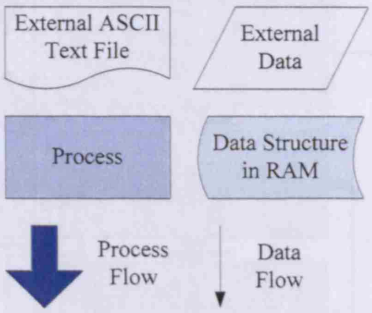

Figure 4-2: High level overview of simulator

In order that multiple simulations can be performed quickly, input and model processing, where relevant geometry is extracted from the initial VRML file, occurs only once. Correspondingly, reading and processing of simulation settings and of parameters for satellite position determination (originating from broadcast ephemeris and SP3 files) are also performed only once. The settings file controls all aspects of simulation, an annotated example is provided in APPENDIX E, and in common with the other input files, is only read and processed once. The simulator outputs consist of a numerical output, detailing the resulting analysis in a proprietary text format and a graphical output, where the results can be examined visually using any VRML viewing software. Full description of the simulator outputs is given in sections 4.3.8 and 4.3.9.

A more detailed and fully complete representation of the simulator is provided in Figure 4-3. Elements shown in this illustration will be described in detail within the following sections. With reference to Figure 4-3, all inputs and outputs that are external to the simulator are shown with a grey background, and the simulator itself is presented within a boundary represented by a solid black line. Data flowing over the software boundary as an input, originates from ASCII text files. Similarly, all output information (with the exception of some runtime information) is sent across the software boundary and written to the appropriate ASCII text file. With the exception of the Geometry-Only file (described later), each file is effected by a dedicated input or output stream only.

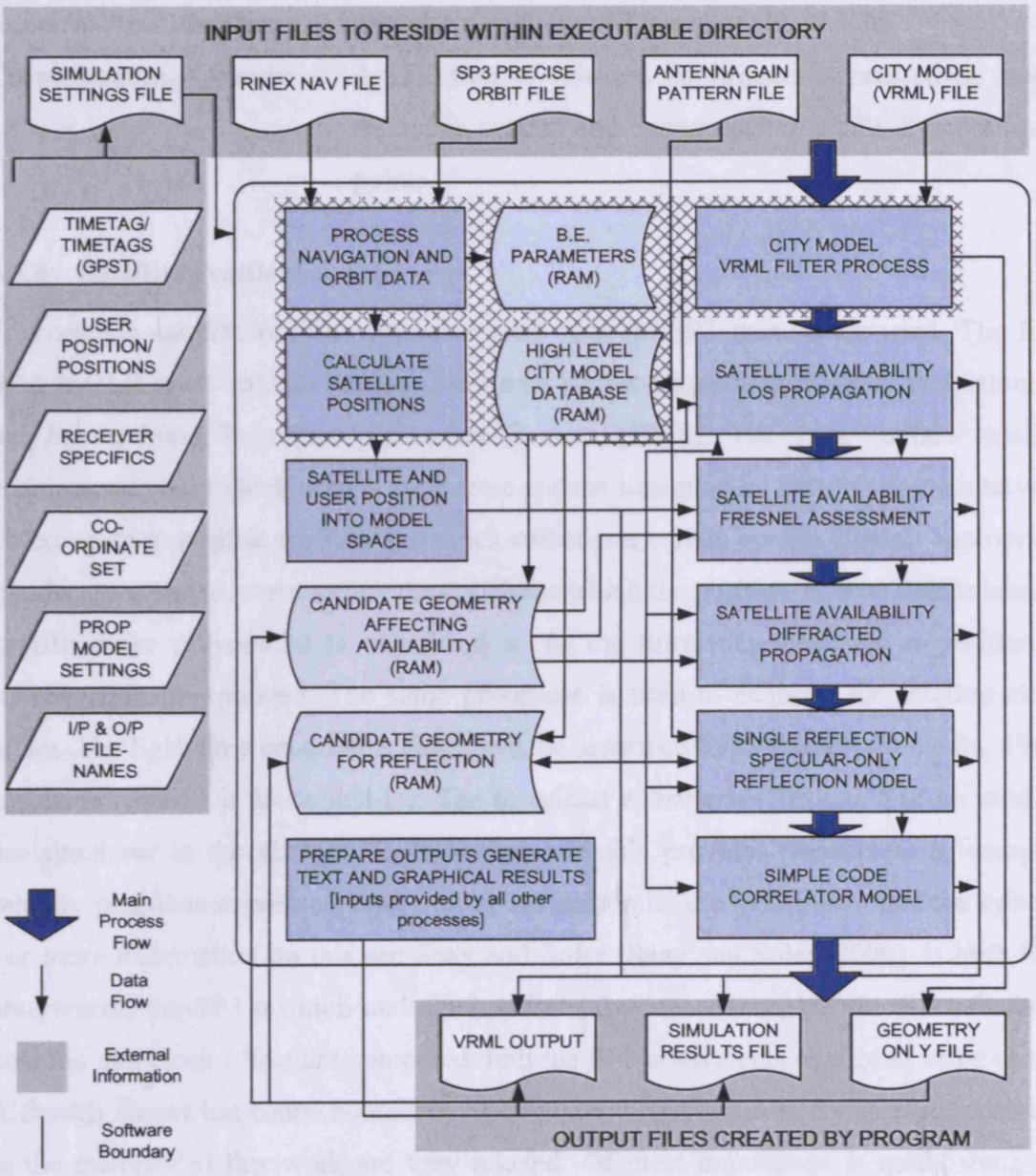

Figure 4-3: Low level overview of the simulator

4.3.3 Simulation Settings

The simulation settings file is used to configure the simulator for a simulation run. Explanation of each setting is given in APPENDIX E along with an annotated example settings file. All settings are categorised and fall under the following headings:

Files: Points the simulator to all input and output files.

Simulation Settings: Initial timetag, initial position, number of simulations, spatial resolution, temporal resolution, etc.

Propagation Models: LOS, Fresnel model, diffraction and all associated settings.

Receiver Specification: Correlator spacing and correlator bandwidth.

Corresponding Coords: A selection of position coordinates expressed in model reference system and corresponding ETRS-89 coordinate points.

4.3.4 Satellite Positions

To compute satellite positions, precise orbit files (in SP3 format) are used. The files used for this work contain satellite orbit data expressed in the ITRF2005 realisation of the International Terrestrial Reference System (ITRS). The files contain satellite positions and their clock offsets at discrete epochs separated by fifteen minute intervals. To compute a satellite position and clock offset at a certain epoch, thirteen appropriate epochs are selected, surrounding the epoch for which the position is to be determined. A twelfth order polynomial is calculated to fit the thirteen points, and a position is subsequently interpolated. The same procedure is used to estimate the satellite clock offset. The light-time equation is employed, as described in [ICD-GPS-200, p.84, 1995] and earth rotation is accounted for. The broadcast ephemeris (BE) can also be used by the simulator in the absence of SP3 files, and this provides parameters to compute satellite positions expressed in the latest realisation of the WGS-84 reference system. For more information on this see Snay and Soler [Snay and Soler, 2000]. If both files are present, the SP3 position and clock offset take precedence, but the BE calculated position and clock offset are compared with the SP3 equivalents as a gross error check. Although somewhat counter-intuitive, the accuracy requirements for satellite positions in the majority of this work are very relaxed. Of most importance is establishing the correct elevation and azimuth (with respect to receiver position) of satellites at defined epochs. For this application, considering the maximum rates of change for elevation and azimuth values, an accuracy of +/- 0.01° is acceptable for both. This is because (with the exception of some analysis described in section 7.8) ranging information is not used within this work.

4.3.5 Reference Frames

Although the environment models are generally available with position data provided in an appropriate Terrestrial Reference Frame (TRF), such as OSGB36 for Great Britain (OSGB36 consists of both a datum and a TRF see [Ordnance Survey, 2007, p.23]), a variety of practical issues make it desirable to transform the model data into a new reference frame, hereon in referred to as the environment model reference frame. The

necessity to create and use a new reference frame is due to practical issues including the display of graphical simulation outputs and also the treatment of numerically large values. By way of example, many CAD packages will export data to different formats in a scientific notation. If measurements consist of large values (consisting of more than 5 digits with three decimal places), then it is possible that scientific notation will be used. If too few decimal places are available (when expressed using scientific notation), then the retention of the initial geometric fidelity can not be relied upon. Other issues are related specifically to the design of algorithms described later in this chapter. The environment model reference frame has no formal definition. For the purposes of this work, coordinate data within an environment model file expressed in an appropriate realisation of a terrestrial reference system, is manually transformed into a newly created reference frame using a CAD tool. As all coordinates are transformed in one procedure, and the transformation is done by the CAD tool, the main error sources in such a procedure are machine induced rounding and numerical instability. These errors occur due to the storage of coordinate values and transformation parameters (within computer memory) to a fixed number of decimal places. Such errors are too small to be significant in this procedure. It would very quickly become apparent, by viewing the model within the environment model reference frame (using a VRML viewer), if any significant transformation induced error was evident. VRML viewers are sensitive to inconsistencies in coordinate values and therefore adjacent structures would become slightly mismatched at their coincident vertices. This would lead to a degraded overall appearance of the model. This was the subject of some crude intial tests whilst initially trialling methods of processing model data. The only constraints upon the newly created reference frame are as follows:

1. It is desirable that the model dataset is located somewhere close to the origin of the system. This is so that the maximum Cartesian component magnitudes, within the coordinates in the model dataset, do not exceed, say 10km.

2. It is beneficial to ensure that the model is orientated such that an upward pointing vector from the initial dataset (normal to a tangential plane located on the ellipsoid model at sea level) is roughly aligned in the environment model space such that it is parallel to the z-component of the system axes. This is because the two-stage availability algorithm (described in section 4.5) is computationally most efficient when this is the case.

Following manual transformation (using CAD software) of all coordinates within the original environment model (according to the considerations given in 1 and 2 above), we can now say that the model exists within the environment model space, as shown in step one of Figure 4-4. It is now necessary to compute transformation parameters in order that satellite positions, initially expressed in the ITRF2005 realisation of the ITRS, can be transformed into the corresponding coordinates within the environment model space. Steps two and three of Figure 4-4 demonstrate how this is achieved. A subset of coordinates existing within the original terrestrial reference frame, are selected. For reduction of any errors due to modelling errors and localised biases, these points should be chosen from locations within the model that are evenly spread across the entire dataset area. For the same reasons, they should also belong to different structures. In addition, they should be easily identifiable, by their position within a dataset coordinate list, or by the physical object to which they belong. A minimum of three coordinates is required, in order to solve for the seven transformation parameters. The chosen coordinates are transformed into coordinates in the ETRF89 reference frame as shown in step 2. As the model datasets used within this research describe environments within the UK, the ETRS89 is used [Ordnance Survey, 2007].

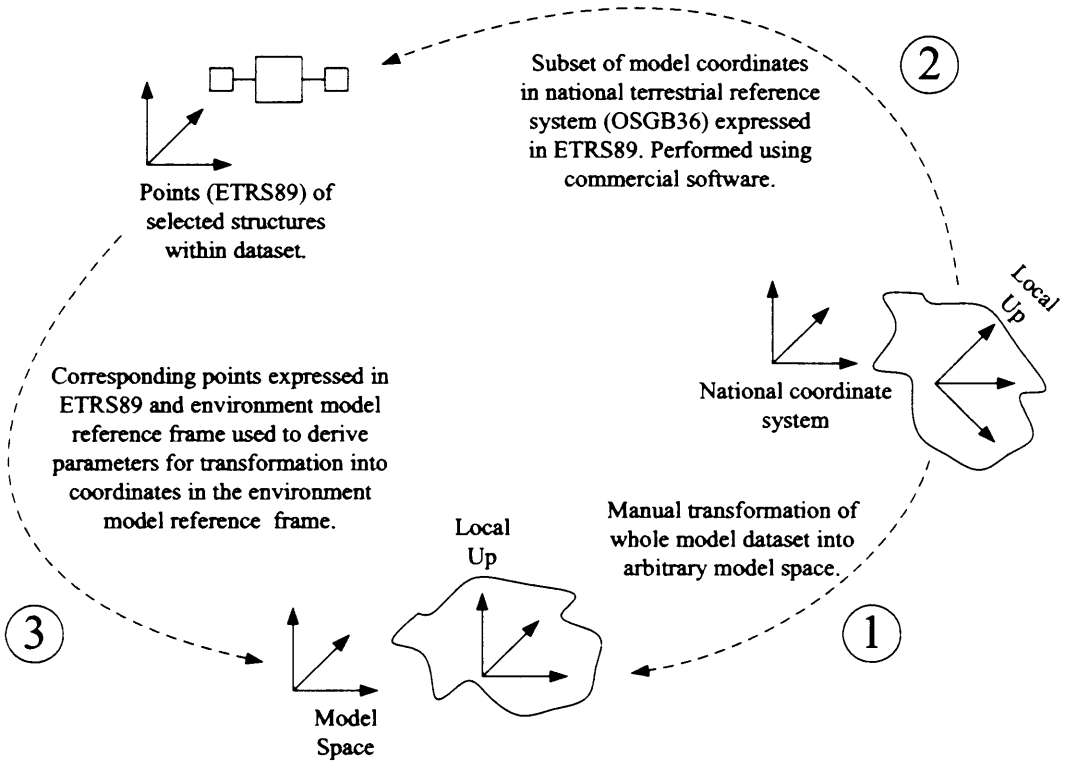

Figure 4-4: Procedure for determination of transformation parameters

The task of establishing corresponding coordinates in the ETRF89 realisation of ETRS89, from the original terrestrial reference frame (such as OSGB36), shown in step 2, is performed externally from the simulator by using commercial software such as Grid InQuest [Ordnance Survey, 2004]. In the absence of such commercial software, some survey work would be necessary in order to establish points that occur on the model in corresponding ETRF89 coordinates. Step three employs a 3D conformal transformation, the parameters for which are derived using a least squares estimation, such as that presented by Wolf [Wolf, 1983]. The least squares estimation permits the inclusion of any number of corresponding points to form the solution. Residuals for each Cartesian component are produced and checked during the process. In order that the software can take any model dataset as input, the transformation parameters are computed within the simulator. It is only necessary to provide the simulator with one set (minimum of three) of corresponding coordinates (coordinates in ETRF89 and corresponding coordinates in the environment model reference frame). This is done by storing the corresponding coordinates in the settings file. From the receiver simulation position, expressed in ITRS coordinates, vector components of the unit local East, North and Up (ENU) directions in the ECEF basis, are produced. This is performed assuming use of the GRS80 ellipsoid. For each simulation, the derived transformation parameters can be applied; the satellite positions (computed for appropriate timetag), ENU vectors, and the simulated receiver position, are all transformed from ITRS coordinates into the equivalent coordinates expressed in the environment model reference space. It is important that correct treatment of the ENU vectors is applied, as these will be used to determine elevation and azimuth angles for satellite positions, reflection points, diffraction points and signals incident upon the antenna.

4.3.6 Antenna Gain Pattern

The antenna response to incoming signals and their copies, predicted by the simulator, can be appropriately scaled by the application of an antenna gain pattern. This takes account of the fact that a receiving antenna exhibits a signal gain that is dependent upon the azimuth and elevation of the incoming signal. Different antenna models have different gain patterns, and a different pattern is generally experienced for different signal polarisations. For example antennae that suppress LHCP signals will exhibit lower gain values over the entire surface of an antenna for LHCP than RHCP. Figure 4-5 illustrates the reduction of LHCP, however, it can be seen that the LHCP signal is not completely suppressed. The relative response to the signal copy to the LOS signal

will be a function of the incoming elevation and azimuth of both signals. An example pattern and multipath situation is provided in Figure 4-5. The dimensionless gain values for the LOS signal ($g_{L)}$ and for the reflected signal (g_R) are extracted from a pattern originating from manufacturer experiments [provided by Leica], involving assessment of antenna response in an anechoic chamber. The attenuation of the reflected signal with respect to the LOS signal is given by the following ratio (η_a):

$$\eta_a = \frac{g_L}{g_R} \qquad \text{(eqn. 4-1)}$$

Gain pattern models initially exist in the form of plots provided by an antenna manufacturer, such as that shown in Figure 4-5 [Leica] and that given in [Spilker, 1996, vol 1, p.722].

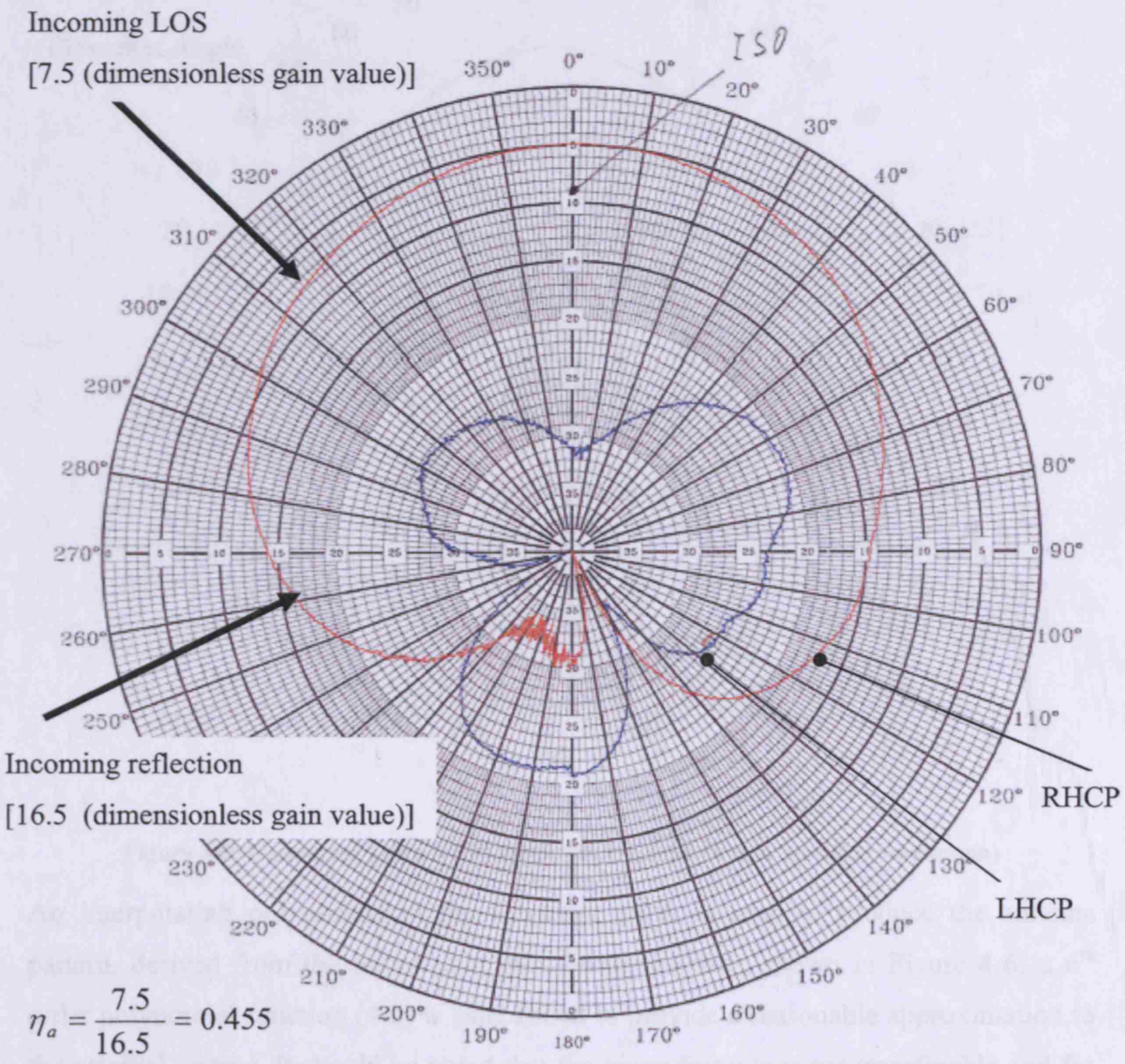

Figure 4-5: Antenna gain pattern (vertical cross-section) Leica AT502 (RHCP and LHCP)

A plot requires translation into a machine readable file. The following is an appropriate method, developed for this research:

1. Initial plot is manually sampled at discrete elevation intervals (e.g. 5°).
2. Polynomial coefficients are determined for a function to fit the sampled data.
3. Gain values at a required resolution (e.g 0.25°) are computed.
4. An XML file is produced to hold the antenna data.

An example antenna gain file, in an XML schema, is provided in APPENDIX F. The result of this process, applied to the antenna plot in Figure 4-5 for RHCP only, is given in Figure 4-6 below.

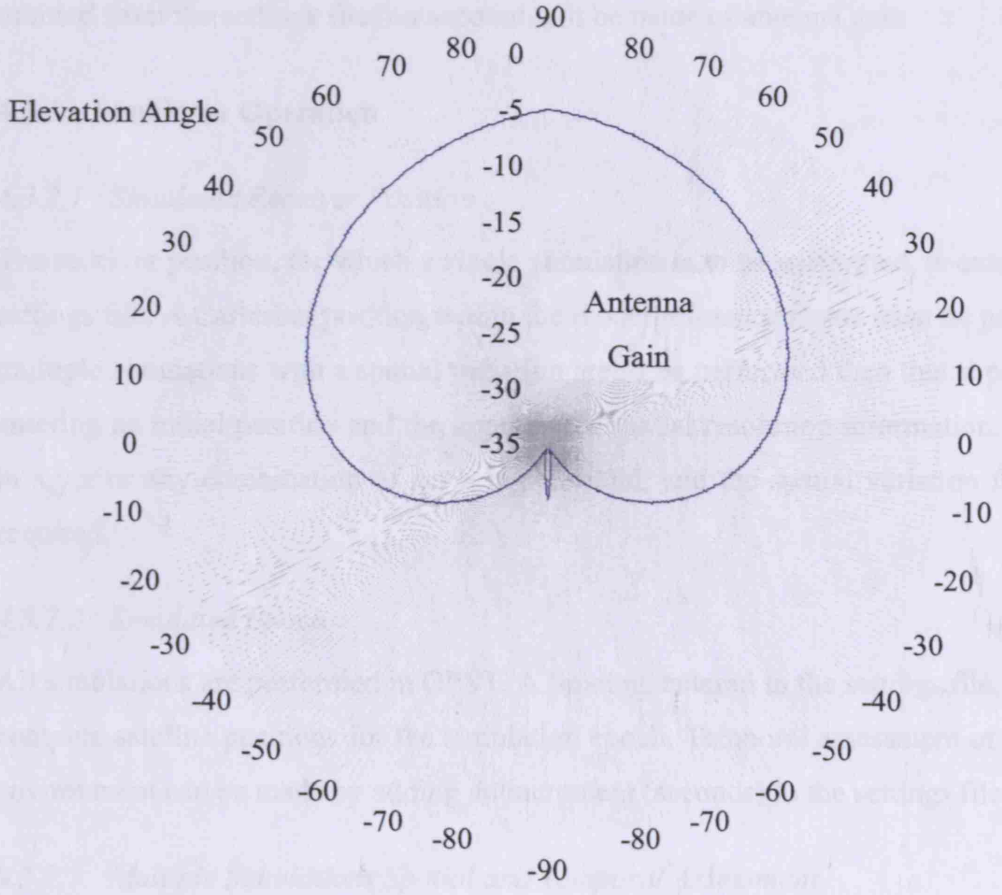

Figure 4-6: Generated Leica AT502 gain pattern (shown as a vertial cross-section)

An interpolating polynomial in the Lagrange form is used to produce the antenna pattern, derived from the initial gain plot. In the instance shown in Figure 4-6, a 6^{th} order polynomial function (4-2) is established to provide a reasonable approximation to the original pattern. It should be noted that the given formula is not transferable and for

other antenna gain patterns another interpolating polynomial will need to be created in the fashion described by this section.

$$y = 0.00005968x^6 - 0.00413x^5 + 0.10101x^4 - 1.149x^3 + 6.126x^2 - 9.65x - 30$$

(eqn. 4-2)

Where:

y	=	gain value (dimensionless).
x	=	elevation angle (degrees).

Application of an antenna gain pattern is optional, and only affects the estimate of signal degradation in the presence of multipath. If the antenna gain pattern filename is omitted from the settings file, no account will be made of antenna gain.

4.3.7 Simulator Operation

4.3.7.1 Simulated Receiver Position

The receiver position, for which a single simulation is to be performed, is entered in the settings file. A Cartesian position within the model reference frame must be provided. If multiple simulations with a spatial variation are to be performed then this is possible by entering an initial position and the appropriate spatial resolution information. Variation in x,y,z or any combination of x,y,z is permitted, and the spatial variation for each is required.

4.3.7.2 Simulated Epoch

All simulations are performed in GPST. A timetag, entered in the settings file, is used to compute satellite positions for the simulation epoch. Temporal assessment of the signal environment can be made by adding an increment (seconds) to the settings file.

4.3.7.3 Multiple Simulations Spatial and Temporal Assessment

As indicated in sections 4.3.7.1 and 4.3.7.2, multiple simulations based upon spatial and temporal variation can be performed. If both spatial and temporal variation is required, then the simulator will perform simulations for all epochs in a certain position, average the results, and then move to the next position until the simulation run is completed.

4.3.8 Simulation Results

An ASCII file of numerical results is produced following simulation. The format of this output file is different for a single simulation to a multiple simulation run. Examples of the output files, together with parameter definitions are provided in APPENDIX G.

4.3.9 VRML Output

For verification of correct simulator operation and as a tool to aid the understanding of results, a VRML output file is produced following simulation. Any VRML viewer can be used to visualise the results. The graphical representation of the scenario shows all predicted signal propagation paths and contains the original model data. It is possible to fly around the scene and view elements of interest in detail. Standalone VRML viewing software, such as *Cosmo VRML Viewer* [Platinum Technology, 1997] or plugin tools for internet explorer such as *Cortona Client* [Parallel Graphics, 2007], can be used for this purpose. If a single simulation is performed, the results are a static representation. If a single position multiple epoch simulation has been performed then an animation of signal propagation over time is produced. Multiple position simulations also produce an animated output, with the receiver changing position over time. Simulations with temporal and spatial variation are also possible. Screenshots from this output are used in later sections of this thesis.

4.4 City Model Processing

4.4.1 City Model Input

Environment data encapsulated within a VRML file forms the input for environment model data in this research. Equally, any file format that fulfils the following main requirements can be used, although a modified environment model reader must be developed to allow deviation from VRML. The format must be:

- Vector-based.
- Express floating point numbers to a minimum of 3 decimal places.
- Allow representation of objects comprised of planar facets (e.g. triangles) rather than geometric primitives only.

The VRML standard is described in section 3.3.2. Original city model datasets often exist in a format other than VRML. The initial format can be specific to a particular

CAD software package. Tools such as Rhinoceros [Robert McNeel and Associates, 2001] can export datasets held within many different file types, into a VRML file format, with no disruption to the initial data quality.

A brief description of VRML is given in section 3.3.2. A detailed account of the VRML format is given by the VRML 2.0 specification [Bell et al., 1995], and also by Ames [Ames et al., 1997].

4.4.2 City Model Processing

Prior to the use of any data held within a city model dataset, the entire file is processed by the VRML reader element of the simulator, see Figure 4-3. A sample object expressed in VRML is provided in APPENDIX H. Typically, an entire model dataset is comprised of many thousands of objects. In reading the model file, the model reader processes objects individually and in turn. The reader element is described by way of a flowchart presented in Figure 4-7. Individual processes are subsequently described.

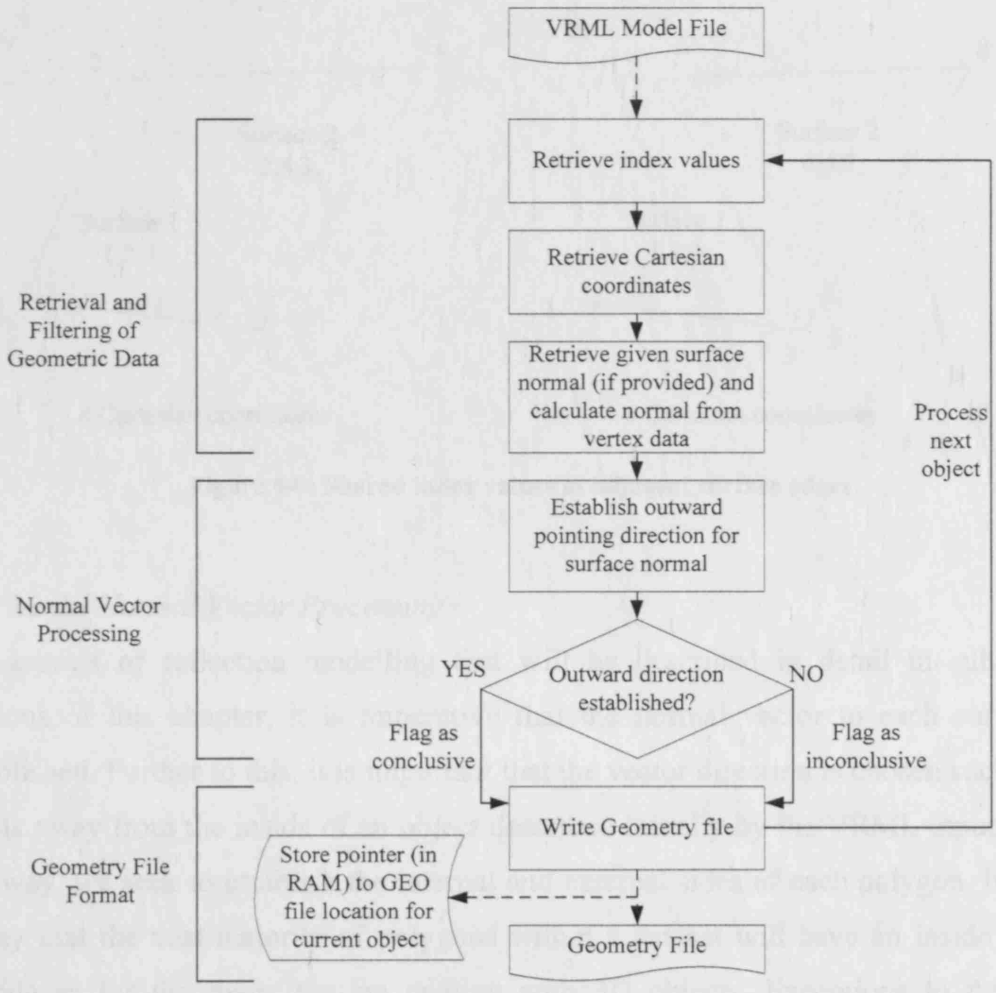

Figure 4-7: Flowchart for model processing element of simulator

Retrieval and Filtering of Geometric Data

The coordinate index list, coordinate values and surface normal vectors (if provided) are extracted from the VRML file, and stored in individual vector arrays in RAM. These arrays are destroyed upon moving to the next object. Extraneous data that may reside within a VRML file is filtered, as the reader searches only for index integers, 3D Cartesian coordinates, and VRML normal vectors. With reference to the VRML format, an example of which is provided in APPENDIX H, it is shown that an object is comprised of a list of index values, coordinate values (referenced to the index list) and surface normal vectors. Typically, each object contains more than one planar facet. A description of a collection of facets that share two or more coordinate points, and therefore have adjacent edges, may be given in two ways. With reference to Figure 4-8, index values may be shared by the two surfaces or coordinate points maybe duplicated and an additional index entry supplied. The former is a more logical approach, and results in smaller file sizes. Any VRML processing software must be designed to cope with either approach, or a mixture of the two.

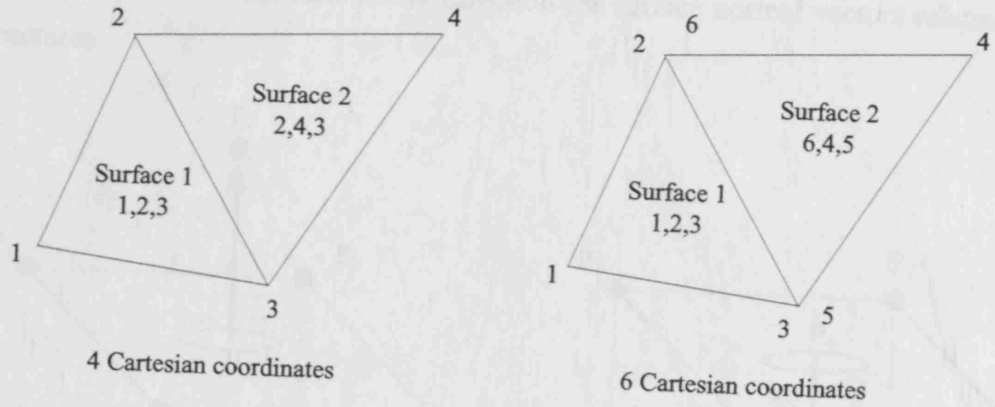

Figure 4-8: Shared index values at adjacent surface edges

City Model Normal Vector Processing

For aspects of reflection modelling that will be described in detail in subsequent sections of this chapter, it is imperative that the normal vector to each surface be established. Further to this, it is important that the vector direction is chosen such it that points away from the inside of an object described initially by the VRML input file. In this way, we seek to establish the internal and external sides of each polygon. It is true to say that the vast majority of polygons within a dataset will have an inside and an outside as for the main, we are dealing with 3D objects. Exceptions to this, with reference to models of urban environments are some free-standing walls.

Conventionally, the polygon winding (order in which the polygon list is expressed) dictates the direction of a surface normal. The surface normal is computed by forming the cross-product of vectors formed by two planar polygon sides. This convention is obeyed within VRML. However, it is not necessarily the case that the given vector direction points away from the inside of a structure. Interpreters designed for use with VRML files still produce consistent lighting effects despite this peculiarity. A strategy has been developed in this study, involving some novel algorithms, that seeks to produce a result as to whether the outward direction (where outward is with respect to the object to which the surface belongs) for a surface vector can be established.

Although not always the case, objects in VRML (referred to as shapes in VRML) tend to define individual structures or sections of structures. This is certainly the case with VRML generated using the Rhinoceros [Robert McNeel and Asscoiates, 2001] software. It is rare that a single object will contain a section of one structure and a section of another. This property allows the consideration of objects as 3D enclosed volumes, expressed in triangular meshes. A technique is now described for the identification of the outward facing direction for surface normal vectors relating to 3D structures.

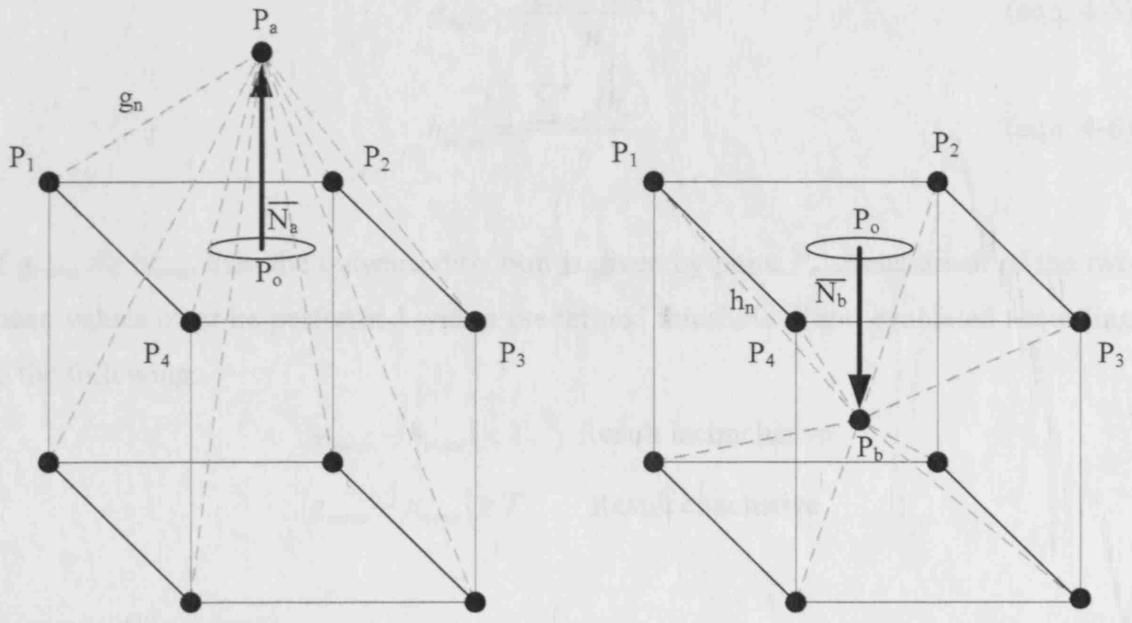

Figure 4-9: Identification of outward facing direction for surface normal vectors

With reference to Figure 4-9, the outward facing direction is sought, for the normal to the surface described by the top four coordinates of the given cube. An expression for the normal is found by the following:

$$\begin{aligned}\overline{V_1} &= \overline{P_2} - \overline{P_1} \\ \overline{V_2} &= \overline{P_2} - \overline{P_3} \\ \overline{N_n} &= \overline{V_1} \times \overline{V_2}\end{aligned} \qquad \text{(eqn. 4-3)}$$

Where P_1 and P_2 are, for the purpose of this example, coordinates that describe the top surface of the given cube. It should be remembered that a single object may contain thousands of individual coordinates. The case for consideration of the outward direction in both directions is given in Figure 4-9, denoted direction *a* and *b*. Point P_0 is first established. This is done by computing the centre of gravity of the surface under consideration. This point needs to reside within the polygon under consideration, although its precise location is not required. Points P_a and P_b can then be determined by selecting a suitable distance *d* from the surface. One metre is chosen when dealing with objects such as buildings.

$$\overline{P_a} = \overline{P_o} + \overline{dN_n} \qquad \overline{P_b} = \overline{P_o} - \overline{dN_n} \qquad \text{(eqn. 4-4)}$$

The 3D distance from P_a to every coordinate in the object is calculated. Likewise for P_b all 3D distances are determined. The mean average 3D distance for P_a and for P_b is then determined:

$$g_{mean} = \frac{\sum_{n=0}^{n}(g_n)}{n} \qquad \text{(eqn. 4-5)}$$

$$h_{mean} = \frac{\sum_{n=0}^{n}(h_n)}{n} \qquad \text{(eqn. 4-6)}$$

If $g_{mean} >> h_{mean}$ then the outward direction is given by point P_a. Assessment of the two mean values must be performed with a predefined threshold *T* and evaluated according to the following:

$|g_{mean} - h_{mean}| < T$ Result inconclusive

$|g_{mean} - h_{mean}| \geq T$ Result conclusive

Geometry File Format

A proprietary file format has been developed specifically for the tools created during this research. An ASCII text file with the extension '.GEO' is produced during operation of the reader element. The reader element of the simulator processes each object in the initial VRML file in turn. The final stage of processing is to output retrieved data into a text file that can be used by subsequent processes within the

simulator. Conversion of the initial city model file to a separate format, is carried out for the following reasons.

- The use of VRML can remain detached from the workings of the simulator. The degree of separation afforded by such a strategy allows any input format to be adopted with a minimum of disruption to the simulator.
- Some data processing may take place at the moment the data is retrieved. An example of this is the rejection of VRML given normal vectors in favour of computed alternatives.
- Object data processed by the reader can be written to the geometry file and a pointer to the file location of the relevant object held in memory. Thereby facilitating rapid searches of the geometry file during subsequent simulator operations. Memory useage is also kept to a minimum as no geometry data is stored in lists.

APPENDIX I provides a sample object expressed in a '.GEO' format. A description of the format is now given.

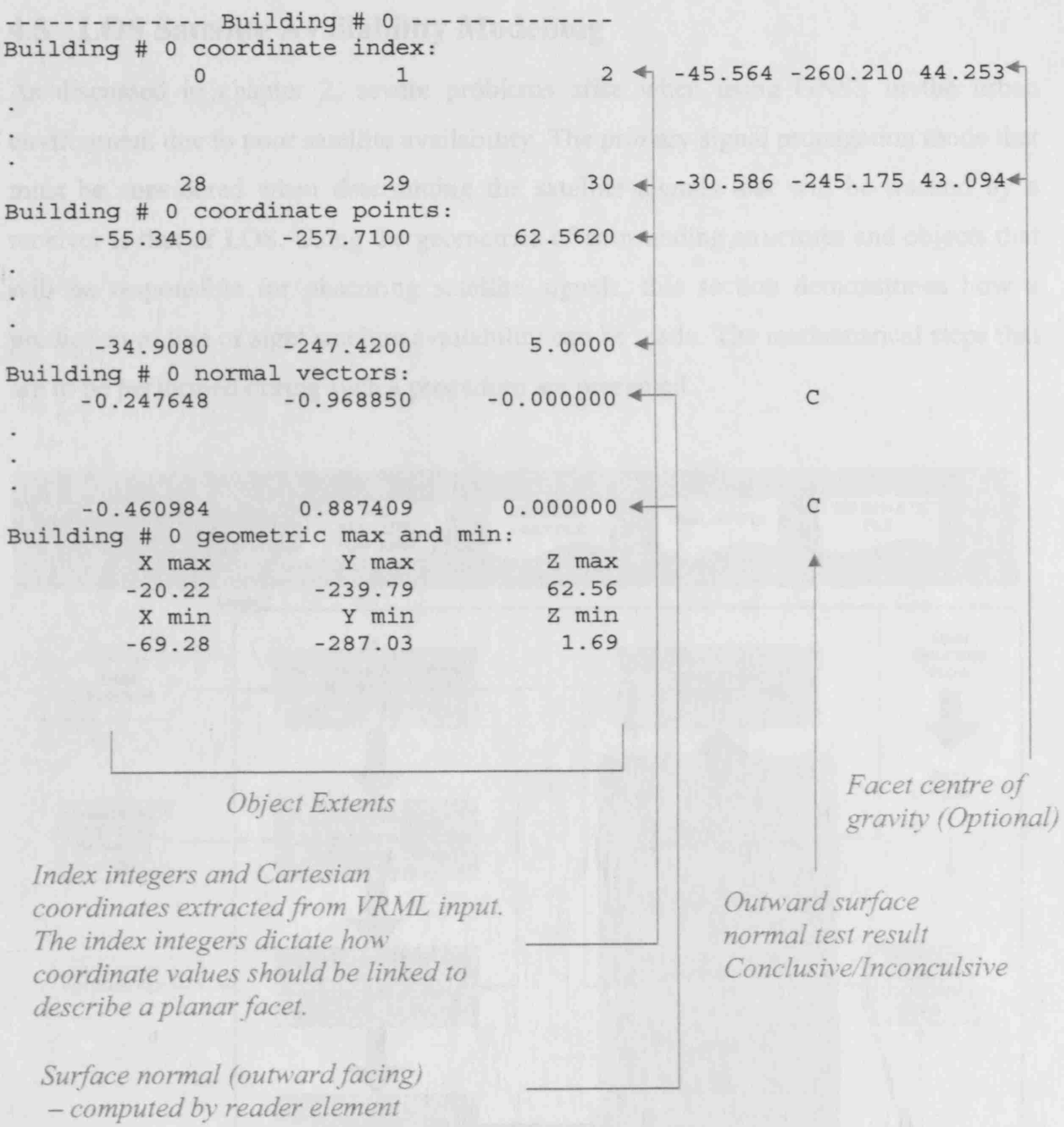
---------- Building # 0 ----------
Building # 0 coordinate index:
0 1 2 -45.564 -260.210 44.253
28 29 30 -30.586 -245.175 43.094
Building # 0 coordinate points:
-55.3450 -257.7100 62.5620
-34.9080 -247.4200 5.0000
Building # 0 normal vectors:
-0.247648 -0.968850 -0.000000 C
-0.460984 0.887409 0.000000 C
Building # 0 geometric max and min:
X max Y max Z max
-20.22 -239.79 62.56
X min Y min Z min
-69.28 -287.03 1.69
Object Extents
Facet centre of gravity (Optional)
Index integers and Cartesian coordinates extracted from VRML input. The index integers dictate how coordinate values should be linked to describe a planar facet.
Outward surface normal test result Conclusive/Inconclusive
Surface normal (outward facing) – computed by reader element

4.5 LOS Satellite Availability Modelling

As discussed in chapter 2, severe problems arise when using GNSS in the urban environment due to poor satellite availability. The primary signal propagation mode that must be considered when determining the satellite signals that will be tracked by a receiver is that of LOS. Using the geometries of surrounding structures and objects that will be responsible for obscuring satellite signals, this section demonstrates how a prediction of line of sight satellite availability can be made. The mathematical steps that are to be performed during such a procedure are presented.

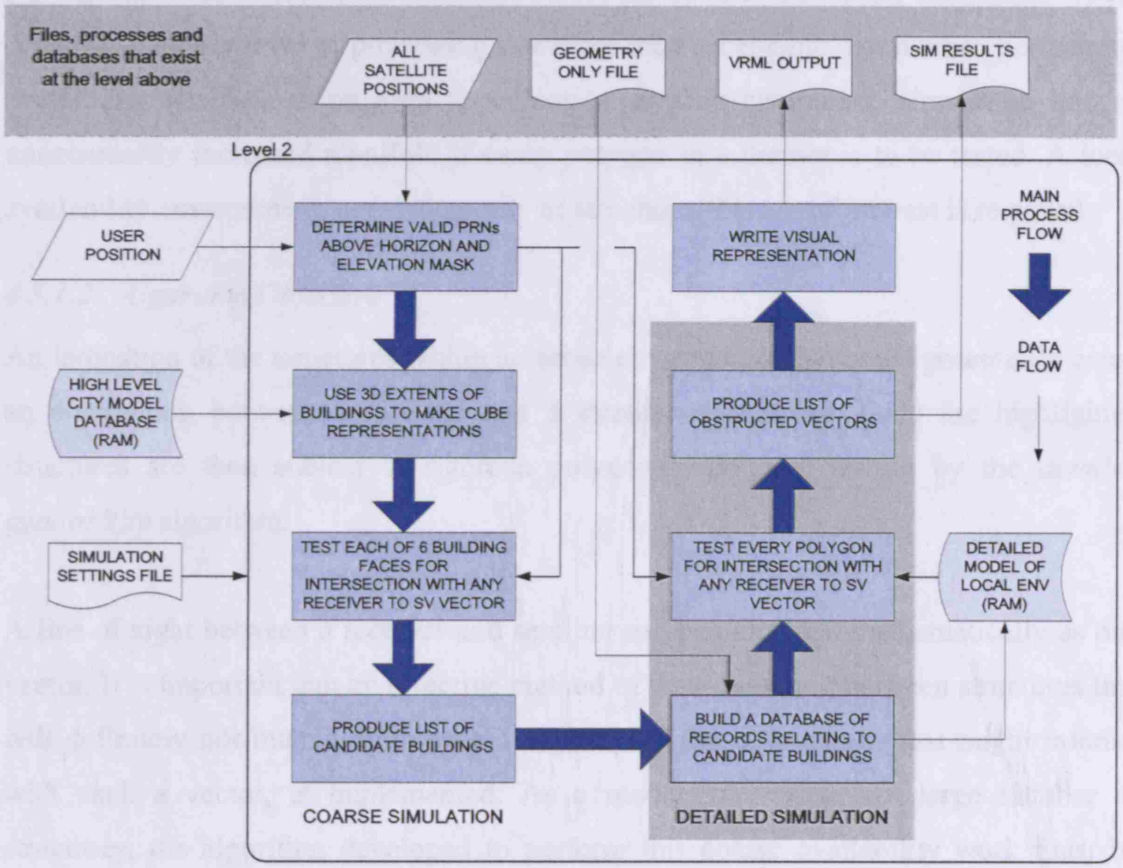

Figure 4-10: LOS propagation element of simulator

Two algorithms are combined to provide an overall LOS availability result. The first is designed to rapidly assess all structures in the urban environment, and produce a list of structures requiring further, more intensive assessment. Use of this first algorithm is termed *coarse simulation*. Further assessment is undertaken by a *detailed simulation*, which yields the actual LOS availability result. Figure 4-10 presents a decomposition of the LOS propagation element shown in Figure 4-3. The Coarse and Detailed availability algorithms are now described.

4.5.1 Coarse Availability Algorithm

4.5.1.1 Problem Definition

A detailed environment model will contain many hundreds of thousands or even millions of individual polygons. The number of polygons is a function of the area captured, the detail captured, and the resolution with which the data is presented. When a subset of a model is considered, as would be acquired by a mobile device over a wireless communications network, the subset will still contain a vast number of polygons. To perform rigorous availability testing on every polygon for even a small local urban area, with a low structure density, captured at a medium resolution, would consume a higher level of processing resources than acceptable. Even when performing availability simulations on high specification desktop computers, simulation time is unnecessarily increased manifold if every polygon in a dataset is to be tested. A local availability environment, consisting only of structures that are of interest is required.

4.5.1.2 Algorithm Objective

An indication of the structures within an urban environment that could potentially cause an obstruction between a receiver and a satellite is required. Only the highlighted structures are then subject to rigorous polygon-by-polygon testing by the *detailed availability* algorithm.

A line of sight between a receiver and satellite can be described mathematically as one vector. It is important that an effective method of discriminating between structures that will definitely not interact with such a vector, and those structures that might interact with such a vector, is implemented. As a model may contain a large number of structures, the algorithm developed to perform this coarse availability work must be capable of rapid assessment of each structure, and must also ensure efficient use is made of memory resources.

4.5.1.3 Coarse Algorithm Description

Algorithm Inputs

1. Geometry only file (section 4.4.2).
2. Number of satellites above elevation mask (section 4.3.3).
3. Satellite positions (section 4.3.4).
4. User position (section 4.3.3).

Algorithm Outputs

1. List of buildings identified as potentially interacting with one or more receiver to satellite vectors.

Algorithm Description

Each object within the geometry only file is considered in turn by looping over the file structure held in RAM. Knowledge of the maximum and minimum values along each coordinate axis (determined during the VRML filter process) enables each structure to be modelled as a cuboid orientated such that each vertex is parallel to a coordinate axis. As shown in Figure 4-11, this method ensures that all of the structure is contained. It is important that no error occurs such that any part of a structure lies outside of this coarse representation.

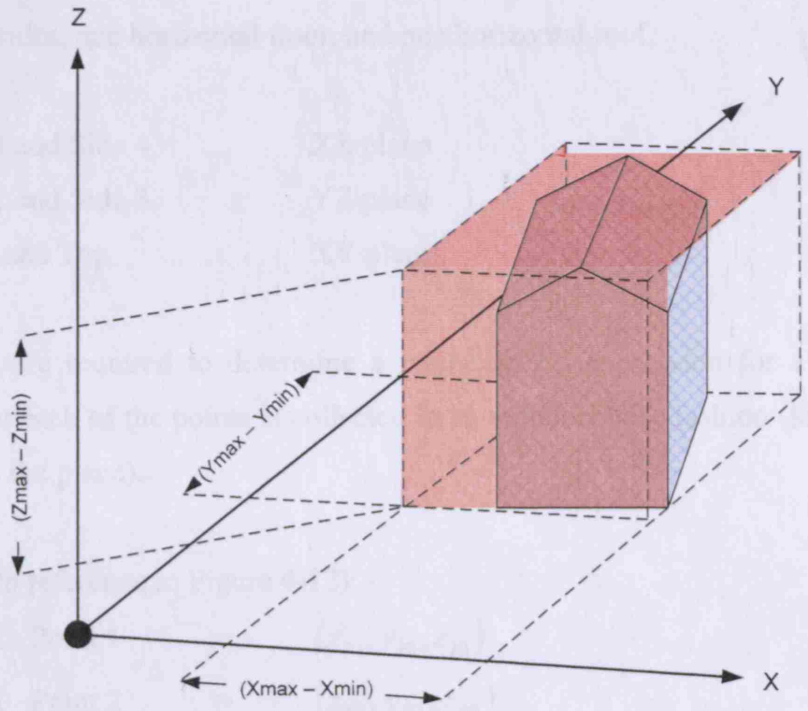

Figure 4-11: Coarse building representation

It is clear from Figure 4-11 that a vector that intersects the cube may not necessarily intersect any polygon in any part of the actual building. For this reason, the coarse evaluation alone is not valid as a satellite availability test. The six cube faces are individually tested for interaction with any of the receiver to satellite vectors to give an indication as to whether the building requires detailed polygon-by-polygon testing. Processing of six polygons (cube faces) as opposed to perhaps many hundreds of thousands, reduces the processing overhead significantly. Furthermore, the processing of these six polygons is less intensive than processing of actual building polygons. This is because there is no need to rotate the cube faces into 2D systems when testing to see if a vector intersects with a surface (see step 5 below). The following is a description of the formation of the coarse model. Mathematical demonstration is provided for how each of the coarse model faces are tested for interaction with receiver to satellite vectors. The mathematical procedure is described at length as it forms an important element of the simulator, and is applicable to all propagation models in some way.

Step 1 – Consider a structure

Select the first / next structure listed in the geometry file.

Step 2 – Collect planar surfaces

With reference to Figure 4-12, the selected structure is coarsely represented by taking the minimum and maximum coordinate values from the '.geo' file and then considering four vertical sides, one horizontal floor, and one horizontal roof.

Side 1 and Side 4	XZ plane
Side 2 and Side 3	YZ plane
Floor and Top	XY plane

Three points are required to determine a mathematical expression for a plane. It is important that each of the points is collected in an anticlockwise fashion (looking down the normal to the plane).

Example (with reference to Figure 4-12):

Side 1 Point 1 = (x_{P1}, y_{P1}, z_{P1})

Side 1 Point 2 = (x_{P2}, y_{P2}, z_{P2})

Side 1 Point 3 = (x_{P3}, y_{P3}, z_{P3})

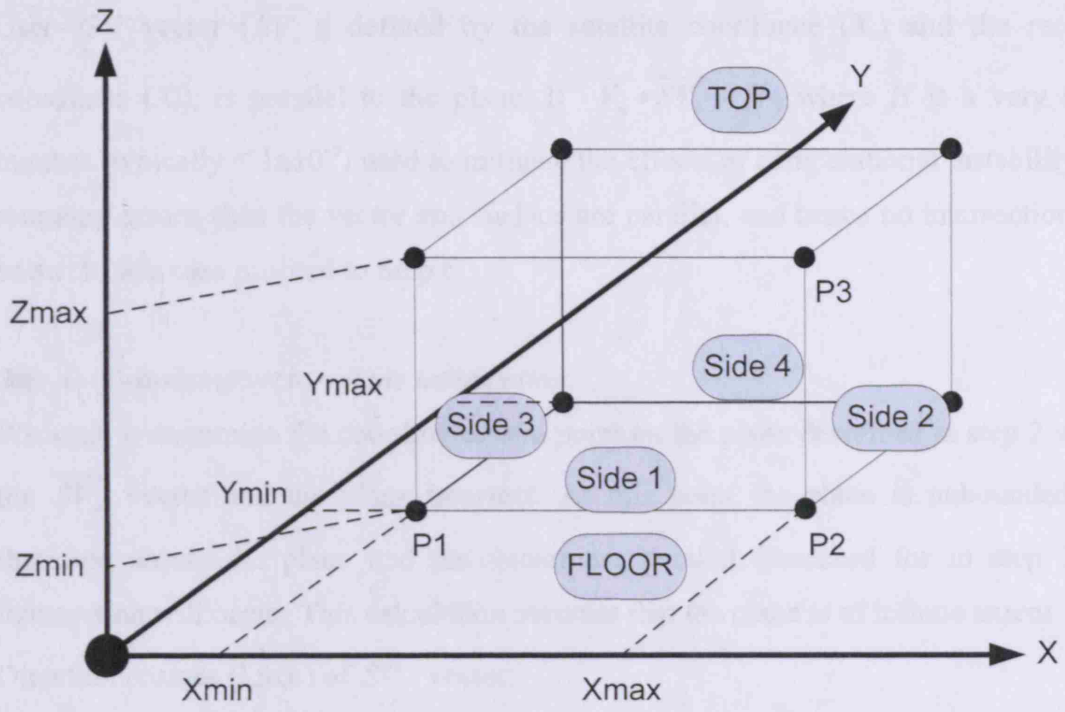

Figure 4-12: Assignment of face and point identifiers for coarse availability algorithm

Equation of a plane:

$$Px + Qy + Rz + S = 0$$

$$ax + by + cz = 1 \qquad \text{(eqn. 4-7)}$$

Methods to determine the equation of a plane are well established and can be found in many mathematical texts (e.g. [Carnegie Mellon, 2007]).

The coefficients a,b,c are found by constructing three simultaneous linear equations in matrix form and solving as follows:

$$\underline{\mathrm{M}} = \begin{bmatrix} X_{P1} & Y_{P1} & Z_{P1} \\ X_{P2} & Y_{P2} & Z_{P2} \\ X_{P3} & Y_{P3} & Z_{P3} \end{bmatrix} \quad \text{and} \quad \underline{\mathrm{M}} * \begin{bmatrix} a \\ b \\ c \end{bmatrix} = \begin{bmatrix} 1 \\ 1 \\ 1 \end{bmatrix} \quad \text{and} \quad \begin{bmatrix} a \\ b \\ c \end{bmatrix} = \underline{\mathrm{M}}^{-1} \begin{bmatrix} 1 \\ 1 \\ 1 \end{bmatrix}$$

Step 3 – Calculate surface normals

Determine each of the surface normal vectors. With reference to Figure 4-12:

$$\overline{V_1} = \overline{P_2} - \overline{P_1}$$
$$\overline{V_2} = \overline{P_2} - \overline{P_3} \qquad \text{(eqn. 4-8)}$$
$$\overline{V_n} = \overline{V_1} \times \overline{V_2}$$

This step is for both error checking, and also allows us to test for the case whereby the User->SV vector ($\overline{SV_n}$), defined by the satellite coordinate (X_s) and the receiver coordinate (X_r), is parallel to the plane. If $\overline{V_n} \bullet \overline{SV_n} = H$, where H is a very small number (typically < $1x10^{-5}$) used to mitigate the effects of computational instability and rounding errors, then the vector and surface are parallel, and hence no intersection will occur. In this case proceed to Step 6.

Step 4 - Determine vector-plane intersection

We seek to determine the coordinates of a point on the plane described in step 2 where the $\overline{SV_n}$ vector and the plane intersect. At this point the plane is unbounded and therefore unless the plane and the vector are parallel (screened for in step 2) an intersection will occur. This calculation assumes that the plane is of infinite extent.

Direction cosines (l,m,n) of $\overline{SV_n}$ vector:

$$l = \frac{a}{\sqrt{a^2 + b^2 + c^2}} \qquad m = \frac{b}{\sqrt{a^2 + b^2 + c^2}} \qquad n = \frac{c}{\sqrt{a^2 + b^2 + c^2}}$$

(eqn. 4-9) (eqn. 4-10) (eqn. 4-11)

where a,b,c are coefficients of the $\overline{SV_n}$ vector. $\overline{SV_n} = ai + bj + ck$.

It can be shown that:

$$l^2 + m^2 + n^2 = 1 \qquad \text{(eqn. 4-12)}$$

(X_i,Y_i,Z_i) is the point of intersection between the plane and the vector to be determined and

(X_o,Y_o,Z_o) is the point of origin of the vector – for our purposes the Rx position.

The following parametric equations can be used to determine the required intersection coordinates:

$$X_i = X_o + lt \qquad Y_i = Y_o + mt \qquad Z_i = Z_o + nt$$

(eqn. 4-13) (eqn. 4-14) (eqn. 4-15)

where

t is the distance of the intersection point along the vector from the receiver to the satellite, originating at the point of origin of the vector (X_o,Y_o,Z_o).

Substituting values from equations 4-13, 4-14 and 4-15 into the plane equation 4-7 gives the condition for the plane and the vector to intercept:

$$P(X_o + lt) + Q(Y_o + mt) + R(Z_o + nt) + S = 0 \qquad \text{(eqn. 4-16)}$$

$$PX_o + Plt + QY_o + Qmt + RZ_o + Rnt + S = 0 \qquad \text{(eqn. 4-17)}$$

and

$$PX_o + QY_o + RZ_o + S = -(Plt + Qmt + Rnt) \qquad \text{(eqn. 4-18)}$$

rearranging equation 4-18 yields a value of t where the line intersects the plane

$$\frac{PX_o + QY_o + RZ_o + S}{(Pl + Qm + Rn)} = -t \qquad \text{(eqn. 4-19)}$$

Using t in the parametric equations 4-13, 4-14 and 4-15 yields the cartesian intersection between the $\overline{SV_n}$ vector and the plane.

Step 5 – Test intersection point

Using logical tests based on the bounding coordinate values of the surfaces, simple numerical tests are performed to ensure that the intersection point:

1. Resides on the 2D plane
2. Resides within the polygon described by the coarse building representation.

No rigorous point in polygon tests are performed at this level, as each of the 6 polygons in the coarse building model is 2D within the XZ,YZ and XY planes.

Step 6 – Repeat for all 6 faces

For each of the 6 faces in the coarse model representation perform steps 4 and 5

Step 7 – Next structure

Return to Step 1, taking the next structure on the list. Continue the entire process until the end of the buildings database has been reached.

Output

The output of the *course availability* algorithm is a list of structures that will definitely not obstruct LOS between the receiver and any of the satellites. For the structures where an obstruction is possible, the PRN(s) of the satellite(s) with possible LOS obstructions is/are stored. The *detailed availability* algorithm can now be employed to assess signal obstruction based upon the results of the *course availability* algorithm.

4.5.2 Detailed Availability Algorithm

4.5.2.1 Problem Definition

A number of structures within an entire urban model dataset have been identified as requiring detailed availability testing following a coarse availability simulation. This defines the local availability environment. Each of the structures within this environment is comprised of a number of polygons. The total number of polygons being dependent upon the physical dimensions of the structure, the resolution at which the geometrical measurement data was originally captured (equivalent to the level of detail), and the resolution at which the dataset was exported to a mesh type model (where applicable). Although it is most often the case that a VRML dataset will be constructed using a triangular mesh network, there is no reason as to why polygons with more than three vertices should not be included in a model. However, all the points in a polygon must reside within the same plane.

4.5.2.2 Algorithm Objective

An indication of the polygons within a local availability environment that could potentially cause a LOS obstruction between a receiver and a satellite is required. Each receiver to satellite vector (as used in the coarse modelling algorithm) requires testing for intersection with every polygon of every structure in the local availability environment. Once this has been completed, the satellites for which an unobstructed line of sight is present, can be identified.

4.5.2.3 Detailed Algorithm Description

Algorithm Inputs

1. Geometry only file (section 4.4.2).
2. Number of satellites above elevation mask (section 4.3.3).
3. Satellite positions (section 4.3.4).
4. User position (section 4.3.3).
5. Output of Coarse availability algorithm.

Algorithm Outputs

1. List of polygons identified as potentially interacting with one or more receiver to satellite vectors.

Algorithm Description

Each polygon is considered in turn. Three coordinate points, extracted from the geometry file, are required for each polygon. Checks are performed to ensure that these points are not collinear. Three points are required in order that an expression for the plane in which a polygon lies can be determined. The plane is considered, in the first instance to be infinite in extent. From this assumption it follows that for any given vector, there will be a point at which intersection between the plane and vector occurs, unless the vector is parallel to the plane. For vectors not parallel to the plane, this point is calculated. In the next step the intersection point and the vertices of the polygon are transformed into a common 2D plane. This is done in order that the intersection point can be tested to determine whether or not it exists within the region bounded by the polygon. This is performed via a series of rotations about selected axes, leaving the transformed coordinates each displaying a constant x, y or z. Prior to the system transformation, a process is performed in order to establish the best system, constant x, constant y or constant z. A 2D system now lends itself to a point in polygon test, which is undertaken to determine whether the intersection point lies within the polygon.

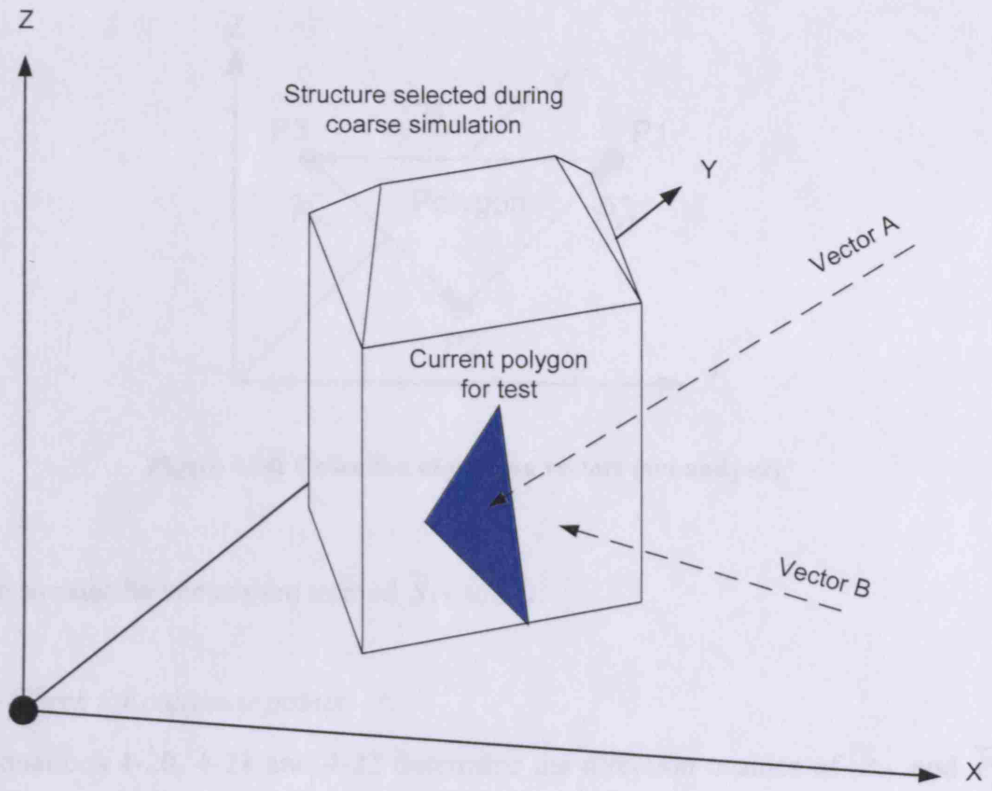

Figure 4-13: Structure selected during coarse availability simulation

The following is a detailed description of how each polygon within a selected structure (see Figure 4-13) is tested for intersection with receiver to satellite vectors.

Step 1 – Consider a structure

Select the first / next structure listed in the output of the Coarse simulation.

Step 2 – Consider a polygon

Select the first / next polygon listed for the current structure.

Step 3 – Polygon points, polygon vectors and receiver to satellite vectors

As the polygon normal ($\hat{n}$) is already known, determined during the VRML filter process, there is no need to obey a winding convention when collecting the polygon coordinates. A vector for each side of the polygon must be produced. With reference to Figure 4-14:

$$\overline{P}_{v1} = \overline{P}_1 - \overline{P}_2 \qquad \text{(eqn. 4-20)}$$

$$\overline{P}_{v1} = \overline{P}_2 - \overline{P}_3 \qquad \text{(eqn. 4-21)}$$

$$\overline{P}_{v3} = \overline{P}_3 - \overline{P}_1 \qquad \text{(eqn. 4-22)}$$

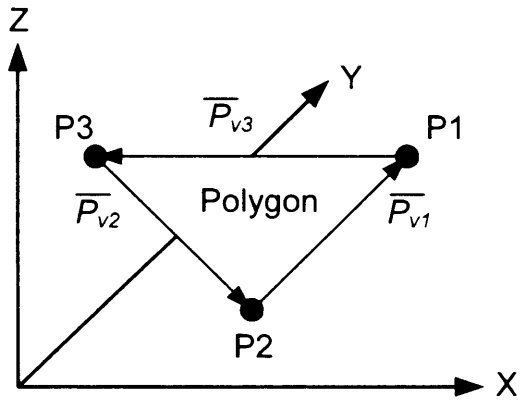

Figure 4-14: Collection of polygon vectors (*pv1* and *pv2*)

Receiver to satellite vectors are termed $\overline{S}_{v1}$ to $\overline{S}_{vn}$.

Step 4 – Check for collinear points

Using equations 4-20, 4-21 and 4-22 determine the direction cosines of $\overline{P}_{v1}$ and $\overline{P}_{v2}$, where:

l_1, m_1, n_1 are the direction cosines of $\overline{P}_{v1}$

and

l_2, m_2, n_2 are the direction cosines of $\overline{P}_{v2}$

then

$$\theta = \cos^{-1}((l_1 l_2) + (m_1 m_2) + (n_1 n_2)) \qquad \text{(eqn. 4-23)}$$

where θ is the angle between $\overline{P}_{v1}$ and $\overline{P}_{v2}$.

Mathematically, if $\theta = 0$, then this is a straight line and not a polygon, and therefore must be disregarded. When implemented on a computer, θ is tested to ensure its magnitude is less than a small number (typically < 1×10^{-5}) to account for numerically instability and rounding effects associated with solutions calculated on a computer. Return to step 2 or to step 1 depending on whether this is the last polygon in the structure or not.

Step 5 – Determine an expression for the plane

An expression for the plane in which the polygon resides is required. This is a well established method and can be found in many mathematical texts (e.g. [Carnegie Mellon, 2007]).

Using (1), the equation of a plane can be expressed as:

$$Px + Qy + Rz + S = 0$$

$$ax + by + cz = 1 \qquad \text{(eqn. 4-23)}$$

The coefficients a,b,c are found by constructing three simultaneous linear equations in matrix form and solving as follows:

$$\underline{M} = \begin{bmatrix} X_{P1} & Y_{P1} & Z_{P1} \\ X_{P2} & Y_{P2} & Z_{P2} \\ X_{P3} & Y_{P3} & Z_{P3} \end{bmatrix} \quad \text{and} \quad \underline{M} * \begin{bmatrix} a \\ b \\ c \end{bmatrix} = \begin{bmatrix} 1 \\ 1 \\ 1 \end{bmatrix} \quad \text{and} \quad \begin{bmatrix} a \\ b \\ c \end{bmatrix} = \underline{M}^{-1} \begin{bmatrix} 1 \\ 1 \\ 1 \end{bmatrix}$$

Step 6 - Determine vector->plane intersection

Perform step 4 of the Coarse availability algorithm (4.5.1) in order to calculate the intersection vector. This calculation assumes that the plane is of infinite extent.

Step 7 – Transform polygon and intersection points into a shared plane

In order to determine whether the intersection point lies within the area bounded by the polygon vertices, it is necessary to transform the polygon coordinates and the intersection point to be tested, into the target plane parallel to the XY, XZ or YZ planes.

If the target plane is to be parallel to the X, and Y axes, then the resulting Z coordinate values will be the same for all points.

If the target plane is to be parallel to the Y, and Z axes, then the resulting X coordinate values will be the same for all points.

If the target plane is to be parallel to the X, and Z axes, then the resulting Y coordinate values will be the same for all points.

For a transformation into a plane of constant X values, use is made of a general 3x3 rotation matrix. Details of rotation matrices can be found in Wolf [Wolf, 1983]. Let:

$\underline{P}_n$ = Point in the initial system

$\underline{H}_n$ = Point in required target plane

R = 3D rotation matrix

ω = Rotation about x-axis

l = Rotation about y-axis

k = Rotation about z-axis

const = Constant

The general 3x3 rotation matrix:

$$R = \begin{bmatrix} \cos l \cos k & \cos\omega \sin k + \sin\omega \sin l \cos k & \sin\omega \sin k - \cos\omega \sin l \cos k \\ -\cos l \cos k & \cos\omega \cos k - \sin\omega \sin l \sin k & \sin\omega \cos k + \cos\omega \sin l \sin k \\ \sin l & -\cos l \sin\omega & \cos l \cos\omega \end{bmatrix}$$

If $\underline{H}_n = R\underline{P}_n$:

and $\underline{H}_n = \begin{bmatrix} D_n \\ E_n \\ F_n \end{bmatrix}$ and $\underline{P}_n = \begin{bmatrix} A_n \\ B_n \\ C_n \end{bmatrix}$

then $\begin{bmatrix} D_n \\ E_n \\ F_n \end{bmatrix} = R \begin{bmatrix} A_n \\ B_n \\ C_n \end{bmatrix}$

In order to solve for the rotation parameters ω, l and k, three points in the initial system are required. The following equations can then be constructed :

$$A_1(\cos l \cos k) + B_1(\cos\omega \sin k + \sin\omega \sin l \cos k) + C_1(\sin\omega \sin k - \cos\omega \sin l \cos k) = const$$
$$A_2(\cos l \cos k) + B_2(\cos\omega \sin k + \sin\omega \sin l \cos k) + C_2(\sin\omega \sin k - \cos\omega \sin l \cos k) = const$$
$$A_3(\cos l \cos k) + B_3(\cos\omega \sin k + \sin\omega \sin l \cos k) + C_3(\sin\omega \sin k - \cos\omega \sin l \cos k) = const$$

Dividing by cos(ω) and then by cos(l) gives:

$$A_1 + B_1\left(\frac{\tan k}{\cos l}\right) + C_1(-\tan l) = const \qquad \text{(eqn. 4-24)}$$

$$A_2 + B_2\left(\frac{\tan k}{\cos l}\right) + C_2(-\tan l) = const \qquad \text{(eqn. 4-25)}$$

$$A_3 + B_3\left(\frac{\tan k}{\cos l}\right) + C_3(-\tan l) = const \qquad \text{(eqn. 4-26)}$$

(4-24)- (4-25)

$$(A_1 - A_2) + (B_1 - B_2)\left(\frac{\tan k}{\cos l}\right) - (C_1 - C_2)\tan l = const \qquad \text{(eqn. 4-27)}$$

(4-25)- (4-26)

$$(A_2 - A_3) + (B_2 - B_3)\left(\frac{\tan k}{\cos l}\right) - (C_2 - C_3)\tan l = const \qquad \text{(eqn. 4-28)}$$

Rearranging (4-27) and (4-28) and expressing result in matrix form gives:

$$\begin{bmatrix} B_1 - B_2 & C_2 - C_1 \\ B_2 - B_3 & C_3 - C_2 \end{bmatrix} \begin{bmatrix} \left(\frac{\tan k}{\cos l}\right) \\ \tan l \end{bmatrix} = \begin{bmatrix} A_2 - A_1 \\ A_3 - A_2 \end{bmatrix} \qquad \text{(eqn. 4-29)}$$

Finding the inverse of the l.h.s yields the result for transformation into a plane of constant X values.

$$\frac{\tan k}{\cos l} = \frac{(C_3 - C_2)(A_2 - A_1) + (C_1 - C_2)(A_3 - A_2)}{(B_1 - B_2)(C_3 - C_2) - (B_2 - B_3)(C_2 - C_1)} \qquad \text{(eqn. 4-30)}$$

and

$$\tan l = \frac{(B_3 - B_2)(A_2 - A_1) + (B_1 - B_2)(A_3 - A_2)}{(A_1 - A_2)(C_3 - C_2) - (B_2 - B_3)(C_2 - C_1)} \qquad \text{(eqn. 4-31)}$$

and

$$\omega = 0$$

For a transformation into a plane of constant Y values, the same method as above is used to derive ω and k with l=0. It can be shown that for this transformation:

$$\frac{\tan k}{\cos \omega} = \frac{(C_3 - C_2)(B_1 - B_2) + (C_1 - C_2)(B_2 - B_3)}{(A_1 - A_2)(C_3 - C_2) - (A_2 - A_3)(C_2 - C_1)} \qquad \text{(eqn. 4-32)}$$

and

$$\tan \omega = \frac{(A_3 - A_2)(B_1 - B_2) + (A_1 - A_2)(B_2 - B_3)}{(A_1 - A_2)(C_3 - C_2) - (A_2 - A_3)(C_2 - C_1)} \qquad \text{(eqn. 4-33)}$$

and

$$l=0$$

For a transformation into a plane of constant Z values, the same method as above is used to derive ω and l with k=0. It can be shown that for this transformation:

$$\frac{\tan l}{\cos \omega} = \frac{(B_3 - B_2)(C_2 - C_1) + (B_1 - B_2)(C_3 - C_2)}{(A_1 - A_2)(B_3 - B_2) - (A_2 - A_3)(B_2 - B_1)} \qquad \text{(eqn. 4-34)}$$

and

$$\tan\omega = \frac{(A_3 - A_2)(C_2 - C_1) + (A_1 - A_2)(C_3 - C_2)}{(A_1 - A_2)(B_3 - B_2) - (A_2 - A_3)(C_2 - C_1)} \qquad \text{(eqn. 4-35)}$$

and

k=0

Step 8 – Point in polygon test

With all polygon points and the vector->plane intersection point in a 2D space, it is now possible to perform a point in polygon test. This test will determine whether the intersection point lies within the area bounded by the polygon vertices. Several methods exist to do this. The particular method used for this work [Taylor, 1994] is the ray intersection method.

Step 9 – Next polygon / Next structure

Return to step 2 or to step 1 depending on whether this is the last polygon in the structure or not.

4.6 Fresnel Zone Model for Satellite Availability

The importance of the Fresnel zone for assessment of signal propagation between transmitter and receiver is discussed in section 3.1.2. Consideration of the volumeless LOS propagation mode alone is insufficient, and therefore a means to determine the level of signal obstruction within the Fresnel zone is required.

4.6.1 Problem Definition

Given that signal propagation within a defined volume must be considered, a method is required to estimate the maximum obstruction present at any point between the transmitter-receiver pair. The transmission zone is defined by concentric spheroids of calculable dimensions between the receiver and the transmitter. The maximum obstruction to the cross-section at any distance h_n from the receiver is sought. A representation of this problem is given in Figure 4-15.

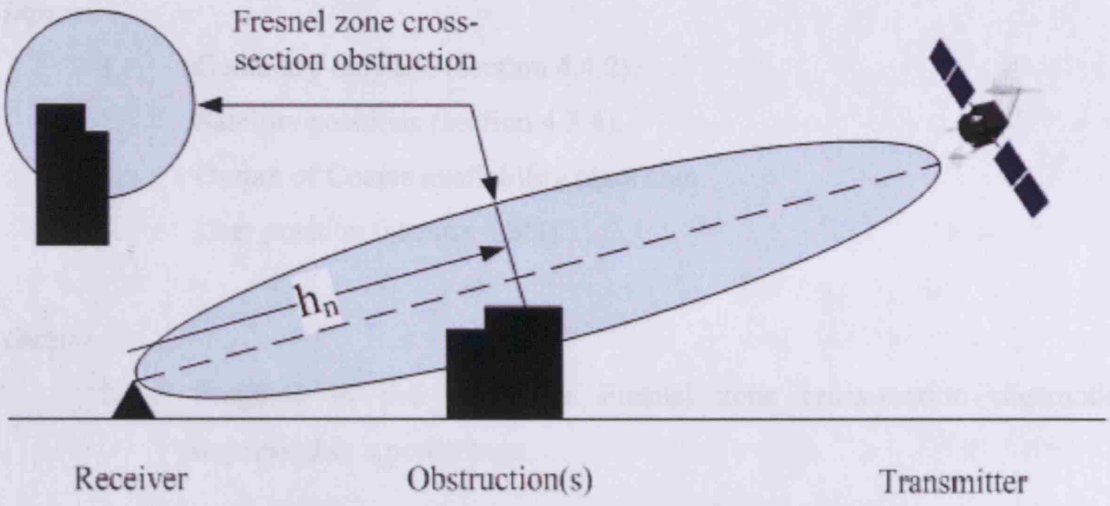

Figure 4-15: 3D analysis of Fresnel zone obstruction

In addition, the process must be performed for multiple signals to be received in environments that are densely populated with irregularly shaped obstructing objects. Fresnel zone dimensions are a function of signal frequency, and both L1 and L2 are to be considered. To complicate this problem further, the radius of the Fresnel zone cross-section increases with distance from the receiver. Therefore, across the range from the receiver where obstruction is present within the Fresnel zone, the zone radius varies. In addition, the shape of the obstructing object(s) may also change dramatically within this range. A procedure that utilises the LOS algorithms described in section 4.5, and shares much of the same mathematical detail, is now described.

4.6.2 Fresnel Zone Obstruction

Creation of a planar grid of points, orthogonally aligned to the direction of transmission at a specified distance from the receiver, permits the determination of a collection of vectors that are parallel to the satellite to receiver LOS vector. A subset of these vectors will reside within the area described by the Fresnel zone at the specified distance from the receiver. These vectors intersect a plane (the description of which follows) defined by the receiver position. Treatment of the satellite as a light source allows a shadow of the obstructing object profiles to be projected on the receiver defined plane. By assessing the area occupied by both obstruction shadow and the projected Fresnel zone cross-section, the level of obstruction can be determined. This procedure is performed for a range of distances from the receiver, and gives an estimate as to the maximum obscuration experienced by the transmission path. A detailed description is now provided.

Inputs

1. Geometry only file (section 4.4.2).
2. Satellite positions (section 4.3.4).
3. Output of Coarse availability algorithm.
4. User position (section 4.3.3).

Output

1. Estimate of the maximum Fresnel zone cross-section obstruction expressed as a percentage.

Step 1 – Select satellite and frequency

This procedure is performed individually for each satellite above the elevation mask angle. The radius of the Fresnel zone is a function of the signal frequency and as such the procedure is performed for both L1 and L2.

Step 2 - Establishing a local user plane

The North and Up vectors (see section 4.3.5) are used to define a plane that is specific to the user position, where the Up vector is normally incident to the defined plane. A plane defined by the local user terrain is considered unsuitable. By using the receiver position as one of the plane coordinates (P_1) the E and N unit vectors (expressed in the model space) can be used establish P_2 and P_3, each at one unit length from P_1:

$$\overline{P}_2 = \overline{P}_1 + \overline{E} \qquad \text{(eqn. 4-36)}$$

$$\overline{P}_3 = \overline{P}_1 + \overline{N} \qquad \text{(eqn. 4-37)}$$

The equation of a plane:

$$Px + Qy + Rz + S = 0$$

$$ax + by + cz = 1 \qquad \text{(eqn. 4-38)}$$

Where:

x,y,z is the coordinate of a point the plane.

The coefficients a,b,c are found by constructing three simultaneous linear equations in matrix form and solving as follows:

$$\underline{\mathrm{M}} = \begin{bmatrix} X_{P1} & Y_{P1} & Z_{P1} \\ X_{P2} & Y_{P2} & Z_{P2} \\ X_{P3} & Y_{P3} & Z_{P3} \end{bmatrix} \quad \text{and} \quad \underline{\mathrm{M}} * \begin{bmatrix} a \\ b \\ c \end{bmatrix} = \begin{bmatrix} 1 \\ 1 \\ 1 \end{bmatrix} \quad \text{and} \quad \begin{bmatrix} a \\ b \\ c \end{bmatrix} = \underline{\mathrm{M}}^{-1} \begin{bmatrix} 1 \\ 1 \\ 1 \end{bmatrix}$$

Step 3 - Local environment for Fresnel analysis

The local environment for satellite availability, as defined by the coarse algorithm, is reused for Fresnel analysis. If the satellite LOS vector is not obscured by the coarse representation of the objects surrounding the receiver, then it is almost certain that over 50% of the Fresnel zone cross section will be clear, and that the signal would be tracked by the receiver. The case whereby an aperture may allow the LOS signal, but little contributing signal energy from the Fresnel zone, is likely to result in a coherent signal present at the antenna unless the aperture is incredibly small. Reuse of the coarse availability candidate object list is a pragmatic approach. Expressions are formed for vectors originating from the satellite passing through each coordinate present in all objects within the local environment. The intersection of each of these vectors with the plane defined in step 2 is found (for intersection calculation see step 4 of section 4.5.1.3). In this way, the satellite has been treated as a point light source, and the shadowed area resulting from all objects in the coarse environment is determined.

Step 4 – Defining the Fresnel zone cross-sections

During coarse availability processing, the maximum and minimum distance, h_{max} and h_{min}, of the obstructing object components from the receiver are established. This is necessary as the radius of the Fresnel zone, given in section 3.1.2 [equation 3-2], reduces as the signal approaches the antenna. This is shown below in Figure 4-16a.

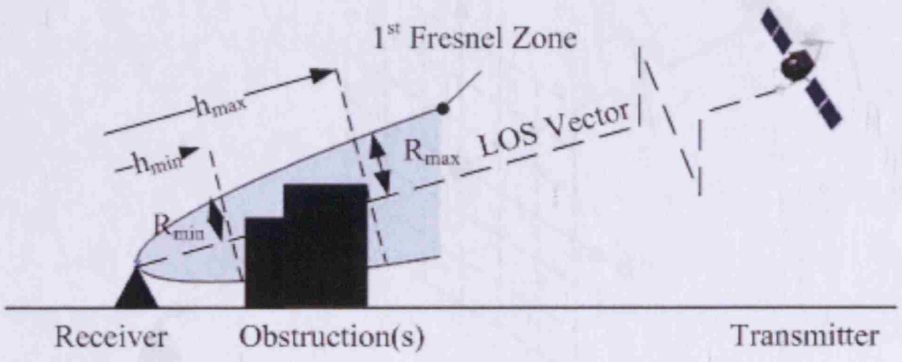

Figure 4-16: Fresnel zone radius change over the obstructed transmission path

A computationally efficient method to assess the maximum cross-section obstruction between h_{min} and h_{max}, is to sample the range at equally spaced discrete intervals. Figure 4-16 shows how this can be achieved by substituting h_{min} to h_{max} for h_1 to h_{10}. It must be realised that the distance between sample points is a function of the range h_{min} to h_{max} and the chosen number of samples. A trade-off exits between the rigour of the solution

and acceptable computation time. For the purpose of this work, 10 samples are used. This decision is based upon the typical physical scale of objects in the urban environment, relative to the radius size exhibited at GPS signal frequencies, in typical proximities to the receiver of not more than 100m. For different applications, this should be adjusted as required. Distances from the receiver to each sample point are used to compute the appropriate Fresnel zone cross-section radii using equation 3-2.

Step 5 – Select a single sample

Each sample is considered individually. A sample point P_n is now chosen, where P_n is the point on the satellite to receiver vector at a distance of h_n from the receiver.

Step 6 – Grid orientation and orthogonal grid axis

At each sample position P_n a grid is to be implemented, the dimensions of which are established during later steps. Each grid of points exists on a single plane orientated such that the LOS vector is normally incident. A right handed coordinate system is formed by producing two perpendicular vectors that are both orthogonal to the LOS vector. The orientation of the two vectors, about the LOS vector is arbitrary. With reference to Figure 4-17 we have now defined a coordinate system, with axial components LOS, *u* and *v*.

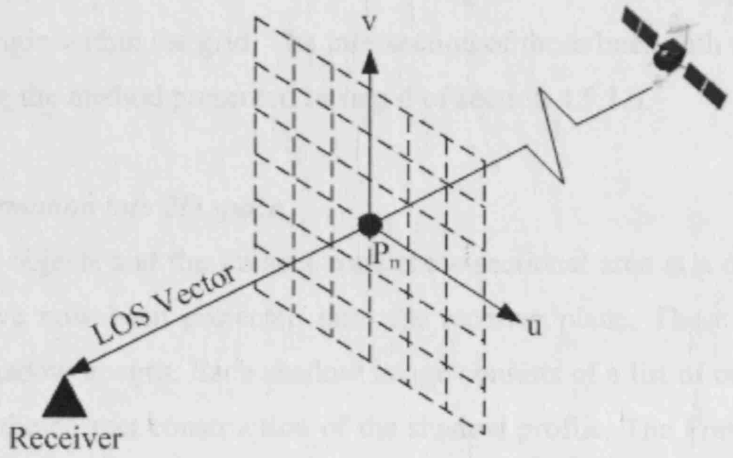

Figure 4-17: Definition of LOS based coordinate system

Step 7 – Grid formation and grid point selection

It is now possible to produce a collection of vectors defining a set of points within the *uv* plane for an appropriately orientated grid produced at P_n. As with selection of the number of samples, the number of points per grid will impact upon both the rigor of the solution and the computational overhead. For this work, again considering the nature of

the problem in terms of signal frequency and physical scale, a 144 point grid has been chosen. The physical area of each grid is given by:

$$G = (2 \times r)^2 \qquad \text{(eqn. 4-39)}$$

Where:

G = Grid area (m^2).

r = Fresnel zone cross-section (m).

Each grid is to consist of i points (in this case 144) and therefore the point spacing for both u and v components is given by:

$$\rho = \frac{2 \times r}{\sqrt{i} - 1} \qquad \text{(eqn. 4-40)}$$

Where:

ρ = Point space (m).

i = number of points in entire grid.

The coordinate axis u and v, defined earlier, can now be used to construct the grid. The grid must be centred on P_n, and the grid spacing between points is ρ. The Euclidean distance from each grid point to P_n is now found. Any point with a distance exceeding the Fresnel radius value at P_n is discarded. All valid points are now considered as a point source. Expressions for lines are formed using the LOS vector expression and the coordinate of origin within the grid. The intersection of these lines with the user plane is now found using the method presented in step 4 of section 4.5.1.3.

Step 8 – Tranformation into 2D space

The obstructing objects and the Fresnel zone cross-sectional area at a distance h_n from the receiver have now been projected onto the receiver plane. These projections are referred to as shadow images. Each shadow image consists of a list of coordinate points and indices for the correct construction of the shadow profile. The Fresnel zone cross-section projection consists of a coordinate list. All coordinate values are now transformed into a 2D space using the same procedure as described in step 7 of section 4.5.2.3.

Step 9 –Zone obstruction at h_n

At a distance h_n from the receiver, the total zone obstruction can now be determined. By application of a suitable point in polygon test such as Taylor [Taylor, 1994] the number of Fresnel zone cross-section points that reside within the projected shadow area is compared to the number of uncontained points to yield a percentage obstruction. The percentage of obstructed points relative to the total number of projected points is now determined.

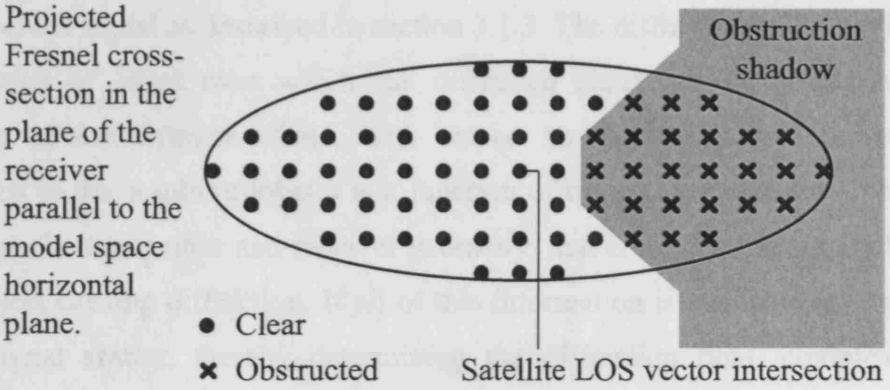

Figure 4-18: Point in polygon to determine obstruction of Fresnel cross-section at Pn

Step 10 – Next Sample

Steps 5 to 9 are to be performed for samples 1 to n. If all n samples have not been processed, increment *n* and continue from step 5. If all samples have been processed, return to step 1 to consider a new satellite or frequency from the first sample onwards.

4.6.3 Further Consideration of the Fresnel Zone for Signal Propagation

The Fresnel zone analysis is effectively an enhancement to the LOS propagation model, however, it should be noted that by considering signal propagation within the concentric volumes surrounding a satellite to receiver LOS vector (see section 3.1.2), we are also considering signal power that contributes to the diffraction field. In this way the Fresnel model should be considered in conjunction with a diffraction model.

4.7 Diffracted Propagation Model

In order to account for all modes of propagation between transmitter and receiver, consideration of signal power present in the diffracted field is necessary. This is particularly important in urban environments where signal interaction with objects around the receiver is inevitable.

4.7.1 Problem Definition

Electromagnetic energy resulting from the diffracted field can contribute signal power to the received signal as described in section 3.1.3. The diffracted field describes a lobe or formation of lobes over which the diffracted signal power is distributed. The properties of the diffracted field, with respect to the total signal power and the dimensions of the resulting lobe(s) is a function of the geometry of the object causing diffraction, the transmitter and receiver geometry, and crucially, the material attributes of the object causing diffraction. If all of this information is available, it is possible to predict signal scatter, thereby determining the diffraction field, complete with an estimate of signal attenuation in any direction from the point of diffraction. Currently, material attributes are not available at a high enough quality or over enough structures in urban models. It is therefore not possible to attempt to numerically model the diffracted field. It is unlikely that even future models will contain material attribuite data of sufficient quality to attempt rigourous numerical modelling of diffracted propagation fields. Even if such attributes were available, the scale of the problem from a computational perspective would be prohibitive. However, the tracking of diffracted signals in urban environments, and subsequent range measurement, is apparent from field work. A crude experiment as described in section 2.1, can be performed whereby a receiver is noted to track signals from satellites with elevation and azimuth angles that indicate the LOS signal is lost. Where reflected propagation is ruled out, this reception is via the diffracted mode. This occurrence is termed a diffraction event. The effect of such an event is that for a satellite that is rising above an obstruction, the signal appears earlier than would be expected. For a satellite that is setting behind an obstruction, the signal remains visible for longer than predicted by any LOS assessment. It is hoped that characterisation of the diffracted field can be achieved by determining when these events are likely to occur and for what period of time they will result in an available signal. Further to this, the disruption to the signal measurement is sought. Multiple transmission paths require testing, each of which will be affected by a different subset of objects within the urban environment.

4.7.2 Diffracted GPS Signal Model

A model for the detection of geometrical configurations that could give rise to the reception of diffracted signals is described. For a receiver at a position within an area that is described by an urban model, diffraction of GPS signals across object edges is considered. Effectively this equates to a knife-edge diffraction model, although no attempt is made to establish the resulting signal behaviour from an attenuation perspective. The model is most applicable when the LOS signal is obscured, however, the model can be used in combination with LOS assessment. An example of this case is provided below.

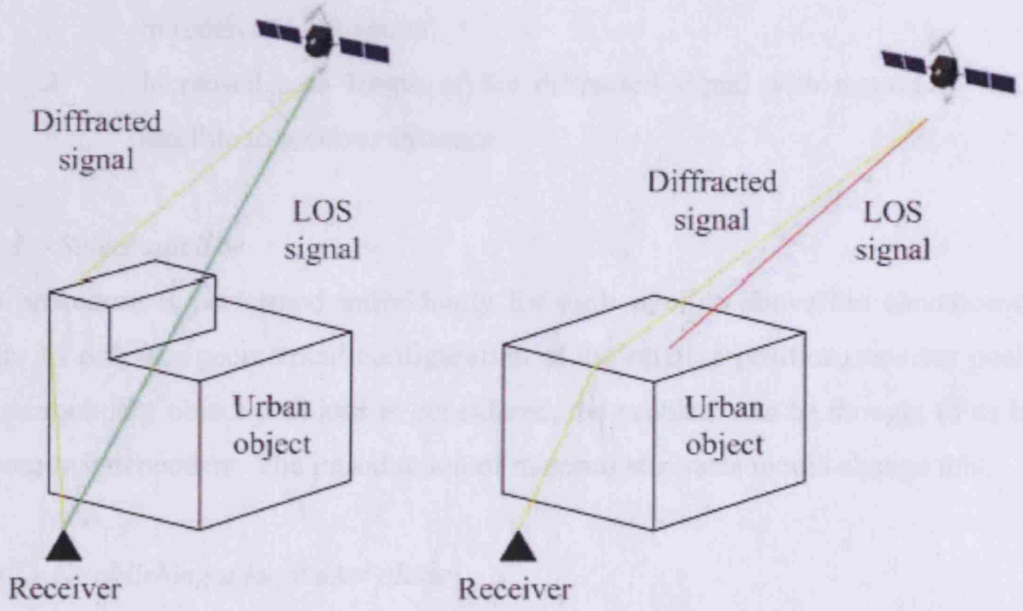

Figure 4-19: Diffracted propagation – LOS clear and obscured

The first problem that is tackled by the described method is to establish the object edges that could give rise to diffracted propagation, where an edge is defined by two planar facets with two or more adjacent vertices (as shown in Figure 4-8). This is achieved by treating the satellite as a light source and projecting a shadow of the object under investigation onto a plane defined by the user position and the local Up vector. This results in a collection of polygons existing within the defined plane. A technique is applied to determine the polygon sides that form the boundary of the projected object on the defined plane. A sequential test routine is then adopted to establish the point on the boundary that yields the minimum angle through which a propagation path would be disrupted to reach the receiver. A detailed description is now provided.

Inputs

1. Geometry only file (section 4.4.2).
2. Satellite positions (section 4.3.4).
3. Output of Coarse availability algorithm.
4. User position (section 4.3.3).
5. Maximum angle through which signal diffracted angle can be tracked.

Output

1. Coordinates of the origin of a diffracted signal.
2. Angle through which the signal is diffracted with respect to the satellite to receiver LOS vector.
3. Increased path length of the diffracted signal with respect to the true satellite to receiver distance.

Step 1 – Select satellite

This procedure is performed individually for each satellite above the elevation mask angle. As only the geometrical configuration of the satellite position, receiver position, and surrounding object positions is considered, the problem can be thought of as being frequency independent. The introduction of material attributes would change this.

Step 2 - Establishing a local user plane

The North and Up vectors (see section 4.3.5) are used to define a plane that is specific to the user position, where the Up vector is normally incident to the defined plane. A plane defined by the local user terrain is considered unsuitable. The mathematical procedure to establish an expression for the plane is given in step 2 of 4.6.2.

Step 3 - Local environment for the diffraction model

The local environment for satellite availability, as defined by the coarse algorithm, is reused for the diffracted propagation model. Diffraction may occur from structures that obstruct the satellite to receiver LOS vector. If the satellite to receiver LOS vector is not obstructed, then due to the consideration of only very small diffraction angles (typically <5°), diffraction will only occur from objects that are very close to obstructing the LOS vector. As such, the coarse availability representation will have identified these objects. As with the reuse of the coarse availability algorithm output for Fresnel zone analysis, this is a pragmatic approach. Expressions are formed for vectors originating from the

satellite passing through each coordinate present in all objects within the local environment. The intersection of each of these vectors with the plane defined in step 2 is found (for intersection calculation see step 4 of section 4.5.1.3). In this way, the satellite has been treated as a light source, and the shadowed area resulting from all objects in the coarse environment is determined. There now exists a collection of polygons that are coincident with the user defined plane. The collection of polygons is categorised according to the object to which it belongs.

Step 4 – Diffraction object profiles

The profile of each object within the coarse environment is now required. The profile is comprised of the outside edges of the object when viewed from the receiver in the direction of the satellite. Only these edges will give rise to diffraction, and it should be noted that the edges that comprise the profile will vary for individual geometrical configurations. It should also be noted that VRML, in common with other formats, gives no indication as to which polygon sides are external to a modelled structure. Effectively, the process we are applying is working with a list of polygons that are grouped according to the object to which they belong. The method to determine these external polygon sides employs a point in polygon test, consequently the entire collection of polygons that currently exist on the user plane is transformed into a 2D space using the same procedure as described in step 7 of section 4.5.2.3.

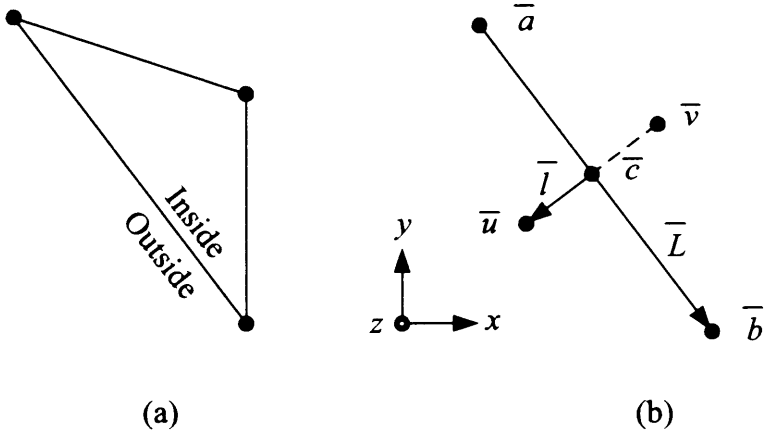

Figure 4-20: Determination of external polygon sides

With reference to Figure 4-20a, the inside and outside of the polygon with respect to an individual polygon side is required. Figure 4-20b shows how this is performed for a single polygon side. Firstly, two Cartesian points $\bar{a}$ and $\bar{b}$ are used to establish a mid point, $\bar{c}$:

$$x_c = x_b + \frac{(x_a - x_b)}{2} \qquad \text{(eqn. 4-41)}$$

$$y_c = y_b + \frac{(y_a - y_b)}{2} \qquad \text{(eqn. 4-42)}$$

The normal to the plane of reference $\overline{N}$ is given by 0i+0j+1k, as we are working in a 2D space within a 3D coordinate system. In this situation we consider constant z values.

A vector expression $\overline{L}$ for the line under consideration is found by considering point *a* to point *b*:

$$L_i = x_a - x_b, \qquad \text{(eqn. 4-43)}$$

$$L_j = y_a - y_b, \qquad \text{(eqn. 4-44)}$$

$$L_k = z_a - z_b = 0 \qquad \text{(eqn. 4-45)}$$

It follows that a perpendicular, $\bar{l}$, to the line $\overline{L}$ can be found by:

$$\bar{l} = \overline{N} \times \overline{L} \qquad \text{(eqn. 4-46)}$$

A distance *d* units from the line is used with the perpendicular vector to establish two points, $\bar{u}$ and $\bar{v}$, as follows:

$$\bar{u} = \bar{c} + (d \times \bar{l}) \qquad \text{(eqn. 4-47)}$$

$$\bar{v} = \bar{c} - (d \times \bar{l}) \qquad \text{(eqn. 4-48)}$$

Considering the size and general form of polygons within the environment models, a distance of 0.2 has been chosen. This should be adjusted if this process is to be applied to a different application. Coordinate points $\bar{u}$ and $\bar{v}$ are established for every polygon side of every polygon, and are stored in indexed arrays. Every $\bar{u}$ and $\bar{v}$ coordinate is subjected to a point in polygon test such as [Taylor, 1994], and for each polygon, there now exists a list of $\bar{u}$ and $\bar{v}$ coordinates that are external to the polygon from which they were derived. The remaining $\bar{u}$ and $\bar{v}$ variables are the subject of further point in polygon tests with all other polygons within the polygon list. Each $\bar{u}$ and $\bar{v}$ coordinate is considered in turn, and if it is found to exist within a polygon, the next $\bar{u}$ or $\bar{v}$

coordinate is selected. There now exists a list of $\bar{u}$ and $\bar{v}$ coordinates that do not exist inside any polygons. The associated line segments of these coordinates identify the sides that comprise the object profile. This is performed for multiple structures and for multiple satellites. As an example, a plan view of a scenario involving several satellites and only one regular shaped object is given in Figure 4-21.

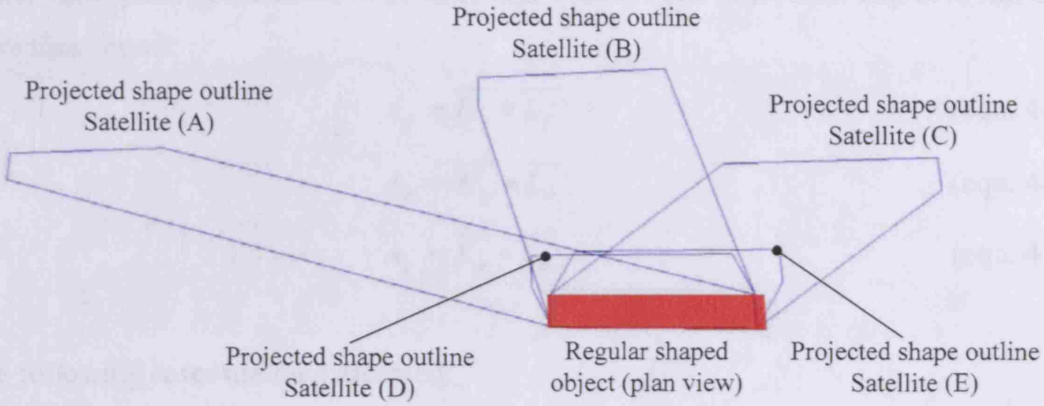

Figure 4-21: Identification of a structure profile for multiple satellites

As shown in Figure 4-21, the object profile is identified. The profile itself is comprised of a number of individual line segments, and is a projection onto the user defined plane. Each of these lines relates to a polygon side that originates from the original object polygons. As all coordinates projected onto the user defined plane are indexed, they can be linked back to the original structure coordinates.

Step 5 – Determining the diffraction angle

Diffracted propagation results in a deviation from the satellite to receiver vector at some point within the transmission path. For the purpose of this model, deviation occurs due to interaction with object edges. The above steps have identified object edges that may give rise to diffraction for a specific geometrical configuration of satellite, receiver and object. To determine if the object would give rise to a diffraction event, the minimum angle through which diffraction would occur, for a specific geometric configuration is now sought. Each identified edge is defined by a coordinate pair, f and g. A coordinate m is found that exists half way along the side described by f and g. For each, the following is performed:

$$\overline{K_f} = \overline{X_{Rx}} - \overline{X_f}, \qquad \overline{K_m} = \overline{X_{Rx}} - \overline{X_m}, \qquad \overline{K_g} = \overline{X_{Rx}} - \overline{X_g}$$

(eqn. 4-49) (eqn. 4-50) (eqn. 4-51)

and

$$\overline{L_f} = \overline{X_f} - \overline{X_{sat}}, \qquad \overline{L_m} = \overline{X_m} - \overline{X_{sat}}, \qquad \overline{L_g} = \overline{X_g} - \overline{X_{sat}}$$

(eqn. 4-52) (eqn. 4-53) (eqn. 4-54)

These vectors are normailised to become unit vectors. The diffraction angles at f,m and g are thus found:

$$A_f = \overline{K_f} \bullet \overline{L_f} \qquad \text{(eqn. 4-55)}$$

$$A_m = \overline{K_m} \bullet \overline{L_m} \qquad \text{(eqn. 4-56)}$$

$$A_g = \overline{K_g} \bullet \overline{L_g} \qquad \text{(eqn. 4-57)}$$

The following cases are then assessed:

Case 1: If $Af<Am<Ag$ then Af is the smallest diffraction angle for that edge.

Case 2: Conversely, if $Ag<Am<Af$, then Ag is the smallest diffraction angle for that edge.

Case 3: If $Am<Af$ and $Am<Ag$ then a successive algorithm that defines mid points between Am and Af or Ag as appropriate is employed iteratively until the solution converges upon the smallest angle. The criteria for this convergence are set to be a minimum change from one angle solution to another, 0.1° is suitable.

In this way, the minimum diffraction angle for the entire object profile is found. However, an organised list of all minimum angles for each edge within the object profile must be retained. A maximum diffraction angle value is provided in the simulator settings file. If the minimum possible diffraction angle, computed within this step, is above the provided threshold, then no diffraction is expected to rake place from this satellite on the structure under consideration. If this is the case, then Step 6 is omitted.

Step 6: LOS assessment for diffracted propagation

Although the edge profile has been successfully determined, and the minimum diffraction angle across the edge profile is determined, it may be the case that an obstruction exists in the receiver to diffraction point zone, or in the diffraction point to satellite zone. For this reason, the detailed availability algorithm, as described in 4.5.2, is employed. Each receiver to diffraction point and diffraction point to satellite LOS is tested, starting with the scenario that displays the smallest diffraction angle. The process is halted when a clear propagation channel is established.

Step 7: Next satellite

Steps 2 to 6 are performed for each satellite above the elevation mask angle. The diffraction model is only applied to satellites with an obstructed LOS.

4.7.3 Failure Modes and Special Cases

The described algorithm performs well in the general case. Consideration of a specific case under which the algorithm will fail, is now made. The contingency for this occurrence is described.

Diffraction model special case: Extremely low elevation angles

The diffraction algorithm relies upon the projection of structures onto a plane defined by the user position. If the elevation of the satellite from which the projection is made is extremely low, then the algorithm is likely to fail as the extents of the projected object outline tend toward an infinite distance from the receiver. The elevation angle at which this occurs is a function of the geometrical configuration of the situation under consideration.

In the event that this situation occurs, a null result is produced. However, it will be clear from employment of the Fresnel zone analysis, that a diffracted propagation is likely. The Fresnel zone analysis model employs a similar projection strategy to the diffraction model, however, it is unaffected by this problem.

4.8 Specular Reflection Model

Reflection of GNSS signals by objects surrounding the receiver can result in the reception of a satellite signal even if the LOS is obscured and reception via diffracted propagation is impossible. If the LOS path is clear, then the reception of time-delayed reflected copies of the original GNSS signal will lead to multipath. Aspects of the reflected propagation mode, including a full description are provided in section 3.1.4. A discussion regarding the conditions for reception of the reflected signal, including the effect of polarisation is also given. Irrespective of these issues, the simulation of GNSS signal propagation requires an appropriate means to predict the reflection of signals.

4.8.1 Problem Statement

Given that the occurrence and subsequent range measurement disruption of the reflected signal is to be accounted for, a means to predict the presence and properties of this propagation mode is required. With knowledge of satellite positions, receiver position and the geometry of objects surrounding the receiver, a method for the prediction of reflecting surfaces that can re-radiate the GNSS signal is sought. In common with the other propagation models presented in this thesis, this problem begins with the organisation and processing of vast geometrical datasets in order to achieve the desired objective. The inclusion of material characteristics would permit the estimation of signal attenuation following reflection. In this case, a diffuse reflection model could be applied in order to characterise signal scatter upon reflection. Current models of urban environments lack suitable description of material attributes. Consequently, any attempt to assess the signal attenuation upon a reflection would be of little value. However, it is desirable that an estimate of the total area available to re-radiate signal energy be included in the reflected propagation model. This can then be compared to the expected required surface area according to the incident signal Fresnel zone, the principles of which are described in section 3.1.4. A single reflection only model is required, this is consistent with the findings of Ercek [Ercek et al., 2006] where the signal power contribution of primary reflections was observed to be of most significance. Also, at this stage, only specular reflection is considered. This decision is taken for two reasons, firstly, most reflected signal energy is likely to result from the specular reflection mode. Secondly consideration of diffuse reflection requires intimate knowledge of surface material attributes. In addition, consideration of any other model than specular, for a

computational engine that works with environments containing so many geometrically modelled objects would be infeasible at this stage.

4.8.2 Reflected Propagation Model

A three stage technique is presented for the rapid and efficient determination of the surfaces within a model of any size that could give rise to a reflection. The list is referred to as the *candidate list of surfaces for reflection*. As the ratio of the number of surfaces that cause multipath effects compared to the total number of surfaces in an entire city model is extremely low this process begins with the organisation of model data within memory as shown in Figure 4-22.

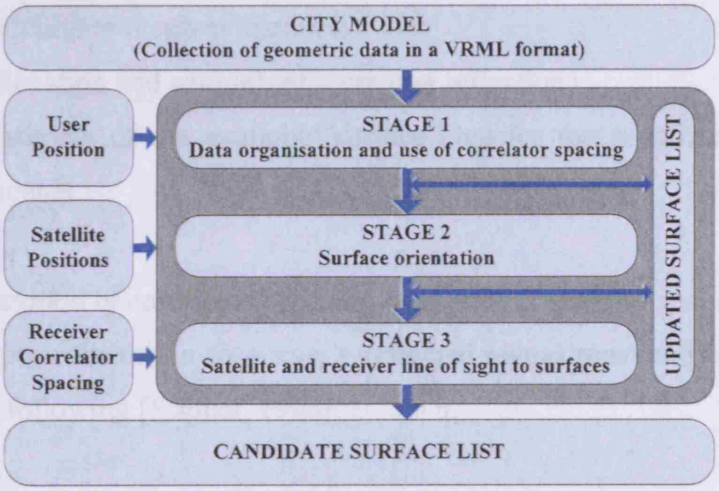

[Bradbury et al., 2007]

Figure 4-22: Three stage technique for determining candidate reflectors

Within this stage, use of the receiver specification in the form of the correlator spacing is made. This acknowledges the differences in response to multipath of different receiver correlator implementations. Surface orientation is assessed during stage two, and surfaces with outward facing normals that render the surface inadequate for signal reflection, with respect to the geometrical configuration of the satellites, objects and the receiver, are rejected. Finally, once an initial list of candidate reflectors is found, by virtue of geometrical properties, a check needs to made that there exists an unobstructed LOS between the receiver and reflection point and the reflection point and the satellite. This is in common with the final stage of the diffraction model, and is of particular importance in densely built urban environments. A full constellation of above horizon satellites is to be considered. The three-stage technique will now be described in detail.

Inputs

1. Geometry only file (section 4.4.2).
2. Satellite positions (section 4.3.4).
3. User position (section 4.3.3).
4. Correlator spacing.

Output

1. List of surfaces predicted to cause a specular reflection.
2. Corresponding reflection point coordinates.
2. Increased path length of the reflected signals with respect to the true satellite to receiver distance.
3. Elevation and azimuth of incoming reflections.
4. Estimate of the available surface area for the re-radiation of reflected signals.

Step 1 – Consideration of candidate reflector range and correlator spacing

For correlation peak distortion to occur, a reflected signal must exhibit a path length according to the following [Kaplan, 1996]:

$$P \leq 1 + \frac{\tau}{2} \qquad \text{(eqn. 2-1)}$$

For C/A code: $$R = P \times ChipLength(C/A) \qquad \text{(eqn. 2-2)}$$

For P code: $$R = P \times ChipLength(Pcode) \qquad \text{(eqn. 2-3)}$$

P = Difference between direct and reflected signal path lengths (chips).

τ = Correlator Spacing, generally 1 for Standard, 0.1 for Narrow (chips).

R = Range measurement error (m).

A pointer to the geometry file location of each urban object is stored in RAM following the process described in section 4.4. More specifically, the pointer is referenced to the file locations of the information regarding the extents of each object. The object extents held in the geometry-only file are inspected by jumping to the file locations, and each building number is subsequently stored in memory or disregarded depending on the distance between the receiver and the furthest object point with reference to P. The original VRML geometry data has now been organised such that rapid assessment of the

geometry can be made. Further to this, the specification of the receiver hardware that will have a bearing on the code correlation process (correlator spacing) has also been accounted for. A local environment now exists, defined in terms of the list of objects that could contribute to code multipath. Each of these objects is likely to consist of many thousands of surfaces, each of which is now a member of the current candidate surface list. The following stages describe the reduction of this list.

Stage 2 – Surface orientation

The orientation of every surface within the candidate surface list, relative to the receiver and to every satellite above the horizon, must be tested to determine whether or not it can act as a reflector. At this point, if an antenna that rejects signals below a specified elevation mask is to be considered, surfaces with all coordinate points existing below the mask angle can be discarded. Figure 4-23 below shows the general scenario for testing a surface within a candidate object, and introduces the notation used.

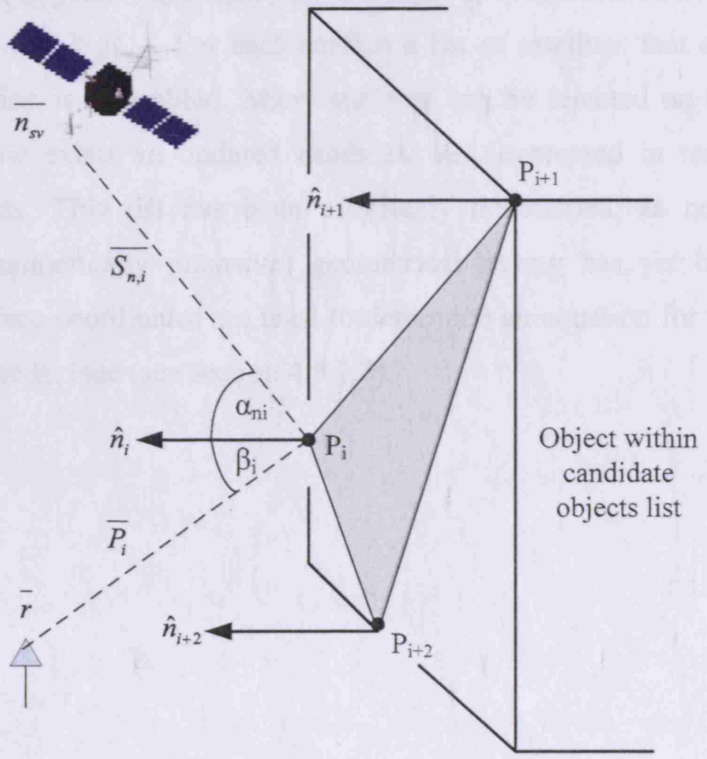

Figure 4-23: Surface rejection by orientation

For each satellite ($\overline{n_{sv}}$) above the horizon at the simulation epoch, the following are determined for each surface point (i):

1. $\bar{r}$ Receiver position.
2. $\overline{n_{sv}}$ Satellites above horizon.
3. $\overline{S_{n,i}}$ Satellite (n) to surface point (i).
4. $\overline{P_i}$ Receiver to surface point (i).
5. $\hat{n}_i$ Surface normal at surface point (i).
6. β_i Angle between $\overline{P_i}$ and $\hat{n}_i$.
7. α_{ni} Angle between $\overline{S_{n,i}}$ and $\hat{n}_i$.

$\hat{n}_i \bullet \overline{P_i}$ yields β_i. A value greater than or equal to 90° means that the receiver is behind, or positioned on the plane described by the surface, and therefore the surface is immediately rejected. The following is then performed for each satellite above the horizon. Angles α_{ni} and β_i are collected for each point describing the surface. These are then assessed to yield α_{max}, α_{min}, β_{max} and β_{min}. Specular reflection cannot occur if $\alpha_{max} < \beta_{min}$ or if $\alpha_{min} > \beta_{max}$. For each surface a list of satellites that could result in a multipath reflection is assembled. Many surfaces can be rejected on the basis of the above. There now exists an updated candidate list, expressed in terms of surfaces instead of objects. This list has been efficiently determined, as no rigorous (and therefore more numerically intensive) geometrical testing has yet been performed. Three of the surface coordinates are used to determine an equation for the plane which is described by the surface (see section 4.5.1.3).

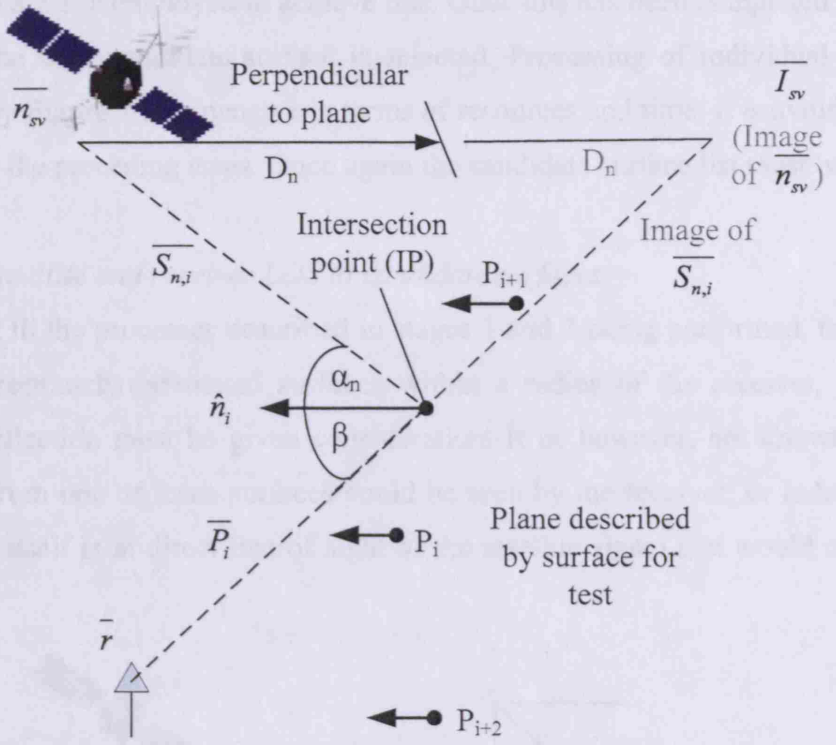

Figure 4-24: Intersection calculation

8. $\overline{I_{sv}}$ Image of satellite above horizon.
9. D_n Perpendicular distance from $\overline{n_{sv}}$ to plane described by surface points.
10. $\overline{Q}$ Intersection point of $\overline{S_{n,i}}$ with plane described by surface points.

Figure 4-24 illustrates the process whereby an intersection point ($\overline{Q}$) on that plane is sought. $\overline{Q}$ is described as the point at which $\alpha_{ni} = \beta_i$ on the plane described by the surface under test. This is done by first calculating the Cartesian position of the mirror image of $\overline{n_{sv}}$ in the plane, denoted by $\overline{I_{sv}}$. A vector between $\overline{I_{sv}}$ and $\overline{r}$ is now established. It is then possible to determine the point at which this vector intersects the plane ($\overline{Q}$), by using parametric equations and knowledge of the perpendicular distance between $\overline{n_{sv}}$ and the plane. Finally, a point in polygon test, such as that described by Taylor [Taylor, 1994], is employed to reveal whether $\overline{Q}$ exists inside (valid surface) or outside (invalid surface) of the area bounded by the vertices of the surface under test. In order that a point in polygon test can be performed, it is necessary to transform all polygon points and $\overline{Q}$ into a 2D space. The same mathematical procedure as described

in section 4.5.2.3 is employed to achieve this. Once this has been completed for all valid satellites, the next candidate surface is selected. Processing of individual surfaces as described by Figure 2 is expensive in terms of resources and time. It is avoided as far as possible by the preceding steps. Once again the candidate surface list must be updated.

Stage 3 – Satellite and receiver LOS to candidate surfaces

Subsequent to the processes described in stages 1 and 2 being performed, there exists a list of appropriately orientated surfaces within a radius of the receiver, such that a resulting reflection must be given consideration. It is, however, not known whether a reflection from one of these surfaces could be seen by the receiver, or indeed, whether the surface itself is in direct line of sight of the satellite signal that would cause such a reflection.

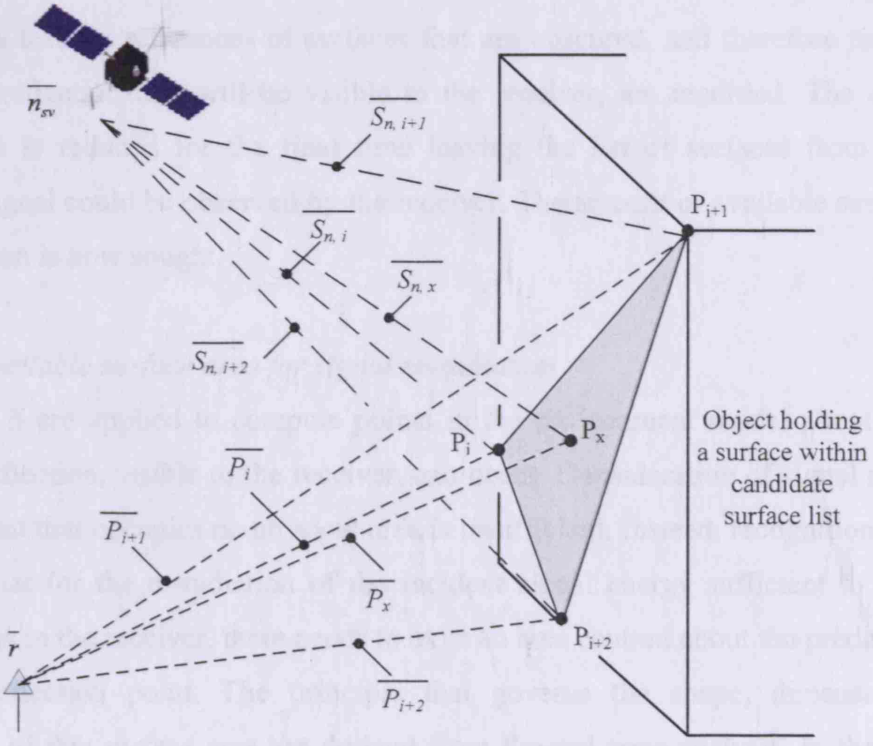

Figure 4-25: Surface LOS testing

Stage 3 deals with this, the most computationally intense part of determining the reflected propagation. LOS testing must now be performed for receiver to reflection point $\overline{Q}$ and for $\overline{Q}$ to the satellite emitting the incident signal. In addition, as a first pass at determining how much of a surface is available to re-radiate the signal, every point of every polygon held within the candidate surface list can be tested for line of sight to the receiver, and then to each satellite. In addition, to mitigate the risk of failure due to the

fact that it is possible that the line of sight to all points is obstructed, but that the receiver can still see a portion of the surface, a mid point (P_x) is also determined and tested. This situation is unlikely to occur, but must be accounted for. More artificial points could be established and tested if it is found that failures occur. With reference to Figure 3, vectors $\overline{S_{n,i}}$, $\overline{S_{n,x}}$, $\overline{P_i}$ and $\overline{P_x}$ are to be tested for intersection with any other surface in the entire city model. The coarse and detailed LOS algorithms (see section 4.5) are reused at this stage for determining the reflecting surfaces. A collection of vectors, (e.g those shown in Figure 4-25) are taken and assessed against all of the objects in the whole model at a coarse level. This is done by again using the extents of the object coordinates, and rapidly concludes if intersection between any of the vectors and objects is likely to occur. Detailed testing of individual surfaces within the identified objects, for intersection with each vector is then feasible. Throughout the above LOS testing, references of surfaces that are obscured, and therefore not able to provide a reflection that will be visible to the receiver, are recorded. The candidate surface list is reduced for the final time leaving the list of surfaces from which a reflected signal could be observed by the receiver. The amount of available surface area per reflection is now sought.

Step 4 – Available surface area for signal re-radiation

Steps 1 to 3 are applied to compute points in the environment model about which a specular reflection, visible to the receiver, can occur. Consideration of signal reflection about a point that occupies no physical area is insufficient. Instead, recognition needs to be made that for the re-radiation of the incident signal energy sufficient to induce a ranging bias in the receiver, there needs to exist an area centred about the predetermined specular reflection point. The principle that governs the shape, dimensions, and orientation of this surface area are derived from Fresnel zone analysis. In the point to point signal propagation case, all signal energy arriving from any point within the first Fresnel zone will contribute constructive signal energy to which the antenna will respond. This can be extended to encompass the energy originating from signal reflection about a planar surface. Provided the additional path length travelled by the signal, along the incident plus reflected path, is less than or equal to the incident plus reflected length at the reflection point plus lamda/2, then reflected signal energy will constructively interfere with the received reflection. A diagram and the appropriate equations for this principle are given in section 3.1.4.

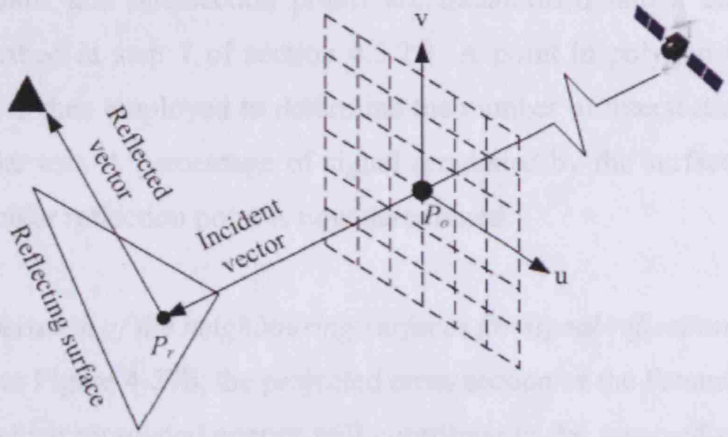

Figure 4-26: Terms and geometrical constructs used to determine the available surface area for signal re-radiation

A modified version of the Fresnel zone analysis model (section 4.6) is employed for this purpose. Again, a planar grid of points is established. This grid is orientated orthogonally with respect to the signal transmission path, in this case, the incident signal path. The grid describes points of origin for a number of lines that are contained within the Fresnel zone, and these lines are tested, in this case for intersection with the surface containing the reflection point, as shown in Figure 4-26. Some important points must be noted. The radius of the Fresnel zone that is used to select the lines for test, based upon the dimensions of the zone, must be calculated at point P_r, as this is where the result is required for. However, in order for the intersection test to be applied correctly, the origin of the lines (planar grid) must be positioned such that it exists without interacting with the surface under test, an arbitrary distance is selected, resulting in point P_o. Specular reflection will only occur for incident angles (measured with respect to the surface normal) of >0°. Therefore the intersection pattern with the plane described by the reflecting surface will always be that of an ellipse, as shown in Figure 4-27.

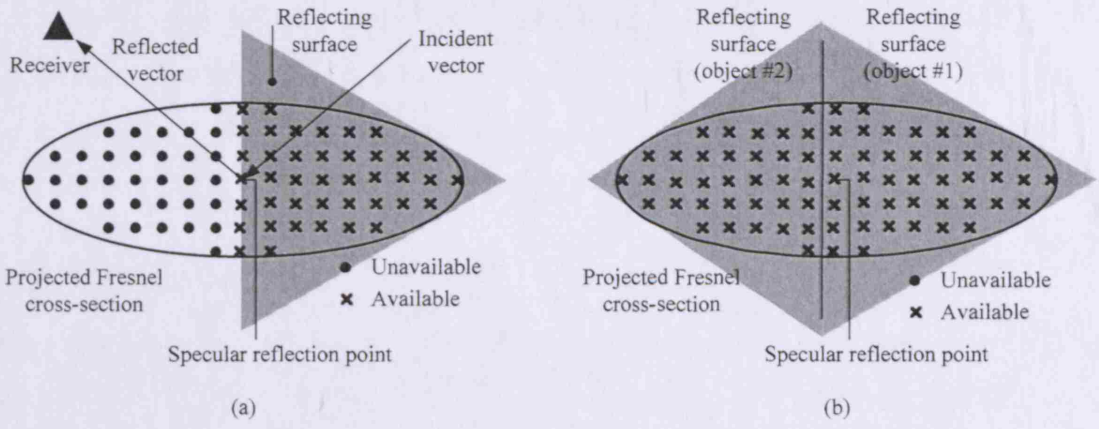

Figure 4-27: Projected incident signal (Fresnel zone cross section)

All polygon points and intersection points are transformed into a 2D space, by the procedure described in step 7 of section 4.5.2.3. A point in polygon test (see Taylor [Taylor, 1994]) is then employed to determine the number of intersection points within the surface under test. A percentage of signal reradiated by the surface containing the established specular reflection point is now determined.

Step 5 – Consideration of the neighbouring surfaces for signal reflection

With reference to Figure 4-27b, the projected cross section of the Fresnel zone describes the area from which reradiated energy will contribute to the received signal. This area may overlap onto several surfaces. Furthermore, these surfaces may belong to other physical structures. A further process is described to estimate the surface area held by neighbouring surfaces to the surface containing the specular reflection point. A proximity test (from the specular reflection point) is first employed to seek out the applicable neighbouring surfaces. Each of these surfaces must be similarly orientated to the original surface in order that energy is reradiated in the same direction. Intersections with the grid array are then performed for these neighbouring surfaces and an estimate of their contribution is also made. The addition of the primary surface percentage, and that of the neighbouring surfaces must not exceed 100% or an error has occurred.

It should be understood that steps 4 and 5 offer a practical solution to an extremely complex geometric problem. It is not expected that all special cases are accounted for by the above method. An expansion to the above method would produce a more reliable solution, on the basis of a study of the special cases. For these reasons, the described process offers an indication only, of the available surface area, and should be treated as an approximation.

4.9 Code Multipath Model

Increases in the sophistication of environment model data collection and model construction, means that it will soon be possible to derive material types and associated properties from later versions of the environment models used in this research. With this in mind, there is an imperative to extend the simulator capabilities, such that corrections to predicted pseudoranges, operating in multipath environments, will be possible. The current lack of material information leaves two unpredictable properties of the reflected signals.

1. Signal attenuation upon reflection.
2. Change in signal polarisation upon reflection (a function of dielectric constant of reflecting material and incident angle [Spilker, 1996, vol1 p.332].

Without the ability to calculate the above parameters, a meaningful estimation for the effect of the presence of reflected signals on the range measurement process is impossible. However, an estimate as to the significance of reflected signals upon the range measurement can be made. By using the information provided following application of the models described above, three very important parameters are established.

1. The number of sources of reradiated signals visible to the receiver.
2. The extended path length of all signal copies.
3. The elevation and azimuth of the reflected and diffracted signals.

The severity of the multipath environment can thereby be assessed using the above. To achieve this, a generally accepted correlator model is used. The code correlation model is presented in section 3.2.3.1 and can be found in Nelson [Nelson et al., 1997] and also in Jones [Jones et al., 2004]. Although no direct comparison with observation data is possible, mapping the predicted multipath severity over an area is a desirable output of the simulator, and is addressed in section 9.

4.9.1 Problem Definition

The observed geometric range between the receiver position and a satellite will be contaminated by multipath, resulting from the presence of reflected and diffracted signals. Several, but not all, properties of the reflected and diffracted signals are

predicted by reflection and diffraction models applied in the simulator. Using these predictions, a correction to the geometric range is required. The computation of these corrections must be based upon the workings of a GNSS receiver. As there are many designs of GNSS receivers, a generic receiver model is assumed.

4.9.2 Range Correction in the Presence of Disrupted Signals

The computation of range error is based upon the principles detailed in section 3.2.3.1. An estimate of the magnitude and form of correlator peak disruption is sought. The LOS signal and reflections are combined to form a composite correlator peak. Subsequently, a mathematical process that models the application of correlator peak samples in a receiver can be applied.

Inputs (per satellite receiver pair)

1. Geometric range (satellite to receiver).
2. Reflected and diffracted signal extra path lengths.
3. Reflected and diffracted signal elevation and azimuth values.
4. Arbitrary phase shift.
5. Arbitrary attenuation factor (*w.r.t.* LOS signal).

Output

1. A correction to the true geometric range, that accounts for the effect of multipath.

Step 1 – Constructing the independent variable axis

The composite function will be formed from the summation of all samples of LOS and reflected signals over a period of time. As with a receiver correlator, this period of time, or correlator window, is two chip widths. The peak occurs at the half way point. This is described by equation 3-5, section 3.2.1. As such, a sample interval is required. This is defined within the settings file (see section 4.3.3), and is typically set to be 1000 samples per chip space. The independent variable axis is therefore 2000 units in length. The axis, referred to as the x axis, is expressed as ranging from -1000 to 1000.

Step 2 – Formation of the LOS function

A triangular LOS response ranging from -1000 to 1000 along the x-axis, with peak at zero is modelled. The maximum output is 1, and a linear response is modelled. An array of two thousand elements holds the LOS y-axis value at each sampled point. The LOS response within the correlator model is presented in Figure 4-28.

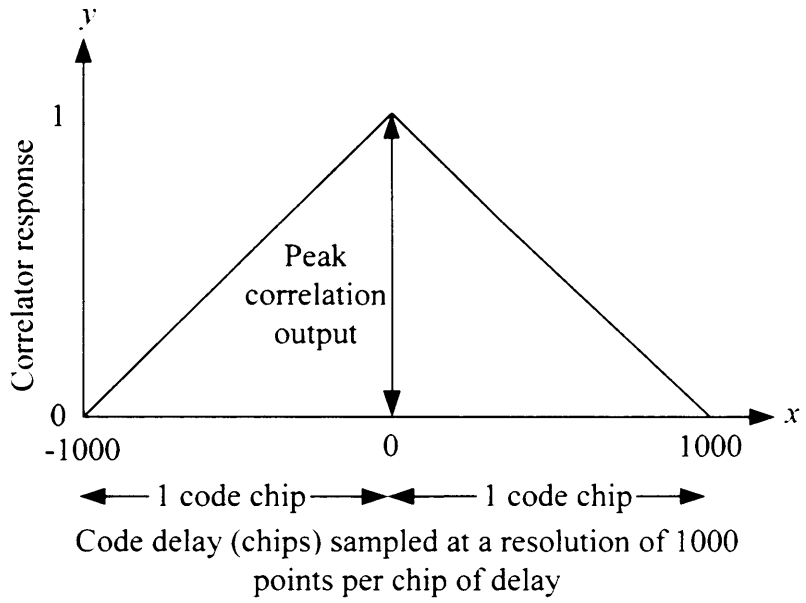

Figure 4-28: Formation of the LOS correlator model response

Step 3 – Provision of the reflected and diffracted signals

The reflected and diffracted signals are time delayed and attenuated copies of the LOS signal. A time delay is computed from the extra path length predicted during propagation modelling, and is then converted into a delay in code chips, as follows:

$$t_{code} = \frac{path\_delta}{chip\_length} \Rightarrow \qquad t_{C/A} = \frac{path\_delta}{293.05} \qquad t_P = \frac{path\_delta}{29.31}$$

(eqn. 4-58) (eqn. 4-59) (eqn. 4-60)

T_{code}	=	Code delay (chips).
$t_{C/A}$	=	C/A code delay (chips).
t_p	=	P code delay (chips).
path_delta	=	Extra path length travelled by reflected or diffracted signal (m).
chip_length	=	Physical length of one code chip.

The attenuation factor (see section 4.3.3) is applied such that the peak value of the reflection or diffraction response is that of the attenuation factor value (as LOS peak is 1). In addition, if antenna gain pattern is to be accounted for, then the reflected/diffracted signal is further scaled according to the antenna gain pattern as presented in section 4.3.6. If a phase reversal is desired (see section 4.3.3), then this is achieved by inverting the attenuation factor. A y-axis function is then computed, assuming a linear response whereby the correlation value (y) will increase from zero to the scaled maximum value over the period of one chip (starting at the appropriately delayed x value). Over the second chip (starting at the appropriately delayed x value plus one chip), the linear response will decrease from the maximum scaled value to zero over the one chip period. Individual arrays are used to hold each reflected and diffracted y-axis value.

Step 4 – Formation of the composite function

The composite value, at a specific value of x, is the sum of all signal samples at x.

$$C(x) = \sum_{n=0}^{n} R_n(x) \qquad \text{(eqn. 4-61)}$$

Where:

C	=	Composite function.
R	=	Response due to reflected/diffracted signal.
n	=	The total number of signal copies from reflection/diffraction.

The composite function is then stored in an array in the same manner as the individual signal functions.

Step 5 – Application of code correlators

Three correlators are applied in order to establish the signal time of flight. The peak of the correlation function is detected by applying early and late correlators that are separated by the specified correlator spacing. As the correlation function is triangular (excepting the distortion caused by additional signal copies), only one point on the correlator function will exhibit this separation. The correlation peak will be at the centre of this separation, and is detected by application of the prompt correlator. The correlator spacing given in the settings file (see section 4.3.3) is observed to set the correlator separation. A progressive test of all samples in the composite function is applied. Starting from the beginning of the x-axis, samples that are one correlator space apart are

compared. The difference in the sample value is recorded and the test window moves to the adjacent samples until all samples are tested. The recorded differences are checked and the minimum recorded difference indicates the sample position at which the peak occurs. This is represented in Figure 4-29.

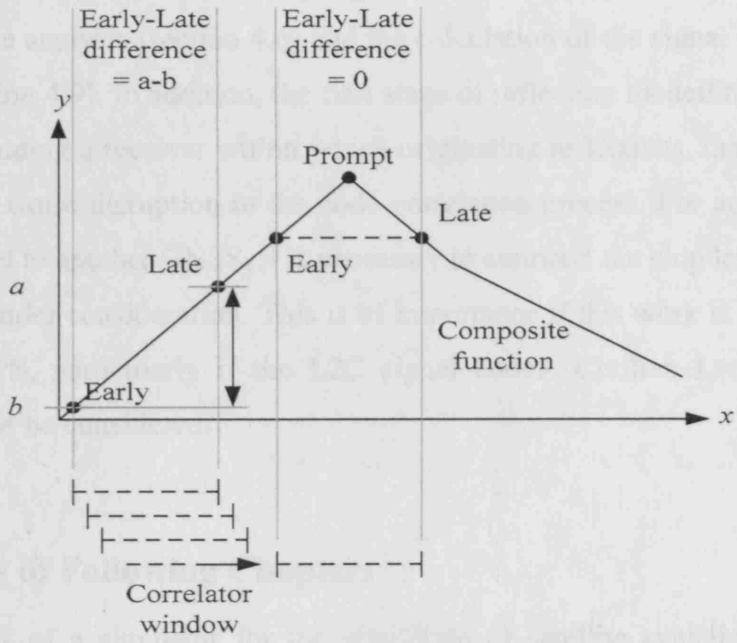

Figure 4-29: Detection of the composite function distorted peak

In this way, a generic model for the operation of a reciver under multipath conditions is created. Due to differences in the design of receivers between manufacturers, the model will not necessarily provide results that are consistent with the performance of an individual receiver. The commercial sensitivity that surrounds receiver design and the complexity of signal processing are barriers to obtaining details of the exact specification and operation of an individual receiver. This however, is not necessarily important. The generic model described above is based upon the operation of GNSS receivers and will deal with the presence of multipath signals (from reflection and diffraction), with a variety of time delay and attenuation charactristics relative to a received LOS signal. As such it will provide a fair and appropriate means to determine the likely level of measurement distortion. Even if the magnitude of measurement error, determined by the correlator model, is not consistent with that which occus within a particular receiver, the application of this model for simulations performed over multiple positions will allow relative determination of signal disruption at individual positions. This allows signal degradation to be mapped over a specified area. The same applies for simulations performed over multiple epochs at a single location, where the disruption due to multipath is being examined over time.

4.10 Consideration of GPS and Other Systems

It is possible to apply this work equally to any GNSS, provided that necessary alterations to the signal frequencies under consideration are made within the software simulator. Although no rigorous electromagnetic propagation modelling is undertaken within this work, the frequency of any signal under consideration is required for both the Fresnel zone analysis (section 4.6) and the calculation of the signal footprint during reflection (section 4.9). In addition, the first stage of reflection modelling is to calculate the area surrounding a receiver within which originating reflections, that may reach the receiver, could cause disruption to the code correlation process. For application of the reflection model to another GNSS, it is necessary to ammend the chip length of the code measurement under consideration. This is of importance if this work is to be applied to modernised GPS, particularly if the L2C signal codes (Civilian Long and Civilian Moderate) are to be considered.

4.11 Preview of Following Chapters

All components of a simulator for the prediction of satellite availability and GNSS signal propagation, in environments described by computerised models, have been presented within this chapter. This is a logical point to detail the contents of the remaining chapters. Chapter 5 presents a description and the results of testing undertaken on various components of the simulator. Chapter 6 details the assessment of city model data, before chapter 7 validates the signal propagation models within the simulator by analysis of simulation results compared to real world observations. Chapters 8 and 9 present availability and reflection modelling results varied over space and time, before chapter 10 details some performance aspects of the simulator. Conclusions are presented in chapter 11.

5 SIMULATOR VERIFICATION

With reference to Figure 4-3, each component of the simulator has been tested in isolation and as an integrated part of the whole simulator during a verification stage.

5.1 Verification Definition

For the research presented in this thesis, the definition of verification is now given. The verification stage is comprised of a number of individual tests. Testing assesses how well the individual simulator components perform with reference to anticipated performance and defined benchmarks. These tests establish that the expected response is obtained from individual elements of the simulator. Tests performed during the verification stage can make use of artificial data. This step is necessary to identify potential strengths and weaknesses before the simulator output is compared with observed data as part of the validation stage and for the generation of final results.

5.2 Objective

The objective of the tests performed on the simulator software is to ensure the following:

- Correct operation of the software.
- Weaknesses in the implementation of the algorithms and models are identified.
- Special cases and unforeseen problems that may not have been envisaged during the methodology design stage are identified.

5.3 Approach

Each component of the simulator requires a different test strategy. This is due to the complexity of the algorithms and models implemented, the number of simulation specific parameters (see section 4.3.3), and also the numerous modes of operation that can be selected. The approach is therefore different for each simulator element. In the first instance, each component is considered as a unique system. A set of inputs are chosen and their associated results are determined using independent software, hand-worked solutions, spreadsheets (e.g. using Excel [Microsoft, 2003]), published results, etc. Correct operation is then verified by comparison of the simulator component output with the calculated result. Some simulator components are tested with data as a one-off procedure following their development. However, the simulator employs a battery of tests during operation to ensure that the individual components are producing correct

results. There are also tests that are performed following simulation to verify that the obtained results are realistic. Description of the three test procedure groups is provided below.

Procedure name	**Specifics**
One-off procedure	Generally performed following software development. Often uses artificial data. Accompanied by runtime procedure(s).
Runtime procedure	Performed on the data within a simulation during runtime. Includes routines written specifically for test. *Gross error checks* - where a failure would be detected if a result was significantly outside of a typical range, normally indicating a computational error in the simulator software coding. These tests are usually applied to interim results during a computational procedure. *Breach of threshold checks* - where results are compared with expected ranges for the parameter under test. Usually applied to the final result of a computation.
Subsequent procedure	Numerical or graphical data produced by simulator for subsequent checking.

5.4 Simulator Verification

5.4.1 Reference Frame Transformation Parameter Calculation

5.4.1.1 Objective

The imperative for performing simulation within an environment model space is stated in section 4.3.5. A test is required to ensure correct operation by the software to calculate transformation parameters between ETRF89 coordinates and the environment reference frame (a full description is provided in section 4.3.5).

5.4.1.2 Test Procedures

(One-off procedure)

Two sets of corresponding coordinates are provided in the settings file (section 4.3.3). One set is expressed in ETRF89 (for datasets in Europe), and the other set is comprised of the corresponding coordinates in the environment model reference frame. A seven parameter 3D conformal transformation model is determined from the coordinate data using least squares analysis. To test the operation of the software that computes the seven transformation parameters, the following is performed. Using the Rhinoceros [Robert McNeel and Associates, 2001] CAD tool, individual artificial structures can be created and grouped. The original geometry data is then exported to a raw triangles (.raw) file format which contains only coordinate data. The original model is then manually transformed within the Rhinoceros tool into a separate, arbitrarily chosen coordinate system. A second geometry file in the raw triangles (.raw) format is then created. The same model (collection of geometric artifical structures) now exists in two different reference frames. Corresponding coordinates can be extracted from both geometry files, and these are then fed to the reference frame transformation component of the simulator. The parameters to transform between one space and the other are then determined, an example of which is provided below.

REFERENCE FRAME TRANSFORMATION PARAMETERS		
Scale:	0.9998461525	
Translation X:	-962.259	units
Translation Y:	20989.250	units
Translation Z:	-6364109.050	units
Rotation about X (Omega):	2.470	radians
Rotation about Y (Phi):	3.158	radians
Rotation about Z (Kappa):	1.593	radians

The post-fit residuals of this process are then examined to ensure that the software has operated correctly. An example is provided below.

REFERENCE FRAME TRANSFORMATION RESIDUALS				
XYZ	REF FRAME 1	REF FRAME 2	COMPUTED 2(m)	RESIDUAL(m)
X	3977685.176	-227.533	-227.534	-0.001
Y	-5804.628	-123.027	-123.026	0.001
Z	4969217.290	26.542	26.548	0.006
X	3977450.542	-77.658	-77.662	-0.004
Y	-5646.768	169.832	169.827	-0.005
Z	4969386.059	12.482	12.491	0.009
X	3977757.686	-231.908	-231.907	0.001
Y	-5809.871	-152.136	-152.141	-0.005
Z	4969261.913	106.603	106.595	-0.008
X	3977495.588	-116.408	-116.403	0.005
Y	-5684.605	206.692	206.701	0.009
Z	4969503.659	132.600	132.593	-0.007

The above test is also applied each time a new environment model dataset is used, as a new set of corresponding ETRS89 and environment model space coordinates are required. The output shown above is presented in the simulation results file (section 4.3.8) for all single simulations performed.

(Runtime procedure)
Determined parameters and residuals undergo a gross error check during simulation.

5.4.2 Transformation of Receiver Position into Model Reference Frame

5.4.2.1 Objective

The receiver position, presented to the simulator from the settings file, is expressed within the environment model reference frame. However, the receiver position will initially be determined (by survey) in a terrestrial reference frame (e.g. OSGB36). As the model is transformed from the initial reference frame (e.g. OSGB36) to the environment model reference frame manually, and therefore by a separate process, it is reassuring to check that the manual process by which the receiver is transformed into the model space, is performed correctly.

(Subsequent procedure)
A graphical output is produced by the simulator (see section 4.3.9). This can be used to verify that the receiver is correctly positioned with reference to the surrounding objects.

5.4.3 Satellite Positions in ITRS2005 Realisation of ITRS

5.4.3.1 Objective

For each simulation epoch, satellite positions are initially computed in the ITRS2005 realisation of the ITRS. Although significant errors in satellite position would become evident very quickly, one-off and runtime test procedures are considered prudent.

5.4.3.2 Test Procedures

(One-off procedure)
The primary method for calculation of satellite position and satellite clock information, for the simulator, is via interpolation of SP3 file data (see section 4.3.4). Following development of this element of the simulator, satellite positions were determined at fifteen minute intervals. These positions can be compared with corresponding epochs in the original SP3 data.

(Runtime procedure)

It is preferable to present the simulator with both SP3 and an ephemeris file (BRDC or broadcast navigation file). In this case, satellite positions will be computed by SP3 interpolation and also computed using the ephemeris parameters. A comparison of the two is then performed. An error is flagged if a significant (>100m) discrepancy is in satellite position is detected. A large figure is used as this is only a coarse check to ensure no major miscalculation has occurred. This check takes place for every satellite in every epoch of simulation.

(Subsequent procedure)

Azimuth and elevation values produced by the simulator can be compared with the same information computed by an independent software package. Examples of such packages used during this research include Leica GeoOffice [Leica Geo Office, 2005], and SimGEN software [SPIRENT Communications, 2004] (for the control of SPIRENT hardware simulators).

5.4.4 Satellite Positions in the Model Reference Frame

(Runtime procedure)

The receiver position is known at the outset, expressed in the ITRF2005 realisation of the ITRS. Satellite positions are initially computed, by the simulator, in the same system. During runtime the true geometric ranges between the receiver and each satellite are computed. The receiver and the satellite positions are then transformed into the model reference frame, and again the ranges are computed. The real-world ranges are compared with the model space ranges and a threshold test is applied. It should be noted that any scale factor within the transformation parameters will affect the range, and so the calculation becomes:

$$D = \left(\left(\frac{R_m}{R_{ITRF2005}} \right) - Scale \right) \times R_m \qquad \text{(eqn. 5-1)}$$

Where:

D	=	Discrepancy in range (m).
Rm	=	Satellite to receiver range (m) in model space.
$R_{ITRF2005}$	=	Satellite to receiver range (m).
$Scale$	=	Scale factor determined during transformation parameter calculation.

The scale factor is that determined during the transformation parameter calculation, and should be close to the scale factor for the receiver position applicable to the mapping projection of the original national coordinate system (if applicable). The quality of this figure, with reference to the true scale factor, is dependent upon the quality of the environment model. Again, this is a coarse check to ensure that no serious miscalculation has occurred within the software.

(Subsequent procedure)

With reference to section 4.3.8, the numerical output file contains satellite elevation and azimuth values. These can be compared with the output of commercial software. In this case, several epochs of different simulations were compared against two independent packages, Leica Geo Office [Leica Geosystems, 2005], and SPIRENT SimGEN [SPIRENT Communications, 2004].

PRN	Elevation	Azimuth
11	26.098	145.497
17	40.147	245.968
20	63.928	74.872
30	0.73	5.975
5	1.767	344.512
25	23.324	127.02
12	4.178	336.47
13	32.78	198.877
4	32.67	301.131
31	21.239	50.746
23	61.962	172.636
1	25.928	46.901

(a)

Chan	ID	Type	Echo	PRN	Elev	Azim
1	11*	GPS L1	-	11	26.1	145.5
2	17*	GPS L1	-	17	40.1	-114.0
3	20*	GPS L1	-	20	63.9	74.9
4	30*	GPS L1	-	30	0.7	6.0
5	5	GPS L1	-	5	1.8	-15.5
6	25	GPS L1	-	25	23.3	127.0
7	12	GPS L1	-	12	4.2	-23.5
8	13	GPS L1	-	13	32.8	-161.1
9	4	GPS L1	-	4	32.7	-58.9
10	31	GPS L1	-	31	21.2	50.7
11	23	GPS L1	-	23	62.0	172.6
12	1	GPS L1	-	1	25.9	46.9

(b)

Figure 5-1: Verification of satellite azimuth and elevation using SPIRENT SimGEN software

(a) Results from simulator developed for this research (b) SPIRENT SimGEN software

It can be seen that in the above example that the correct azimuth and elevation values are determined using the simulator. Furthermore, this has been performed in the model space, and therefore confirms that the transformation from the ITRS2005 realisation of ITRS into the model reference frame, for both receiver and satellite positions, has been performed correctly. It also confirms that the simulator is correctly applying GPST and that no errors in the treatment of PRN numbers are occurring. In addition, SimGEN provides predicted pseudoranges. These contain satellite clock error, and modelled

atmospheric errors. By applying the clock offset (determined from SP3 at the same time as satellite position) we can then compare the simulator pseudorange with the output from SimGEN. The ranges differ due to the addition of atmospheric models etc within SimGEN. However this range comparison test is good enough to ensure that the application of the light-time equation and appreciation of earth rotation during signal time of flight by the simulator is correct.

5.4.5 LOS Tests

5.4.5.1 Objective

The LOS algorithms, described in section 4.5, are used extensively throughout the propagation models within the simulator. It is imperative that these algorithms perform as expected. Tests using artificial data are required and must consider even the most difficult of geometrical configurations.

5.4.5.2 Test Procedure

(One-off procedure)

Using the Rhinoceros [Robert McNeel and Associates, 2001] CAD tool, individual artificial structures can be created, grouped and then exported into a VRML file. By selecting an appropriate receiver position within the group of structures, and fixing satellite positions, the most difficult geometric situations can be constructed. The LOS vectors can be visualised within the Rhinoceros tool. The simulator then independently predicts LOS availability. A comparison of the clear and obstructed vectors within Rhinoceros, and from the simulator, is then possible.

(Subsequent procedure)

With reference to section 4.3.9, a graphical representation can be produced by the simulator. All objects in the environment and the LOS vectors from satellite to receiver are presented in this output. This output can be examined to ensure that the LOS algorithms have not produced erroneous results.

5.4.6 Fresnel Tests

5.4.6.1 Objective

The procedure for estimation of the maximum cross-section obstruction of the first Fresnel zone is described in section 4.6. A vast amount of numerical data is processed in order to arrive at this estimation. The complexity and unique nature of each geometric configuration within this problem mean that there are few convenient tests that can be applied. Some simple tests are required to ensure that the algorithm is formulated and coded correctly

5.4.6.2 Test Procedure

(One-off procedure)

As with other propagation model tests, Fresnel zone analysis can be tested by the creation of artificial scenarios within a CAD tool such as Rhinoceros [Robert McNeel and Associates, 2001]. A single structure is created and exported to VRML. Satellite and receiver positions are then manipulated such that a range of geometrical configurations are tested.

(Subsequent procedure)

A VRML output showing the projected Fresnel cross section of the ground plane described by the user position (see section 4.6.2) can be produced. However, only one satellite to receiver pair can be tested. In addition, it can be difficult to view such a graphical output in urban environments that are densely populated with large structures. For these reasons, this VRML output is not included as a general option in the list of outputs of the simulator.

5.4.7 Diffraction Tests

5.4.7.1 Objective

Diffracted propagation occurring due to the interaction of an incoming signal with the profile of a building (described by the satellite to receiver configuration), is described in section 4.7. Tests are required that ensure the determined solution could feasibly give rise to such an event.

5.4.7.2 Test Procedure

(One-off procedure)

An artificial environment is created using a CAD tool such as Rhinoceros [Robert McNeel and Associates, 2001]. A single uniform structure is produced and exported to into a VRML format. A constellation of satellite positions and a receiver position are assigned, and the diffraction algorithms are tested. The generation of a VRML output file allows examination of the results. With reference to Figure 5-2, a plan view of the scenario can be examined. The dark rectangle shows the top of the artificial structure. The projection of the structure by incoming signals, as described in section 4.7.2, can also be seen. With respect to the given illustration, the yellow lines indicate diffracted propagation. A failure in the process can be detected using this method.

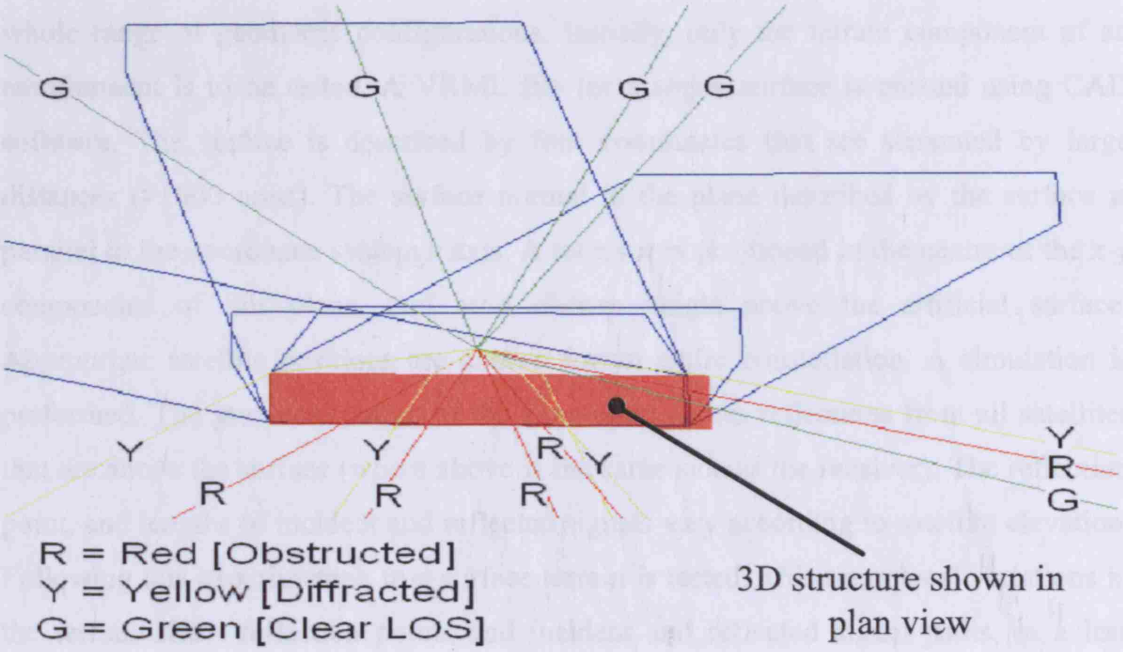

Figure 5-2: Diffracted propagation prediction test

(Subsequent procedure)

Following simulation, a graphical output, such as that of Figure 5-2 can be produced and checked. It should be noted that this becomes more difficult with an increased complexity in the modelled shapes. However, the test is still valid, and ensures that no errors have occurred. Such errors could include the determination of a diffracted propagation that is obstructed by objects separate to the diffracting object. The possibility of any such error can quickly be eliminated by inspection of the graphical output.

5.4.8 Reflection Tests

5.4.8.1 Objective

A single specular reflection model is implemented in the simulator, see section 4.8. The algorithms within the model must be capable of processing large environment models, employing the three stage technique as described in section 4.8.2. A set of tests ensures that the implementation of this technique is correct, and is sufficient for the task of establishing surfaces that could give rise to signal reflection that is visible to the receiver.

5.4.8.2 Test Procedure

(One-off procedure)

As with the other propagation models, use can be made of artificial data to rapidly test a whole range of geometric configurations. Initially, only the terrain component of an environment is to be tested. A VRML file for a single surface is created using CAD software. The surface is described by four coordinates that are separated by large distances (>1000 units). The surface normal to the plane described by the surface is parallel to the coordinate system z axis. A receiver is positioned in the centre of the x-y components of this plane, and at a chosen height above the artificial surface. Appropriate satellite positions are chosen for an entire constellation. A simulation is performed. The graphical output of the simulation shows reflections from all satellites that are above the surface (where above is the same side as the receiver). The reflection point, and lengths of incident and reflected signals vary according to satellite elevation. Following this experiment, a true surface terrain is tested. This time, local variations in the terrain affect reflection points and incident and reflected signal paths, in a less predictable way. Depending upon the standard deviation of the surface disruption, incident signals can be blocked by the local terrain for satellites with very low elevation angles.

(One-off procedure)

Following successful completion of the above tests, a simple artificial object is placed near to the receiver. The resulting simulated reflections are checked graphically and numerically.

(One-off procedure)

As an indication of correct operation, the number of surfaces that are excluded from the candidate reflectors list following each stage of the technique can be checked. It should be seen that stage one roughly halves the initial number of candidate reflectors. Stage two should then dramatically reduce this figure again, in order that the LOS stage has as few surfaces to deal with as possible.

(Subsequent procedure)

Each simulation (including multiple simulations) can be made to produce a graphical representation of the predicted reflections. This is checked to ensure that all reflections are viable.

6 ENVIRONMENT MODEL DATASETS USED IN THIS RESEARCH

In order to test the capabilities of the simulator when presented with different types of environment model, several different models have been exported from CAD formats into VRML. For the work presented in this thesis, two urban models are focussed on. This chapter describes the models that are used for validation of the propagation models and for generation of the results presented in this thesis. A description of the terminology surrounding model quality is first given. The approach toward the selection of individual model datasets for this work is provided. One of the two model datasets has been the subject of an extensive validation exercise (separate to the work presented in this thesis) to quantify aspects of model quality. The results of this validation, and their impact upon the accuracy of simulator results, are presented and assessed.

6.1 Factors Dictating the Quality of Environment Models

Any CAD model expressed in the VRML format can be used with the simulator. The quality of any model, with respect to geometry data only, is dictated by the following:

Quality of survey data

The absolute and relative position accuracy of all modelled objects within the dataset will affect the quality of the signal propagation predictions. This is especially true with regard to establishing the clear and obstructed LOS paths. With respect to the corresponding true objects, the orientation, scale and shape of the modelled objects describes the quality of the model.

Level of detail

The resolution at which the geometry data is captured during a survey will affect the quality of survey data as described above. For the extraction of geometry data by photogrammetric methods, a great deal of importance is placed upon how rigorous are the manual or automatic processes employed. Producers may decide to neglect objects below a certain size, or may choose to model some very complex components using geometric primitives. Additionally, the resolution at which data is exported from a CAD format into VRML is of relevance.

Geographical extents of model coverage

A relationship exists between the planimetric area covered by the model and the density of objects surrounding the simulated position. In dense urban locations, a small area may contain all objects that will affect signal propagation between the satellite and the receiver. As the density of objects around the receiver is reduced, a larger area must be considered. This is due to the fact that all propagation models are related in some way to the consideration of surfaces that are visible to the receiver.

6.2 Approach to Model Selection

The strategy adopted for the generation of results presented in this thesis is based upon the following requirements:

Datasets from different areas must be used

This requirement ensures that peculiarities that may be evident in one dataset, due to production techniques etc, do not affect overall conclusions. To ensure that peculiarities in a particular locality do not influence results, different areas are preferable.

More than one model of different qualities must be used

A tradeoff between the quality (in terms of extent and density) of a model and the simulator performance, in terms of processing time and resource useage exists. An interesting experiment is to assess the quality of results obtained using different environment models. It is not the intention of this research to rigorously assess the differences in simulator performance in terms of highest and lowest quality environment models. It is more important to gain an appreciation of the effect that different model quality might have on simulator performance. For this reason, the use of two models of different quality is considered acceptable. Further research might consider the rigorous assessment of simulator performance with different model quality, if it is considered beneficial to do so. It is likely that this would be the case when considering integrating such a software simulator into hardware, for example.

At least one model must be validated to assess the geometric data quality

Validation is an intensive activity, and requires vast resources in terms of man-hours and surveying equipment. Whilst working with what is considered to be a state of the art environment model, it is only necessary (in the case of this research) for one dataset to be validated. This is provided that all datasets employed have similar quality

characteristics and are believed to be produced using the same data collection and processing techniques. The results of validating one model can be used to form conclusions regarding the quality of other models produced by the same methods. Caution should be applied, as this is only true if the model datasets are located in the same general geographical area and have been produced by the same techniques. Most importantly, comparison of real world observations with simulated predictions, combined with a quantified assessment of the model quality, allows validation of the signal propagation models used within this work.

A model must be selected according to the desired severity of the environment

The most notable contribution of this work is the characterisation of the signal environment for a receiver operating in challenging locations. It is almost certain that applications of this work will be centred around signal prediction in dense urban environments. Therefore, selection of models that describe environments known to cause high levels of signal propagation disruption is considered appropriate. It is the intention of this work that an environment considered to be severely disruptive to signal propagation is used. Favourable results in such an environment would reasonably lead to the conclusion that results in more benign environments would be consistently good.

6.3 Overview of Models Used

Two urban models have been selected for the signal propagation model validation and for the generation of results, both of which are the subject of following chapters. The models have been selected such that the criteria outlined above are fulfilled as far as is possible. It is acknowledged that in some cases commercial sensitivity surrounds some details of some models with respect to exact production techniques etc, and that this impacts upon their fulfilment of the stated criteria. This section provides a description of the chosen models.

6.3.1 Dataset 1

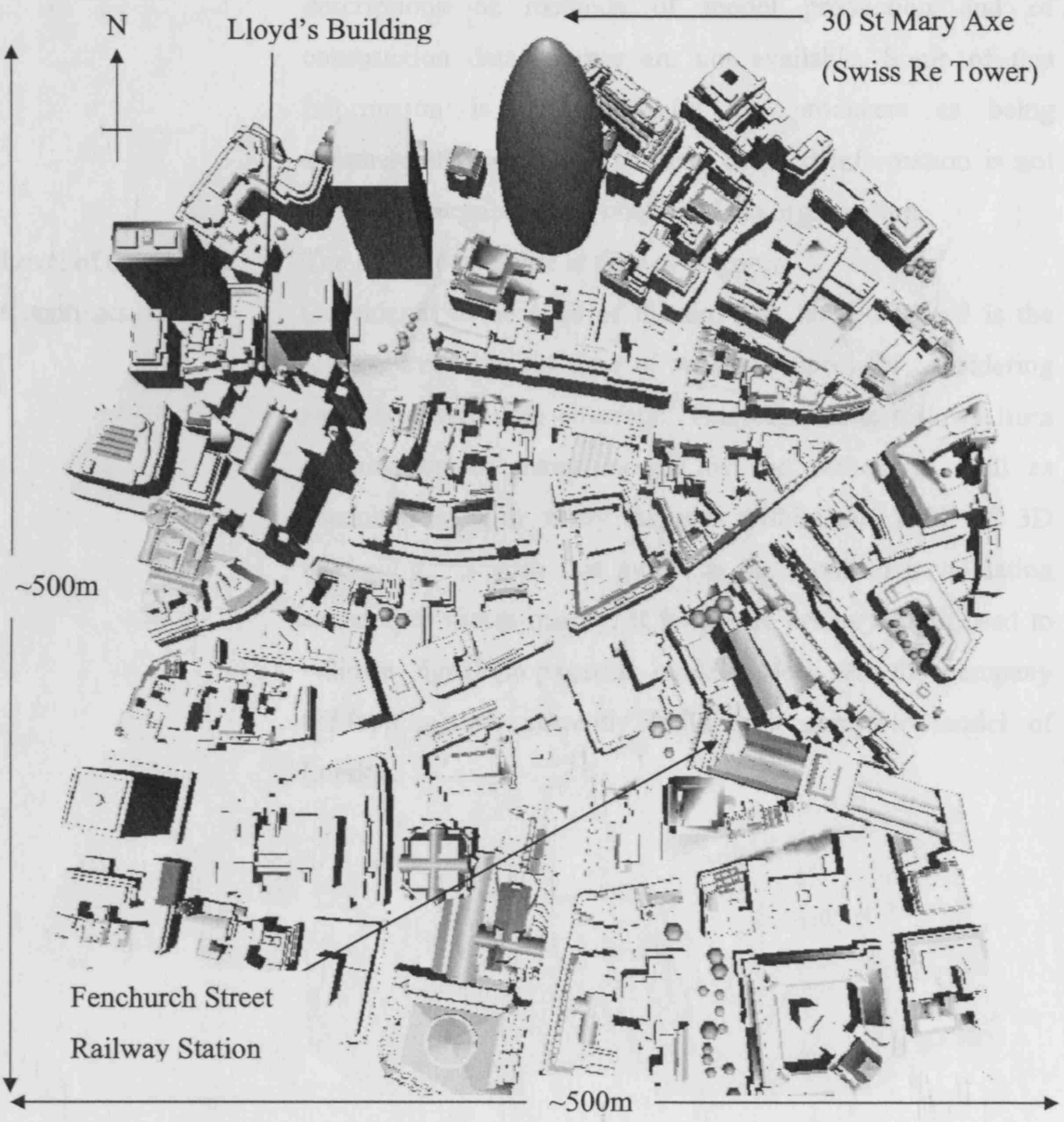

Figure 6-1: Dataset 1 (viewed with Cortona plugin for Internet Explorer)

Model name:	Dataset 1.
Location:	Fenchurch Street area, City of London.
Physical size:	500m x 500m.
CAD file type:	Autodesk drawing (.DWG).
CAD file size:	4.6MB.
VRML file size:	6.5MB.
Originator:	ZMapping Ltd.
Year:	Early 2006.

Dataset derived from:	Aerial photogrammetry with GPS/Grid InQuest [Ordnance Survey, 2004] derived ground control. Comprehensive descriptions of methods of model production and of construction data sources are not available. Some of this information is considered by the producers as being commercially sensitive. As such, detailed information is not available for publication outside of the organisation.
Level of detail:	The highest available at time of research.
Comments:	Considered to be state of the art. The level of detail is the highest available (at time of writing) especially considering such extensive area coverage. This conclusion follows from examination of many models by the author, as well as consultation with many experts within the field of 3D modelling. As such this model is the focus of a validation exercise to assess quality. It forms the primary input used to validate signal propagation models. Note that the company (ZMapping) are currently building a complete model of London.

6.3.2 Dataset 2

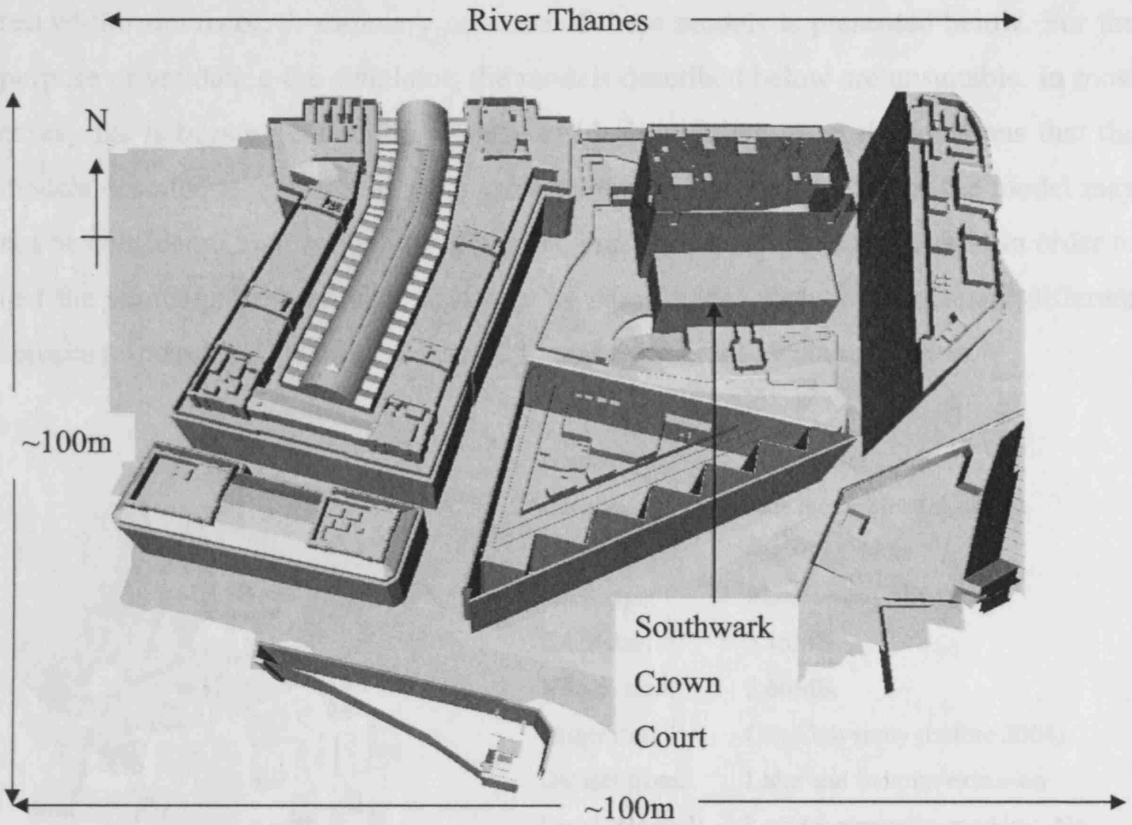

Figure 6-2: Dataset 2 (viewed with Cortona plugin for Internet Explorer)

Model name:	Dataset 2.
Location:	London Bridge area, London.
Physical size:	100m x 100m extracted from initial 500m x 500m dataset.
CAD file type:	Autodesk drawing (.DWG).
CAD file size:	1.74MB.
VRML file size:	1.89MB.
Originator:	ZMapping Ltd.
Year:	2007
Dataset derived from:	Aerial photogrammetry with GPS/Grid InQuest [Ordnance Survey, 2004] derived ground control. Methods of construction and full list of data sources unknown as commercially sensitive.
Level of detail:	The highest available at time of research.
Comments:	A small enclosed area consisting of objects with relatively simple geometry has been selected. Area exhibits little traffic flow that might disturb data collection.

6.3.3 Other Datasets Used During this Work

It is worth noting that many other datasets have been used during the development and test of the simulator. A summary of some of these models is presented below. For the purpose of validating the simulator, the models described below are unsuitable. In most cases, this is because collection of real-world observations from the locations that the models describe is impractical within this research. Also, the quality of the model may not be considered high enough for generating results presented in this thesis. In order to test the simulator with as wide a variety of input model data, from as many different sources as possible, it is of great benefit to make use of all available models.

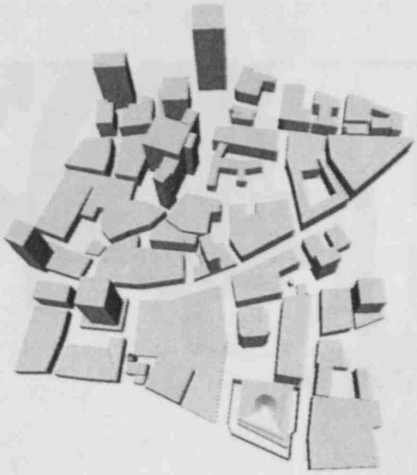

Figure 6-3: Dataset 3 (low resolution model)

Name:	Dataset 3.
Location:	Fenchurch Street, London.
Physical size:	~ 400m x 400m
CAD type:	Rhinoceros (.3DM)
CAD size:	3.15MB.
VRML size:	2.66MB.
Originator:	City University (before 2004).
Dataset from:	Lidar and footpint extrusion
Level of detail:	Low (compared to modern). No terrain model.
Comments:	Applicable to low resource devices.

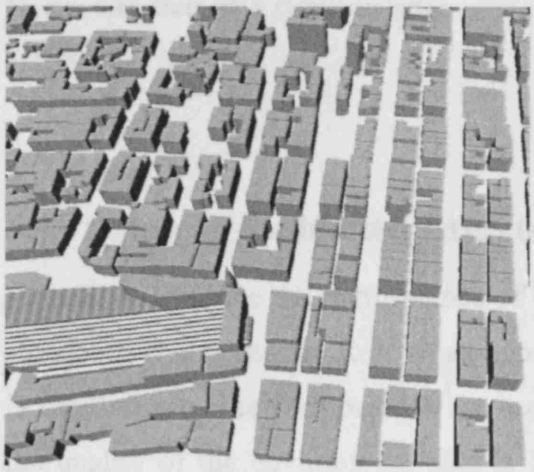

Figure 6-4: Dataset 3 (low resolution model)

Name:	Dataset 4.
Location:	Glasgow.
Physical size:	25 square km
CAD type:	Design Exchange Format (DXF)
CAD size:	Separate files. Size dependent
VRML size:	on number of files used.
Originator:	VR Glasgow (before 2004).
Dataset from:	Lidar? Footpint extrusion
Level of detail:	Low (compared to modern). No terrain model.

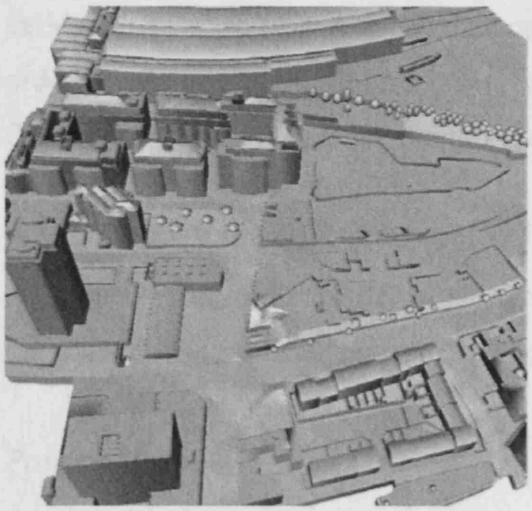

Figure 6-5: Dataset 3 (low resolution model)

Name:	Dataset 5.
Location:	Brighton.
Physical size:	~ 360m x 400m
CAD type:	Autodesk drawing (.DWG)
CAD size:	1.426MB.
VRML size:	2.099MB.
Originator:	ZMapping Ltd (around 2005).
Dataset from:	Aerial photogrammetry
Level of detail:	State of the art
Comments:	Area unsuitable for validation. Too sparse.

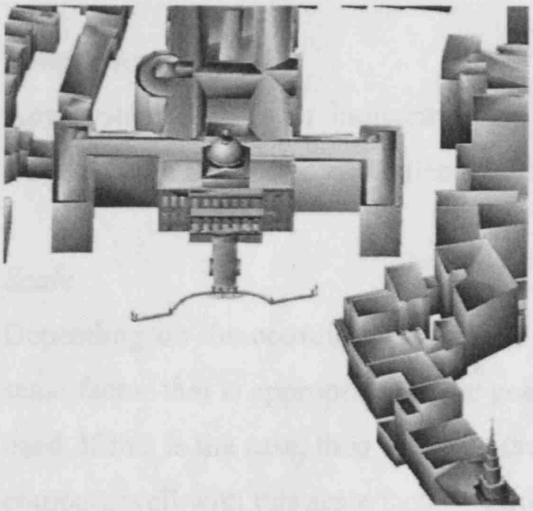

Name:	Dataset 6.
Location:	Tokyo.
Physical size:	Unknown – Consists of many individual tiles.
CAD type:	Autodesk drawing (.DWG).
CAD size:	~5MB per tile.
VRML size:	~6MB.
Originator:	Unknown.
Year:	Around 2005.
Dataset from:	Unknown
Level of detail:	Simple block model. No terrain.
Comments:	Primarily for visualisation?

Figure 6-6: Dataset 3 (low resolution model)

6.4 Dataset 1 Validation Exercise

In order to evaluate the performance of the signal propagation models employed in the simulator, it is necessary to have an appreciation of the quality of all input data. Errors in satellite and receiver positions are accounted for and are well understood. However, the quality of the environment data is largely unknown. This section summarises the methodology and the results of a validation exercise performed for Dataset 1 [Chamberlin, 2006]. It should be noted that although this validation exercise was performed as a distinctly separate project from this research, the exercise was designed such that it would validate Dataset 1 and was specifically aimed at providing information for the work detailed in this research. The author assisted in all areas of the

validation exercise (especially in data collection) and acted in a supervisory capacity in order to ensure that the correct data was collected using appropriate methods. The findings are directly applicable to this work.

6.4.1 Validation Objectives and the Definition of Modelling Quality

An appreciation of the quality of a city model is sought. The quality is defined, for the purposes of this research, by consideration of the following:

Position accuracy

Assessment of the absolute and relative position accuracy of modelled components with respect to the real-world equivalents.

Orientation

Any systematic bias or indiscriminate errors in orientation of modelled objects with respect to the real-world equivalents must be detected.

Scale

Depending on the coordinate system in which the dataset is expressed, there maybe a scale factor that is appropriate to the position of the objects and the mapping projection used. If this is the case, then the scale factor at the corresponding model location should compare well with this scale factor. Aside from the mapping projection scale factor, any systematic or random variation in the scale of the modelled objects with respect to the real-world objects must be determined.

Size and shape

The modelled objects will capture the size and the shape of the real-world objects at some level. As the shape is to some extent a function of the level of modelled detail in complex environments, this can be difficult to quantify. Again, any systematic bias in the size of the objects must be detected. An example of how the assessment of size differs from that of scale is that it could be the case that positions of the objects are accurately scaled (according to any map projection), but an error in the modelling of the object size could occur.

6.4.2 Validation Description

Assessment of every object contained within a city model, with respect to the corresponding real world object, is unachievable. A practical approach to this problem is to select a subset of the model objects and perform an assessment based on those objects only. The quality of the sampled objects is then determined. For the validation exercise cited in this thesis, the following provides a description of the data collection tasks undertaken. Note that the scale effects in the data should be horizontal only as the mapping projection scale would only be applied to horizontal coordinates.

Site Selection

Three localised areas within the model area were surveyed. The areas were chosen based upon the following:

- Availability of real-world points with clearly corresponding identifiable points within the model dataset.
- A range of roof designs affords the validation an understanding of the techniques used for roofscape morphology modelling.
- Availability of GPS. Sites with potential for more than one GPS position to be determined were favoured.
- Site separation. Longer baselines between sites allows calculation of a reliable scale factor.

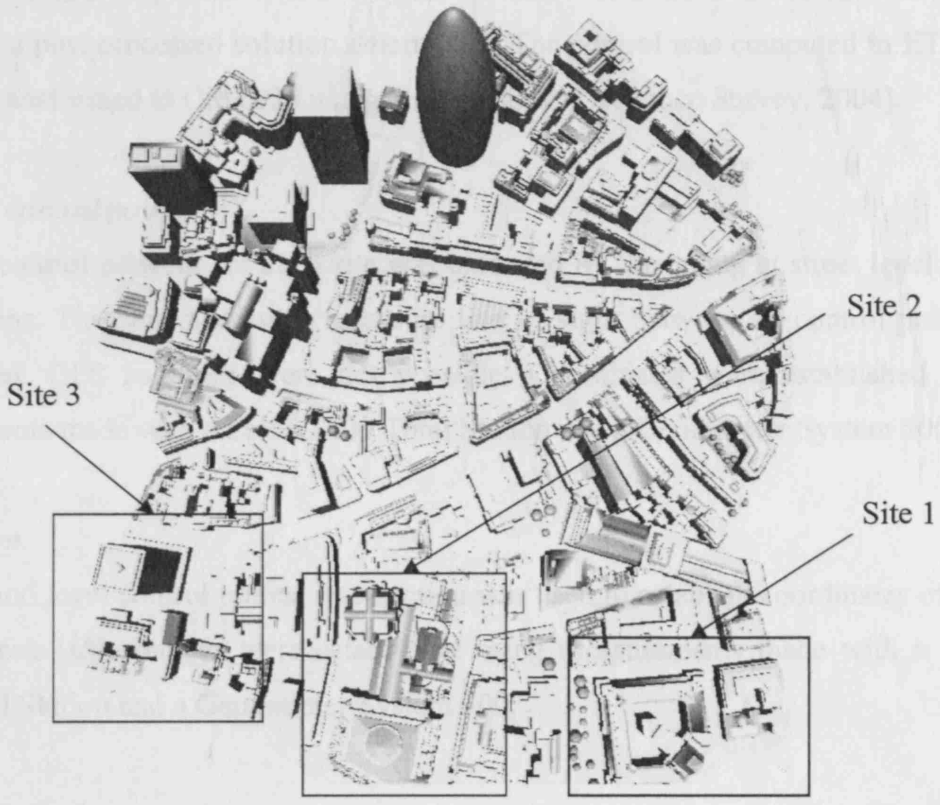

Figure 6-7: Dataset 1 validation exercise, site selection

As illustrated in Figure 6-7 the three localised sites chosen for the validation exercise reside within the southern section of the area covered by the model. The southern section of the area is slightly less densely populated by structures and contains objects with more identifiable artefacts. Also, better visbility between surveyed points is afforded in this area. On the whole, the area was less occupied by traffic and pedestrian movement, and due to the surrounding architecture better sky coverage was apparent, leading to better GPS availability. In addition, permission was granted to collect data from a roof top in the southern section, something that is difficult to obtain due to issues relating to insurance and potential terrorism attacks. Ideally, a site to the north would have been chosen in place of one of the three southern sites. However, for the reasons given, it was considered that a more reliable validation could be performed using the southern sites. Within each of the the three chosen areas, the collected data is well distributed in both east-west and north-south directions, and as such, any north-south effects would still be well detected using data from the chosen sites.

GPS control points

GPS control points were established where possible (due to urban canyon difficulties) for each of the three sites. Leica System 500 reference and rover receivers, with baselines < 5km, were used as a static pair for this work. OS active station data was added and a post processed solution determined. The control was computed in ETRS89 and then transformed to OSGB36 using Grid InQuest [Ordnance Survey, 2004].

Traversed control points

The GPS control network for each site was extended by traversing at street level using total stations. This was necessary to ensure line of sight between all control points in areas where GPS solutions were not possible. Coordinates were established using measurements made with a Leica T400 Total Station and a Geodimeter System 500.

Intersection

From ground level control points, intersection was used to establish coordinates of real-world objects. Coordinates were established using measurements made with a Leica T400 Total Station and a Geodimeter System 500.

If the assumptions are made that additional datasets are constructed by the same set of techniques, and that the model datasets are not spatially separate by any significant amount, then the results of such a validation exercise can give an indication to the quality of other datasets. Therefore, this test over a small sample of the city model is assumed indicative of overall model quality.

6.4.3 Validation Conclusions

Following data collection as described in section 6.4.2, many thousands of individual coordinate points referring to the absolute position of real world objects were available to be compared with corresponding model data coordinates. Analysis of the collected data concluded the following points regarding Dataset 1.

Conclusion 1: Planimetric accuracy

Planimetric accuracy for the three sites was found to be good.

Site 1 (RMS): 0.3339m E and 0.3042m N

Site 2 (RMS): 0.3447m E and 0.6468m N

Site 3 (RMS): 0.1497m E and 0.2746m N

Conclusion 2: Modelled heights

Modelled heights were consistently underestimated with respect to the corresponding real world heights.

Site 1 (RMSE): -0.554m

Site 2 (RMSE): -0.7207m

Site 3 (RMSE): -0.8977m

(-ve indicates direction of error is an underestimation)

Literature examined during the validation exercise indicated that underestimation of height data was typical in 3D models, particularly those derived from photogrammetry.

Conclusion 3: Model scale factor

A total of 2590 baselines were used to establish the scale factor of the model. The model was shown to exhibit a scale factor of 0.999575, for the calculations performed. For the area covered by this model, a scale factor of 0.99984 [Ordnance Survey, 2007] is expected. A slight underestimation in the size of 2D shapes was also noted, and this also accounts for error in the established scale factor.

Conclusion 4: Orientation

The mean orientation difference between the real world and the model was calculated from 2590 baselines. A very small systematic difference of +0.05° (clockwise) was concluded. A standard deviation for the orientation error of 0.16353° was calculated with 98.88% of samples falling within 1 sigma.

Conclusion 5: Shape

As a trend, modelled shapes were found to be slightly smaller than the real world equivalents. This is in part due to the very slightly smaller scale factor (conclusion 2). Eight shapes were tested. The model exhibits the following size discrepancies with respect to the corresponding real world shapes.

Shape 1:	-17.586%
Shape 2:	-4.05%
Shape 3:	-0.117%
Shape 4:	-0.197%
Shape 5:	-0.955%
Shape 6:	-1.8686%
Shape 7:	+6%
Shape 8:	+6%

6.5 Consideration of Model Quality

Simulator performance is measured in terms of resource useage and processing time. There exists a relationship between the quality of an environment model (described in section 6.1) and achievable simulator performance. An increase in the quality of an environment model results in an increase in the number of surfaces to be processed. Examination of this relationship is a large topic and requires generation of the same model in a range of qualities. It is not within the scope of this research to investigate this factor. However, it is acknowledged that model quality has a bearing on accuracy of the simulation results. For this work, the highest quality model available has been sourced, validated and examined in detail. This strategy permits assessment of the best achievable results, and opens up further avenues of research for the afore mentioned model quality test. It is envisaged that lower quality models could be used for integration of this work with GNSS hardware, especially with regard to mobile device useage.

The validation exercise performed for Dataset 1 has assessed the quality of the environment used to validate signal propagation models used within this research. Validation of other datasets (produced using other techniques and other data sources) is outside the remit of this work. However, future work that might focus on using environment models sourced from a variety of producers, or constructed using different techniques, must ensure that a similar validation of model quality is performed before the results of any GNSS signal propagation modelling can be relied upon. The quality of model geometry with respect to the real world has been quantified. Other aspects of quality, such as the optimum model area coverage for a particular location, have been considered. It is, however, imperative that consideration of the receiver position is made on the basis of relative and absolute position. An absolute position should be established, and then adjusted appropriately according to any local model biases (such as model height biases). This ensures that the best receiver position, relative to the surrounding objects, is used for simulation. Due to the geometrical configuration of nearby objects and the relative distance of transmitters (satellites), these minor adjustments will have negligible effect on the satellite azimuth and elevation angles. Typically, we are considering adjustment of the order of 0.5m, which for a 20,200,000m transmission, is of no consequence. Range assessment, when compared to observed range data, will need to account for any slight adjustment in simulated receiver position.

7 PROPAGATION MODEL VALIDATION

The work presented in this chapter aims to validate the individual signal propagation models applied within the simulator. To achieve this, experiments are described whereby collected observation data is compared with corresponding simulator outputs. An analysis of the results is provided.

7.1 Validation Definition

Validation assesses how well the software achieves the overall objectives, in this case the simulation of available signals and characterisation of the signal environment within which a receiver operates. Observed data is used to validate individual propagation models implemented in the software. Artificial data is not used in validation, as the aim of this step is to predict the observation data, and furthermore assess the level of agreement between observed and simulated data. An important consideration of the validation process is that observed data and simulated data are completely independent. All treatment of observed and simulated data is undertaken separately.

7.2 Validation Approach

A set of experiments performed at different locations, covering different epochs and using different environment models are described. Observation data collected at three locations, two on one dataset and one on another are presented as the truth data against which simulated data is assessed. More observation data than can be presented in this thesis has been gathered and analysed during this research. The observation data chosen for presentation within this thesis has been selected such that it captures the best distribution of events for a rigorous validation of the signal propagation models. Three locations are presented in section 7.3. The collected observation data for each location is then presented. Section 7.4 presents the application of the LOS propagation model and assesses the ability of this mode in isolation to predict the observed data. Section 7.5 demonstrates consideration of the Fresnel zone for signal transmission, and again the simulated results using this propagation model are presented with reference to the observed data. Section 7.6 examines the performance of the diffraction model, again providing a full comparison of simulated results against observed data. Section 7.7 demonstrates the existence of reflected only-signal measurement in observed data, and demonstrates the ability of the simulator to independently predict such events.

7.3 Collected Data

The observation data collected at three locations on two models is presented in this section. For reasons detailed in section 6.2 locations that exist on two different models have been chosen. Selection of the positions at which to collect data has been made following consideration of factors such as the likelyhood of observing satellites that will rise and set over the top of structures in the environment. This provides a good means by which to test the ability of the simulator to predict satellite availability. Collection of GNSS observation data in urban environments is often difficult due to movement of people and traffic around the receiver (as described in chapter 2). For this reason, often relatively short data collection periods have been captured. A more important reason for the collection of data over short period is due to the lack of availability in urban canyons. Restricted areas of unobstructed sky often results in only few visible satellites. This in turn results in poor satellite geometry and consequently high DOP values. Many receivers (including the Leica GPS System 530) will refuse to track signals when certain conditions occur. This includes the case whereby few satellites are visible and the DOP value is beyond a defined threshold. Short data collection periods do not cause a problem for this work, as the occurrence of events, such as satellite signal availability transitions between available and not available are of most importance to this validation. If there was to be any averaging of observed data over time, then this would need consideration.

7.3.1 Location 1

A description of Location 1, including a graphical representation from the model dataset is provided in section 7.3.1.1. The observation data collected at Location 1 is detailed in section 7.3.1.2.

7.3.1.1 Location 1 Deep Urban Canyon

Location 1 is a deep urban canyon, typical of a poor environment in terms of satellite visibility. Surrounding objects consist mainly of structures with vertical sides and intricate roof morphologies as presented in a screen capture from the model dataset of the surrounding area (see Figure 7-1). Satellites visible to the receiver will generally exhibit high elevation angles. Roads in the surrounding area partition the objects surrounding the receiver and produce corridors. These corridors provide sets of azimuth values, relative to the receiver position, along which satellites with lower elevation

angles can be visible by LOS. The chosen position is visible at the intersection of the illustrated LOS vectors.

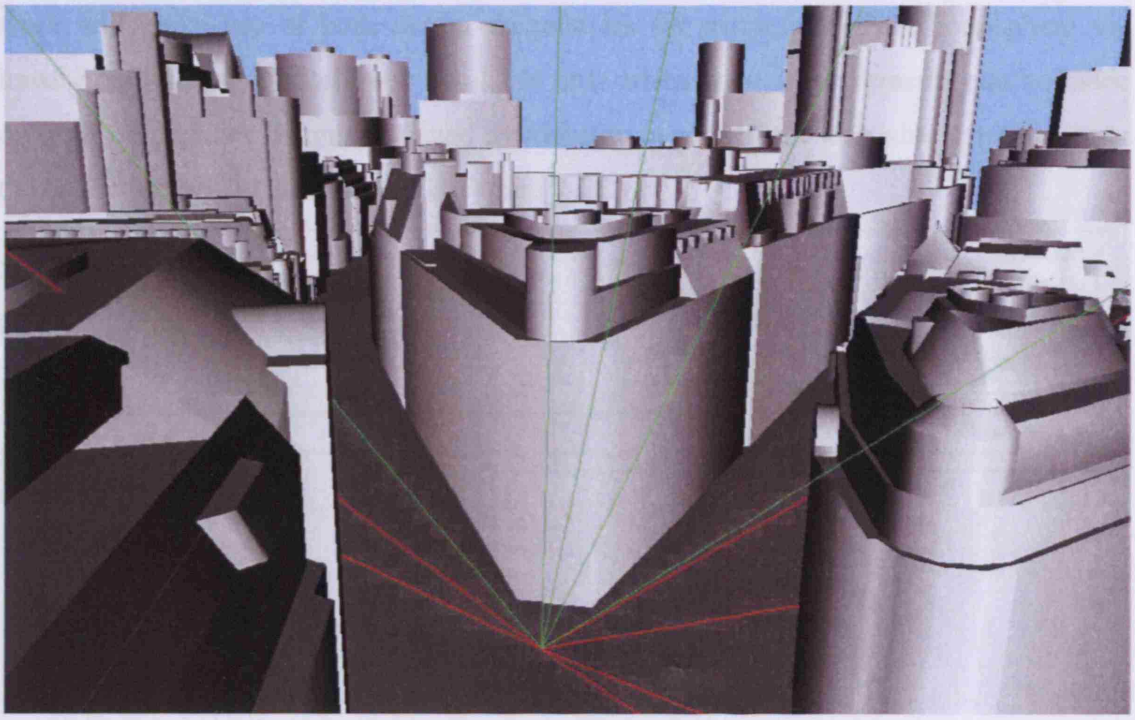

Figure 7-1: Location 1 screen capture of model representation

The selection of the chosen position is based upon a trade-off, whereby a poor environment for signal availability is sought as well as a position where satellites will be available for tracking over a reasonable period of time.

7.3.1.2 Location 1 Observed Data

Location reference:	Location 1
Location:	Fenchurch Street, London
Data collection:	Leica GPS System 530, AT502 antenna.
WGS-84 coordinates:	X = 3977535.915, Y = -5406.441, Z = 4969323.041
GPST start:	2007 1 31 10 33 25.0
GPST end:	2007 1 31 12 51 38.0
Collection rate:	1 second
Missed epoch records:	1

Measurements:

PRN	C1	L1	P2	L2	C1,L1,P2,L2
3	8293	8293	8293	8293	8293
8	20	20	0	0	0
11	28	28	0	0	0
16	4853	4853	3183	3183	3183
18	5593	5593	5340	5340	5340
19	8293	8293	8242	8242	8242
21	6120	6120	5767	5767	5767
22	3304	3304	2679	2679	2679
27	17	17	0	0	0

As described in section 2.4, a definition of availability is required. In light of the popularity of dual frequency receivers, and the likelihood that all applications for this work will make use of both carrier frequencies for extraction of the ionosphere via linear combination, a satellite is available only when code measurements can be made on both frequencies. Having defined availability, a plot of the available satellites over the collection period is presented in Figure 7-2.

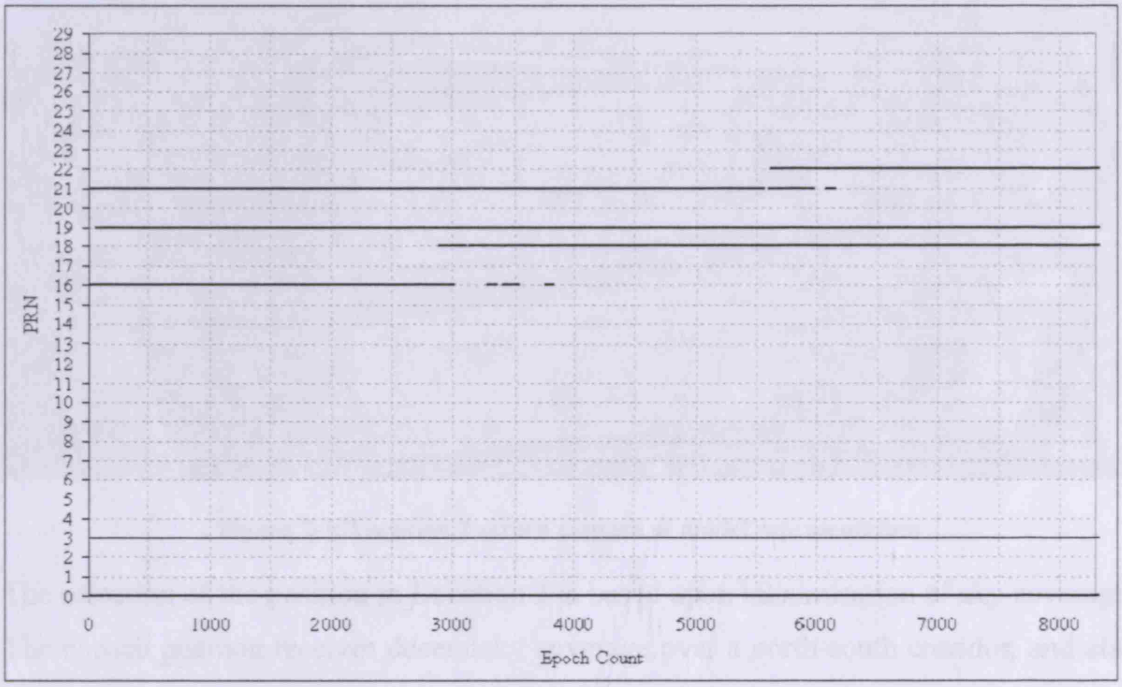

Figure 7-2: Location 1 observed availability (C1,L1,P2,L2)

7.3.2 Location 2

A description of Location 2, including a graphical representation from the model dataset is provided in section 7.3.2.1. The observation data collected at Location 2 is detailed in section 7.3.2.2.

7.3.2.1 Location 2 Typical Urban Environment

Location 2 is considered to be a typical urban environment. Fewer structures surround the receiver than would be found in an extremely dense urban environment such as that in Location 1. The structures are also relatively simple in their form with the exception of some intricate roof designs as presented in a screen capture from the model dataset of the surrounding area (see Figure 7-3). Satellites are visible in this environment with a greater range of elevation angles than exhibited by Location 1. The chosen position is visible at the intersection of the illustrated LOS vectors. An important consideration in the selection of this location is that there exists a large open area surrounded by

modelled structures. In other words, for virtually all azimuth values with respect to a receiver position within the location, the environment is appropriately modelled.

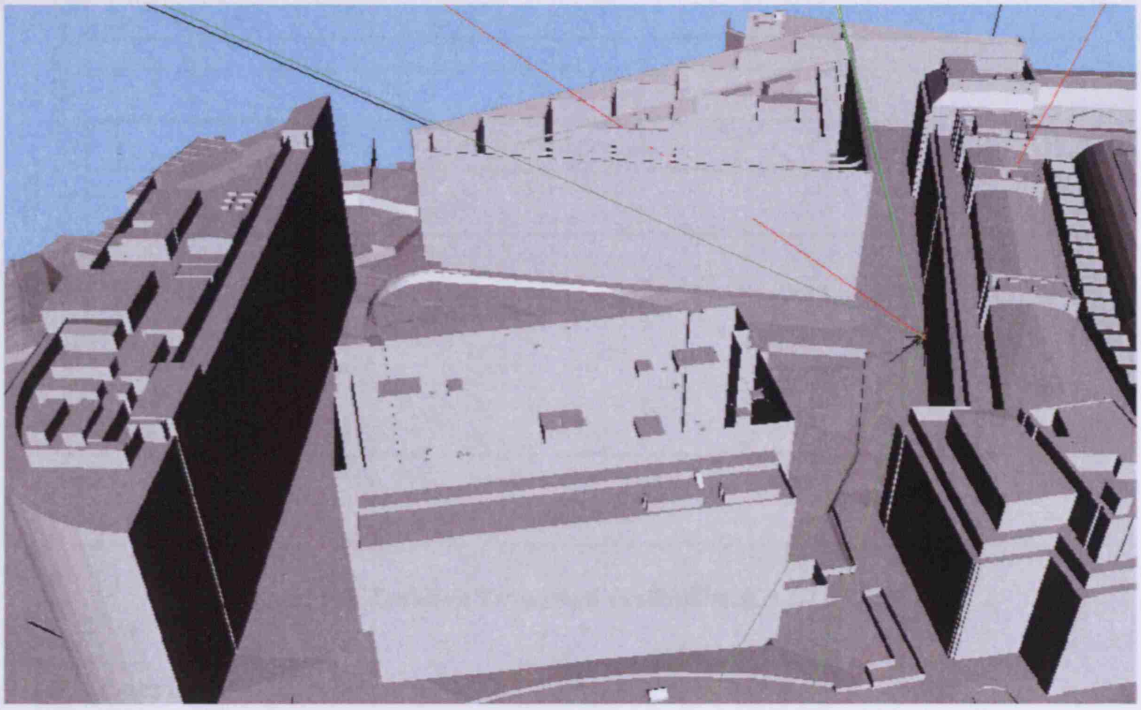

Figure 7-3: Location 2 screen capture of model representation

The selection of the position in Location 2 is based upon maximisation of sky coverage. The chosen position receives decent sky coverage over a north-south corridor, and also good eastward coverage across the central open space.

7.3.2.2 Location 2 Observed Data

Location reference:	Location 2
Location:	London Bridge, London
Data collection:	Leica GPS System 530, AT502 antenna.
WGS-84 coordinates:	X =3978189.266, Y =-5783.005, Z =4968787.542
GPST start:	2007 04 03 13 17 14
GPST end:	2007 04 03 14 21 59
Collection rate:	1 second
Missed epoch records:	

Measurements:

PRN	C1	L1	P2	L2	C1,L1,P2,L2
1	749	749	554	554	554
2	382	382	341	341	341
13	3876	3876	3859	3859	3859
17	3878	3878	3854	3854	3854
20	3737	3737	3675	3675	3675
23	3876	3876	3859	3859	3859
25	3853	3853	3833	3833	3833
31	809	809	736	736	736

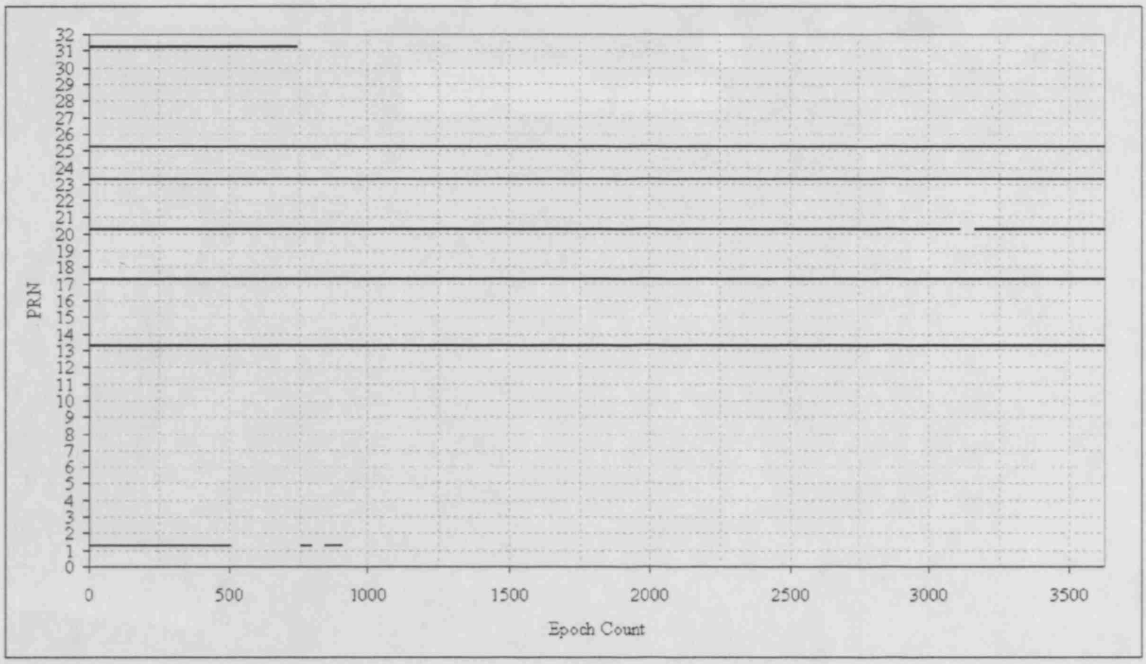

Figure 7-4: Location 2 observed availability (C1,L1,P2,L2)

7.3.3 Location 3

A description of Location 3, including a graphical representation from the model dataset is provided in section 7.3.3.1. The observation data collected at Location 3 is detailed in section 7.3.1.2.

7.3.3.1 Location 3 Typical Enclosed Urban Environment

Location 3 is an enclosed space surrounded by tall structures, as shown in Figure 7-5. The horizon is obscured for all azimuth values with respect to the chosen receiver position. The minimum elevation angle at which satellite signals have been observed is 24°, and this occurs at an azimuth of 158.46°. As with Location 2, for all values of azimuth angle, objects are well captured within the environment model. This is with the exception of a small segment at around 90-95° of azimuth. Within this area construction work, ongoing at the time of data collection, has produced small structures around 100m from the receiver that supercede the date of creation of the environment model. The pace of change of urban environments is an important factor for work that relies upon such models.

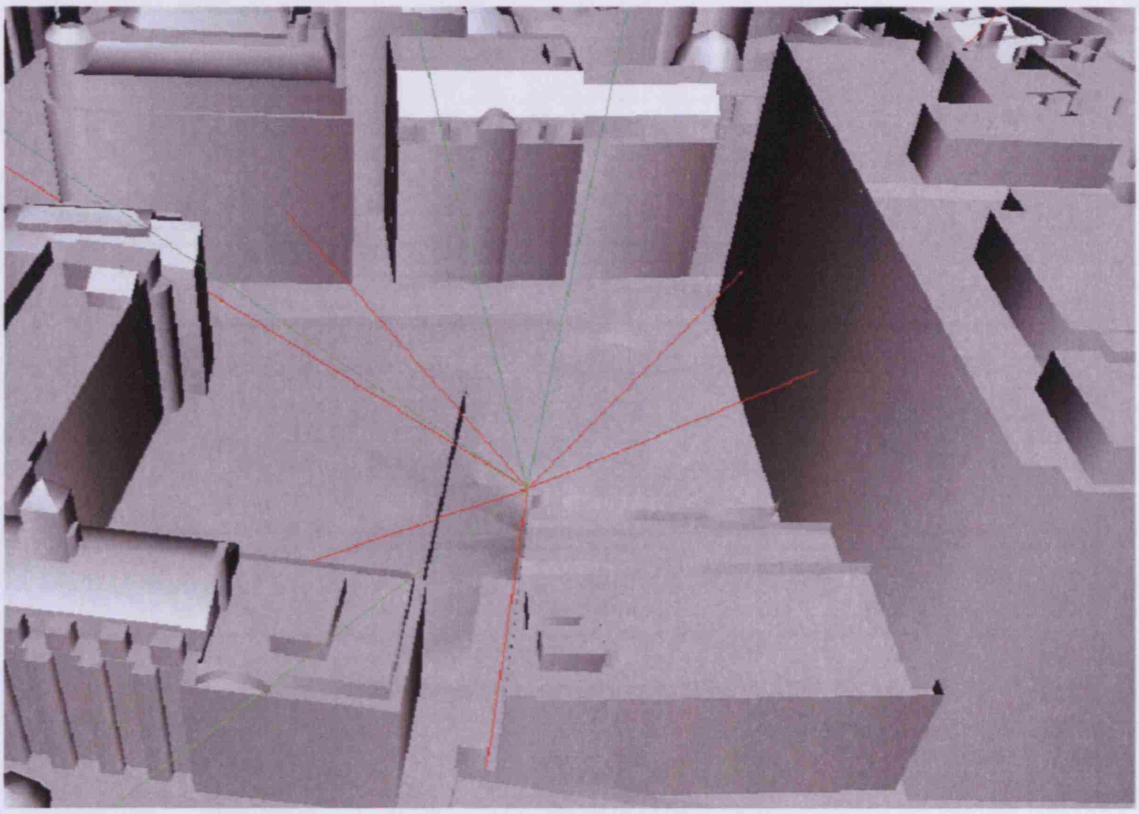

Figure 7-5: Location 3 screen capture of model representation

The selection of the position in Location 3 is based upon maximising the chances of interaction between incident signals and surrounding structures. For this reason, the position is as central as could practically be achieved within the chosen area.

7.3.3.2 Location 3 Observation Data

Location reference:	Location 3
Location:	Mitre Square, London
Data collection:	Leica GPS System 530, AT502 antenna.
WGS-84 coordinates:	X = 3977476.451, Y = -5408.333, Z = 4969369.409
GPST start:	2007 04 04 10 35 7
GPST end:	2007 04 04 11 21 02
Collection rate:	1 second
Missed epoch records:	99 of which 95 from receiver configuration changes

Measurements:

PRN	C1	L1	P2	L2	C1,L1,P2,L2
1	2657	2657	2657	2657	2662
11	2657	2657	2657	2657	2657
14	2634	2634	2504	2504	2504
17	788	788	530	530	530
19	2154	2154	1964	1964	1964
20	2657	2657	2657	2657	2662
28	22	22	0	0	0

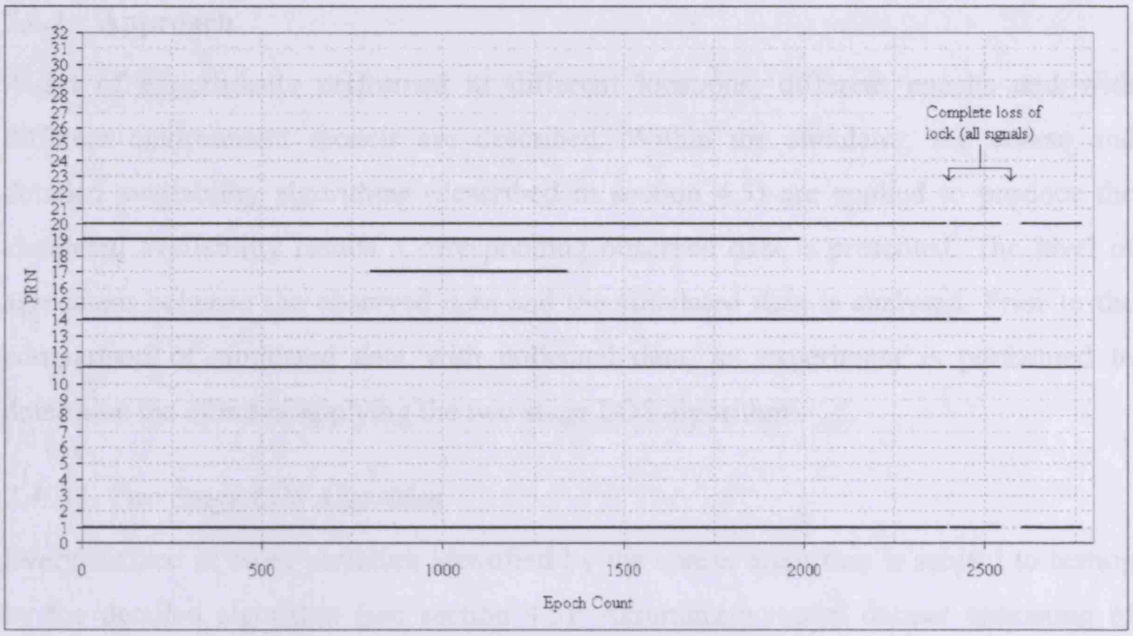

Figure 7-6: Location 3 observed availability (C1,L1,P2,L2)

7.4 LOS Propagation Model Validation

The primary signal propagation mode for consideration is LOS. An unobstructed LOS between a satellite and receiver indicates that a range measurement will be made based on the direct signal, although it must be understood that the range measurement process may be disrupted by the presence of additional signals that reach the receiver by reflected and diffracted propagation paths. If the LOS signal is obstructed, then a range measurement may still be possible, based upon signal propagation through diffracted and reflected transmission modes. The simulations performed using the LOS propagation model, are based upon the assumption that propagation is via a volumeless transmission path.

7.4.1 Objective

The first propagation mode for consideration is that of LOS. An indication of the satellites with unobstructed and obstructed LOS propagation paths is sought by provision of the following:

1. Suitable model of the environment surrounding the receiver.
2. Simulation epoch.
3. Simulation position.

7.4.2 Approach

A set of experiments performed at different locations, different epochs and with different environment models are described. Within the simulator, the coarse and detailed availability algorithms (described in section 4.5) are applied to produce the simulated availability results. Corresponding observed data is presented. The level of agreement between the observed data and the simulated data is analysed. Prior to the comparison of simulated data with collected data, an experiment is performed to determine the effect of applying the two stage LOS algorithm.

7.4.2.1 Two Stage LOS Algorithm

Every surface in every structure identified by the coarse algorithm is subject to testing by the detailed algorithm (see section 4.5). Assuming a model dataset consisting of 4953 structures, with a total of 78780 individual surfaces, and 9 satellites above the elevation mask, for which LOS is to be tested, Table 7-1 demonstrates the effectiveness of the two stage algorithm. In the given case, a 62% reduction in the number of LOS tests to be performed is achieved. This will result in a significant reduction in both memory usage and processing time.

	Structures for Test	Surfaces for Test	Total LOS Tests
Single stage	4953	78780	709020
Stage 1	4953	29718	267778
Stage 2	53	316	

Table 7-1: Single versus two stage availability algorithm

7.4.2.2 Location 1 Simulated Data

Location reference:	Location 1
Location:	Fenchurch Street, London
Dataset:	Dataset 1
Antenna coordinates:	X= 165.437, Y= 70.405, Z= 17.146
GPST start:	2007 1 31 10 33 25.0
GPST end:	2007 1 31 12 51 35.0
Simulation rate:	10 seconds
Total simulations:	829
Propagation model(s):	LOS only

Multiple simulations have been performed according to the above inputs. The results are the LOS satellite signals that are available and the satellites with obstructed LOS paths. A plot of the LOS availability is provided in Figure 7-7.

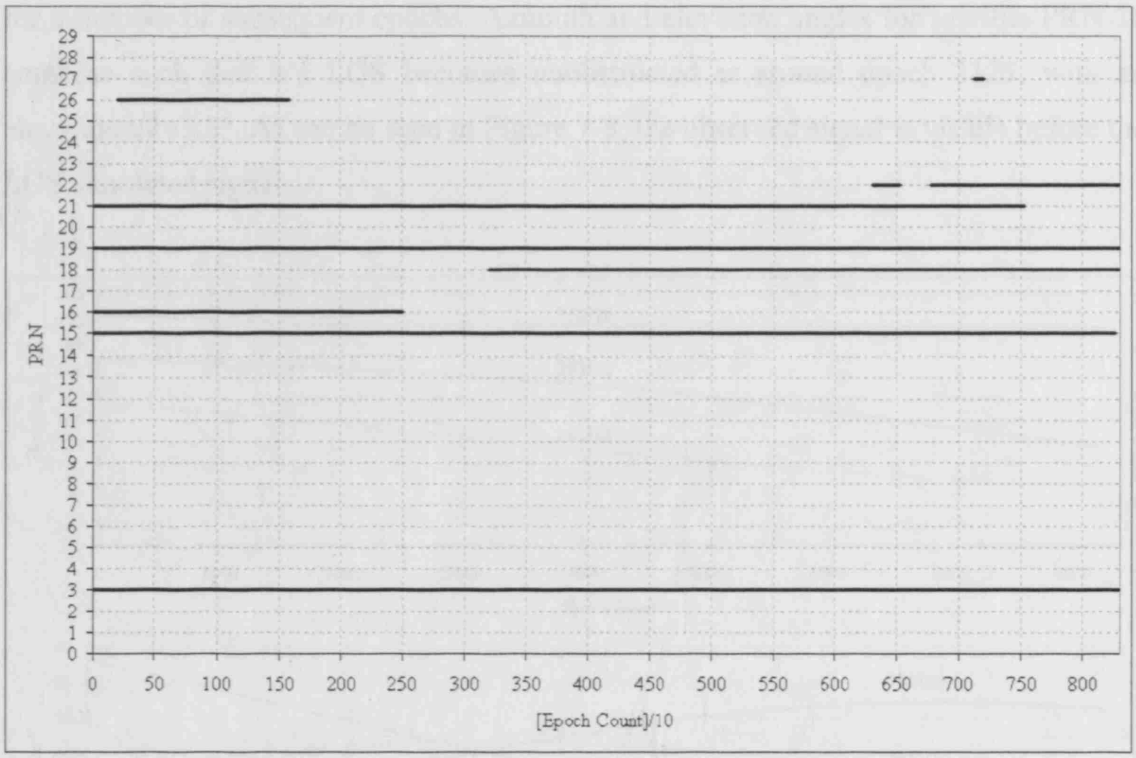

Figure 7-7: Location 1 simulated availability (LOS propagation model only)

Examination of the relevant Navstar GPS Constellation Status [Navstar, 2007] revealed that satellite PRN 15 had been decommissioned. Parameters for the calculation of satellite position within the broadcast ephemeris were still included. Hence, the simulator has computed this satellite's profile, however, the satellite would be disregarded by the receiver during the observation period. Satellite PRNs 21, 26 and 27 are also disregarded. Recent building activity around the azimuth values at which PRN 21 was observed meant that observations to this satellite could not be used. Each of these satellites passes through a small section of sky where distant model data has not been acquired. Although this only has an effect at low elevation angles and no unexpected results occurred, for simplicity of explanation, these satellites are disregarded for this experiment.

7.4.2.3 Location 1 Comparison of Observed and Simulated Data

Figure 7-8 presents the collected observations (heavy dark lines) and the simulated LOS availability (thin lines) on one chart. Only PRN 3 and PRN19 are visible throughout the

entire collection period. In this case, the LOS propagation model is sufficient for the prediction of the available signals. Satellite 16 sets behind a structure in the environment around the receiver. Consequently, at an elevation angle of 46.23°, LOS is lost. However, the observed data reveals that L1 and L2 code measurements are made for a number of subsequent epochs. Azimuth and elevation angles for satellite PRN 18 combine such that it's LOS becomes unobstructed at around epoch 3125, with an elevation of 43.2°. As can be seen in Figure 7-8, the observed signal is visible before the LOS simulated signal.

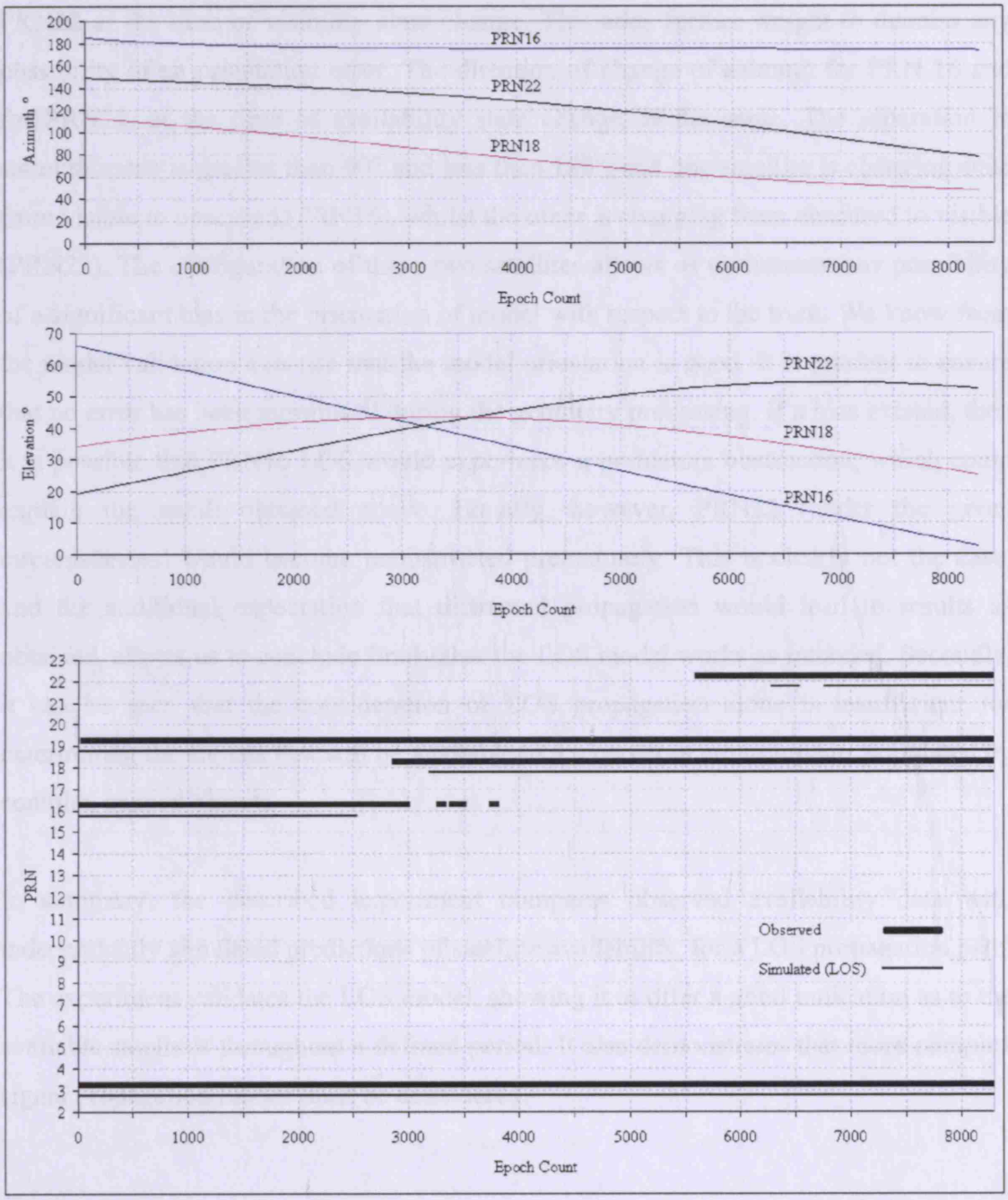

Figure 7-8: Location 1 comparison of observed and simulated availability

Satellite PRN 22 rises above an object in the urban environment, becoming visible at 53.98°. Again, the observed availability begins before the LOS simulated availability. By the software verification presented in section 5.4 and the model validation presented in 6.4, the possibilities of inadequate urban model or orientation errors within the treatment of geometric data, are ruled out. In addition, the results of the above experiment are entirely consistent with the expected presence of a diffracted propagation field. Both visible to obstructed (PRN16) and obstructed to visible (PRN 18 and PRN22) availability state changes are considered. The distribution of azimuth angles is also considered appropriate, with 100° of separation between PRN 16 and PRN22 at the time of visibility state change. This adds further weight to dismiss any possibility of an orientation error. The direction of change of azimuth for PRN 16 and for PRN22, at the time of availability state change, is the same. The separation in azimuth value is greater than 90° and less than 180°, and one satellite is changing state from visible to obscured (PRN16), whilst the other is changing from obscured to visible (PRN22). The configuration of these two satellites allows us to discount any possibility of a significant bias in the orientation of model with respect to the truth. We know from the model validation exercise that the model orientation is good. It is prudent to ensure that no error has been introduced during the geometry processing. If a bias existed, then it is possible that PRN16 LOS would experience a premature obstruction, which could explain the result obtained above. Equally, however, PRN22 (under the given circumstances) would become unobstructed prematurely. This is clearly not the case, and the additional expectation that diffracted propagation would lead to results as obtained, allows us to conclude firstly that the LOS model works as intended. Secondly, it can be seen that the consideration of LOS propagation alone is insufficient for determining the signals that will be available to a receiver in environments populated by complex shaped objects.

In summary, the described experiment compares observed availability data with independently simulated predictions of satellite availability, for a LOS propagation path. The experiment validates the LOS model, showing it to offer a good indication as to the available satellites throughout a defined period. It also demonstrates that more complex signal propagation modes must be considered.

7.4.2.4 Location 2 Simulated Data

Location reference:	Location 2
Location:	London Bridge, London
Dataset:	Dataset 2
Antenna coordinates:	X= -265.008, Y= -11.541, Z= 5.395
GPST start:	2007 4 3 13 17 14.0
GPST end:	2007 4 3 14 17 4.0
Collection rate:	10 seconds
Total simulations:	360
Propagation model(s):	LOS only.

Multiple simulations have been performed according to the above inputs. The results are the LOS satellite signals that are available and the satellites with obstructed LOS paths. A plot of the LOS availability is provided in Figure 7-9.

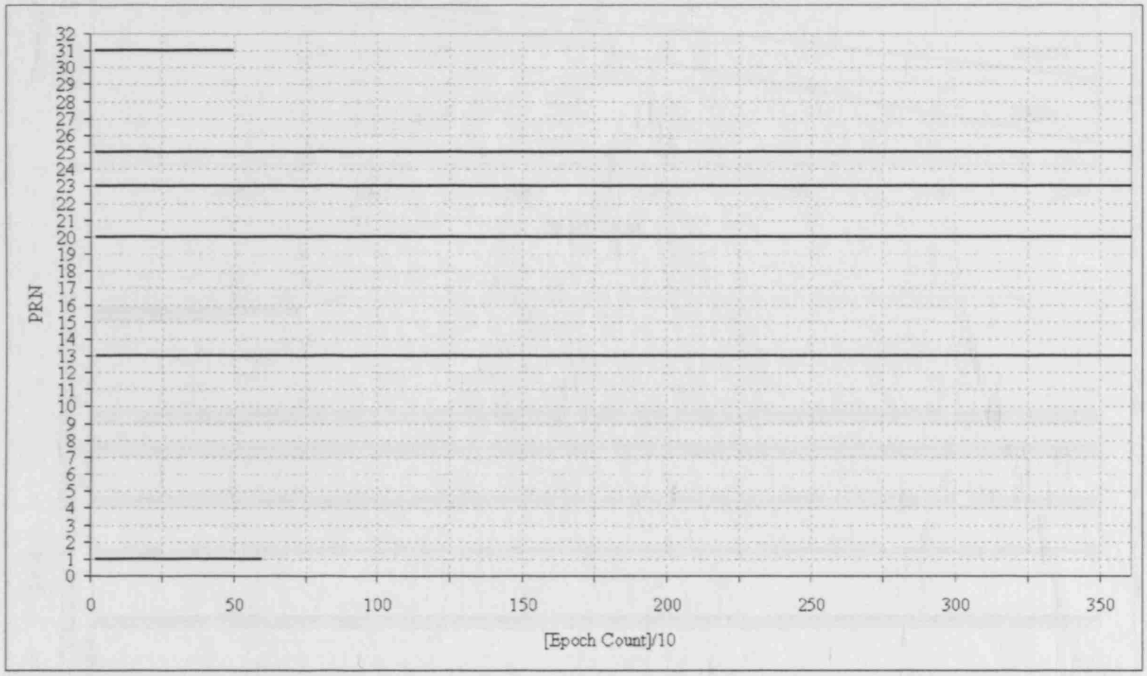

Figure 7-9: Location 2 simulated availability (LOS propagation model only)

Dataset 2 includes an area that is completely enclosed by objects described by the original CAD model. The data collection position, and subsequent simulation position, is within this area. It is therefore the case that no exclusion of any satellite from the analysis be made.

7.4.2.5 Location 2 Comparison of Observed and Simulated Data

Figure 7-10 presents the collected observations (heavy dark lines) and the simulated LOS availability (thin lines) on one chart. Elevation and azimuth plots for PRN1 and PRN31 are also provided, as these satellites undergo availability state change during the period of interest.

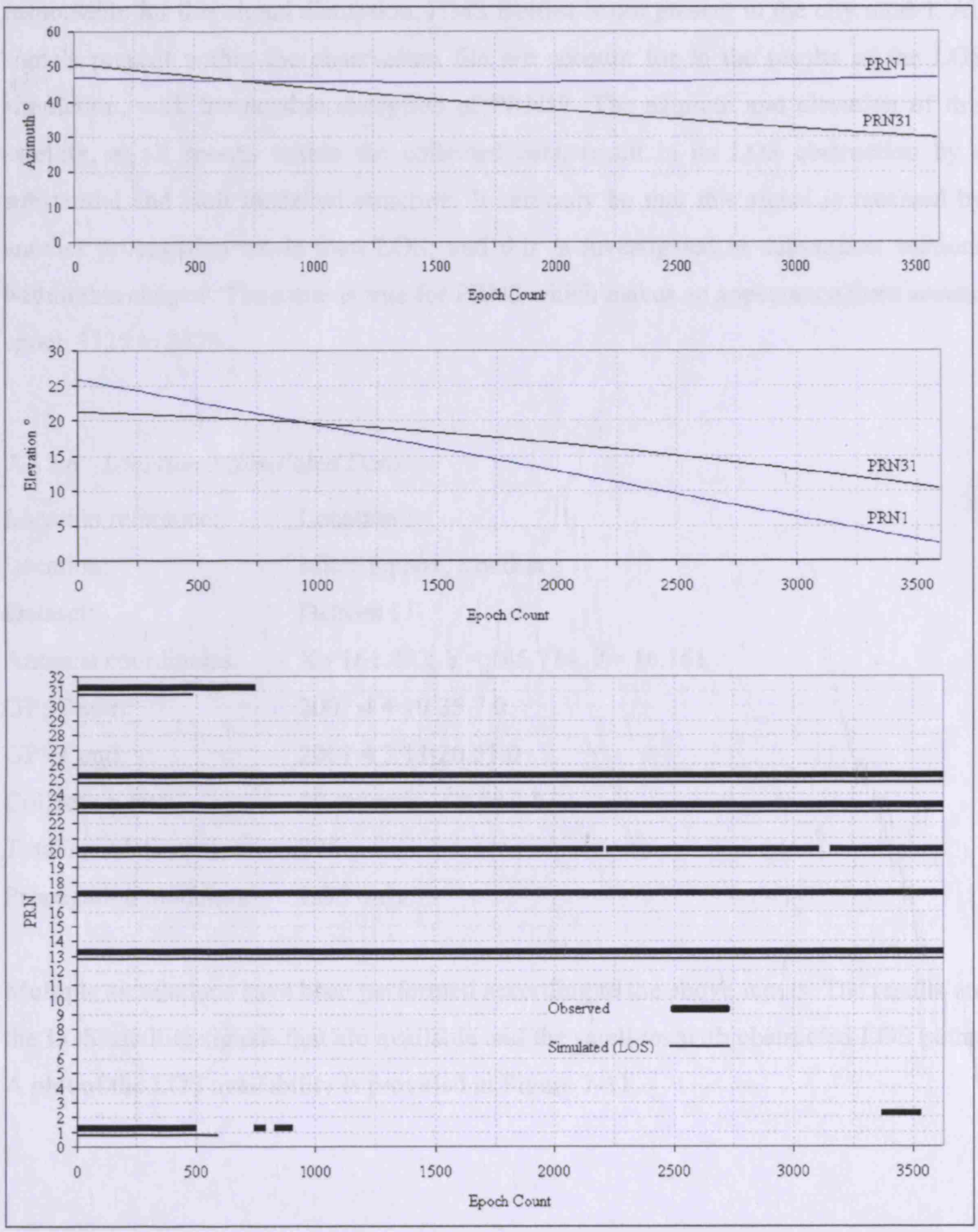

Figure 7-10: Location 2 comparison of observed and simulated availability

With reference to Figure 7-10, satellite PRN31 is visible for a longer period than that determined by the LOS propagation model. This is also true for satellite PRN1, although some notable disruption to the signal is caused between epochs 500 and 750. Upon inspection of the graphical representation of the path described by the satellite motion during this period and examination of the model, it is likely that a boat (HMS Belfast) moored on the river Thames at a distance of <100m from the receiver is responsible for this signal disruption. HMS Belfast is not present in the city model. All signals present within the observation file are account for in the results of the LOS simulation, with the notable exception of PRN17. The azimuth and elevation of this satellite, at all epochs within the collected data, result in its LOS obstruction by a substantial and well modelled structure. It can only be that this signal is received by another propagation mode than LOS, and this is investigated in subsequent sections within this chapter. The same is true for PRN2 which makes an appearance from around epoch 3125 to 3575.

7.4.2.6 Location 3 Simulated Data

Location reference:	Location 3
Location:	Mitre Square, London
Dataset:	Dataset 1
Antenna coordinates:	X= 161.492, Y= 145.714, Z= 16.161
GPST start:	2007 4 4 10 35 7.0
GPST end:	2007 4 3 11 20 57.0
Collection rate:	10 seconds
Total simulations:	276
Propagation model(s):	LOS only.

Multiple simulations have been performed according to the above inputs. The results are the LOS satellite signals that are available and the satellites with obstructed LOS paths. A plot of the LOS availability is provided in Figure 7-11.

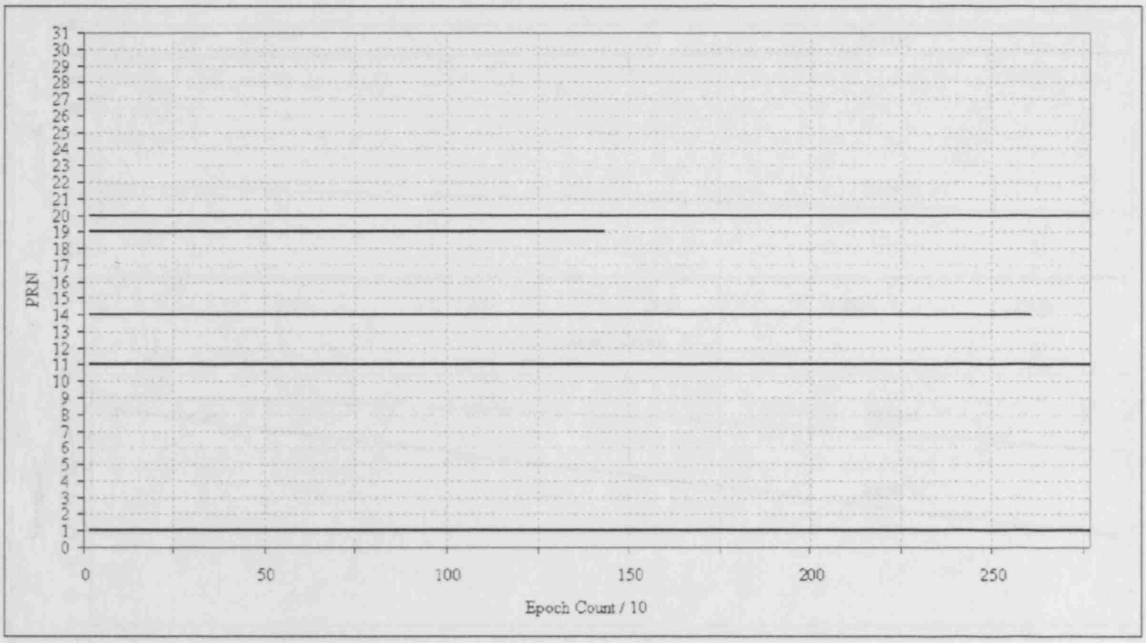

Figure 7-11: Location 3 simulated availability (LOS propagation model only)

7.4.2.7 Location 3 Comparison of Observed and Simulated Data

Figure 7-12 presents the collected observations (heavy dark lines) and simulated LOS availability (thin lines) on one chart. Elevation and azimuth plots for PRN14 and PRN19 are also provided, as these satellites undergo availability state change during the period of interest.

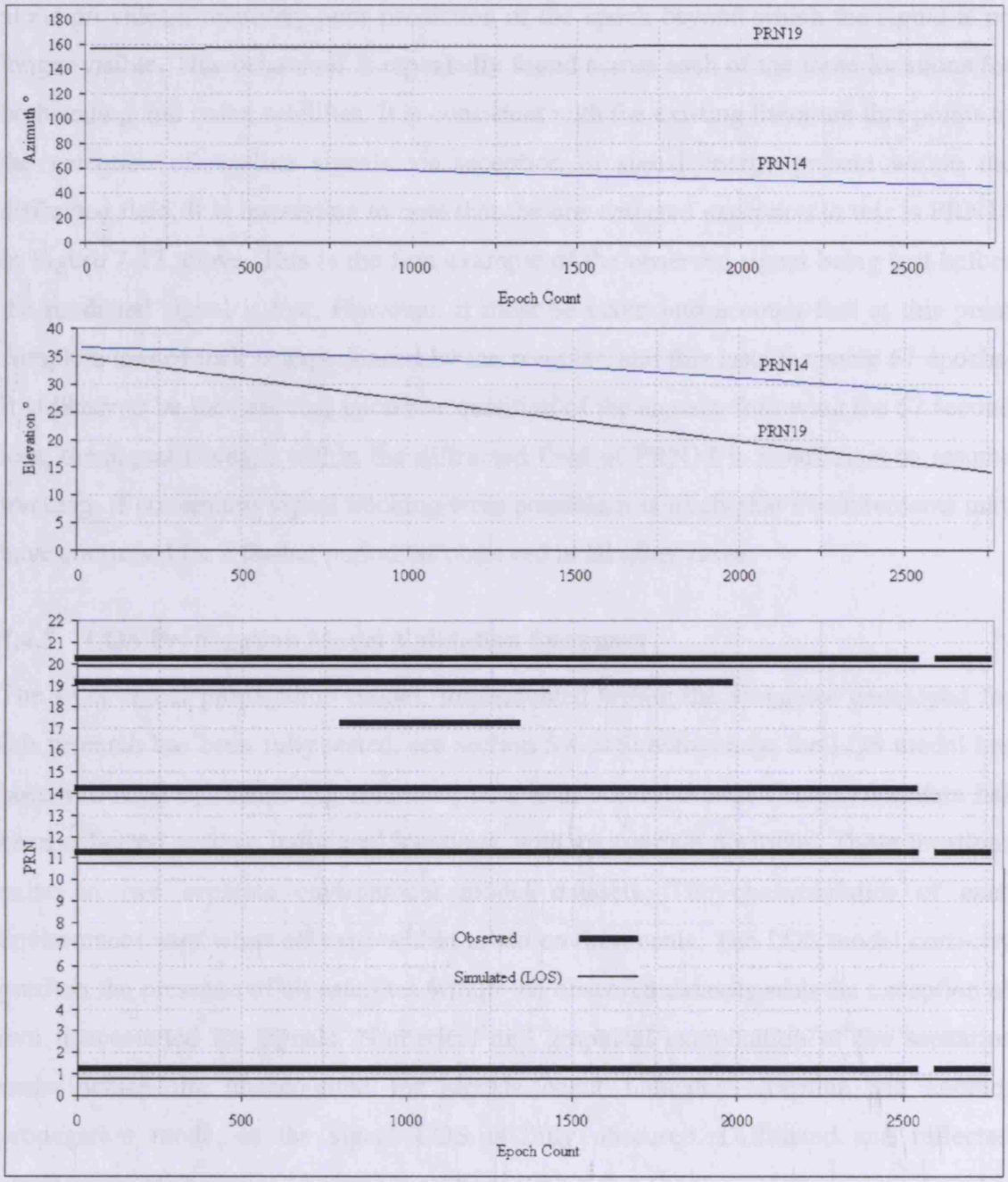

Figure 7-12: Location 3 comparison of observed and simulated availability

As presented in Figure 7-12, simulated satellite availability predicts the presence of all observed satellites. This is with the notable exception of PRN17. Examination of the azimuth and elevation values for PRN17 during the observation time, reveal that there is no possibility of LOS signal reception. A large concrete structure completely obscures the section of the sky from which the PRN17 signal originates. The reception of this signal is examined later, while consideration of other propagation modes is made. The availability state change for PRN19, exhibits the same behaviour as noted for satellites within the previous locations. Essentially, consideration of the LOS propagation mode

alone provides a relatively poor prediction of the epoch beyond which the signal is no longer visible. This behaviour is repeatedly found across each of the three locations for both setting and rising satellites. It is consistent with the existing literature that points to the reception of satellite signals via reception of signal energy present within the diffracted field. It is interesting to note that the one detected exception to this is PRN14 in Figure 7-12 above. This is the first example of the observed signal being lost before the predicted signal is lost. However, it must be taken into account that at this point complete loss of lock is experienced by the receiver, and this lasts for some 67 epochs. It is likely to be the case that upon reacquisition of the signals, following the 67 second loss, the signal strength within the diffracted field of PRN14 is insufficient to resume tracking. If continuous signal tracking were possible it is likely that measurements may have continued for a further period, as observed in all other cases.

7.4.3 LOS Propagation Model Validation Summary

The LOS signal propagation model, implemented within the simulator developed for this research has been fully tested, see section 5.4.5. Subsequently, the LOS model has been validated by comparing simulated data with observed data. Observation data has been collected at three individual locations, with appropriate positions. These locations exist on two separate environment model datasets. The characteristics of each environment vary whist all exist within urban environments. The LOS model correctly predicts the presence of all satellites within the observed datasets with the exception of two unaccounted for signals. Numerical and graphical examination of the scenarios under which the unaccounted for signals occur indicates reception via another propagation mode, as the signal LOS is fully obscured. Diffracted and reflected propagation are examined in further sections within this chapter. Of particular interest is the prediction of availability state change. Events where obscured signals become visible and visible signals become obscured have been focussed upon. A mixture of state change directions have been captured at a mixture of azimuths and elevations, occurring on different structures at different locations. A total of seven state changes have been observed and the according simulation data generated. In six out of the seven cases, the same behaviour is observed, whereby the observed signal is available for longer than that determined by the simulated data. The one instance in which this behaviour did not occur is most likely explained by a total loss of lock for all signals by the receiver, which lasted for a substantial period of time. The behaviour of the observed signal being present for longer periods than that predicted by the LOS model

within the simulator is of no surprise, and is indeed consistent with all literature that discusses the diffraction and reflection of electromagnetic waves. If opposing behaviour had been found in all seven cases, whereby the LOS signal existed for longer than the observed data, then two scenarios would need investigation. Firstly, an error in the simulator would have been possible. Secondly, this may have indicated that the quality of the environment models used would be insufficient for such work. The validation of the LOS propagation model has resulted in a predictable performance. It is now possible to conclude that, as expected, consideration of more sophisticated models of signal propagation is necessary. Diffracted and reflected propagation models have been implemented and tested within the simulator. The continuing sections of this chapter focus on the validation of these models in the same manner as validation of the LOS model.

7.5 Fresnel Zone Model Validation

Consideration of a volumeless transmission path between transmitter and receiver, as made with LOS only models, is insufficient. Appreciation must be made that the signal energy incident upon an antenna is contained within a defined volume, the dimensions of which are dependent upon the geometrical configuration of the transmitter and receiver as well as the signal frequency. As described in section 3.1.2, essentially by employing such theory, we are acknowledging that signal energy that has reached the antenna by travelling only within a defined volume will constructively interfere with any LOS signal between transmitter and receiver. The theory of the Fresnel zone [Spetzler, 2004] is used to determine a volume of space within which diffraction events will contribute energy that will interfere constructively with any direct signal. In addition, telecommunications planners use the Fresnel zone, and estimates of zone blockage, to determine whether a communications link will be capable of transmitting enough signal energy, given obstacles present between a transmitter and a receiver. In this way, an estimate of the signal energy that will propagate between a transmitter and receiver and arrive at the antenna to form a coherent signal can be assessed. In turn it is also a way to quantify the geometric area available for delivery of a diffracted signal when the LOS path is blocked.

7.5.1 Objective

An indication of the total percentage obstruction caused to the cross section of the Fresnel zone between transmitter and receiver is sought by provision of the following:

1. Suitable model of the environment surrounding the receiver.
2. Simulation epoch.
3. Simulation position.
4. Indication of clear and obstructed LOS paths.

7.5.2 Approach

A set of experiments performed at different locations, different epochs and with different environment models are described. Within the simulator, the coarse and detailed availability algorithms (described in section 4.5) are applied to produce the simulated LOS availability results. For signals where the LOS transmission path is obscured, the Fresnel propagation model is employed (described in section 4.6) in order to assess the level of obstruction between the satellite and receiver. Observed data is presented, the details of which can be found in section 7.3. The level of agreement between the observed data and the simulated data is analysed.

7.5.2.1 Location 1 Simulated Data

Location reference:	Location 1
Location:	Fenchurch Street, London
Dataset:	Dataset 1
Antenna coordinates:	X= 165.437, Y= 70.405, Z= 17.146
GPST start:	2007 1 31 10 33 25.0
GPST end:	2007 1 31 12 51 35.0
Simulation rate:	10 seconds
Total simulations:	829
Propagation model(s):	LOS assessment followed by Fresnel zone analysis for obstructed LOS signals.

Multiple simulations have been performed according to the above inputs. The results are the percentage of signal obstruction for satellites with blocked LOS propagation paths. A plot of the Fresnel zone obstruction for satellites that experience an availability state change during the simulations for location 1 are presented in Figure 7-13, Figure 7-14 and Figure 7-15.

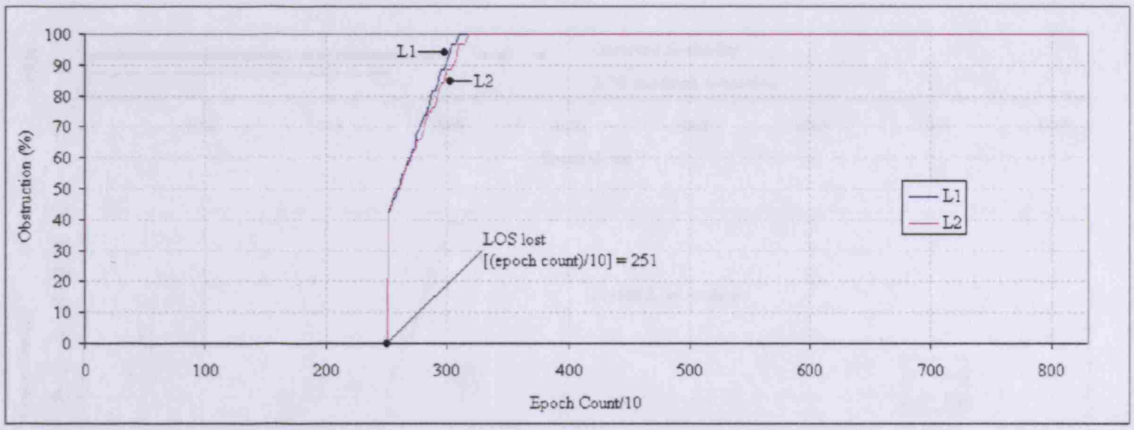

Figure 7-13: Fresnel zone obstruction (L1 and L2) for location 1 PRN16

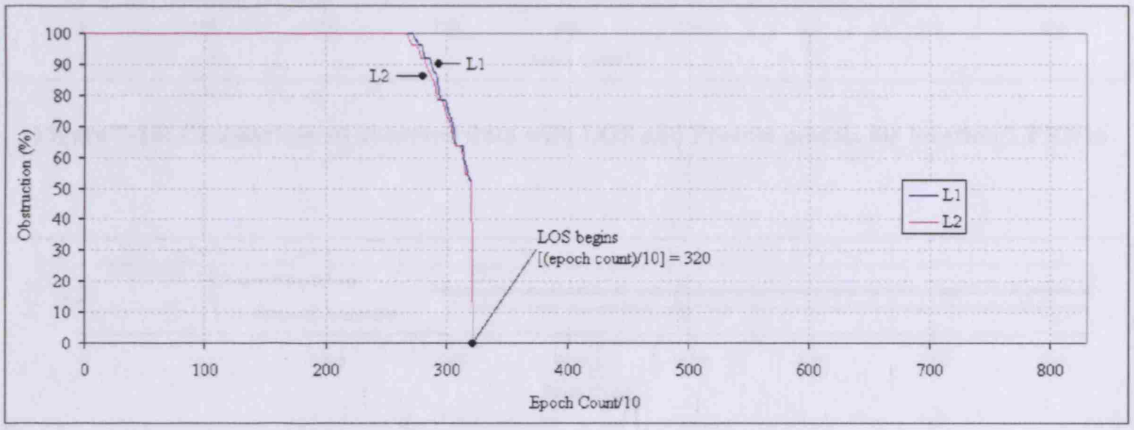

Figure 7-14: Fresnel zone obstruction (L1 and L2) for location 1 PRN18

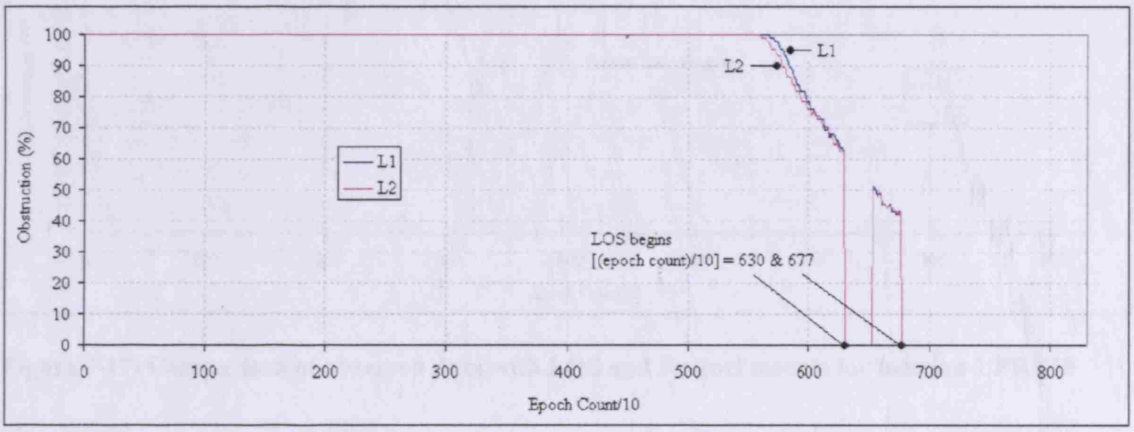

Figure 7-15: Fresnel zone obstruction (L1 and L2) for location 1 PRN22

7.5.2.2 Location 1 Comparison of Observed and Simulated Data

The level of Fresnel zone obstruction throughout a simulation period can be compared to the corresponding observed data. This is shown for the satellites that undergo an availability state change at location 1 by Figure 7-16, Figure 7-17 and Figure 7-18.

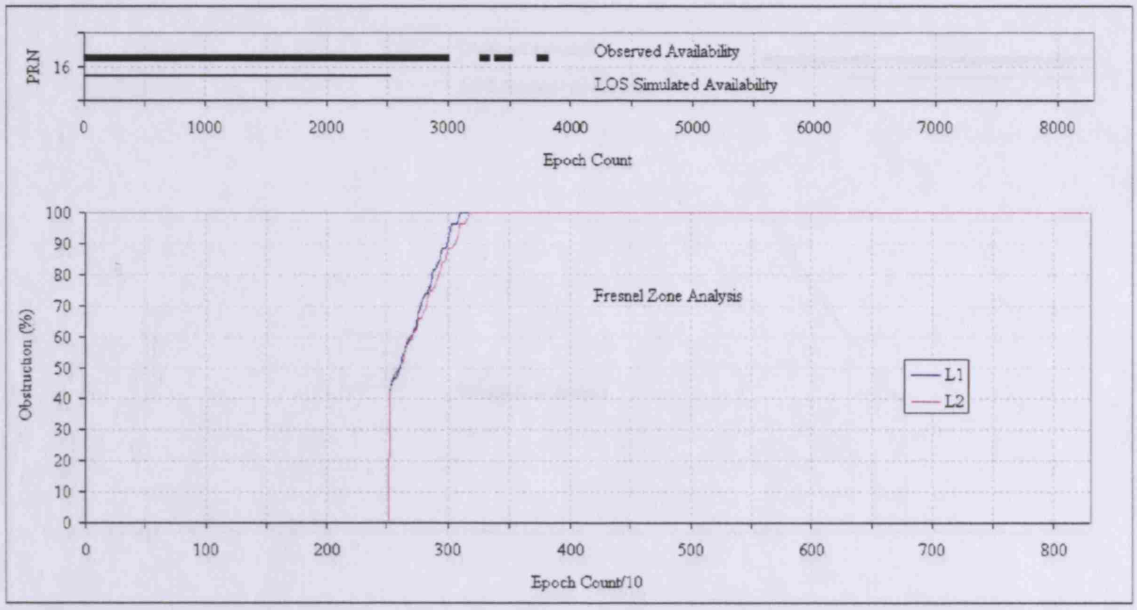

Figure 7-16: Comparison of observed data with LOS and Fresnel models for location 1 PRN16

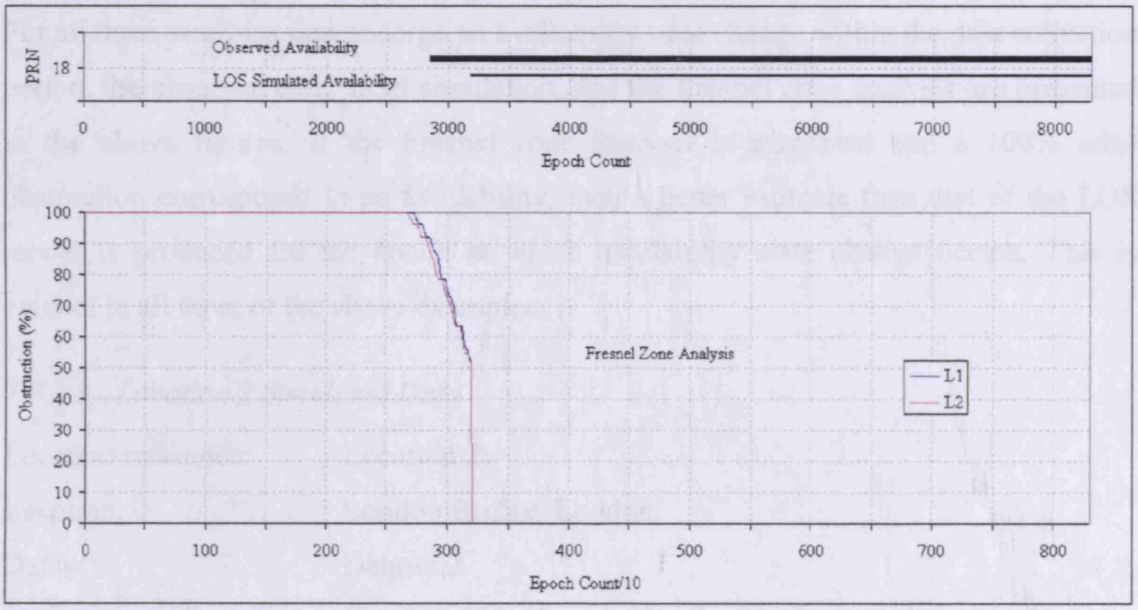

Figure 7-17: Comparison of observed data with LOS and Fresnel models for location 1 PRN18

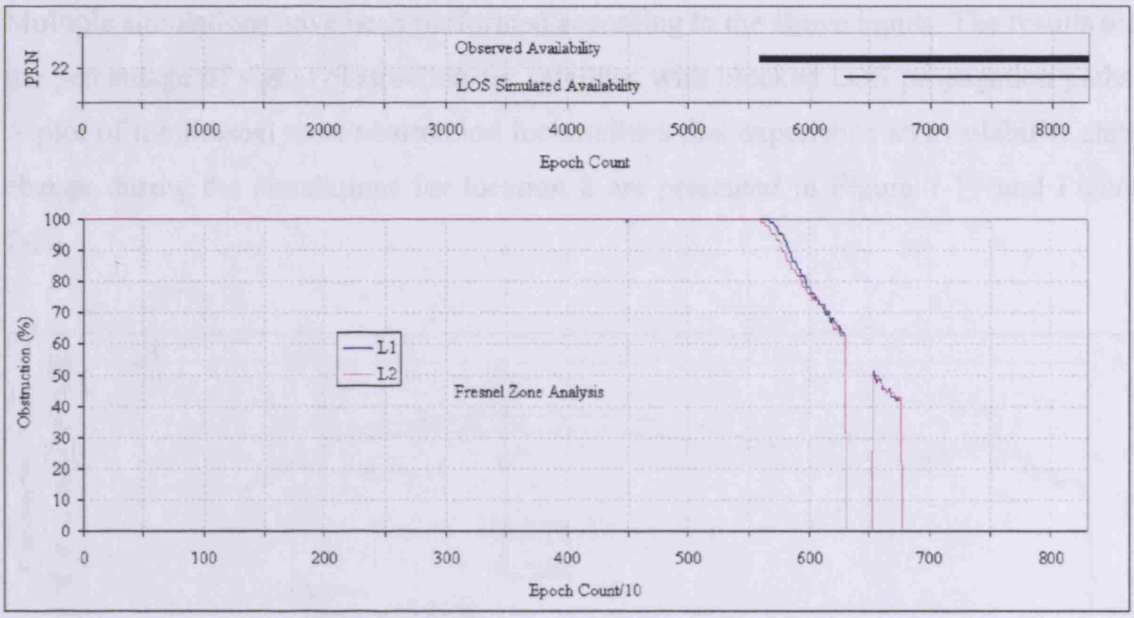

Figure 7-18: Comparison of observed data with LOS and Fresnel models for location 1 PRN22

For all three satellites that undergo an availability state change within the data collection period, the observed data, LOS simulation, and the Fresnel zone analysis are presented in the above figures. If the Fresnel zone analysis is examined and a 100% zone obstruction corresponds to no availability, then a better estimate than that of the LOS model is produced for the epoch at which availability state change occurs. This is evident in all three of the above examples.

7.5.2.3 Location 2 Simulated Data

Location reference:	Location 2
Location:	London Bridge, London
Dataset:	Dataset 2
Antenna coordinates:	X= -265.008, Y= -11.541, Z= 5.395
GPST start:	2007 4 3 13 17 14.0
GPST end:	2007 4 3 14 17 4.0
Collection rate:	10 seconds
Total simulations:	360
Propagation model(s):	LOS assessment followed by Fresnel zone analysis for obstructed LOS signals.

Multiple simulations have been performed according to the above inputs. The results are the percentage of signal obstruction for satellites with blocked LOS propagation paths. A plot of the Fresnel zone obstruction for satellites that experience an availability state change during the simulations for location 2 are presented in Figure 7-19 and Figure 7-20.

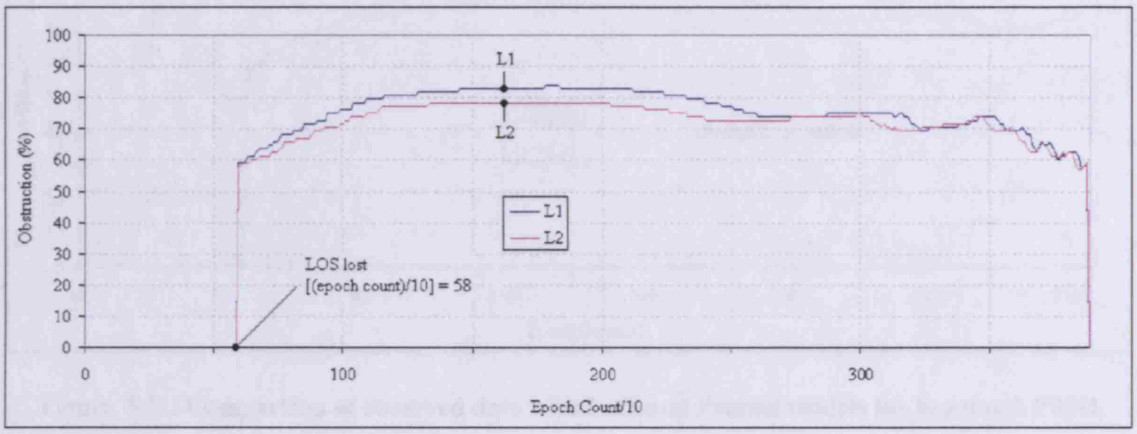

Figure 7-19: Fresnel zone obstruction (L1 and L2) for location 2 PRN1

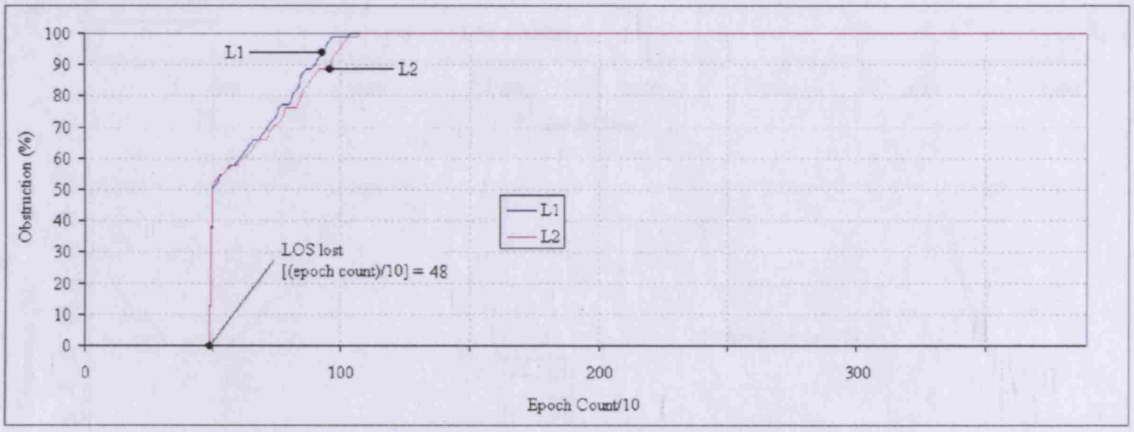

Figure 7-20: Fresnel zone obstruction (L1 and L2) for location 2 PRN31

7.5.2.4 Location 2 Comparison of Observed and Simulated Data

The level of Fresnel zone obstruction throughout a simulation period can be compared to the corresponding observed data. This is shown for the satellites that undergo an availability state change at location 2 by Figure 7-21 and Figure 7-22.

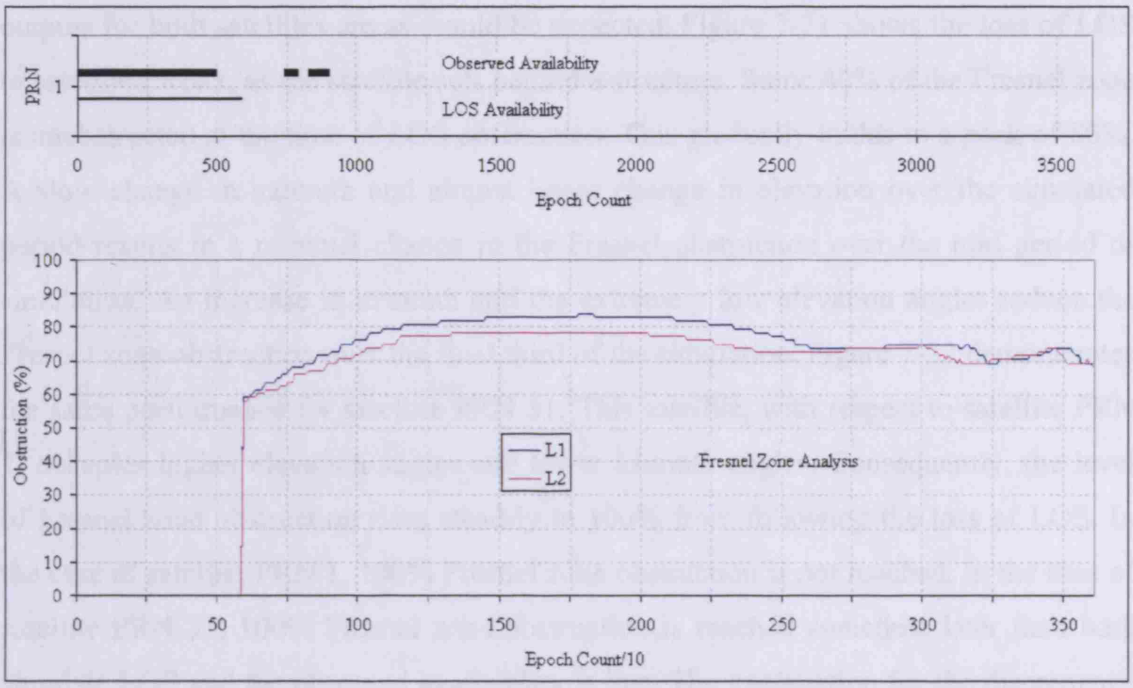

Figure 7-21: Comparison of observed data with LOS and Fresnel models for location 2 PRN1

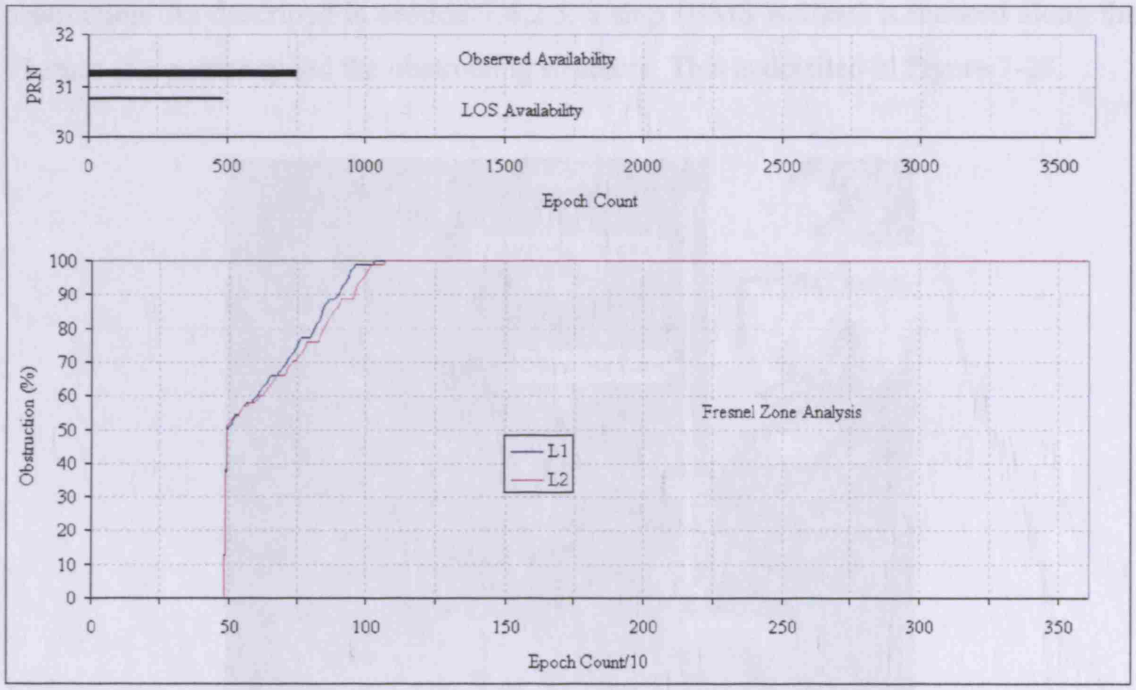

Figure 7-22: Comparison of observed data with LOS and Fresnel models for location 2 PRN31

Comparison of the Fresnel zone obstruction for two satellites with availability state change events in location 2 has been made. Both satellites become obscured by the same building. In contrast to location 1, where satellites became obscured by roof tops, in this location, the two satellites disappear behind a building, such that any diffraction events would be experienced across the side of the profile of the structure. The Fresnel

outputs for both satellites are as would be expected. Figure 7-21 shows the loss of LOS to satellite PRN 1, as the satellite sets behind a structure. Some 40% of the Fresnel zone is unobstructed at the time of LOS obstruction. This gradually builds to a peak of 80%. A slow change in azimuth and almost linear change in elevation over the simulated period results in a minimal change in the Fresnel obstruction over the mid period of simulation. An increase in azimuth and the extremely low elevation angles reduce the Fresnel zone obstruction over the final third of the simulation. Figure 7-22 demonstrates the same performance for satellite PRN 31. This satellite, with respect to satellite PRN 1, occupies higher elevation angles and lower azimuth angles. Consequently, the level of Fresnel zone obstruction rises steadily to 100% from following the loss of LOS. In the case of satellite PRN 1, 100% Fresnel zone obstruction is not reached. In the case of satellite PRN 31, 100% Fresnel zone obstruction is reached sometime later than both simulate LOS and the observed availability is lost. The explanation for the discrepancy between the observed and the simulated data for the Fresnel zone clearance, for both satellites is likely to be due to a missing model component behind the building causing obstruction. As described in section 7.4.2.5, a ship (HMS Belfast) is moored along the Thames at a point beyond the obstructing structure. This is detailed in Figure 7-23.

Figure 7-23: Location 2 obstructing structure and the unmodelled HMS Belfast

It is possible, but by no means certain, that HMS Belfast causes disruption to the incoming signal, and as the ship is not present in the model, the simulation cannot account for this obstruction of the Fresnel zone. This has effect only in the Fresnel zone model, and not in the LOS model.

7.5.2.5 Location 3 Simulated Data

Location reference:	Location 3
Location:	Mitre Square, London
Dataset:	Dataset 1
Antenna coordinates:	X= 161.492, Y= 145.714, Z= 16.161
GPST start:	2007 4 4 10 35 7.0
GPST end:	2007 4 3 11 20 57.0
Collection rate:	10 seconds
Total simulations:	276
Propagation model(s):	LOS assessment followed by Fresnel zone analysis for obstructed LOS signals.

Multiple simulations have been performed according to the above inputs. The results are the percentage of signal obstruction for satellites with blocked LOS propagation paths. A plot of the Fresnel zone obstruction for the satellite (PRN 19) that experiences an availability state change during the simulations for location 3 are presented in Figure 7-24.

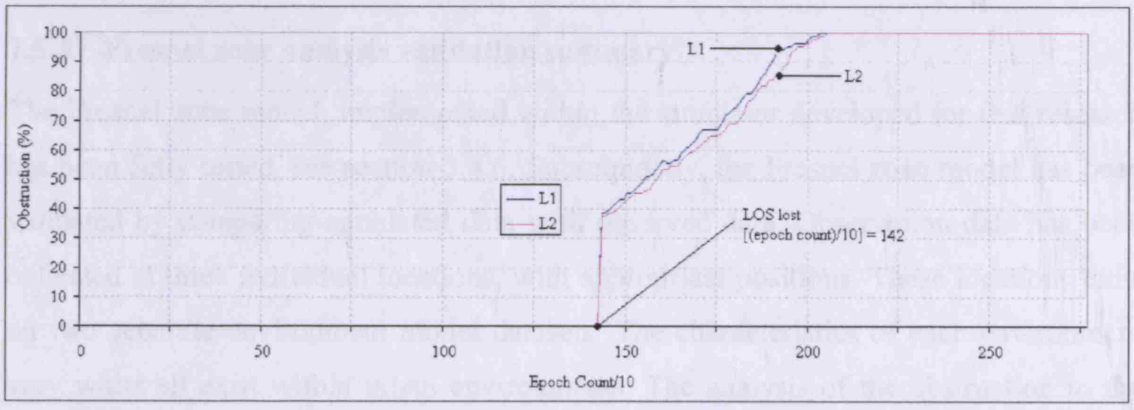

Figure 7-24: Fresnel zone obstruction (L1 and L2) for location 3 PRN19

7.5.2.6 Location 3 Comparison of Observed and Simulated Data

The level of Fresnel zone obstruction throughout a simulation period can be compared to the corresponding observed data. This is shown for the satellites that undergo an availability state change at location 3 by Figure 7-25

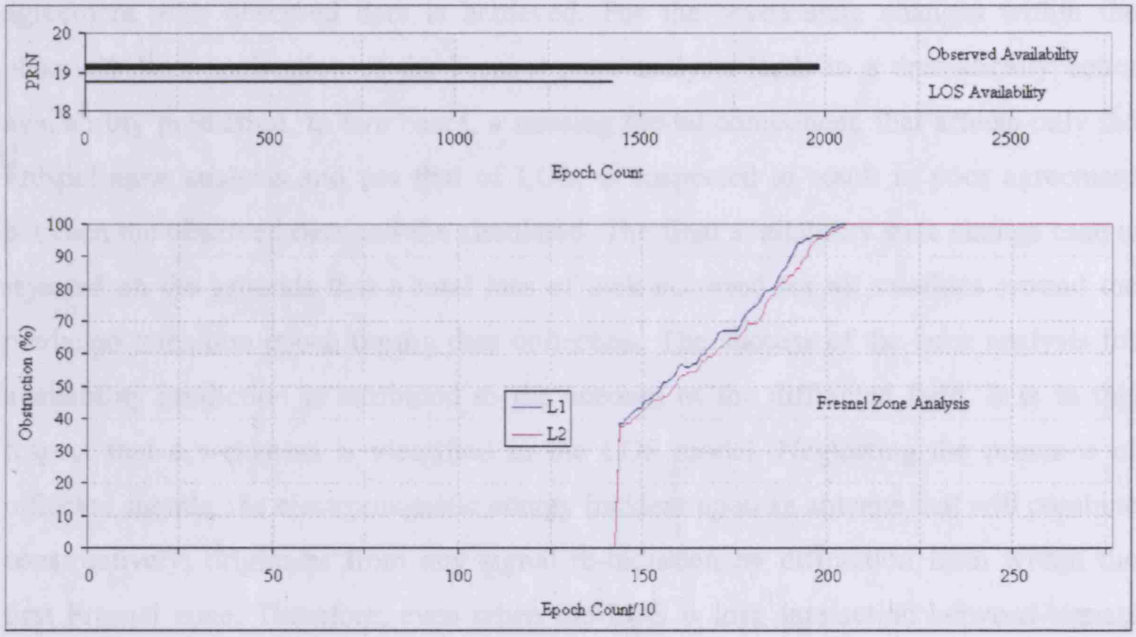

Figure 7-25: Comparison of observed data with LOS and Fresnel models for location 3 PRN19

A marked improvement over the LOS model is again apparent by predicting the loss of satellite availability at the 100% Fresnel zone obstruction point. This is illustrated in Figure 7-25.

7.5.3 Fresnel zone analysis validation summary

The Fresnel zone model, implemented within the simulator developed for this research has been fully tested, see section 5.4.6. Subsequently, the Fresnel zone model has been validated by comparing simulated data with observed data. Observation data has been collected at three individual locations, with appropriate positions. These locations exist on two separate environment model datasets. The characteristics of each environment vary whist all exist within urban environments. The analysis of the obstruction to the Fresnel zone for signals incident upon the antenna has been successfully achieved. Within the collected data, a total of seven satellite availability state changes can be used to assess the performance of the model in the same manner as performed for the LOS model. By comparison of the point at which availability state change occurs in the observed data and in the simulated data, the following conclusions can be made. Firstly,

the LOS model, used in isolation, prematurely predicts the obstruction of a satellite signal that is transiting from available to obstructed. The LOS model belatedly predicts a signal becoming available from a previously unavailable state. Application of Fresnel analysis indicates that the 100% obscuration level can be used to great effect. If this point is used to predict the transition of a signal availability state, a much better agreement with observed data is achieved. For the seven state changes within the observed data, application of the Fresnel zone analysis leads to a dramatically better availability prediction. In two cases, a missing model component, that affects only the Fresnel zone analysis and not that of LOS, is suspected to result in poor agreement between the observed data and the simulated. The final availability state change case is rejected on the grounds that a total loss of lock occurred for all satellites around the predicted transition epoch during data collection. The success of the zone analysis for availability prediction is attributed to the account of the diffracted field. It is in this respect that a weakness is identified in the LOS model. Neglecting the presence of reflected signals, the electromagnetic energy incident upon an antenna that will combine constructively, originates from any signal re-radiation by diffraction from within the first Fresnel zone. Therefore, even when the LOS is lost, interaction between signals and objects within the zone can still transfer electromagnetic wave energy, all of which will constructively interfere and produce a coherent signal at the antenna. This is not to say that the resulting signal displays the same signal to noise ratio as a direct LOS, and it is almost certain that attenuation occurs for all but the most lossless diffraction events. With this in mind, continuous tracking of the diffracted signal energy is likely until such time as the zone is completely obscured, or until the signal to noise ratio falls below a receiver dependent threshold. The case of signal acquisition under such conditions is untested. Some evidence exists within the observed and simulated data to suggest that reacquisition (with the specific equipment used) following a loss of lock under the presented diffracted signal scenario, is not possible. This is a subject for further debate and research. Fresnel analysis has been applied for every satellite with an obstructed LOS for each of the three locations. The output of this activity provides an estimate as to the level of obstruction of this zone. Fresnel zone analysis has been unable to account for the presence of satellite PRN 17 throughout the entire data collection period at location 2 (see Figure 7-4). It has also been unable to account for the presence of satellite PRN 17 from epoch 800 to 1350 at location 3 (see Figure 7-6).

7.6 Diffracted Propagation Model Validation

Treatment of diffracted propagation is made both by the Fresnel zone analysis, and also a ray tracing diffraction propagation model. The latter exists as a model under which a parameter for the maximum tolerable diffraction angle can be configured within the simulator. For the purpose of this work, a 3° maximum angle is used in all simulations. This is in accordance with Walker and Kubik [Walker and Kubik, 1996]. A full description of the model is presented in section 4.7.

7.6.1 Objective

Diffraction points that exist on the profile (with respect to receiver position) of structures surrounding the receiver are sought. In order to reradiate signals, the points must fulfil the following criteria: Firstly, the point must exist such that a diffraction angle below a defined threshold will result; secondly, the point must be visible by both receiver and by satellite from which the signal originates. The diffraction model is only employed when the LOS signal is obscured. The above must be achieved by provision of the following:

1. Suitable model of the environment surrounding the receiver.
2. Simulation epoch.
3. Simulation position.
4. Indication of clear and obstructed LOS paths.

7.6.2 Approach

A set of experiments performed at different locations, different epochs and with different environment models are described. Within the simulator, the coarse and detailed availability algorithms (described in section 4.5) are applied to produce the simulated LOS availability results. For signals where the LOS transmission path is obscured, the diffracted propagation model is employed (described in section 4.7) in order to assess the existence of a point that could yield a diffraction field subsequently detected by the receiver. Observed data is presented, the details of which can be found in section 7.3. The level of agreement between the observed data and the simulated data is analysed.

7.6.2.1 Location 1 Simulated Data

Location reference:	Location 1
Location:	Fenchurch Street, London
Dataset:	Dataset 1
Antenna coordinates:	X= 165.437, Y= 70.405, Z= 17.146
GPST start:	2007 1 31 10 33 25.0
GPST end:	2007 1 31 12 51 35.0
Simulation rate:	10 seconds
Total simulations:	829
Propagation model(s):	LOS assessment followed by diffraction model for obstructed LOS signals.

Multiple simulations have been performed according to the above inputs. For each satellite with an obstructed LOS, assessment is made as to whether a diffracted propagation may occur. If diffraction does occur then details relating to the incoming elevation and azimuth as well as the extra path length travelled by the signal are all computed. The presence of diffracted propagation, as simulated for location 1, is now graphically presented for PRN16, PRN18 and PRN22.

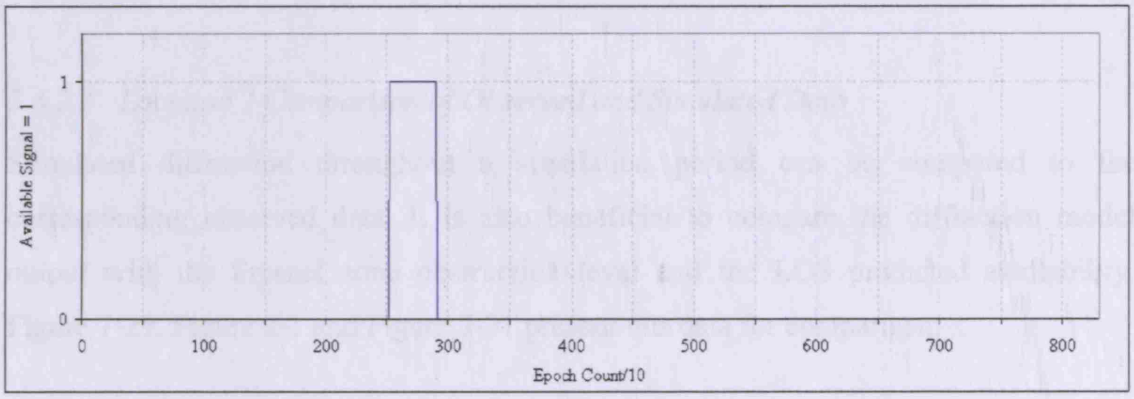

Figure 7-26: Simulated presence of a diffracted signal for location 1, PRN16

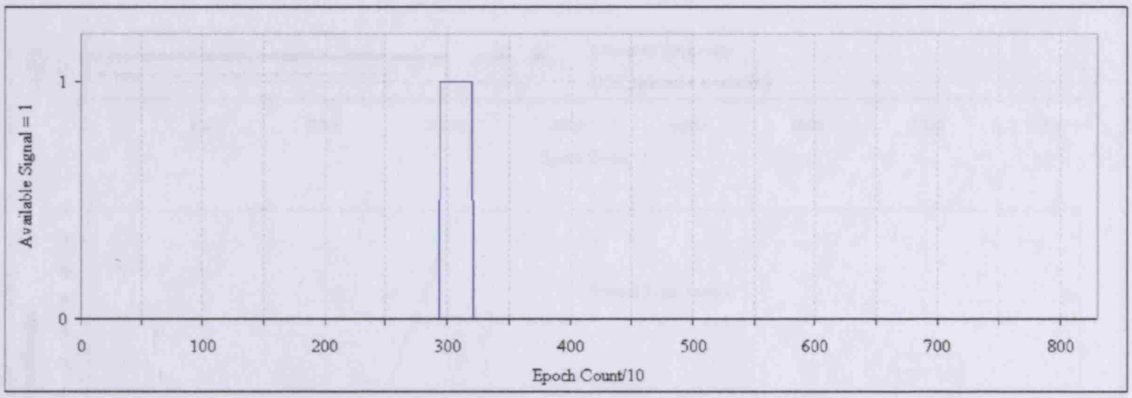

Figure 7-27: Simulated presence of a diffracted signal for location 1, PRN18

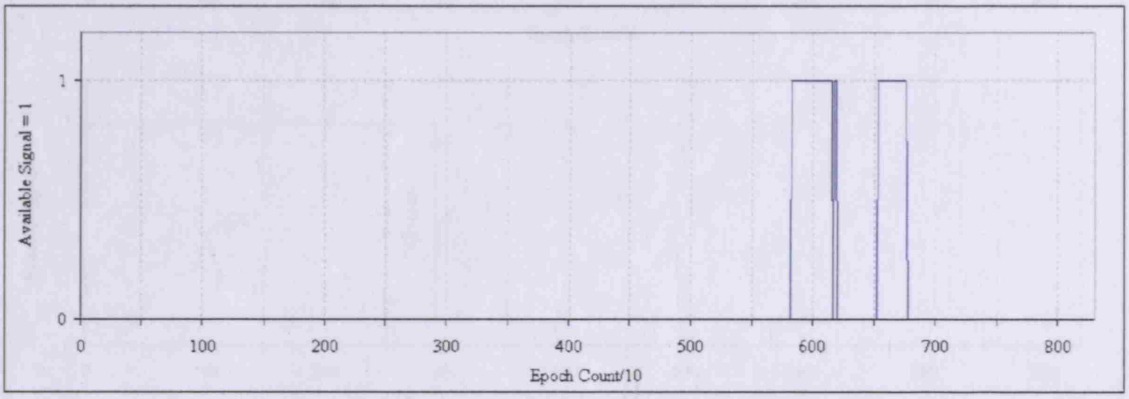

Figure 7-28: Simulated presence of a diffracted signal for location 1, PRN22

7.6.2.2 Location 1 Comparison of Observed and Simulated Data

Simulated diffraction throughout a simulation period can be compared to the corresponding observed data. It is also beneficial to compare the diffraction model output with the Fresnel zone obstruction level and the LOS predicted availability. Figure 7-29, Figure 2-1 and Figure 7-31 present this data for comparison.

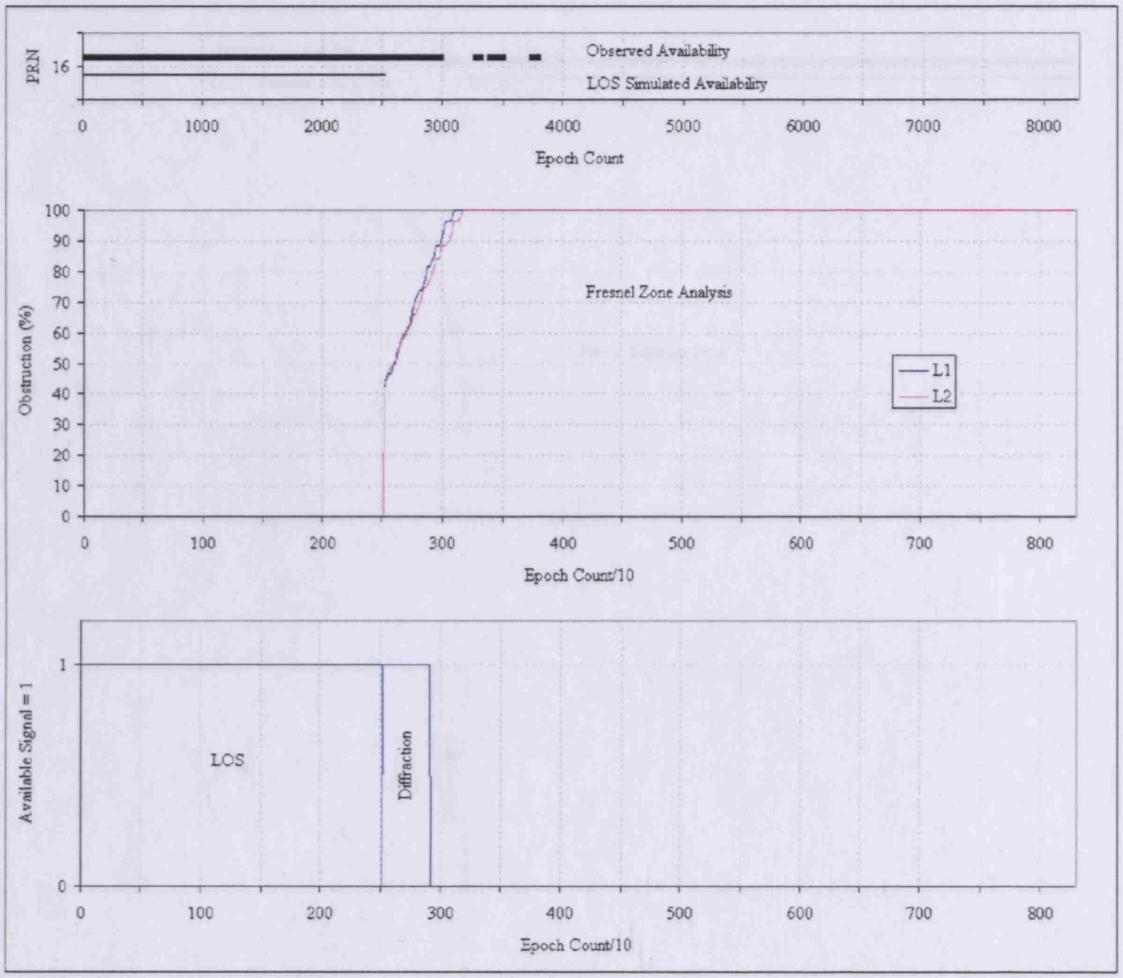

Figure 7-29: Comparison of observed data with LOS, Fresnel and diffraction models for location 1 PRN16

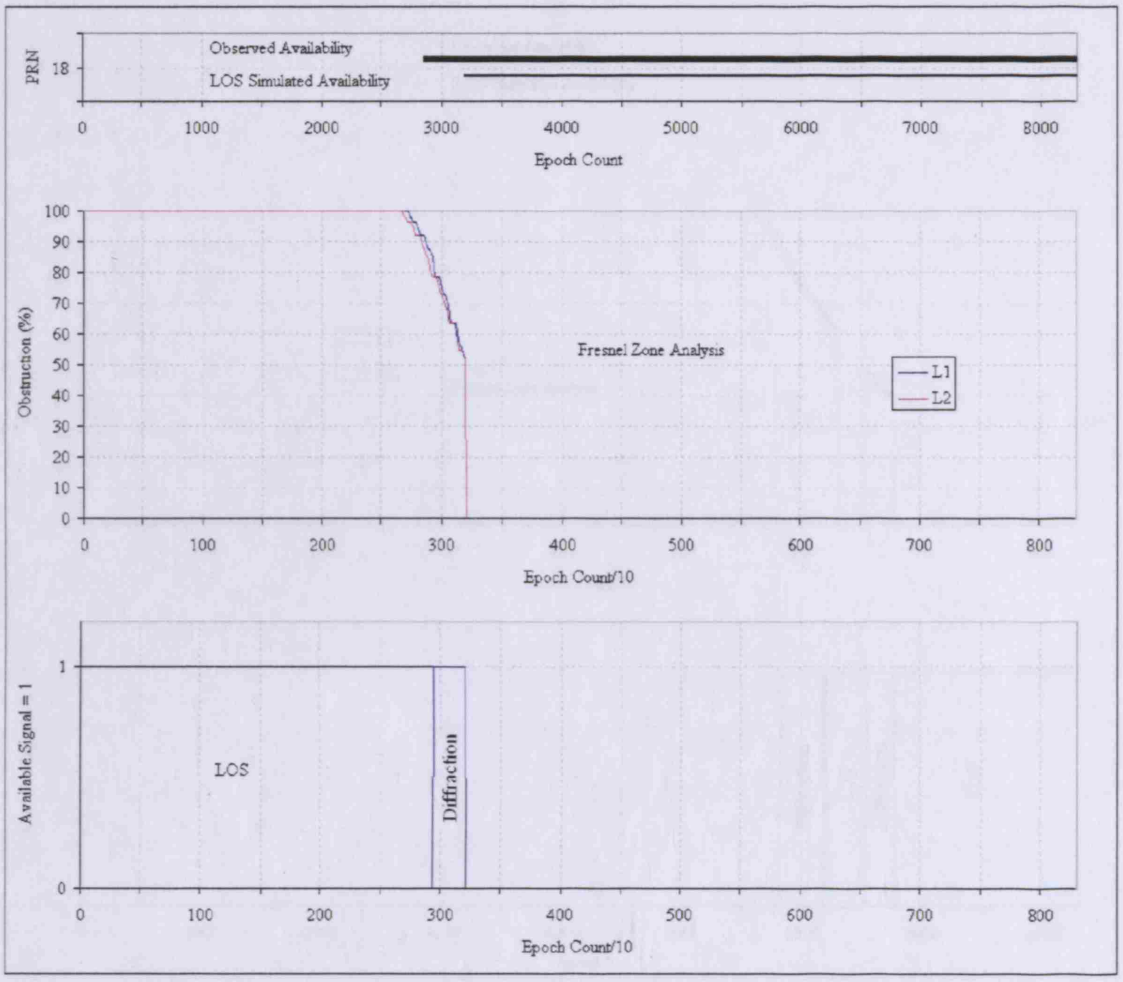

Figure 7-30: Comparison of observed data with LOS, Fresnel and diffraction models for location 1 PRN18

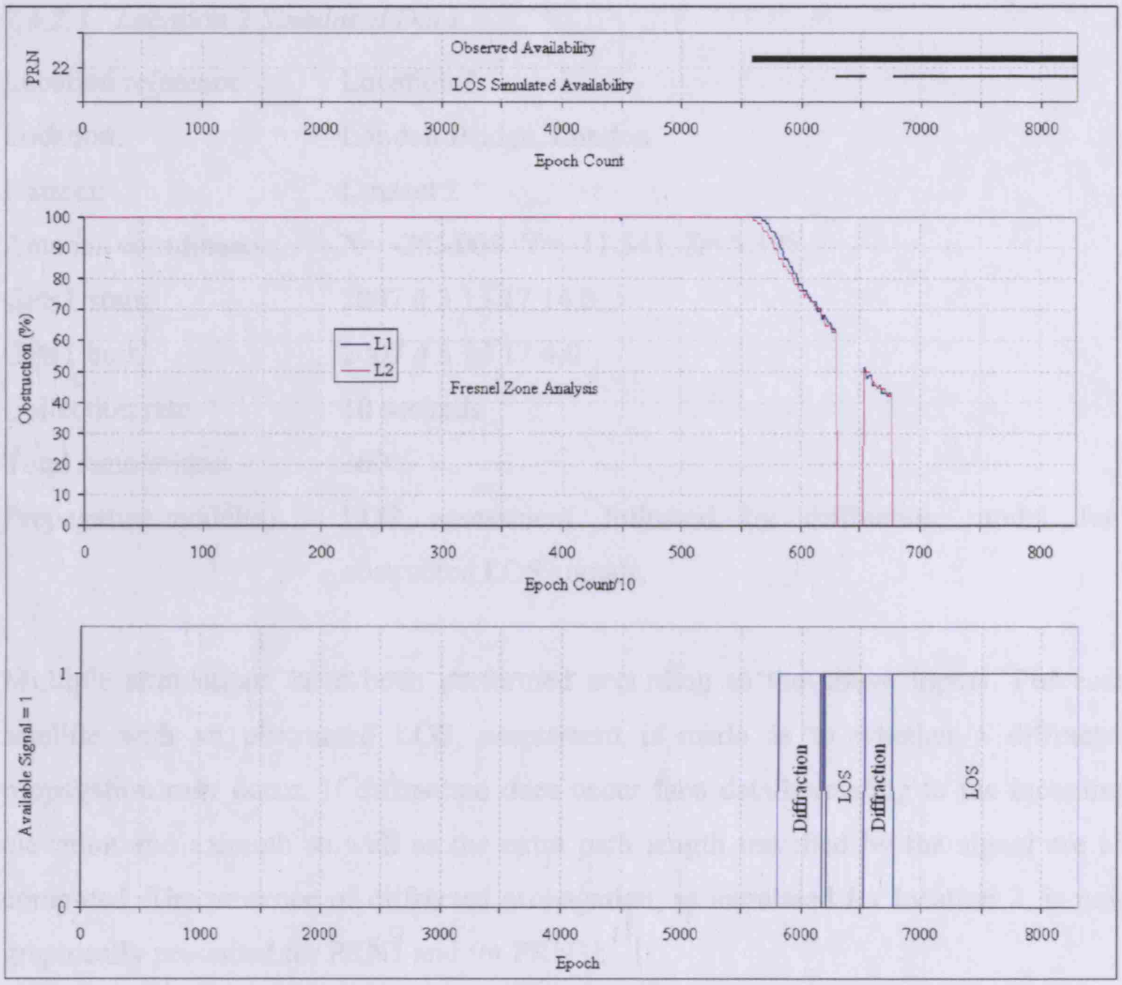

Figure 7-31: Comparison of observed data with LOS, Fresnel and diffraction models for location 1 PRN22

Satellites that experience an availability state change, or number of changes, during the data collection period are applicable for this test. All three applicable satellites at location 1 demonstrate that application of the diffracted propagation model, as an addition to the LOS model, results in a substantial improvement to the predicted period throughout which a satellite signal is available for range measurement. In each case, the application of the diffraction model produces a better estimate of the epoch at which a change in the availability state occurs. The experiments performed at this location cover availability state changes in both directions. Satellite PRN16 changes from available to unavailable, and satellites PRN18 and PRN22 change from unavailable to available. It has previously been established that LOS alone is insufficient in predicting the period through which a satellite is available, and diffracted propagation is believed to be responsible for this. Accounting for the diffracted propagation has proved to deliver better agreement between simulated and observed data.

7.6.2.3 Location 2 Simulated Data

Location reference:	Location 2
Location:	London Bridge, London
Dataset:	Dataset 2
Antenna coordinates:	X= -265.008, Y= -11.541, Z= 5.395
GPST start:	2007 4 3 13 17 14.0
GPST end:	2007 4 3 14 17 4.0
Collection rate:	10 seconds
Total simulations:	360
Propagation model(s):	LOS assessment followed by diffraction model for obstructed LOS signals.

Multiple simulations have been performed according to the above inputs. For each satellite with an obstructed LOS, assessment is made as to whether a diffracted propagation may occur. If diffraction does occur then details relating to the incoming elevation and azimuth as well as the extra path length travelled by the signal are all computed. The presence of diffracted propagation, as simulated for location 2, is now graphically presented for PRN1 and for PRN31.

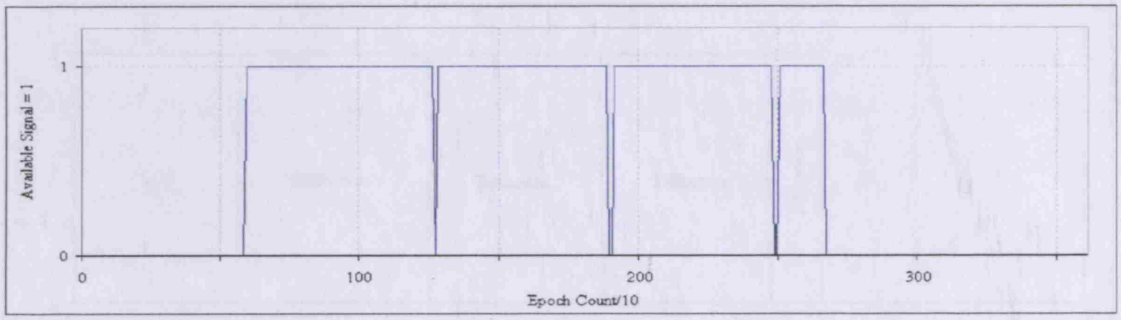

Figure 7-32: Simulated presence of a diffracted signal for location 2, PRN1

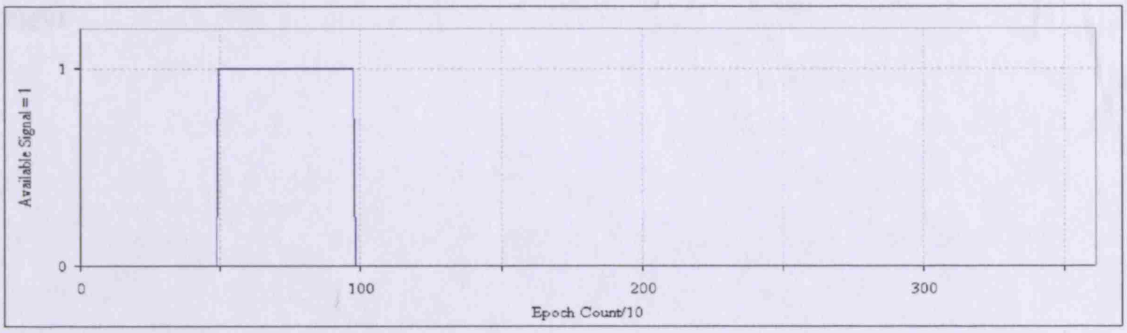

Figure 7-33: Simulated presence of a diffracted signal for location 2, PRN31

7.6.2.4 Location 2 Comparison of Observed and Simulated Data

Simulated diffraction throughout a simulation period can be compared to the corresponding observed data. It is also beneficial to compare the diffraction model output with the Fresnel zone obstruction level and the LOS predicted availability. Figure 7-34 and Figure 7-35 present this data for comparison.

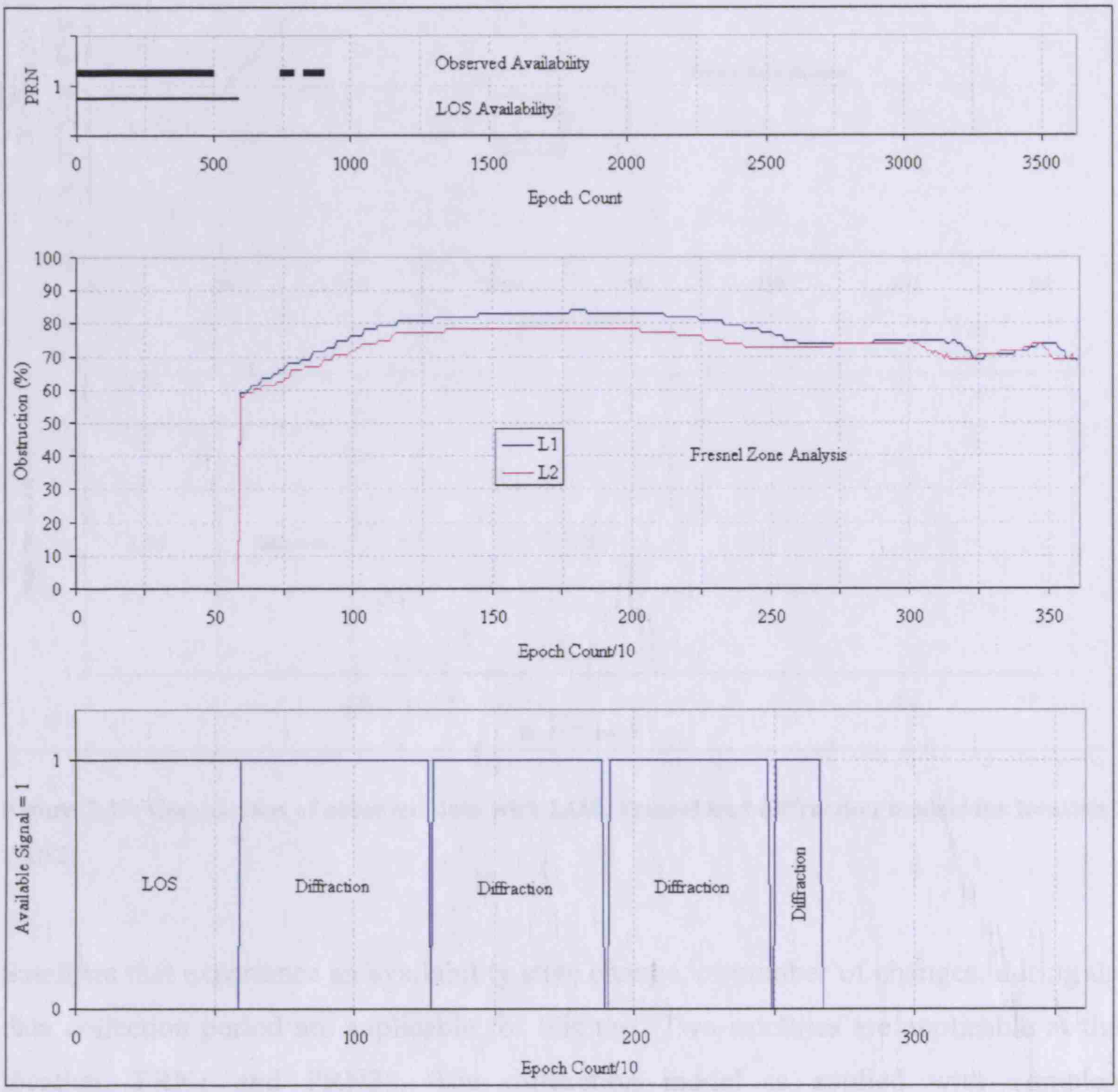

Figure 7-34: Comparison of observed data with LOS, Fresnel and diffraction models for location 2 PRN1

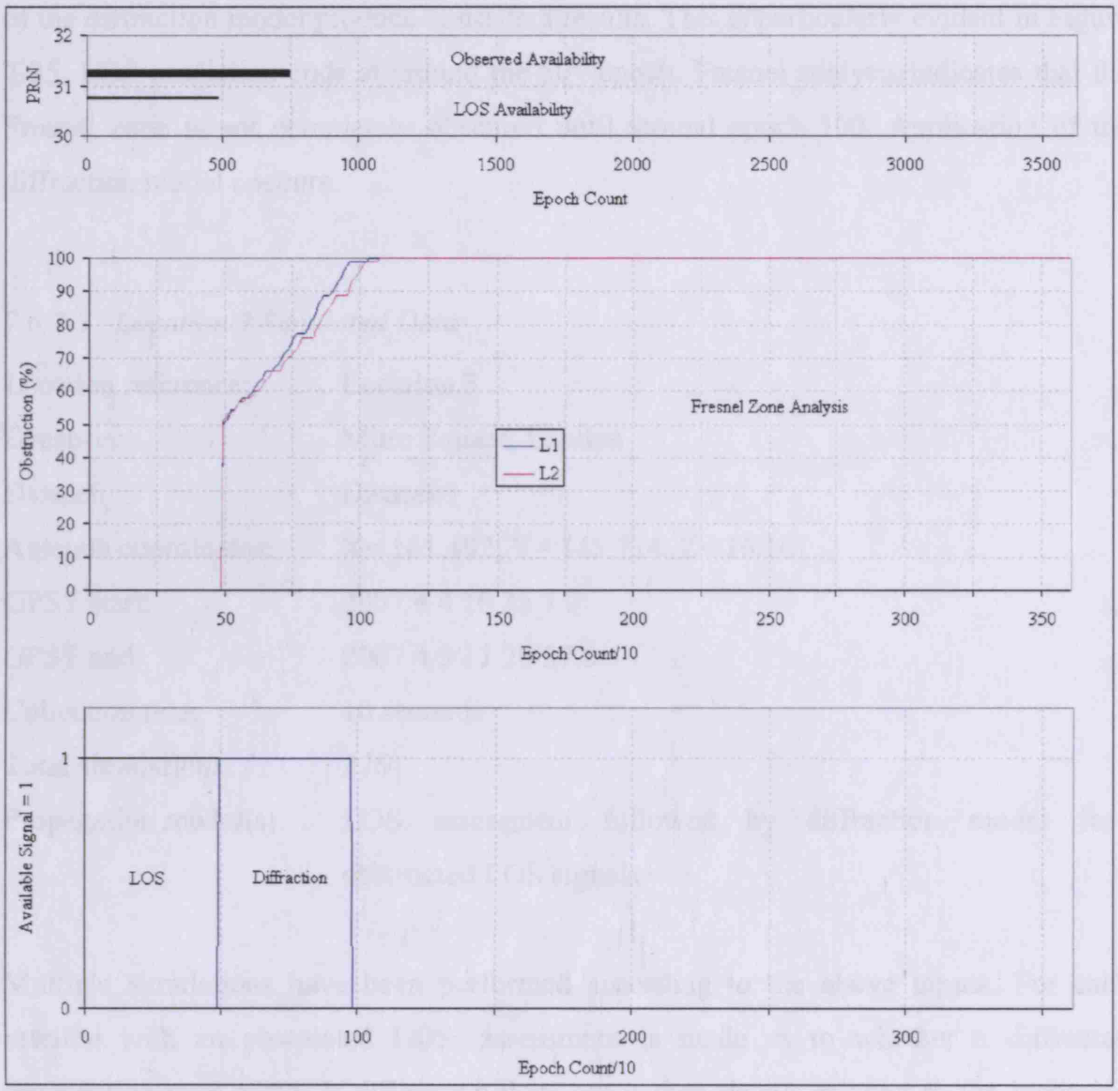

Figure 7-35: Comparison of observed data with LOS, Fresnel and diffraction models for location 2 PRN21

Satellites that experience an availability state change, or number of changes, during the data collection period are applicable for this test. Two satellites are applicable at this location, PRN1 and PRN31. The diffraction model is applied with complete independence from the Fresnel zone analysis. As discovered in section 7.5.2.4, HMS Belfast (not present in the computerised environment model) is likely to be causing obstruction to the real world data. The absence of this component causes no disruption to the LOS model, but is expected to affect the Fresnel zone analysis. The effect on the diffraction model is likely to be similar to that of the Fresnel zone analaysis. It is evident that this is the case. As demonstrated by Figure 7-34 and Figure 7-35, the predicted availability extends far beyond the observed availability, for the reasons mentioned above. It is, however, noted that the Fresnel zone analysis and the application

of the diffraction model produce consistent results. This is particularly evident in Figure 7-35. LOS prediction ends at around the 50th epoch. Fresnel analysis indicates that the Fresnel zone is not completely obscured until around epoch 100. Application of the diffraction model concurs.

7.6.2.5 Location 3 Simulated Data

Location reference:	Location 3
Location:	Mitre Square, London
Dataset:	Dataset 1
Antenna coordinates:	X= 161.492, Y= 145.714, Z= 16.161
GPST start:	2007 4 4 10 35 7.0
GPST end:	2007 4 3 11 20 57.0
Collection rate:	10 seconds
Total simulations:	276
Propagation model(s):	LOS assessment followed by diffraction model for obstructed LOS signals.

Multiple simulations have been performed according to the above inputs. For each satellite with an obstructed LOS, assessment is made as to whether a diffracted propagation may occur. If diffraction does occur then details relating to the incoming elevation and azimuth as well as the extra path length travelled by the signal are all computed. The presence of diffracted propagation, as simulated for location 3, is now graphically presented for PRN 19 (Figure 7-36).

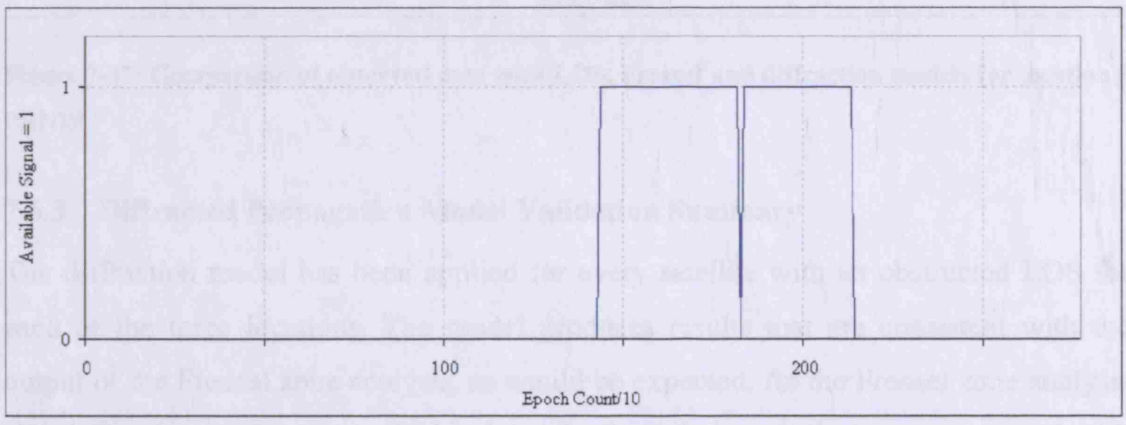

Figure 7-36: Simulated presence of a diffracted signal for location 3, PRN19

7.6.2.6 Location 3 Comparison of Observed and Simulated Data

Simulated diffraction throughout a simulation period can be compared to the corresponding observed data. It is also beneficial to compare the diffraction model output with the Fresnel zone obstruction level and the LOS predicted availability. Figure 7-37 presents this data for comparison.

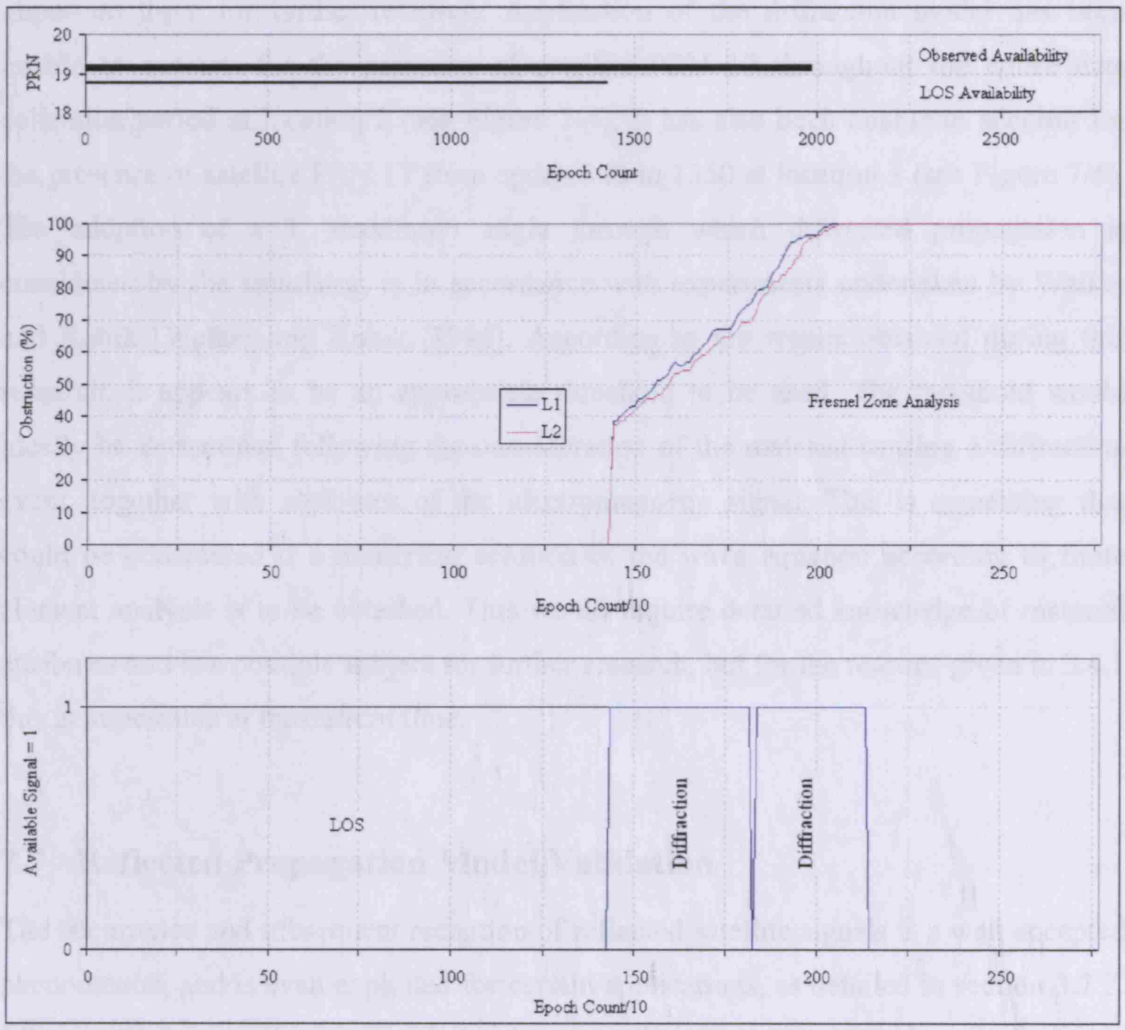

Figure 7-37: Comparison of observed data with LOS, Fresnel and diffraction models for location 3 PRN19

7.6.3 Diffracted Propagation Model Validation Summary

The diffraction model has been applied for every satellite with an obstructed LOS for each of the three locations. The model produces results that are consistent with the output of the Fresnel zone analysis, as would be expected. As the Fresnel zone analysis and diffraction model are applied independently and share little common ground with regard to the techniques and algorithms developed, the level of agreement between the two acts as a validation in itself. Of the seven satellites that experience availability state

change, four cases demonstrate that the application of the diffraction model dramatically enhances the prediction of satellite availability, over the use of an LOS model alone. Two cases are effectively invalid, as it is suspected that disruption to the observed signal is caused by a component that is not present in the computerised model. This highlights the importance, when constructing city models for this type of work, to ensure that not only the objects that are in view of the receiver are present. This is an important topic for further research. Application of the diffraction model has been unable to account for the presence of satellite PRN 17 throughout the entire data collection period at location 2 (see Figure 7-4). It has also been unable to account for the presence of satellite PRN 17 from epoch 800 to 1350 at location 3 (see Figure 7-6). The adoption of a 3° maximum angle through which diffracted propagation is considered by the simulator, is in accordance with experiments undertaken by Walker and Kubik [Walker and Kubik, 1996]. According to the results obtained during this research, it appears to be an appropriate threshold to be used. The threshold would ideally be determined following the consideration of the material causing a diffraction event, together with attributes of the electromagnetic signal. This is something that could be considered if a numerical solution of the wave equation according to finite element analysis is to be obtained. This would require detailed knowledge of material attributes and is a possible subject for further research, but for the reasons given in 3.4.1 this is impossible at the current time.

7.7 Reflected Propagation Model Validation

The occurrence and subsequent reception of reflected satellite signals is a well accepted phenomenon, and is even exploited for certain applications, as detailed in section 3.2.2. When present in combination with the direct satellite to receiver signal, an error due to multipath effects is consequent. It is also the case that a reflected signal can be received when the direct signal is obstructed, referred to as the reflected-only propagation mode. In this case the range measurement error is a function of the extra path length experienced by the incoming signal. The reflected-only propagation mode is exploited during this work to validate the reflected propagation model within the simulator.

7.7.1 Objective

A specular, single-reflection model has been implemented in the simulator. Signals that have arrived at the receiver via reflected transmission paths are to be detected by application of this model. It is undoubtedly the case that signals arriving at the antenna via direct and even diffracted propagation are contaminated by the additional reception of reflected signals, and it is difficult to decorrelate the reflected component from these signals. For this reason, the only way to validate the reflected model is to isolate observed data that has arrived via the reflected-only propagation mode. Within collected data from locations 2 and 3, there exist the presence of satellite signals that are unexplained by LOS, Fresnel zone analysis and diffracted propagation models. It is suspected that these range measurements are made upon a signal that arrives via a reflected transmission path. In this way, the results of simulations including the reflected propagation model can be used for the detection of these signals and subsequent validation of the reflected propagation model.
The above must be achieved by provision of the following:

1. Suitable model of the environment surrounding the receiver.
2. Simulation epoch.
3. Simulation position.
4. Indication of clear and obstructed LOS paths.

7.7.2 Approach

A set of experiments performed at different locations, different epochs and with different environment models are described. For all signals, even those with unobstructed LOS paths, the reflection model is applied. In this way, the signal environment in terms of reflected signals, in which the receiver is operating, is characterised. Reflection modelling produces details of all anticipated reflection paths, including details such as specular reflection point, extra path length, azimuth, elevation, and an estimate of the available surface area for the re-radiation of signal energy. Observed data is presented, the details of which can be found in section 7.3. The level of agreement between the observed data and the simulated data is analysed.

7.7.2.1 Location 2 Comparison of Observed and Simulated Data

Location reference:	Location 2
Location:	London Bridge, London
Dataset:	Dataset 2
Antenna coordinates:	X= -265.008, Y= -11.541, Z= 5.395
GPST start:	2007 4 3 13 17 14.0
GPST end:	2007 4 3 14 17 4.0
Collection rate:	10 seconds
Total simulations:	360
Propagation model(s):	LOS assessment followed by reflection model for PRN 17 only.

Multiple simulations have been performed according to the above inputs. The reflection model is then applied for all satellites above the elevation mask, or as in this case, for a specific satellite. The advantage of running reflected propagation simulations for a single satellite is a much reduced simulation time. The simulation focuses on satellite PRN17, as this satellite appears in the observed data and is not picked up by other propagation models. It is therefore possible that this satellite appears following a reflected transmission path.

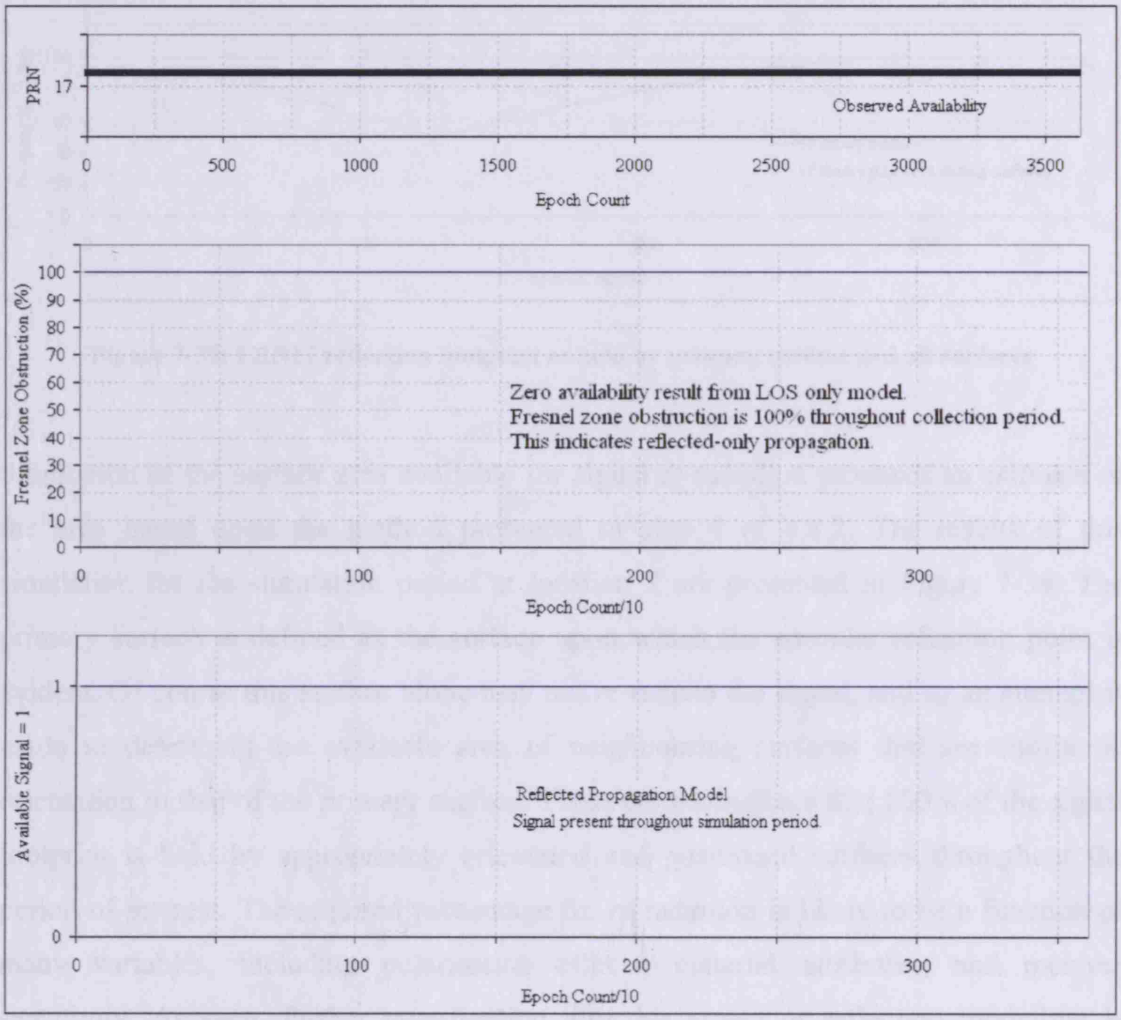

Figure 7-38: PRN17 reflection as observed and as simulated for Location 2

As presented in Figure 7-38, the reflection model picks up the signal of satellite PRN17 via a reflected path. The presence and duration of the signal over the entire data collection period is highlighted in the top graph, showing the collected data. Corresponding simulated data is presented in the next two graphs within the figure. The Fresnel zone obstruction over the entire period is presented in the middle graph, and this shows that both LOS and diffracted propagation cannot be responsible for the reception of this signal, as 100% obstruction is experienced throughout. The third graph in the figure presents the results of the reflection model. This indicates that a specular reflection is responsible for delivering the signal, and that this specular reflection is possible over the entire period of simulation. This is consistent with the observed data. The available surface area for re-radiation of the reflected signal, referred to as the reflection footprint, is subsequently considered.

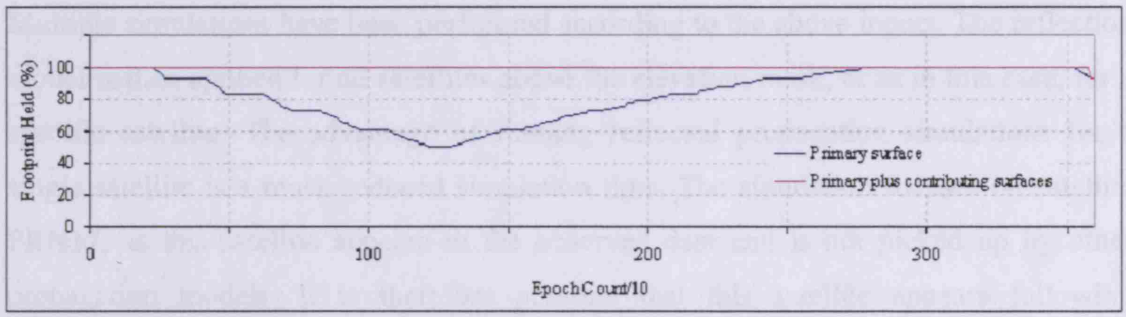

Figure 7-39: PRN17 reflection footprint as held by primary surface and all surfaces

Simulation of the surface area available for signal re-radiation produces an estimate of the area based upon the method presented in step 4 of 4.8.2. The results of this simulation for the simulation period at location 2 are presented in Figure 7-39. The primary surface is defined as the surface upon which the specular reflection point is evident. Of course this surface alone may not re-radiate the signal, and so an attempt is made to determine the available area of neighbouring surfaces that are similar in orientation to that of the primary surface. These results indicate that 100% of the signal footprint is held by appropriately orientated and positioned surfaces throughout the period of interest. The required percentage for re-radiation is likely to be a function of many variables, including polarisation effects, material attributes, and receiver sensitivity. As such, further investigation into this aspect of reflection modelling is outside the scope of this research. The importance of this calculation is that is provides more evidence to indicate that a reflected propagation is responsible for the reception of this signal.

7.7.2.2 Location 3 Simulated Data

Location reference:	Location 3
Location:	Mitre Square, London
Dataset:	Dataset 1
Antenna coordinates:	X= 161.492, Y= 145.714, Z= 16.161
GPST start:	2007 4 4 10 35 7.0
GPST end:	2007 4 3 11 20 57.0
Collection rate:	10 seconds
Total simulations:	276
Propagation model(s):	LOS assessment followed by reflection model for PRN 17 only.

Multiple simulations have been performed according to the above inputs. The reflection model is then applied for all satellites above the elevation mask, or as in this case, for a specific satellite. The advantage of running reflected propagation simulations for a single satellite is a much reduced simulation time. The simulation focuses on satellite PRN17, as this satellite appears in the observed data and is not picked up by other propagation models. It is therefore possible that this satellite appears following propagation through a reflected transmission path.

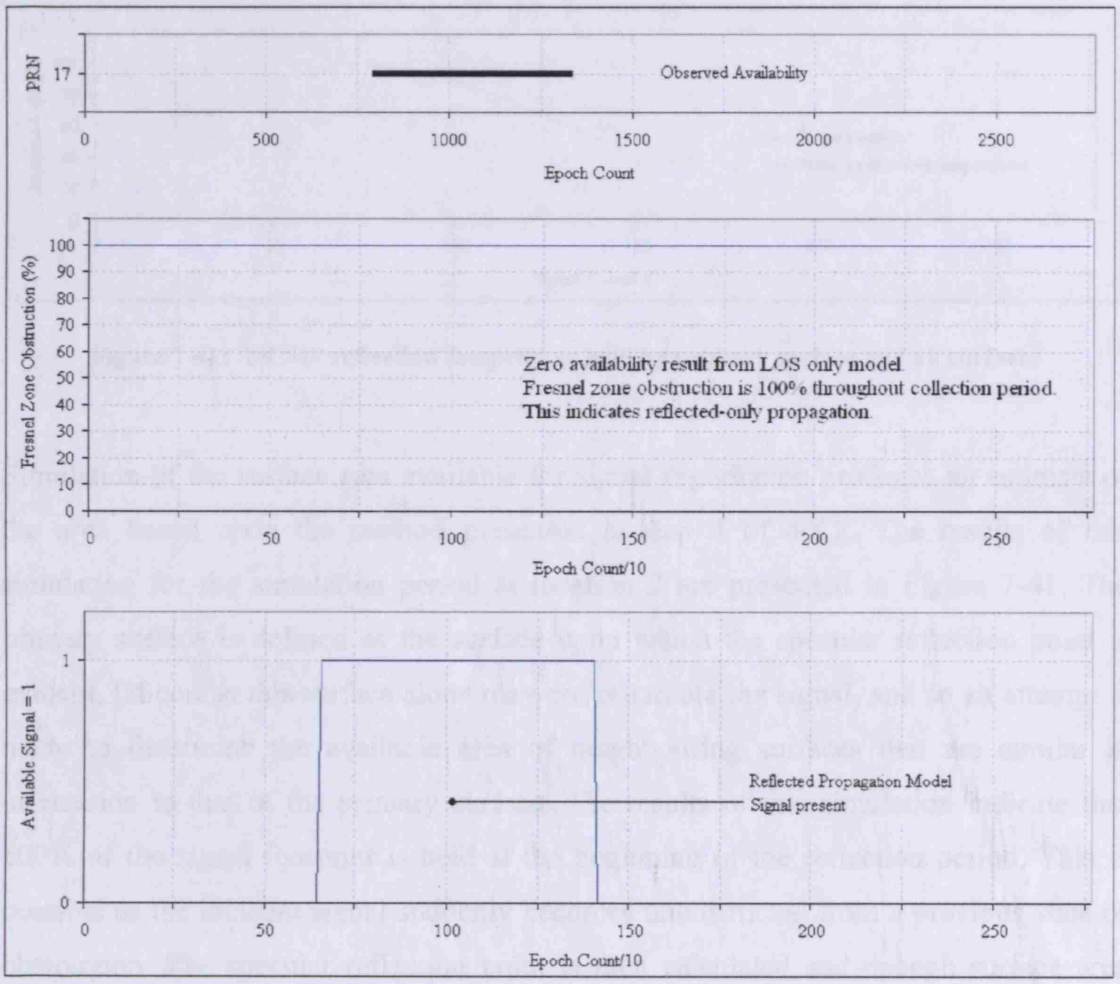

Figure 7-40: PRN17 reflection as observed and as simulated for Location 3

As presented in Figure 7-40, the reflection model picks up the signal of satellite PRN17 via a reflected path. The observed availability of PRN17 is presented in the top graph. Simulated data for the corresponding time period is presented in the next two graphs within the figure. The Fresnel zone obstruction over the entire period is presented in the middle graph, and this shows that both LOS and diffracted propagation cannot be responsible for the reception of this signal, as 100% obstruction is experienced

throughout. The third graph in the figure presents the results of the reflection model. Application of the specular reflection model has detected the received signal. Further to this, the reflection model has produced a good level of agreement to the observed data in terms of the time at which the reflection is visible, and also the duration of this signal. For the example given, the simulated results are highly consistent with the observed data. The available surface area for re-radiation of the reflected signal, referred to as the reflection footprint, is subsequently considered.

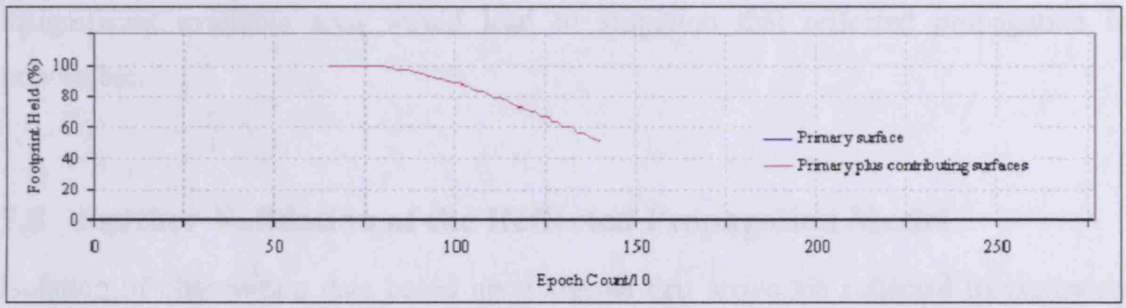

Figure 7-41: PRN17 reflection footprint as held by primary surface and all surfaces

Simulation of the surface area available for signal re-radiation produces an estimate of the area based upon the method presented in step 4 of 4.8.2. The results of this simulation for the simulation period at location 2 are presented in Figure 7-41. The primary surface is defined as the surface upon which the specular reflection point is evident. Of course this surface alone may not re-radiate the signal, and so an attempt is made to determine the available area of neighbouring surfaces that are similar in orientation to that of the primary surface. The results of this simulation indicate that 100% of the signal footprint is held at the beginning of the reflection period. This is possible as the incident signal suddenly becomes unobstructed from a previous state of obstruction. The specular reflection point is then calculated and enough surface area surrounds the point to provide 100% capture of the footprint.

7.7.3 Reflected Propagation Model Validation Summary

Datasets collected at locations 2 and 3 contain observations that have been unexplained by application of the previous propagation models. The reflected propagation model has been applied within the simulator, and simulation results for appropriate time periods at these locations have been generated. One reflected-only signal is present throughout the entire observation time period, and the other appears and disappears within the time

period of data collection. Simulation has confirmed that these observations are based upon propagation via reflected signal paths. In both cases, the models employed within the simulator, accurately predicts the time period throughout which the signal is present. In addition, estimates for the available area to reradiate the electromagnetic energy during a reflection are made. These estimates indicate that, in both of the analysed cases, there is substantial surface area available with respect to the signal footprint that is projected during a Fresnel zone analysis. This gives further weight to the evidence that these signals propagate via reflected only signal paths, as the computation of an insignificant available area would lead to suspicion that reflected propagation is impossible.

7.8 Further Validation of the Reflected Propagation Model

Isolation of observation data based upon signals that arrive via reflected transmission paths, where the LOS is obstructed, has been used to validate operation of the reflected propagation model within the simulator. The model performs well in predicting when range measurements will be made upon reflected signals. This has been established by comparison of observation data with the simulator output. From an availability perspective, this achievement will enhance current applications that rely upon GNSS in urban environments. The ability to rely upon the use of a signal that has been determined to arrive via a reflected signal path, depends upon the ability to correctly determine the range error that has been caused by transmission via the non-direct transmission path. This section aims to compare range error within observed data, attributed to reflection, with simulated range error. This will provide a comprehensive validation of the reflected propagation model, as it will indicate that not only the presence of a simulated reflection is valid, but also the geometry of the transmission path is correct.

7.8.1 Objective

Exploitation of received signals that are established as arriving via reflected-only paths permits validation of the reflected propagation model. This is because the performance of the receiver (in terms of position determination), under the presence of multipath (direct and reflected signals), can be disregarded. We are interested in examining the raw range measurements only. The objective of the work presented in this section is to establish range errors, due to reflected propagation, in the observed data. This can then

be compared with range errors determined by simulation. It should be noted, that as this is a validation exercise, observed and simulated data are treated independently.
The above must be achieved by provision of the following:

1. Precise receiver position.
2. Precise (SP3) satellite positions and clock corrections.
3. Outputs of the reflection model from the simulator.

7.8.2 Approach

At the outset, the use of a code minus carrier solution to determine the effect of multipath was considered. This was neglected due to concerns that proprietary code smoothing techniques used by the receiver maufacturer might have some unknown effect on such a solution. Formation and examination of the MP1 and MP2 observables [Hilla and Cline, 2002] was attempted and subsequently neglected due to concerns that comercially sensitive techniques for decryption of the P-code might affect such calculations. For these reasons, it was considered more prudent not to rely upon observations made to only one satellite in an epoch, and rather to adopt a solution that would make use of all pseudoranges within a measurement epoch. A modified point positioning program is used to determine the atmospheric errors and receiver clock offset present on code pseudorange measurements extracted from a RINEX observation file. The aim is to extract and estimate as many errors from the observed pseudoranges as possible, such that the dominant remaining error is that of multipath. This remaining error can be quantified, as the true geometric range to each satellite is known by virtue of the use of precise satellite orbits and a surveyed receiver position.

7.8.3 Analysis Method

Pseudorange model

$$P_n = r_n + c(dt_{Sat(n)} - dt_{Rx}) + Ion_{(n)} + Trop_{(n)} + \varepsilon_{Rx} + MP_{Code(n)} \qquad \text{(eqn. 7-1)}$$

Where satellite (PRN denoted by n) and:

P_n = Pseudorange as extracted from the RINEX observation file (m).
r_n = True geometric range (m).
c = Speed of light (m/s).
$dt_{Sat(n)}$ = Clock offset from GPST (s).

dt_{Rx} = Receiver clock offset from GPST (s).

Ion_n = Ionospheric delay (m).

$Trop_n$ = Tropospheric delay (m).

ε_{Rx} = Receiver noise (m).

$MP_{Code(n)}$ = Code multipath (m).

Calculation of the true geometric range

For each satellite to receiver vector pair, the true geometric range is computed according to the following:

$$r_n = \left| \overline{X}_{S(n)} - \overline{X}_R \right| \qquad \text{(eqn. 7-2)}$$

Where:

r_n = True geometric range.

$\overline{X}_{S(n)}$ = Satellite position at signal transmission time. Corrected for Earth rotation .during signal flight time.

$\overline{X}_R$ = Receiver position at measurement epoch.

For the purposes of this analysis, it is assumed that the following are sufficient. Satellite positions are computed using the appropriate SP3 precise orbit file, as detailed in section 4.3.4. No correction for the antenna phase centre is made, for two reasons. Firstly, this offset is assumed to map into the range measurement between satellite and receiver by a negligible amount. Secondly, we are dealing only with code measurements. No carrier observables are used in this analysis, with the exception of the formation of linear combinations. In addition, the same treatment of the receiver position is made. The absolute centre of the antenna is used, rather that the phase centre. An enhancement to this analysis in subsequent research may seek to update this, although it is deemed to have no effect on the analysis described within this thesis.

Formation of the ionosphere free observable

This analysis can only be applied to observed data containing dual frequency measurements. The formation of the ionosphere free observable can be found in [ICD-GPS-200, 1995]. As there are a variety of implementations of this linear combination, the chosen version and source are now provided.

$$P_{ion} = \frac{P_2 - \gamma P_1}{1 - \gamma} \qquad \text{[ICD-GPS-200, 1995, Page75]} \qquad \text{(eqn. 7-3)}$$

Where:

$$\gamma = \left(\frac{f_{L1}}{f_{L2}} \right)^2 \qquad \text{[ICD-GPS-200, 1995, Page 74]} \qquad \text{(eqn. 7-4)}$$

P_{ion} = Ionosphere free pseudorange observable.

P_n = Pseudorange measured on L-band indicated by the subscript.

In the absence of dual frequency observations, an ionospheric model is provided in [ICD-GPS-200, 1995, Page 106a].

Estimation of the tropospheric error

A Modified Hopfield model is used to compute an estimate of the pseudorange error due to tropospheric delay. A full description of this model can be found in [Kaplan, 1996]. The following parameter values are used:

Temperature:	20° C
Pressure:	980 mbar
Relative humidity:	50%
Empirical constant a_1:	77.624 K/mbar
Empirical constant a_2:	-12.92 K/mbar
Empirical constant a_3:	371,900 K^2/mbar

Satellite clock offset correction

As described in section 4.3.4, the correction for each satellite clock offset is determined via interpolation of the data provided within the appropriate SP3 precise orbit file. Each observed pseudorange is corrected.

Determining estimates of code multipath range error on observed pseudoranges

With reference to Figure 7-42, the extraction of satellite clock range error and atmospheric errors produces pseudoranges that contain receiver clock range error and multipath error. For the reflected-only signal case (where the direct signal is obstructed), the receiver clock error is accompanied by the increased path length over which the reflected signal has travelled. The illustrated case assumes that receiver noise is neglected and precise satellite and receiver positions have been determined. It is

acknowledged that any residual errors within the atmospheric modelling, and in particular any localised atmospheric effects that have not been extracted by the ionospheric and troposheric models will polute the solution and as such will map into either the receiver clock estimate (described subsequently), or into the estimate of an increased path length due to reflected propagation. This is not considered to be problematic, as the extra path length to be determined is expected to be the dominant error source and depending upon the geometrical configuration of any reflection, can easily be of the order of tens of metres. Additionally, due to the urban canyon effect, satellites within the solution tend to exhibit high elevation angles due to obstruction by surrounding objects. Therefore, any residual error component that is a function of the elevation angle will be applicable to all satellites and will subsequently map into the receiver clock error estimate to be extracted from all ranges. In this approach, the receiver clock error estimate is required only such that it can be extracted from all observations. In this way, it is of no consequence if the estimate also soaks up any residual errors from other error models, provided that any such error applies to all observations.

A property of this approach is that all pseudoranges within the measurement epoch contain the same range error due to receiver clock offset from GPST. Establishing the receiver clock offset is conventionally achieved by application of a least squares adjustment, as used in a traditional PVT solution. However, this would result in some of the reflected signal path mapping into the solution for the clock offset, and therefore a realistic estimate of the extra path length would not be achieved. The occurrence of a pseudorange within the measurments made at a specific epoch, that is definitely made upon a direct signal and that had no multipath error, could be used to solve for the clock error.

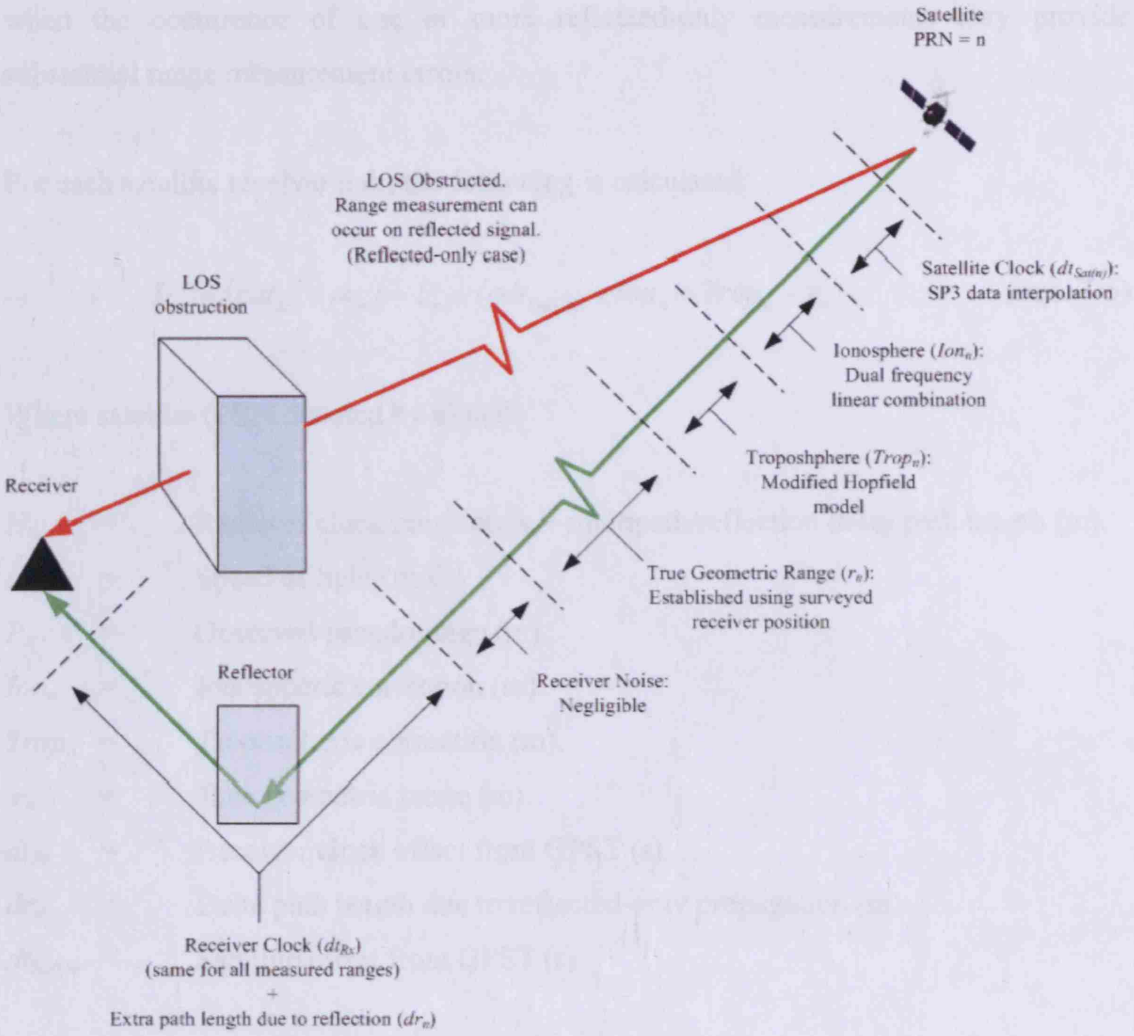

Figure 7-42: Extraction of errors from observed pseudoranges for reflected-only propagation

Due to the nature of correlator peak distortion (as described in section 3.2.3), code multipath can induce a negative range error. In the reflection-only case, the correlator peak occurs at a phase shift of the internally generated PRN code replica, that is greater than that of the direct signal (see section 3.2.2). Therefore, the reflected-only case will always result in an increased time of flight measurement by the receiver. In order to determine the receiver clock offset we need to minimise the distortion of the estimated clock term by code multipath. By finding the observation with satellite clock range error and atmospheric effects accounted for, that is closest in magnitude to the appropriate true geometric range, we are automatically selecting the range with the minimum multipath error. This is by virtue of the fact that the clock error is the same for all pseudorange measurements. The clock error can then be computed using this chosen range. It should be noted that any multipath error present on that range will map into the receiver clock estimate, however, this is a better situation than allowing the receiver clock estimate to soak up multipath errors from all range measurements, especially

when the occurrence of one or more reflected-only measurements may provide substantial range measurement errors.

For each satellite receiver pair, the following is calculated:

$$H_n = (cdt_{Rx} + dr_n) = P_n - (cdt_{Sat(n)} + Ion_n + Trop_n + r_n) \qquad \text{(eqn. 7-5)}$$

Where satellite (PRN denoted by n) and:

H_n = Receiver clock range error + multipath/reflection delay path length (m).
c = Speed of light (m/s).
P_n = Observed pseudorange (m).
Ion_n = Ionospheric correction (m).
$Trop_n$ = Tropospheric correction (m).
r_n = True geometric range (m).
dt_{Rx} = Receiver clock offset from GPST (s).
dr_n = Delta path length due to reflected-only propagation (m).
$dt_{Sat(n)}$ = Satellite offset from GPST (s).

The minimum value of H_n is sought. This occurs at a specific PRN denoted by a. At Ha it is assumed that dr_a is small, such that dr_a is set to zero. The receiver clock offset from GPST can then be calculated:

From equation 7-5:

$$(cdt_{Rx} + 0) = P_a - (cdt_{Sat(a)} + Ion_a + Trop_a + r_a) \qquad \text{(eqn. 7-6)}$$

and

$$dt_{Rx} = \frac{P_a - (cdt_{Sat(a)} + Ion_a + Trop_a + r_a)}{c} \qquad \text{(eqn. 7-7)}$$

It is now possible to determine dr_n for the satellite(s) to receiver pair(s) that exhibit reflected-only propagation. Determination of dr_n for other pseudoranges will yield an estimate of the range error due to multipath.

7.8.3.1 Location 2 Analysis of Reflected-Only Signal

As indicated in section 7.7.2.1, a reflected-only signal has been detected by simulation. The simulated result directly corresponds to the observed signal from the same satellite, in terms of the duration of the signal presence. It is now desirable to analyse the observed signal, by the method described in section 7.8.3. An estimate for the extra path length through which the signal has travelled as a result of reflected propagation is sought from the observed data. This will then be compared with the corresponding extra path length as determined by the simulation.

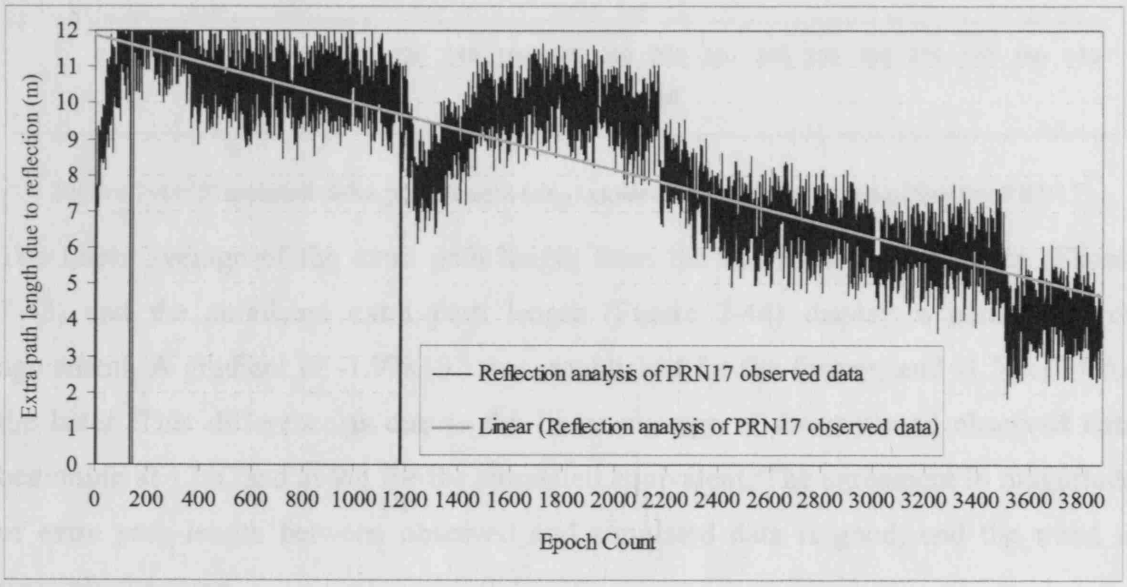

Figure 7-43: Analysed observation for PRN17 location 2

Within the dataset collected at location 2, it has been established that a pseudorange to PRN17 is measured via a reflected propagation path. Measurements made by the receiver to this satellite are made from the start to the end of the dataset. These observations are analysed as previously described, yielding the results given in Figure 7-43. These results can subsequently be compared to the extra path length due to reflection, as presented in Figure 7-44.

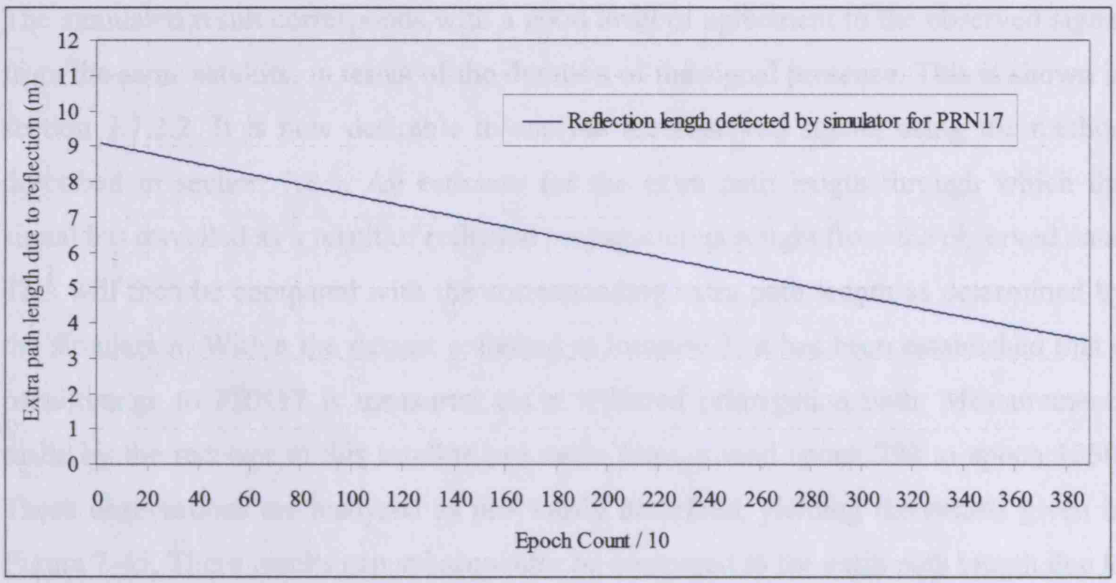

Figure 7-44: Simulated delta path length (dr_{17}) caused by reflected propagation for PRN17

The linear average of the extra path length from the analysed observed data (Figure 7-43) and the simulated extra path length (Figure 7-44) display a good level of agreement. A gradient of -1.97×10^{-3} was established for the former, and -1.51×10^{-3} for the latter. This difference is due to the linear average of the analysed observed data beginning at 12m, and at 9m for the simulated equivalent. The agreement in magnitude of extra path length between observed and simulated data is good, and the trend is certainly the same.

7.8.3.2 Location 3 Analysis of Reflected-Only Signal

As indicated in section 7.7.2.1, a reflected-only signal has been detected by simulation.

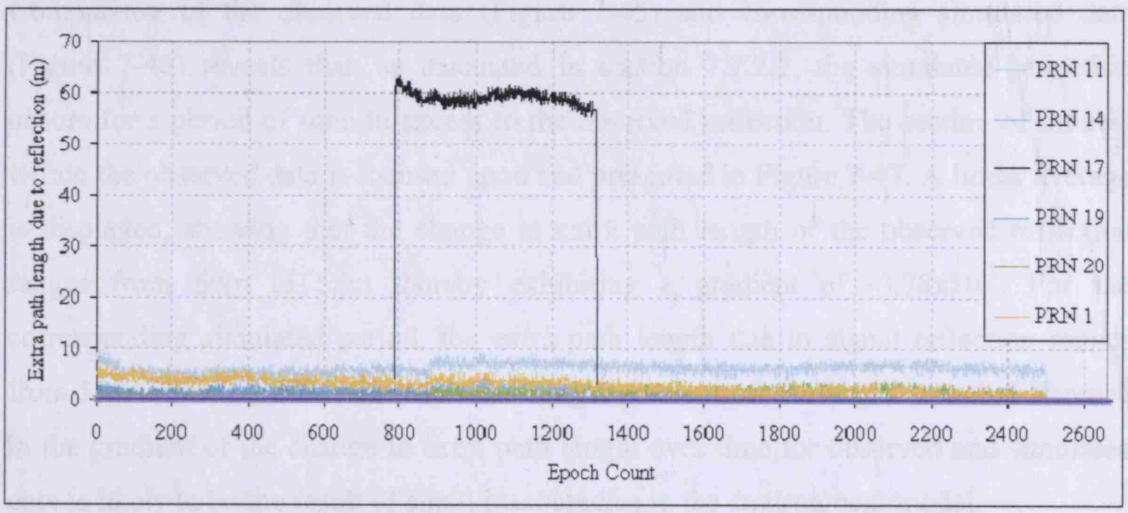

Figure 7-45: Analysed observation for PRN17 location 3

The simulated result corresponds with a good level of agreement to the observed signal from the same satellite, in terms of the duration of the signal presence. This is shown in section 7.7.2.2. It is now desirable to analyse the observed signal, using the method described in section 7.8.3. An estimate for the extra path length through which the signal has travelled as a result of reflected propagation is sought from the observed data. This will then be compared with the corresponding extra path length as determined by the simulation. Within the dataset collected at location 3, it has been established that a pseudorange to PRN17 is measured via a reflected propagation path. Measurements made by the receiver to this satellite are made from around epoch 790 to epoch 1350. These observations are analysed as previously described, yielding the results given in Figure 7-45. These results can subsequently be compared to the extra path length due to reflection, as presented in Figure 7-46.

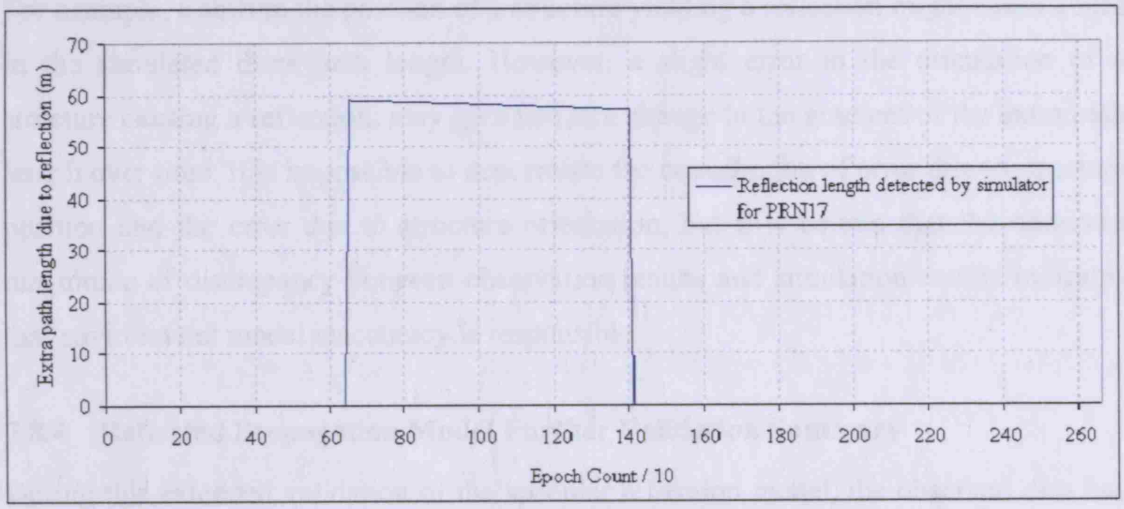

Figure 7-46: Simulated delta path length (dr_{17}) caused by reflected propagation for PRN17

Comparison of the observed data (Figure 7-45) and corresponding simulated data (Figure 7-46) reveals that, as discussed in section 7.7.2.2, the simulated reflection occurs for a period of time in excess to the observed reflection. The section of interest within the observed data is focused upon and presented in Figure 7-47. A linear average is displayed, showing that the change in extra path length of the observed reflection ranges from 60m to 58m thereby exhibiting a gradient of -3.78×10^{-3}. For the corresponding simulated period, the extra path length due to signal reflection ranges from 58.649m to 57.223m thereby exhibiting a gradient of -2.696×10^{-3}. Such difference in the gradient of the change in extra path length over time for observed and simulated data is likely to be the result of small inaccuracies in the environment model.

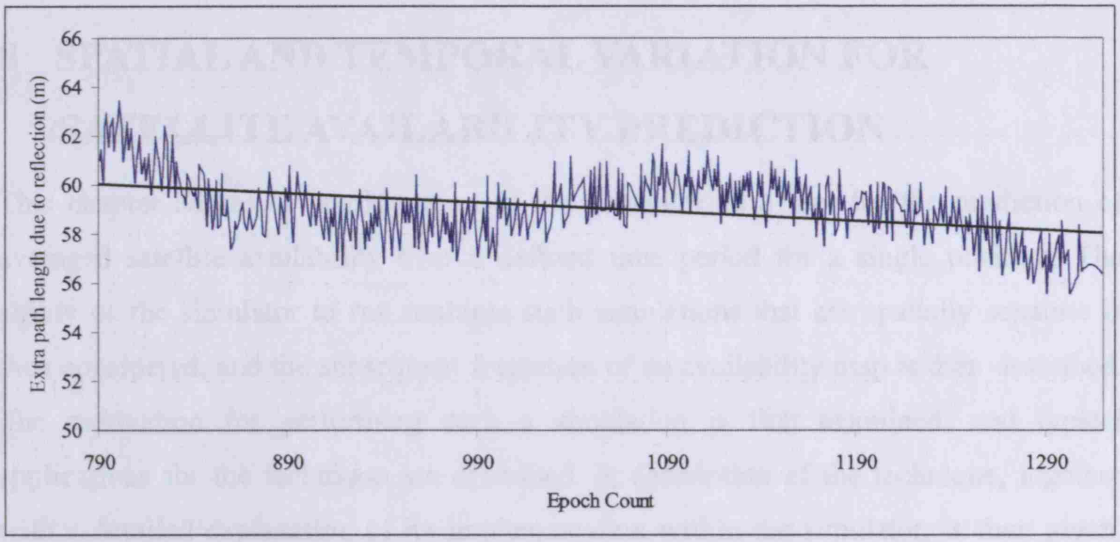

Figure 7-47: Reflected signal within observation data for location 3

For example, a shift in the position of a structure yielding a reflection might cause a bias in the simulated extra path length. However, a slight error in the orientation of a structure causing a reflection, may give rise to a change in the gradient of the extra path length over time. It is impossible to decorrelate the contribution of error due to structure position and the error due to structure orientation, but it is certain that the observed magnitude of discrepancy between observation results and simulation results indicates that environment model inaccuracy is responsible.

7.8.4 Reflected Propagation Model Further Validation Summary

During this extended validation of the specular reflection model, the observed data has been processed, independently of the simulation data, in order to estimate the extended path length through which a reflected signal has travelled, with respect to the direct distance between satellite and receiver. The results have shown, for both examined cases, the extra path length extracted from the observed data agrees with the path length determined by the simulator. Linear averaging of this parameter is performed for the noisy observation data. The gradients of the change in this parameter over the reflected signal period are compared. A good correlation between observed and simulated data is again found. It is expected that any bias in the simulated data is likely to be the result of inaccuracy within the environment model and that due to the complex nature of the geometry involved, a modelled reflection from an inaccurately positioned structure can affect the simulated results by changing the gradient of the change in the extra path length due to reflection.

8 SPATIAL AND TEMPORAL VARIATION FOR SATELLITE AVAILABILITY PREDICTION

This chapter addresses configuration of the simulator as a tool for the prediction of averaged satellite availability over a defined time period for a single position. The ability of the simulator to run multiple such simulations that are spatially separate is then considered, and the subsequent formation of an availability map is then described. The motivation for performing such a simulation is first examined, and typical applications for the technique are described. A description of the technique, together with a detailed explanation of its implementation within the simulator, is then given. The approach toward such a simulation is discussed and an example configuration is given. The results of a simulation based upon the example configuration are then presented and discussed.

8.1 Description

Simulation of satellite availability for single epochs and positions has been described, demonstrated, tested and validated within the preceding chapters. Multiple simulations, whereby the temporal variation in satellite availability is assessed for a single position, have also been demonstrated. Multiple simulations of this type have allowed comparison of observed data with simulated data, and thereby facilitated the validation of signal propagation models employed within the simulator (see chapter 7).

For a single position, it is possible to perform multiple simulations, varying the simulation epoch. These results can then be combined in order to produce representative statistics of the availability at that position. This provides an assessment of the satellite availability at that position, taking account of the fact that availability is a function of time. Multiple simulations, whereby satellite availability is assessed over numerous defined positions, can be performed in order to produce graphical availability maps that are quick and easy to interpret. Such maps are directly applicable to a range of applications involving satellite positioning and navigation. For example, a network of control points may be required as part of a site survey. Where some flexibility in the exact position of control points is permitted, a statistical map of availability will greatly increase the chance of successful capture of these control points using GPS. When configured for multiple simulations, via the settings file (section 4.3.3), an output file is

generated that can be viewed by external software, e.g Excel [Microsoft, 2003], in the form of a 3D surface plot. For the prediction of satellite availability, and focussing on spatial variation, it is possible to perform simulations at all points within a defined 3D area at a defined resolution. The following parameters from the settings file will now be used to demonstrate how this is achieved.

```
SIM X Y Z INC:                2                    Spatial resolution (m)
SIMULATIONS[T,Px,Py,Pz]:      12 100 100 100       Time at X and Y and Z
USER X:                       0                    Initial X
USER Y:                       0                    Initial Y
USER Z:                       0                    Initial Z
SIM EPOCH INC:                3600                 Time increments (seconds)
SIM TIME:                     2007 01 31 10 33 25  Initial timetag
```

The origin of the simulation space is provided by USER X, USER Y and USER Z. The first simulation epoch is provided by SIM TIME. Spatial resolution is configured by setting SIM X Y Z INC in metres and temporal resolution by setting SIM EPOCH INC in seconds. For the above example, the following will be performed. A search space is established (100m x 100m x 100m at a resolution of 2m). This space consists of 1,000,000 simulation positions. For each of these positions, 12 time epochs (separated by 3600 seconds) will be simulated. An RMS value for satellite availability at this point over the 12 hour period is then computed, according to the following equations, and is subsequently stored.

$$Epoch_n = SIM\_TIME + (T_n * SIM\_EPOCH\_INC) \qquad \text{(eqn. 8-1)}$$

$$Availability_{RMS} = \sqrt{\frac{1}{T}\sum_{n=0}^{n=T} A(Epoch_n)^2} \qquad \text{(eqn. 8-2)}$$

Where:

Epoch	=	Current epoch of simulation.
A(Epoch)	=	Integer satellite availability at the specified epoch (given by Epoch).
T	=	Total number of epochs.

The order of precedence for temporal and spatial variation within a multiple simulation run will now be shown. With reference to Figure 8-1 (1), for a given simulator position, the RMS availability is sought by computing availability for each of the appropriate epochs. Figure 8-1 (2)(3) and (4) present the order of precedence for varying X, Y and Z components of the position to be simulated.

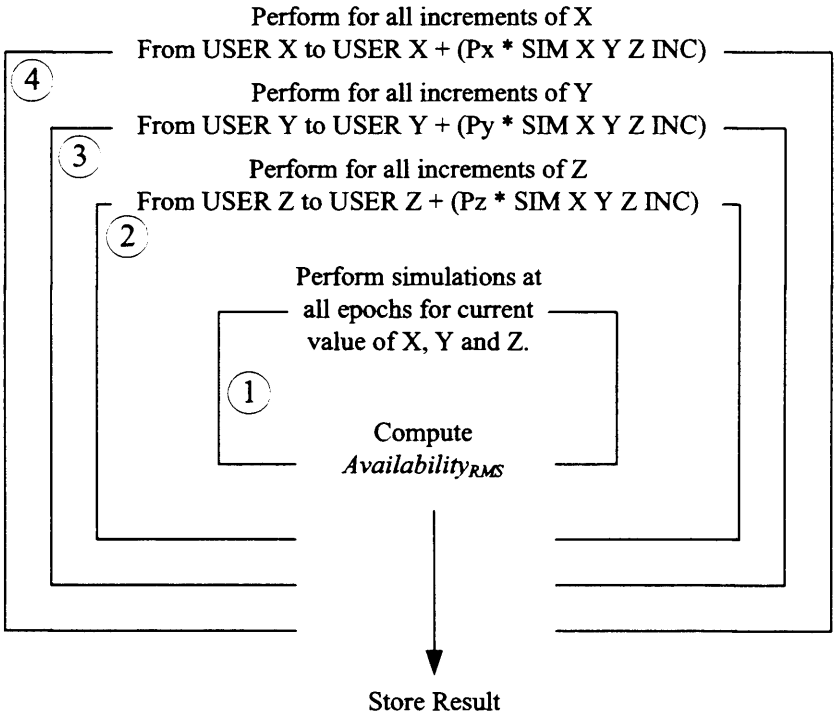

Figure 8-1: Multiple simulations order of precedence for temporal and spatial variation

In order to reduce computation time during a multiple simulation run, a 2D area may be simulated, whereby the Z component of all simulation coordinates has a constant value. This is achieved by setting Pz within the settings file to 1, as shown below.

```
SIMULATIONS[T,Px,Py,Pz]:      12 100 100 1          Time at X and Y and Z
```

Such a strategy is particularly applicable when an availability map is required for an application such as GPS surveying, where a good knowledge of the height range within which the receiver will operate is possessed. Another such example is vehicle navigation. Figure 8-2 demonstrates the considerations when running spatially varied multiple simulations with a fixed coordinate component.

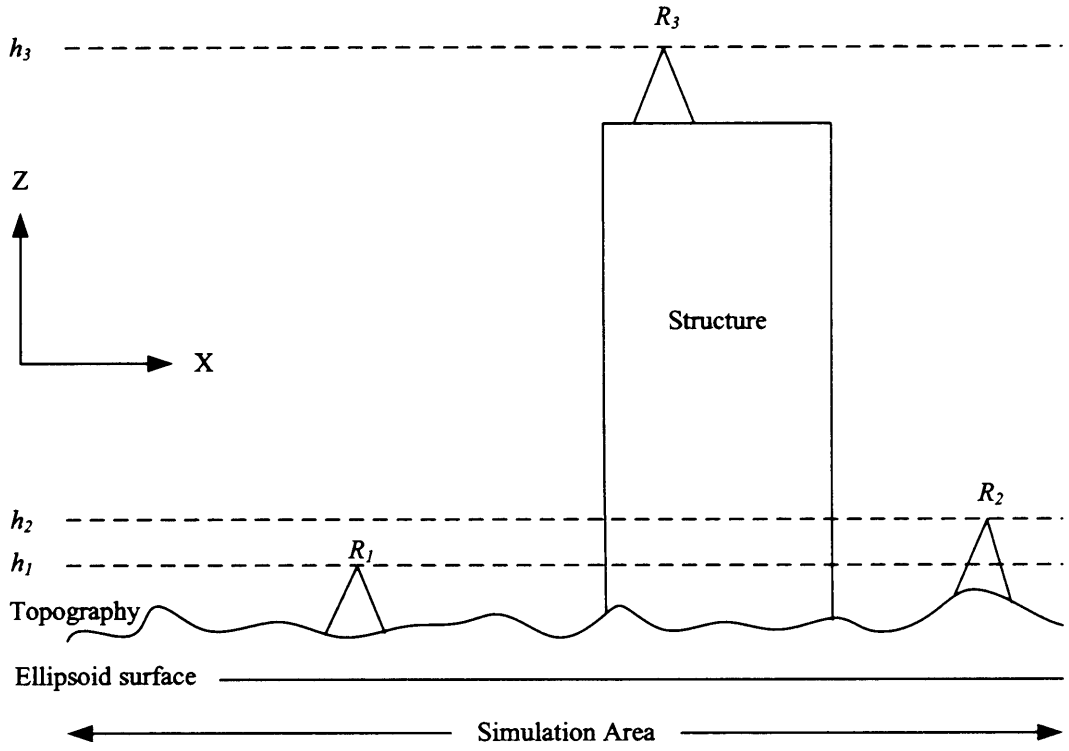

Figure 8-2: Multiple simulation runs, 2D spatial variation (fixed Z component)

For a GPS survey at ground level, involving Cartesian positions R_1 and R_2, h_1 and h_2 represent heights at which the receiver will operate. The difference in h_1 and h_2 is due to local ground height variations. The Z component for this simulation can be fixed as the difference between h_1 and h_2 is small. However, if a survey is to employ receiver positions R_1 and/or R_2, together with R_3, then the variation in height is too great to provide a reasonable assessment of availability at one value of Z. The multiple simulation process with both spatial and temporal variation has been successfully employed during the validation of a model dataset (detailed in chapter 6). During the environment model validation, multiple control networks were required within a location where satellite availability was extremely problematic. An initial trial to capture points within the required areas failed, due to a severe lack of satellite availability. Subsequently, satellite availability was simulated, and a graphical representation of satellite availability over a defined area was generated. The map indicated the spatial variation in satellite availability, where satellite availability for an individual position was averaged over a 12 hour period. In this way, an indication of good and bad locations had been established. By selecting points that existed in high availability spots, according to the simulated data, a far higher success rate in the selection of suitable control points was achieved.

8.2 Approach

This section describes the approach taken to demonstrate a multiple simulation run for the prediction of satellite availability. Both spatial and temporal variation is employed within the simulation as described in section 8.1.

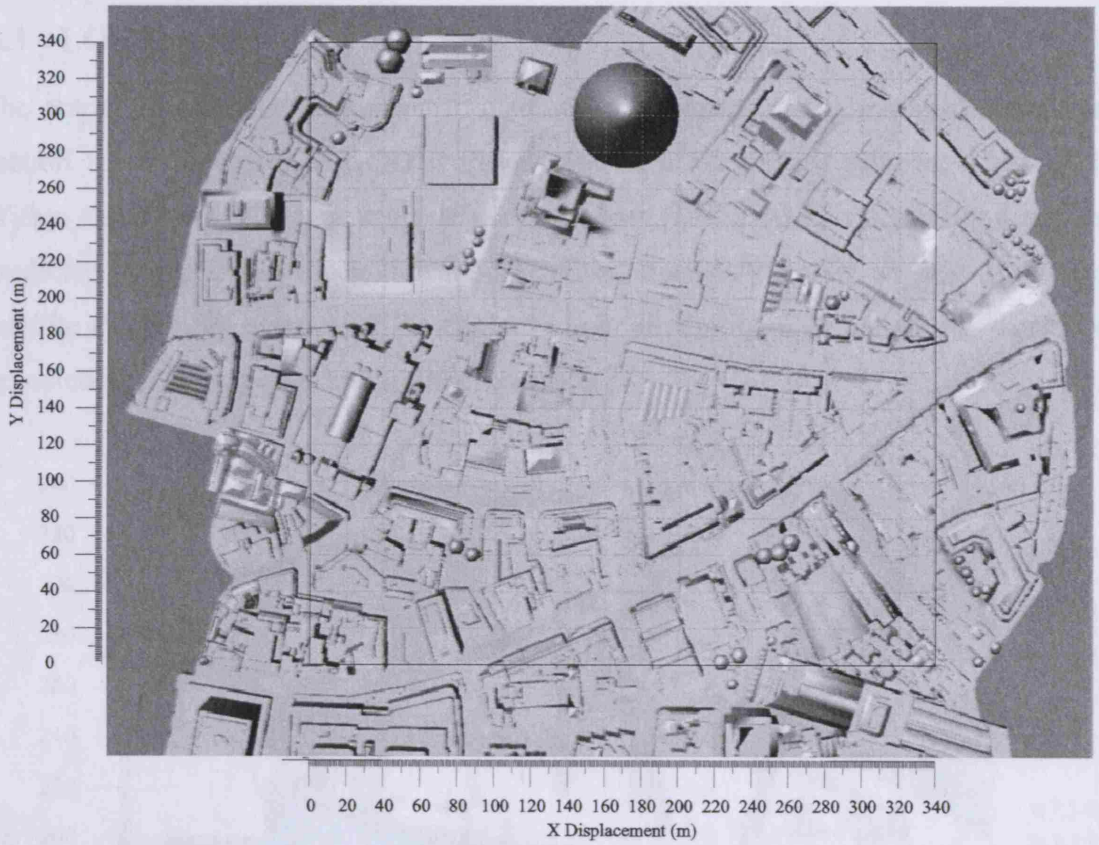

Figure 8-3: Selected area for multiple simulation (availability) within environment model

A test area within the largest environment model dataset (in terms of physical area coverage), has been established. The selected area is presented in Figure 8-3. Multiple simulations are performed according to the following:

- LOS availability is assessed.
- Fresnel zone analysis is assessed. A satellite is deemed obstructed only if the maximum Fresnel zone obstruction exceeds 99.999%.
- Area coverage (X and Y) is 340m x 340m at a spatial resolution of 2m.
- Z is fixed at 18m.
- A 12 hour period is assessed, by 12 individual simulations at each location, with a temporal resolution of 3600 seconds.
- For both LOS and Fresnel assessments, RMS availability is sought.

Such a process reveals the predicted satellite availability over space and time, and produces results for graphical interpretation. In total, 346,800 individual simulations employing both LOS and Fresnel zone analysis (for L1 and L2) are required to complete such a simulation run.

8.3 LOS Results

The output of a simulation run, performed according to the configuration described in section 8.2 is presented as a 2D representation of a 3D surface plot, by Figure 8-4. Within this figure, a colour scale is used to represent the RMS availability level, as predicted by the LOS propagation model. Where the plot presents a white area, zero satellite availability exists over the entire 12 hour simulation time period. As would be expected, this corresponds to building footprints.

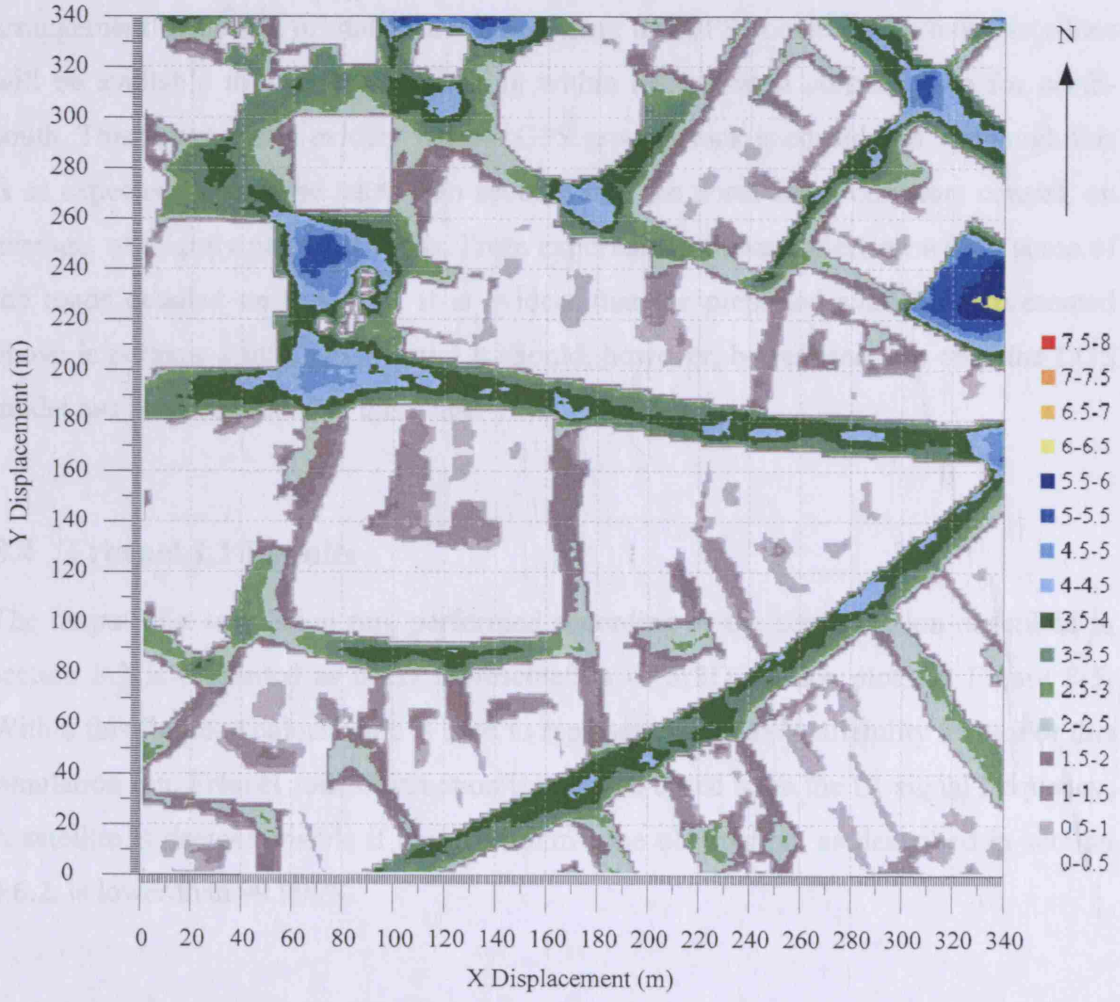

Figure 8-4: LOS satellite availability over a 12 hour period

With reference to Figure 8-4, an example of building footprints can be observed at ~140m to ~195m in the X displacement and ~275m to ~330m in the Y displacement. A circular white area is observed, and this directly corresponds to the footprint of number 30 St Mary Axe (Swiss Re Tower). Examination of the results indicates that the maximum satellite availability, according to the LOS model, within the tested area is around 6-6.5 (RMS average). The location of this level of availability is a square with good sky coverage. The area is called Mitre Square, and has been used for some validation of the signal propagation models due to the good sky coverage. Selection of this location for the propagation model validation was partially based upon the indications of this simulation. Around 5-5.5 (RMS average) satellites can be observed typically at road intersections. However, the area is comprised mainly of urban canyons, and as such, availability by LOS is generally predicted to be around 3-3.5. Satellite availability in the north-south orientated corridors is also seen to be worse than that in east-west orientated corridors. This is consistent with the notion that due to the arrangement of the six orbital planes comprising the GPS constellation, more satellites will be available to a receiver operating within an east-west corridor than for north-south. This is especially evident when a GPS ground track is considered. Although this is as expected, it must be taken into account that the north-south corridors consist, on average, of slightly narrower roads. From experience of data collection within some of the roads detailed on this map, it is evident that the predicted availability presented above is perhaps a little pessimistic. It should, however, be realised that only the LOS model has been employed at this stage.

8.4 Fresnel L1 Results

The output of a simulation run, performed according to the configuration described in section 8.2 is presented as a 2D representation of a 3D surface plot, by Figure 8-5. Within this figure, a colour scale is used to represent the RMS availability level. For this simulation run, Fresnel zone obstruction is assessed based upon the L1 signal frequency. A satellite is deemed visible if the maximum zone obstruction, as described in section 4.6.2, is lower than 99.999%.

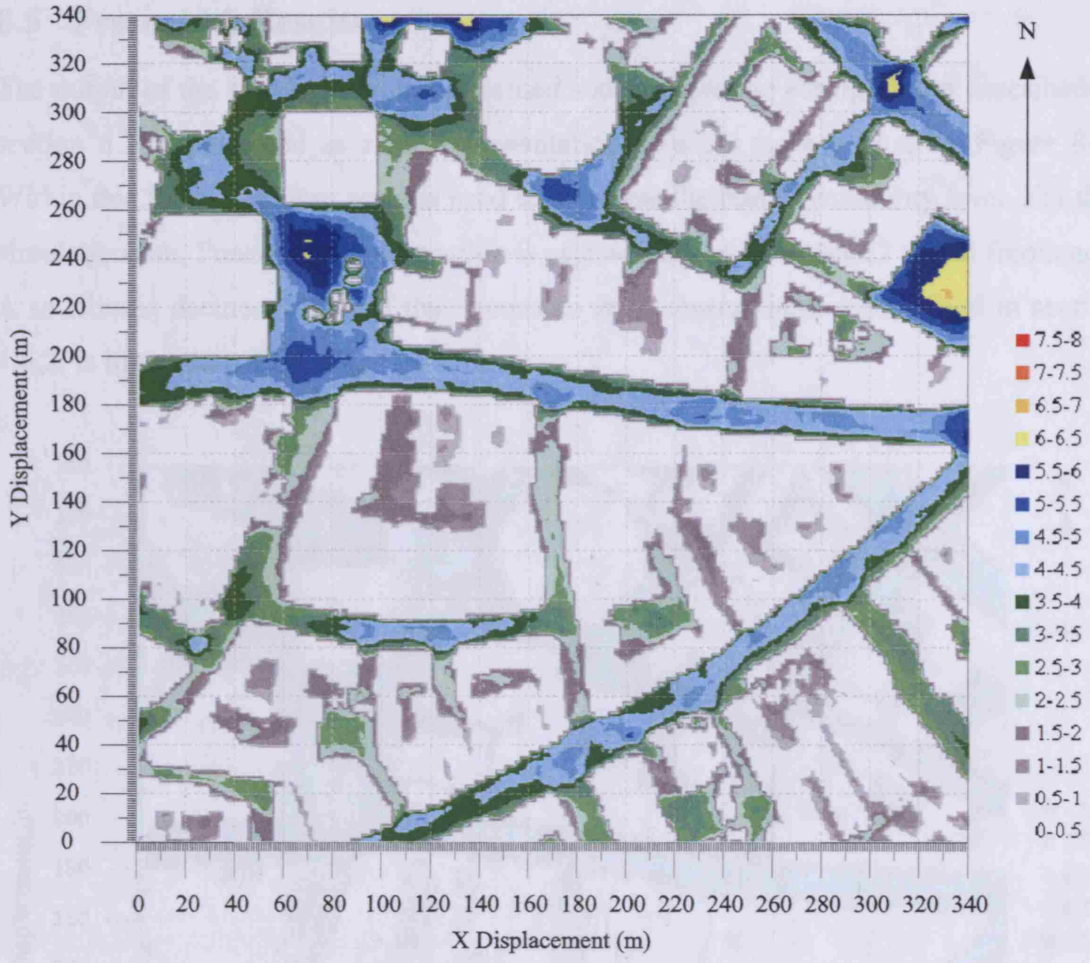

Figure 8-5: Satellite availability over a 12 hour period, determined by L1 Fresnel zone obstruction

As would be expected, the RMS average satellite availability is slightly increased all round with respect to the LOS only availability model. In general, comparison of availability at individual positions for LOS only and for Fresnel zone analysis reveals an increase of around 1 visible satellite for the Fresnel propagation model. This increase results in a greater area amount of positions exhibiting >4 satellites, and is more typically aligned to the experience gained whilst collecting data. It must be remembered that an average visibility of four or more satellites does not by any means guarantee that a position computation will be possible. In fact, given the nature of observation within urban canyons, it is extremely unlikely that the geometrical configuration of four visible satellites will provide low enough GDOP and PDOP values. This fact makes the case for such an availability mapping tool even stronger. In addition to the availability mapping demonstrated within this chapter, the simulator could be configured to output the same representative statistics detailing any of the DOP values. In the same way as for availability mapping, this functionality is of particular importance as a sophisticated planning tool, and forms a novel output of this research.

8.5 Fresnel L2 Results

The output of the simulation run, performed according to the configuration described in section 8.2 is presented as a 2D representation of a 3D surface plot, by Figure 8-5. Within this figure, a colour scale is used to represent the RMS availability level. For this simulation run, Fresnel zone obstruction is assessed based upon the L2 signal frequency. A satellite is deemed visible if the maximum zone obstruction, as described in section 4.6.2, is lower than 99.999%.

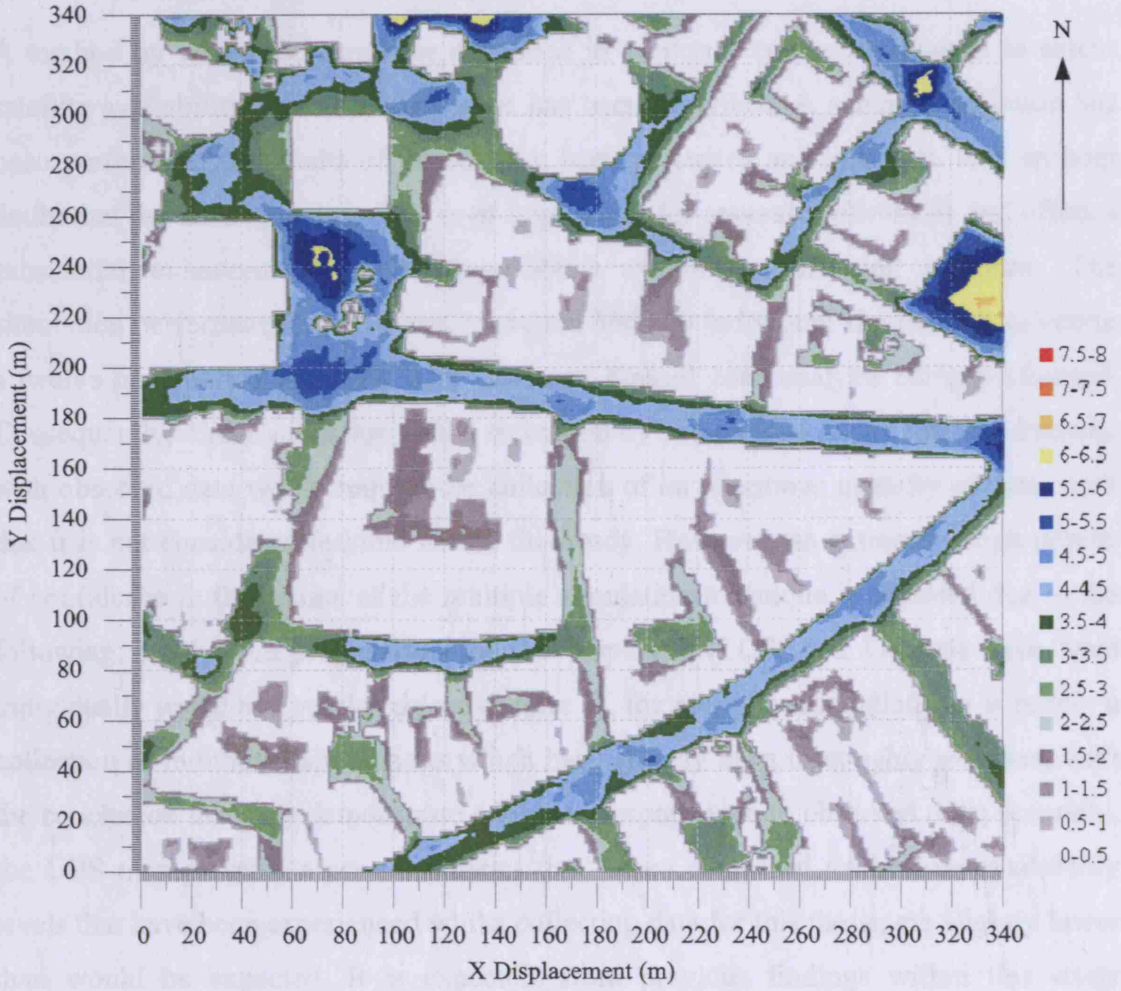

Figure 8-6: Satellite availability over a 12 hour period, determined by L2 Fresnel zone obstruction

Consistent with the expectation that satellite availability determination using analysis of the Fresnel zone should yield higher average availability results than those using an LOS only propagation model, Figure 8-6 demonstrates that this is the case. With reference to the same simulation for the L1 Fresnel zone analysis, this simulation (for the L2 Fresnel zone analysis) presents comparable results, with fractionally higher availability levels all around. This is to expected, as L2 is a lower frequency signal, and

therefore the carrier describes a longer wavelength. This larger wavelength subsequently describes a Fresnel zone of slightly large radius, and therefore an associated higher chance of visible signal for the receiver. The difference, however, is very small. From this, it could follow that there is a greater chance of observing the L2 signal in difficult environments that L1, however, due to the lower signal strength of L2 this is not the case.

8.6 Overall Analysis of Multiple Simulations for Availability

A method by which the simulator described in section 4 can be configured to assess satellite availability over time and space has been described. A sample simulation has been performed, the results of which have been presented and analysed. It is without doubt that the technique described is of importance for several applications and offers a substantial enhancement to existing GNSS availability planning software. The simulation performed for this thesis contained 346,800 individual simulations, covering a twelve hour period and with both LOS and Fresnel zone analysis being performed. Consequently, direct validation of the technique by comparison of the simulated results with observed data would require the collection of an enormous quantity of data, such that it is not considered feasible within this study. However, an extremely high degree of confidence in the results of the multiple simulation technique is afforded due to the following; firstly, the propagation models employed (LOS, and Fresnel) have been individually tested and validated (see chapter 7), the multiple simulation run is purely a collection of individual simulations which have already been thoroughly assessed, with the conclusion that they demonstrate a high correspondence to observed data; secondly, the LOS map presents a set of statistics that, when compared to the true availability levels that have been experienced whilst collecting data for this thesis, are slightly lower than would be expected. It is expected, from previous findings within this study (detailed in chapter 7) and from theoretical knowledge, that LOS alone will produce a pessimistic prediction of satellite availability. Examination of the Fresnel map, provides slightly higher predicted availability, and these results are more reflective of the experience gained whilst collecting observation data.

8.7 Discussion

It has been shown within this chapter that computerised environment models can be used to predict satellite availability over wide areas in addition to individual positions. This chapter has described the configuration of the simulator written for this research to account for the fact that satellite availability is a function of time. Furthermore, it has been demonstrated that multiple simulations can be performed over a defined 3D area and that this feature can produce satellite availability maps that are easy and quick to interpret. The high content of produced simulation data makes formal validation of such a technique almost impossible. It is, however, the case that all results are based upon propagation models that have been individually tested and validated within previous chapters. It is also the case that all outputs display expected characteristics, such as the pattern of availability for east-west versus north-west urban corridors. The presented results focus upon quantity of satellites that are available to the receiver and more specifically the RMS average quantity over a defined time period. It is possible to extend such a process to examine DOP values in the same way. When combined, these outputs will provide highly useful information for survey planning and other such applications.

9 SPATIAL AND TEMPORAL SENSITIVITY TO MULTIPATH

This chapter demonstrates the computation of pseudorange error estimates due to code multipath. A code correlation model is employed to provide a means of combining predicted reflections with the LOS signal (where present) and produce an estimate of the disruption to the range measurement process. The technique is extended to demonstrate that a signal disruption map can be produced in the same manner as for satellite availability mapping. Firstly, the incentive to produce such signal degradation maps is examined and this leads to a discussion of the applications for this work. A description of the technique, together with a detailed explanation of its implementation within the simulator, is then given. The approach toward such a simulation is discussed and an example configuration is given. The results of a simulation based upon the example configuration are then presented and discussed.

9.1 Description

Simulation of satellite signal reflection has been described, demonstrated, tested and validated for the reflected only signal propagation scenario within the preceding chapters of this thesis. This validation provides confidence in the ability of the simulator to predict the occurrence of reflected signals that will be tracked by the receiver. The idea of computing the exact range measurement error that subsequently occurs within the receiver is the next logical step to this work and is considered a topic for further research. Achievement of such an objective will require an intimate knowledge of the specification of an individual receiver, something which is currently unavailable due to commercial sensitivity. Also, as stated in section 4.7 and section 4.8, the absence of material attributes within modelled environments is a barrier to the correct establishment of signal attenuation following diffracted and reflected propagation. It is therefore unrealistic that a meaningful determination of range measurement error due to multipath be achieved at this point in time. The work presented in this thesis indicates that such achievement is possible with the addition of these missing factors. The success of predicting reflected only signals, as detailed in section 7.7 and section 7.8, effectively makes the case for use of a simulation tool such as that developed during this work to characterise the signal degradation due to the addition of signal reflection. This is valid even in the absence of a means to generate a range error prediction. This hypothesis can

be made as there are parameters, key to the magnitude of multipath error, that are determined during reflected propagation simulation. These parameters include the number of reflected signals visible to the receiver, extra path length experienced by the reflected signals, together with elevation and azimuth of the received reflected signals. Such details can, with the use of a generic model of the treatment of received signals, result in the generation of an estimated range measurement error. Although, for the reasons stated above, the result may bare no strict comparison to a true observed error, the generation of such estimates over space and time can be used to map such estimated errors for a specific location. The map would detail the likely severity of signal disruption by assessing the presence and characteristics of reflected copies of the original satellite signal. In addition to producing such a map, the information illustrates the sensitivity of receiver position to the reception of unwanted reflected signals in a certain environment. As with satellite availability, the prediction of such information over spatial and temporal domains is beneficial for applications such as planning GPS surveys in difficult environments. For example, where a degree of flexibility exists in the precise position of control points during a GPS survey, the ability to reject and accept candidate positions based upon factors such as the predicted presence of reflected signals, is of real benefit.

As part of this thesis, a demonstration of signal degradation modelling is presented. The demonstration focuses upon a defined area, and period of time. Estimates of the multipath error are produced by the generic receiver correlator model. As the multipath error is a function of time, discrete time intervals will be sampled by way of simulation. The overall multipath error estimate for a particular location is calculated as the average of all time samples. The results will be presented as a 2D representation of a 3D surface plot, as is the case for the equivalent spatial and temporal variation simulations performed for satellite availability. A description of the technique employed within the simulator to achieve the above will now be presented. For clarity, the simulation will be performed to characterise the signal environment for one signal only. It is possible to perform such simulations for all satellite signals, however, the computational burden becomes unmanageable in the current version of the simulator. It is also more expedient, in terms of presenting the process, to consider only one satellite.

Figure 9-1 presents the graphical output of a single simulation concentrating on satellite PRN6. A specific position and time have been chosen for this illustration and two reflections can be seen by the receiver according to the simulation performed.

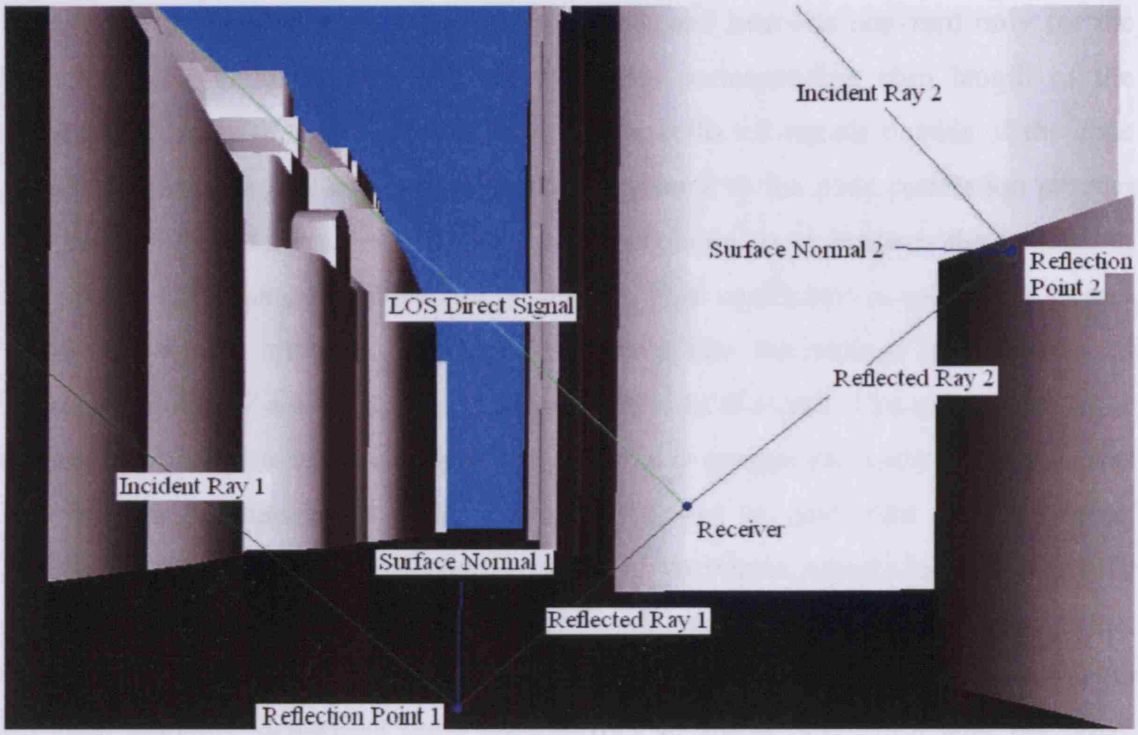

Figure 9-1: Graphical outputs for LOS and reflections at specific time and location for PRN 6

Generation of the graphical representation of simulation results is accompanied by the numerical output, and this will now be examined in order to illustrate the parameters that are determined following simulation.

RECEIVED SIGNALS PREDICTION

#	PRN	D/R	dP(m)	CA Chip	P Chip	R COEFF	Azi(deg)	Ele(deg)
1	6	D	0	0	0	0	76.22	39.05
2	7	D	0	0	0	0	76.52	49.44
3	15	D	0	0	0	0	172.72	45.26
4	16	D	0	0	0	0	294.52	60.07
5	21	D	0	0	0	0	140.75	60.11
6	6	R	2.01	0.007	0.069	0.27	76.74	-38.37
7	6	R	3.82	0.013	0.130	0.75	280.38	39.05

Table 9-1: Received signals prediction including reflection parameters

For the simulation presented in Figure 9-1, the accompanying numerical output is given by Table 9-1. The table represents all signals that are predicted to be visible to the receiver by any of the propagation models included within the performed simulation (in

this case only LOS and reflected modes are considered). Column one assigns a unique identifier to the signal. Column two gives the PRN of the satellite from which the signal originates and column three indicates whether the received signal is visible by the LOS (D for direct) or the reflected (R) propagation mode. Column four presents the extra path length through which a signal has travelled, and hence is non-zero only for the reflected case. Columns five and six show the corresponding chip length of the associated extra path length. This is important as reflected signals outside of the code correlation window will cause little or no disturbance to the code correlation process [Kaplan, 1996] and therefore can be neglected. Column seven presents the coefficient for scaling reflections relative to LOS signals. This coefficient is calculated in two stages. Firstly, an arbitrary coefficient is entered into the settings file to scale all reflected signals by a certain amount relative to the LOS signal. This exists in order to respect the fact that a reflected signal will undergo an attenuation. Later research in this area may be successful in using material attributes to determine this coefficient accurately for individual reflections. For this particular simulation, an arbitrary coefficient of 0.75 is applied to all incoming reflections. This is a reasonable value, though it should be acknowledged that incoming signals will likely be scaled by different amounts, depending upon the specifics of signal interaction with the urban environment. Therefore, in this example, all reflections will be scaled by 0.75 with respect to the LOS signal. Secondly, with reference to section 4.3.6, antenna gain pattern scaling is appropriately applied (see antenna pattern scaling in section 4.3.6) to recognise that the received signal power is not only a function of the electromagnetic signal power incident upon the antenna but is also a function of the elevation angle of the incoming signal. The calculation of this coefficient therefore relies upon the azimuth and elevation angles presented within columns eight and nine respectively. It can be seen from the results presented above that a reflection incident upon the antenna at an elevation of -38.37° incurs a substantial reduction in coefficient value, whereas a reflection incident at 39.05° incurs little or no reduction. This is consistent with the suppression of signals arriving from ground reflections employed by many antenna. It should be noted that the appropriate gain pattern has been used, as demonstrated in section 4.3.6. Application of the received signal coefficient is made within the correlator model described in section 4.9. This generic code correlation model is based upon a standard correlator with a 1 chip early-late correlator spacing, and is used as a means of combining all information regarding LOS and reflected signals in order to produce a composite correlation peak. A corrupted correlation peak will occur in the presence of

reflected signals, see section 3.2.3.1. The level of distortion will depend upon the delay and the attenuation of the reflected signals present.

PREDICTED RANGE ERRORS				
#	PRN	Dir Ref Com	ERROR(m) CA Code	ERROR(m) P Code
1	6	C	-1.76	-1.70
2	7	D	0.00	0.00
3	15	D	0.00	0.00
4	16	D	0.00	0.00
5	21	D	0.00	0.00

Table 9-2: Resulting predicted range errors due to reflected signals for given example

Very low extra path lengths experienced by reflected signals in the given example have resulted in an insignificant distortion of the correlator peak. In this case the estimated error is around -1.76m for the C/A code, and slightly lower at -1.70 for the P code. The distortion in this correlation peak has resulted in a negative error, meaning that the observed range is expected to be less than the true range due to the presence of multipath. It is often assumed that the error due to multipath will always be positive, i.e the presence of multipath will always result in an addition to the true range. This is not always the case. An error that reduces the TOF measurement inside a receiver is a characteristic of correlator peak distortion that can occur (refer to section 2.5). The higher chip rate of the P Code means that, in general, it is less susceptible to multipath error than that of the C/A code [Parkinson, 1996, Vol1, P557 (Braasch)]. The P code is modulated at a rate of 10.23MHz, which is ten times higher than that of the C/A code (1.023MHz). This rate is also referred to as the chipping rate. Only multipath with a relative delay that is within 1.5 times the chip rate [Kaplan, 1996] of the code will cause peak distortion. As such, any experienced delay will be a greater proportion of the 1.5 chip correlator window for the P code than for the C/A code. This is evident in the simulation results above, however, the reflected signals are delayed by very small amounts (with respect to a full chip length) and the result is a small difference in the effect on the code correlation for C/A and P code error estimates.

To a certain extent, it is of little consequence as to whether the performance of this code correlator model is comparable to the performance of a true correlator. Firstly, there are many variations of correlator implementation. The model used for this simulation is a

generic model and as such lacks any multipath mitigation techniques. It is difficult to acquire detailed specifications of correlators within receiver hardware due to commercial sensitivity. As such, any attempt to compare simulated data directly with observed data would likely be fruitless. Secondly, it is of little importance if the performance of the correlator model will lead to similar results to that of an observed set of results for the following reason. The motivation for the use of a correlator model within a simulation of this type is to characterise the level of signal degradation within a defined area and over a period of time. Confidence in the ability of the reflected propagation model to determine the presence of reflected signals, and knowledge that reflected signals degrade range measurement, is enough to produce commentary on the quality of a position in terms of the unwanted signals that will be visible to a receiver. The benefit of the code correlator model is that it allows us to quantify the severity of the combined reflected signals available to the receiver. As all positions and points in time are treated in exactly the same way by the same model, all results will be consistent with each other. For the purpose of mapping, a relative indicator of quality or likely severity of disruptive signals will suffice. The description will now continue with the steps to configure such a simulation.

```
SIM X Y Z INC:                2                     Spatial resolution (m)
SIMULATIONS[T,Px,Py,Pz]:      12 100 100 0          Time at X and Y and Z
USER X:                       -                     Initial X
USER Y:                       -                     Initial Y
USER Z:                       -                     Initial Z
SIM EPOCH INC:                3600                  Time increments (seconds)
SIM TIME:                     2007 01 31 10 33 25   Initial timetag
```

An area is first selected. Within the settings file, the coordinate given by *USER X, USER Y, USER Z* corresponds to $Position_{(0,0)}$, which is the origin of the simulation. Simulations will be performed over an area determined by increments in x,y,z of P_x, P_y, and P_z respectively. The spatial resolution is dictated by *SIM X Y Z INC* and the order of precedence for spatial variation is the same as for a spatially varied availability simulation, see section 8.1. Figure 9-2 illustrates an example area chosen for such a simulation. The blue dots indicate the positions at which simulations will be performed. At each position, a number of simulations will be performed for different epochs. The signal degradation determined for each epoch will then be averaged to give a signal degradation level for that position.

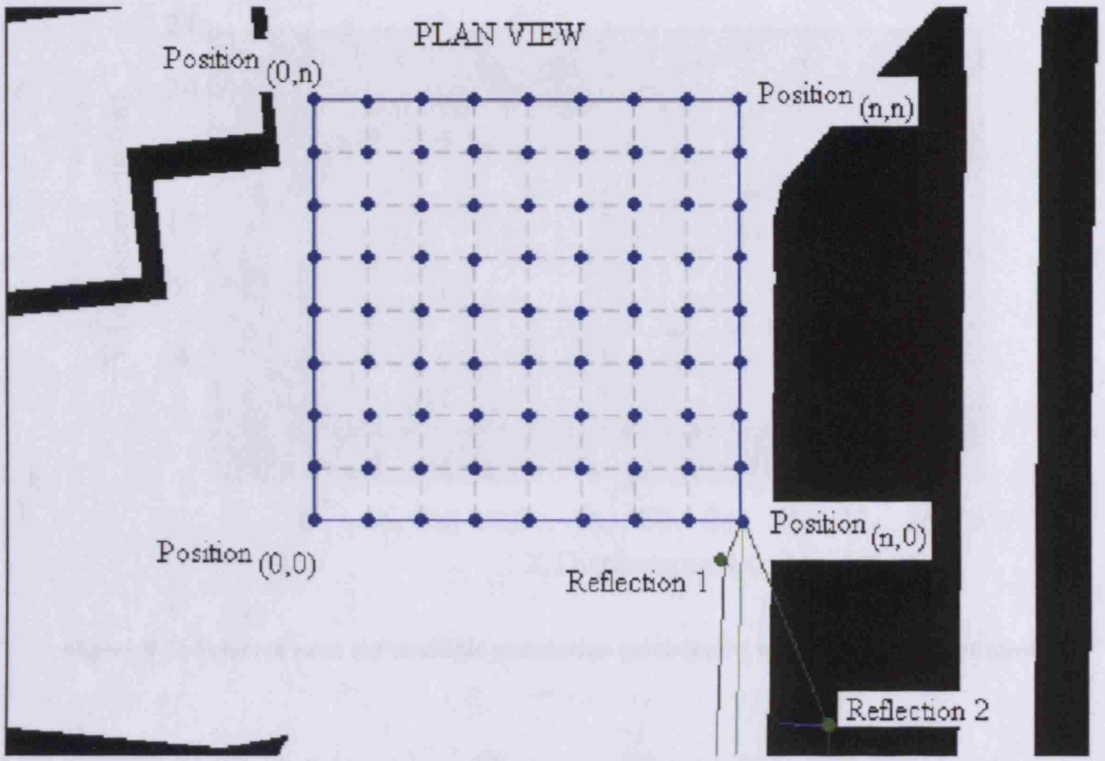

Figure 9-2: Illustration of a selected area for spatially varied signal degradation simulation

Multiple simulations are performed at each location depending upon the SIM TIME (initial simulation time) and SIM EPOCH INC (temporal resolution) variables. Sampling at time intervals in this way respects the fact that the level of signal degradation is a function of time. For a description of the RMS calculation that averages the result for a single position, refer to section 8.1 (equations 8-1 and 8-2).

9.2 Approach

This section describes the approach taken to demonstrate a multiple simulation run for the prediction of satellite availability. Both spatial and temporal variation is employed within the simulation as described in section 9.1. An area within the largest environmental model has been selected for this demonstration. The area is shown in Figure 9-3, and has been chosen based only upon the following factors. Firstly, the area is relatively clear of structures at ground level, thereby allowing a result to be produced for almost all positions within the area. Secondly, the area is surrounded by a mixture of different sized and shaped structures. Finally, the chosen area is typical of an urban environment in which a receiver would be used for surveying and navigation applications.

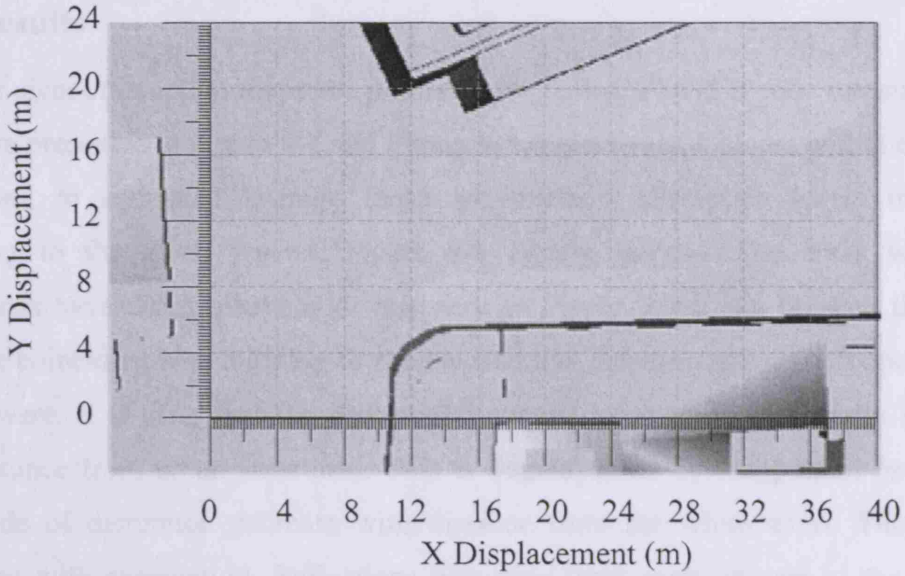

Figure 9-3: Selected area for multiple simulation (multipath) within environment model

A section of the simulation settings file (see section 4.3.3) is given below. As shown, the temporal resolution is 3600 seconds and four simulations will be performed at each location from the initial SIM TIME epoch.

```
SIM EPOCH INC:                  3600
SIM X Y Z INC:                  2
SIMULATIONS[T,Px,Py,Pz]:        4 20 12 1
USER X:                         14.7
USER Y:                         -125.5
USER Z:                         15.653
SIM TIME:                       2007 01 31 06 00 00
```

This configuration has been selected as a previous availability-only simulation was performed to determine that the satellite of interest (PRN6) would be visible to the receiver for this time period. This is important for this demonstration, as we are assessing the signal degradation due to multipath, and therefore it is important that we observe the LOS signal. Twenty simulations at a resolution of 2m are performed in the direction parallel to the X axis and twelve simulations at 2m in the direction parallel to the Y axis. This provides coverage of the area illustrated in Figure 9-3. Finally it is important to note that simulation is performed over a 2D space. This is consistent with the equivalent experiment for satellite availability, and again, a simulation height of 1-2m above local ground height is used in order to assess signal degradation at a height that is of relevance to a typical GNSS user in an urban environment. For more discussion on this topic refer to section 8.1.

9.3 Results

Separate signal disruption maps are produced for both C/A and P code measurements. These are presented in Figure 9-4 and Figure 9-5 respectively. Colours within each map correspond to estimated average range measurement disruption levels in metres according to the given legend. Figure 9-4 clearly shows white areas where no simulations have taken place. With reference to Figure 9-3 it can be seen that these areas are coincident with building footprints, and this demonstrates correct operation of the software. It is clear that the disruption to range measurement generally increases with distance from urban structures. This is demonstrated by the gradual increase in magnitude of disruption estimate with distance from the white areas. This is also consistent with expectation. Reflections occurring from surfaces near to the receiver will have travelled through small extra path lengths, with respect to LOS path length, to reach the receiver. As the simulation moves away from structures, these extra path lengths increase, and consequently induce a more severe correlator peak disruption. This effect is clearly visible in Figure 9-4 by starting at position x=12, y= 4 and increasing y to 14.

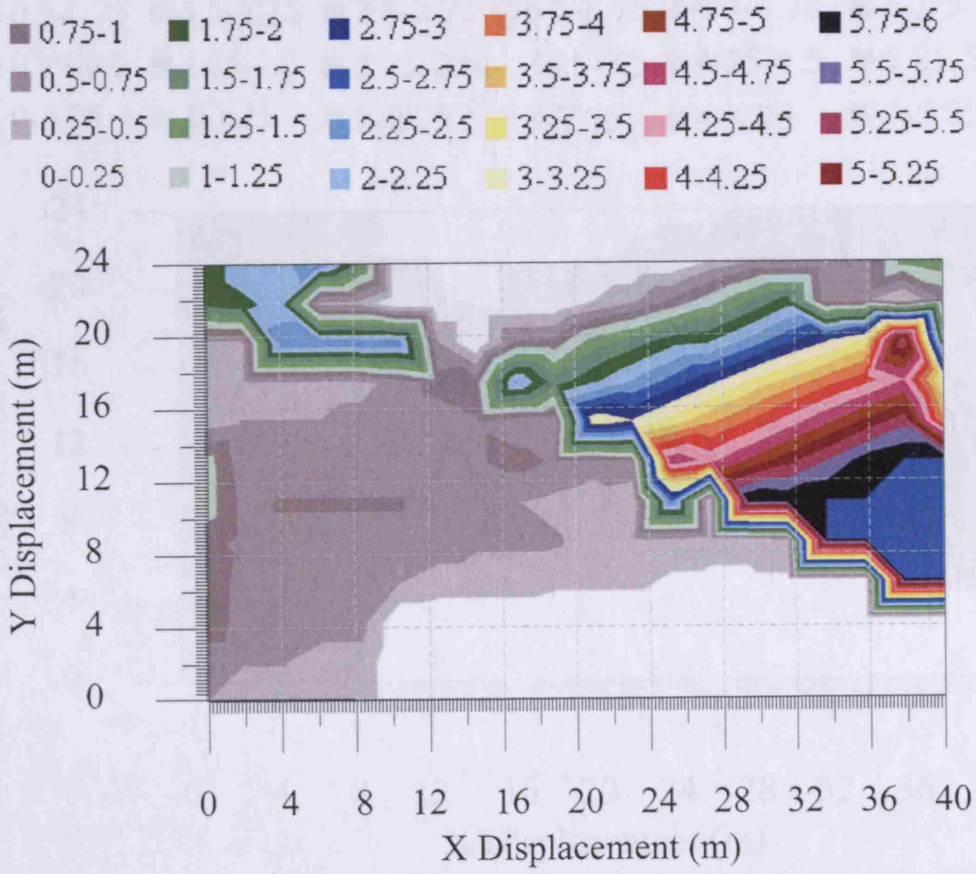

Figure 9-4: Simulated C/A code disruption for PRN 6

The effect is perhaps more noticeable in the mapping that occurs between points x=26, y=24 all the way to x=40, y=4. Within the area surrounding this vector, the full range of disruption (0m to 6m), is experienced.

The signal disruption map for the P code disruption shows the same pattern of signal disruption over the chosen area. However, the magnitude of disruption is slightly lower overall. This can be seen in Figure 9-5, particularly for the large grey area in the left-most third of the map. A lower disruption is expected on the P code, as the chipping rate is higher and therefore the correlator window is smaller. Any delayed signal therefore affects the correlator peak at a later stage than for the C/A code and consequently deforms the peak by a lesser degree. Differences between the prediction of C/A and P code range measurement disruption are very small in this experiment, as the origin of reflected signals is always such that only small extra paths lengths occur. This is a factor imposed by simulation within very enclosed areas.

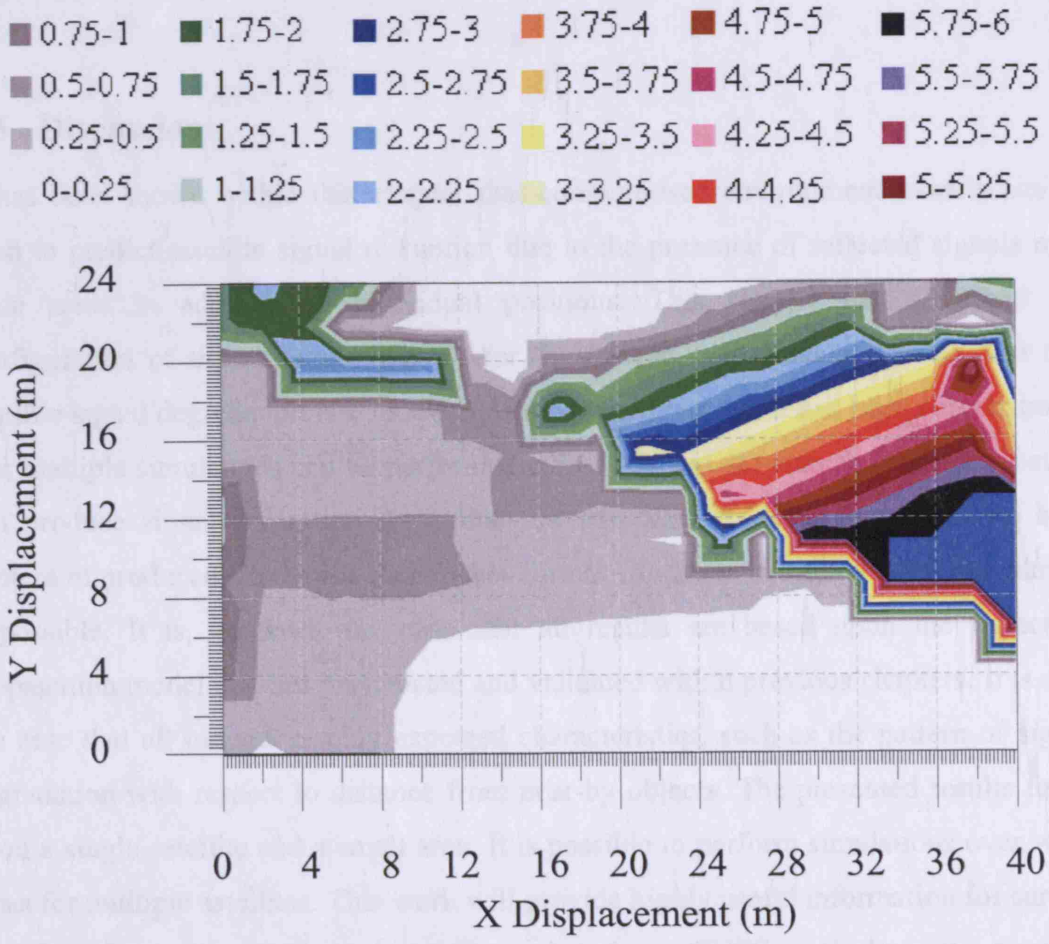

Figure 9-5: Simulated P code disruption for PRN 6

9.4 Analysis

A method by which the simulator described in section 4 can be configured to assess satellite signal disruption over time and space has been described. A sample simulation has been performed, the results of which have been presented and analysed. It is without doubt that the technique described is of importance for several applications and offers a substantial enhancement to existing GNSS planning software. The simulation performed for this thesis covers a relatively small physical area and only considers the signal disruption for a single satellite. However, this is mainly for efficiency in presenting the work. A much larger physical area can be considered and all satellites included in a simulation. The RMS range error (averaged over a four hour period) due to the presence of reflected signals, has been predicted for 240 positions. The output of this type of simulation is a map, such as those presented in Figure 9-4 and Figure 9-5. As with the simulation of satellite availability over time and space (presented in section 8), applications of such work include precise surveying with GNSS. In such an application, positions exhibiting the lowest signal disruption over a period of time can be chosen based upon the outputs of such simulation, leading to more successful surveys.

9.5 Discussion

It has been shown within this chapter that computerised environment models can be used to predict satellite signal disruption due to the presence of reflected signals over wide areas in addition to individual positions. This chapter has described the configuration of the simulator written for this research, to account for the fact that satellite signal degradation is a function of time. Furthermore, it has been demonstrated that multiple simulations can be performed over a defined 3D area and that this feature can produce signal disruption maps that are easy and quick to interpret. The high content of produced simulation data makes formal validation of such a technique almost impossible. It is, however, the case that all results are based upon the reflection propagation model that has been tested and validated within previous chapters. It is also the case that all outputs display expected characteristics, such as the pattern of signal degradation with respect to distance from near-by objects. The presented results focus upon a single satellite and a small area. It is possible to perform simulations over wide areas for multiple satellites. This work will provide highly useful information for survey planning, for example where locations to lay down GNSS control points must be selected. In the cases where there exists a degree of flexibility with regard to the exact

positions that will be occupied to collect GNSS data, locations exhibiting high levels of signal disruption according to the processes described in this section, could be avoided. Other potential uses of signal disruption mapping include route planning applications. A typical example could be emergency services. When a satellite based navigation system within an emergency services vehicle computes possible routes to a destination it will likely be presented with a number of different routes with equal distance or journey time. The system described above could provide a means to choose routes with less signal disruption between start and end point over routes with high signal disruption.

10 SIMULATOR PERFORMANCE

Detailed description of a software simulator developed specifically for this research has been given in preceding chapters of this thesis. The performance of individual signal propagation models, within the simulator, has been assessed. It remains to assess the performance of the simulator as a whole, in terms of resource useage. The results of such work indicate likely achievable performance for optimised and extended simulator versions, that will be applicable to any subsequent research. This chapter begins with a description of the resources consumed by the simulator. Factors affecting the level of resource useage are then given. An experiment to determine resource useage is then described, before a critical analysis of simulator performance is given.

10.1 Simulator Resources

Ultimately, it is hoped that many of the techniques developed within this research, for satellite availability prediction and for signal degradation prediction, will directly impact upon the functionality of mobile positioning devices. It is expected that in the future, simulations to predict satellite signal availability and signal degradation will be performed in near real-time on mobile devices. It is anticipated by the author of this thesis that there will be many applications that will make use of environment models on mobile devices. The simulation of satellite availability and signal degradation is just one such application. Mobile device hardware is generally resource limited. For this reason, the simulator has been developed to make no use of dedicated graphics processing hardware, and has been designed to run on a simple, low specification PC. As such there are only two resource types to be considered; physical memory and processing time. All simulations performed to generate results for this thesis have been performed on a PC with the following specifications:

RAM:	1.0GB
PROCESSOR (x2):	Intel Xeon CPU 2.8GHz with 512KB cache memory
OPERATING SYSTEM:	Windows XP Professional 2002 with Service Pack 2

Achieving the prediction of available signals by considering multiple propagation modes is an extremely complex process. The time taken to perform any simulation is dictated firstly by the propagation modes simulated and the other simulation settings

given in section 4.3.3. Additionally, simulation time is a function of the amount of geometric data that requires processing. In this respect, a relationship exists between the simulation time and the memory used. The following factors affect the memory allocated to a single simulation:

1. Simulations of this type are primarily geometry based activities, and as such, memory useage within any simulation is a function of the size of the initial dataset.

2. The individual scenario, regarding the number of structures that reside in or around the path of signals between the transmitter and the receiver, affects each propagation model in the same way and dictates the number of structures that will be held in memory.

3. Techniques described in section 4.5 ensure that a minimum of geometric data is held in memory for processing. The overhead, in terms of allocated memory for a simulation, is proportional to the density of polygons within individual structures inside the environment model.

With the above objective to extend this work for mobile devices, it is desirable that all resource useage is kept to a minimum. It must, however, be realised that the simulator written for this research is essentially a proof of concept tool, with the primary function of applying the implemented signal propagation models in conjunction with a selection of chosen city models. It should be realised that considerable optimisation of the current tool is achievable. The aim has been to validate signal propagation models using a simulator that is both robust and easily modifiable. Within the developed tool, the functionality to determine memory useage and time taken for a subset of tasks has been added. It is with this functionality that the outputs presented in this chapter are produced.

10.2 Performance Analysis Approach

The aim of the performance analysis is to provide an indication of the typical resource useage for different processes performed by the simulator. This is achieved by establishing a single simulation scenario in terms of simulation settings and model

dataset, performing a simulation, and then recording time taken and memory useage for individual processes. With reference to Table 10-1, a single simulation will produce time and memory useage outputs for all processes indicated by X.

Simulator Process		Time Test	Memory Test
LOS Availability	**Coarse Availability**	X	X
	Detailed Availability	X	X
Fresnel Zone Analysis		X	-
Specular Reflection		X	X

Table 10-1: Memory and time tests performed for individual simulator functions

Memory useage for Fresnel zone analysis is not produced as the process reuses data that has already been stored in RAM during the *detailed availability* process. For this reason, the maximum memory useage for this function is equal to that used during the *detailed availability* process.

The performance assessment outputs have now been defined. The problem is reduced to addressing individually the factors that affect simulation time and memory useage (stated in section 10.1). Factors 1 and 2 are addressed by the use of a single environment model (dataset 2, section 0), together with a defined position and epoch. Factor 3 revolves around a critical part of geometric processing. The number of polygons per structure has a significant effect on the memory useage and also the processing time taken by the simulator. For this reason, the number of polygons per structure will become the independent variable within this approach. The environment model will be modified to express structures that consist of defined numbers of polygons, denoted by N. Each structure will be defined by a specific number of adjacent polygons rather than by any other logical grouping. The number of polygons within the performance assessment ranges between defined limits, in this case five and thirty have been chosen to illustrate performance characteristics. Five polygons represents a large collection of small structures, and thirty polygons is sufficiently different to the lower limit to illustrate a change in performance that is related to number of polygons per structure. Simulations are then performed for the same environment model data expressed as collections of structures that consist of differing numbers of polygons between the defined lower and upper limits (five and thirty respectively). This entire process is presented as a flow diagram in Figure 10-1.

As all processes within the simulator run consecutively, determination of simulation time is a case of noting start and end times and computing the difference. Memory usage is more complex. All propagation models within the simulator work by creating and maintaining individual class instances for each surface under test. Class instances are only destroyed, and therefore memory is reallocated, at the end of an entire process. It is therefore simple to assess the maximum memory usage by noting the memory usage at the start of the process and then at the end (just before memory is reallocated). This is again possible as all processes in the simulator are performed consecutively.

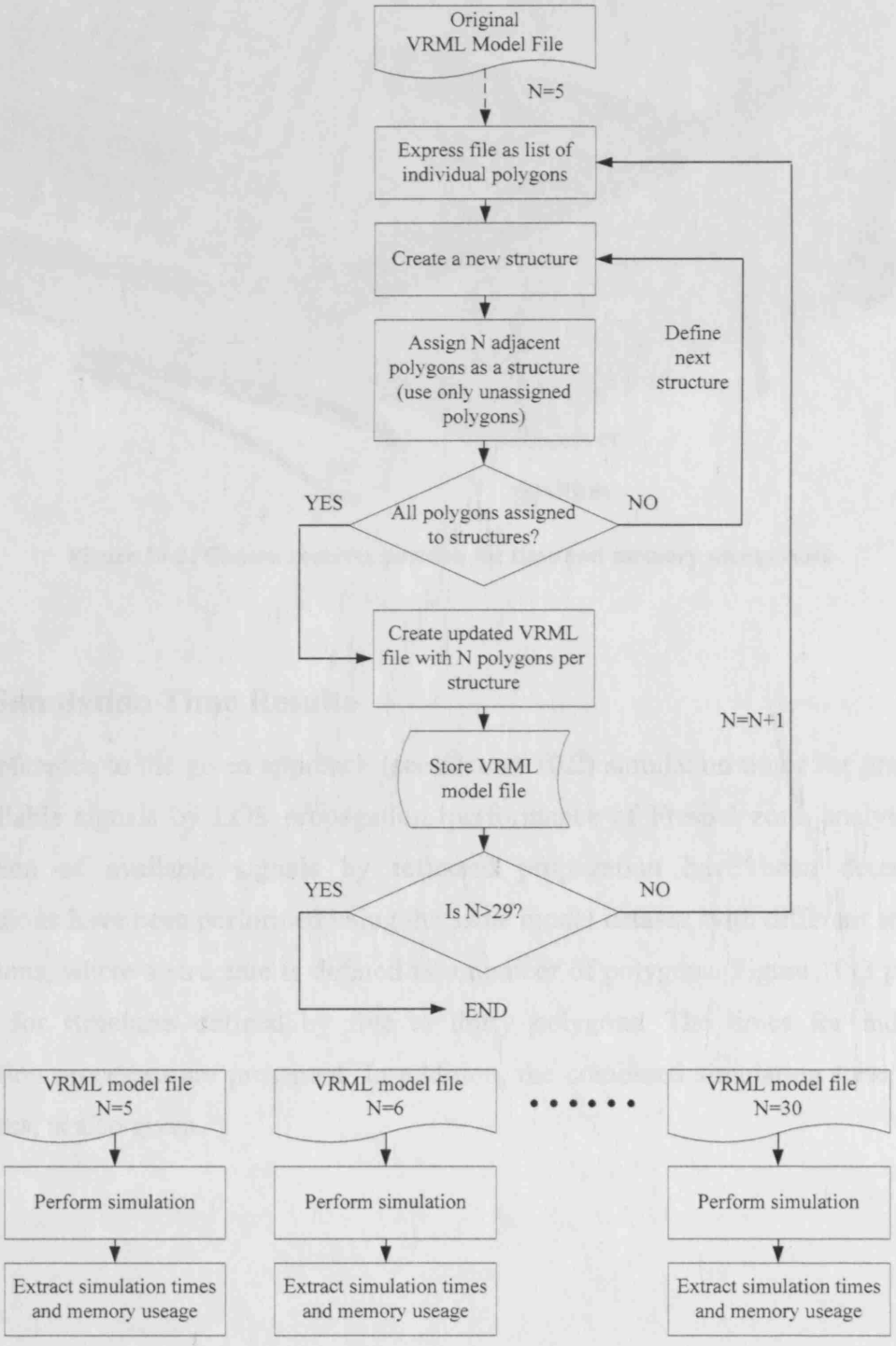

Figure 10-1: Simulator performance accounting for the effect of number of polygons per structure

Having selected an arbitrary simulation epoch, a simulation position within the chosen dataset is required. The chosen position is presented in Figure 10-2.

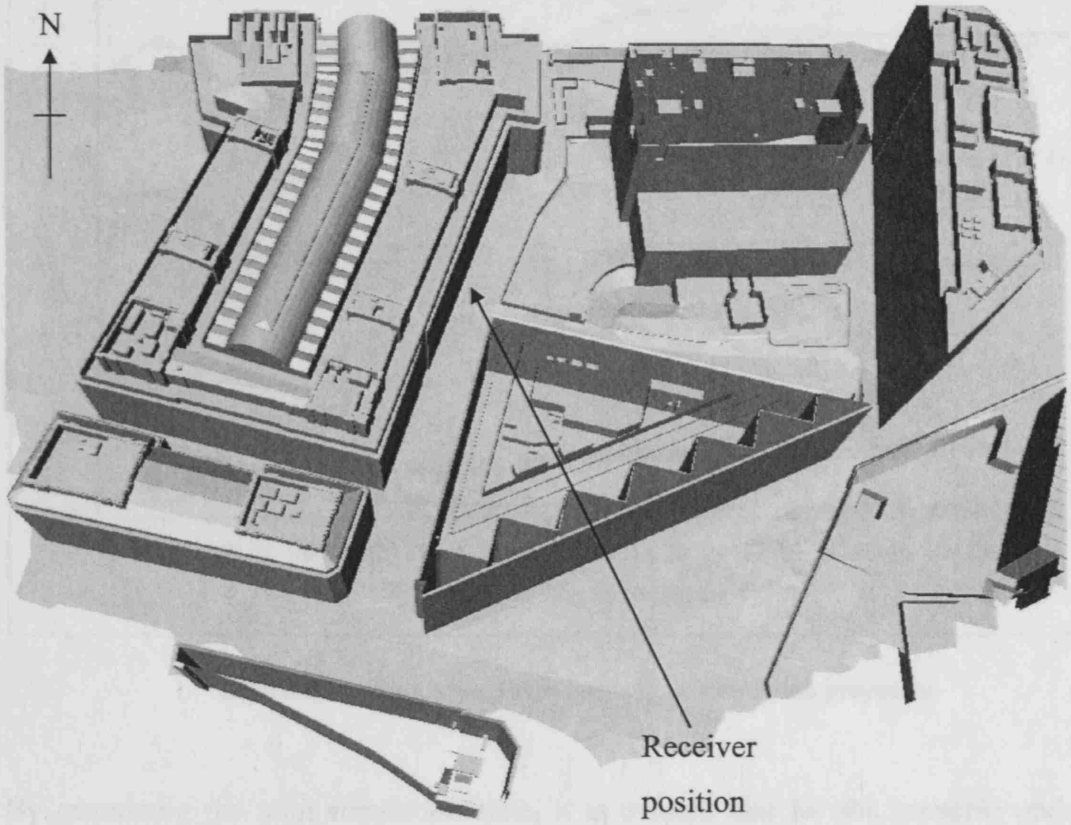

Figure 10-2: Chosen receiver position for time and memory useage tests

10.3 Simulation Time Results

With reference to the given approach (see section 10.2) simulation times for prediction of available signals by LOS propagation, performance of Fresnel zone analysis, and prediction of available signals by reflected propagation have been determined. Simulations have been performed using the same model dataset, with different structure definitions, where a structure is defined as a number of polygons. Figure 10-3 presents results for structures defined by five to thirty polygons. The times for individual simulation processes are presented. In addition, the combined simulation time, for all processes, is also given.

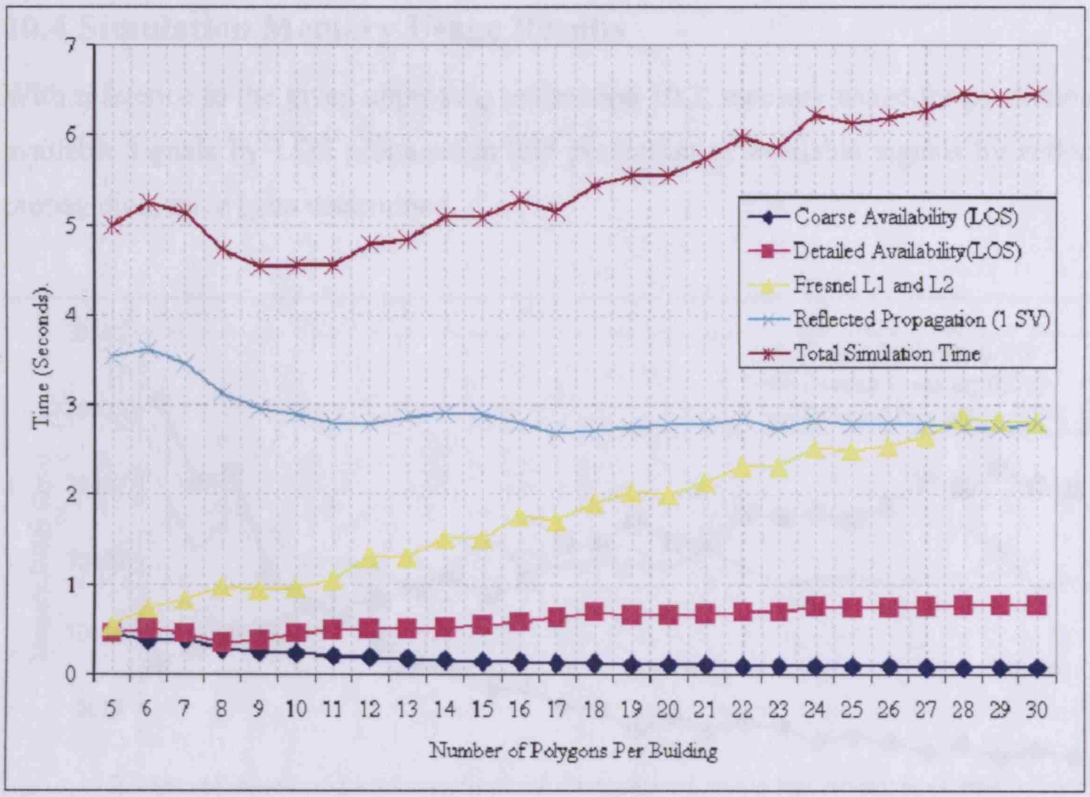

Figure 10-3: Simulation times for various simulation processes

By examining the total simulation time, it is evident that for the scenario under test (defined by receiver position within chosen dataset and also chosen simulation epoch) there exists an optimum number of polygons for the expression of structures within a dataset. At nine polygons per structure, the total simulation time for all processes under consideration within this test is 4.529 seconds. As the number of polygons in each structure is increased, coarse availability processing time decreases. The reason for this is clear. A defined number of polygons exist in the entire dataset and so if only a few polygons are used to define a structure, then the number of structures will be large. Consequently, a high coarse availability time will be experienced. Hence the increase in number of polygons per structure is accompanied by a reduction in the coarse processing time. The inverse is true for the detailed processing. When the number of polygons defining a structure is high, each structure identified as potentially causing a LOS obstruction by the coarse LOS availability algorithm will contain more polygons to be tested, and consequently a higher simulation time is experienced. It is apparent from the above results that the time taken by the Fresnel zone analysis is sensitive to increases in number of polygons used to express individual structures. This is logical, as in the same way as detailed LOS availability, the processing overhead is dictated by the number of polygons that require examination.

10.4 Simulation Memory Usage Results

With reference to the given approach, see section 10.2, memory usage for prediction of available signals by LOS propagation and prediction of available signals by reflected propagation, have been determined.

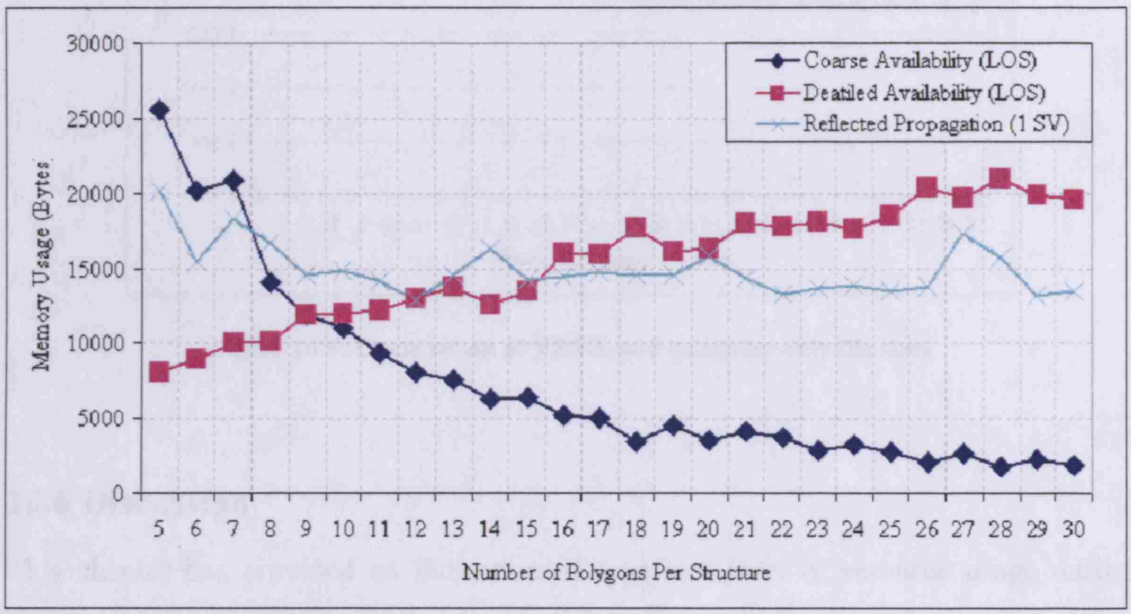

Figure 10-4: Memory usage for prediction of LOS and reflected signal propagation

In addition to indicating the level of memory required by the current version of the simulator, Figure 10-4 demonstrates the relationship between memory usage and simulation time. In all cases, a reduction in simulation time is accompanied by a reduction in memory used. Increases in simulation time are accompanied by increased memory usage.

10.5 Comparison of Geometry File Size and Initial VRML File Size

As described in section 4.4.2, there are several reasons for the creation of a geometry-only file, written in a proprietary format. Noting again that this simulator is a proof of concept tool and that significant optimisation can be performed, it is interesting to compare the sizes of the two files. Also, it should be acknowledged that the geometry-only file contains more information, such as the results of the outward facing normal determination problem (section 4.4.2).

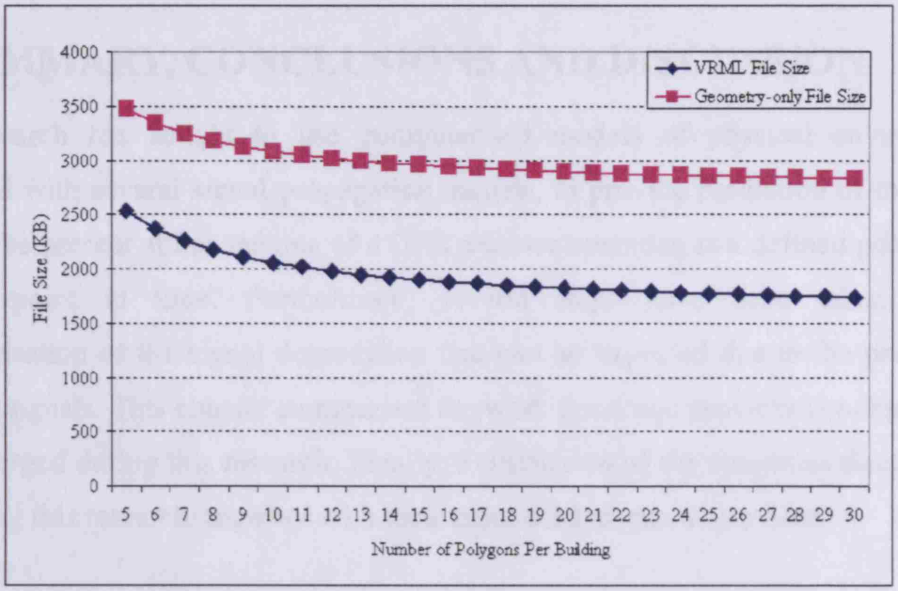

Figure 10-5: Comparison of VRML and geometry-only file sizes

10.6 Discussion

This chapter has provided an indication of type and level of resource usage during simulations performed using the current proof of concept version of the simulator. A strategy has been developed to test individual procedures within the simulator. In order to produce a set of indicative results, an arbitrary position within a single dataset has been chosen and a single arbitrary epoch selected. To appreciate that algorithms within the simulator are sensitive to different model configurations, the definition of a structure within a model has been focussed upon. A group of adjacent polygons forms the base definition of a structure. For monitoring of resource usage it has been beneficial to test the performance of the simulator when dealing with structures containing different numbers of polygons. In order to do this, the chosen model has been replicated in different configurations, whereby all individual structures contain a predefined number of polygons. With the number of polygons per structure acting as the independent variable, it has been possible to assess the effect this factor has on the processes within the simulator. An optimum number of polygons exists whereby resource usage is at a minimum. However, this optimum number of polygons per structure is not constant and is a function of the environment model used and the scenario under test. For an environment model containing a total of 10761 polygons in a dense urban environment, the experiment presented showed that 9 polygons is likely to be the optimum number of polygons per structure. Further investigation would be needed to confirm this, by testing multiple positions and epochs.

11 SUMMARY, CONCLUSIONS AND DISCUSSION

This research has sought to use computerised models of physical environments, combined with several signal propagation models, to provide prediction of the signals that will be present at the antenna of a GPS receiver operating at a defined position at a specific point in time. Furthermore, several steps have been taken towards characterisation of the signal degradation that can be expected due to the presence of reflected signals. This chapter summarises the work done, and provides conclusions that have emerged during this research. Finally, a discussion of the numerous directions for continuing this research, together with their associated merits, is provided.

11.1 Summary

At the outset of this research, two fundamental research questions were posed. These questions centred about the assertion that it is possible to predict the presence of observable GNSS signals, together with some associated signal characteristics, by using computerised models of the physical environments surrounding a receiver. This thesis has been written such that its format depicts the order in which tasks have been undertaken. By way of a summary of this research, the following is provided.

11.1.1 Problem Definition

The first tasks within this research focussed on definition of the problems associated with GNSS signal reception in urban environments. Such problems are not limited simply to the obstruction of LOS between receiver and satellite, but include the disruption to signal quality resulting from the presence of time delayed, reflected copies of the original signal. Additionally, range measurements based upon signals that are observed solely via the reflected propagation path have the potential to cause large position determination errors. The effect of these problems for both static and dynamic GNSS applications was considered. The literature review revealed that the accurate prediction of signals present at an antenna, situated in environments that are densely populated by manmade structures, remained a prominent problem. In particular, consideration of the LOS propagation mode alone by most existing strategies, has led to poor prediction performance when compared with observed data. The problem is compounded by use, prior to this research, of low quality environment models for such tasks. The principles applicable to the propagation of electromagnetic signals have been

investigated, and detailed in appropriate depth for the subject of this research. Methods for the simulation of electromagnetic propagation including computational electromagnetics have been addressed. Although adopting such techniques is desireable, they are largely deemed unsuitable for this work due to the scale of the environment models and the consequent prohibitive levels of numerical processing that would need to be performed. Similarly, consideration at this stage, of multiple reflections is not practical. It is acknowledged that there is value in investigating this propagation mode, however, due to the scale of the environment models considered within this research the computational burden is currently too high. It is also prudent for this research to robustly enhance our understanding of single reflection events before tackling more complex modes. The contribution made made by successive reflections (following the first) is considered to have little effect with regard to causing signal disruption, when compared to that of the dominant single reflection. However, it is acknowledged that reflected propagation will be of great importance when high sensitivity receivers are considered. The same is true with regard to the consideration of propagation through surfaces that feature in an environment model. It should be noted that all development work performed within this research has been careful to allow for future extension to consider both multiple reflections and signal propagation through surfaces.

11.1.2 Managing Input Data

From the outset of this work it became clear that an accepted input format for environment model data would need to be established. In light of the numerous standards and formats that exist for the encapsulation and transfer of data, a lengthy process to determine suitable candidates for use within this project has been necessary. In addition, a proprietary format has been defined to ensure that work performed in this research can be independent of existing formats. Of the 158 file formats identified for the encapsulation of 3D geometric data, VRML was determined to be the most suitable for this work. VRML is a well established standard. It is well defined, with a formal definition [Bell et al., 1995]. Such a rigorous definition is an important indication that the format will be well adhered to. VRML is open source, and as such, data within the format is freely distributable. VRML is a vector based format, and therefore resolution independent. The specification of VRML in terms of character space allocated to hold numbers, and the achievable precision, mean that the geometric fidelity of the initial data within an environment model can be retained. In addition, software packages are freely available to visualise VRML data.

11.1.3 Software Toolkit and Algorithm Development

A software toolkit was written and tested that comprised of modular components combined to form a simulator. All software written for this research has been written completely from scratch and is designed to run without the aid of any dedicated graphics processing hardware. Firstly, input environment files (currently taken in the VRML format) are processed such that geometry data is extracted and copied to a proprietary geometry only file. In addition, during this processing stage, index information is stored in memory that allows algorithms within the toolkit to rapidly access geometry data from the proprietary geometry only file at later stages. This technique allows the initial model file to be processed only once (even when performing multiple simulations). Such a strategy is of great importance when dealing with large volumes of geometric data because continuous accessing of geometric data from large text files can be time consuming. The simulator takes an envrionment model and predicts satellite availability based upon the given receiver location(s) and epoch(s). As a first approximation to satellite signal availability, a LOS signal propagation model is employed. In addition to simple LOS availability, more complex signal propagation modes are considered. These modes are responsible for the reception of signals that occurs even throughout periods where a receiver to satellite LOS is obstructed, as observed using collected data. Within the study it was not assumed that it is sufficient to model the propagation of an electromagnetic signal between a transmitter and a receiver by a volumeless transmission path. There exists a zone in which all incoming signal energy must be considered. It is from within this zone that all incoming signal energy effectively combines to form the composite coherent signal that is tracked by a receiver. This zone is referred to as the Fresnel zone, and a model within the simulator has been implemented such that the maximum cross section obstruction that occurs within this zone, between the transmitter and the receiver, can be determined. A diffracted propagation model has been added to identify possible diffraction events that may give rise to the reception of signals via this mode. A specular reflection model has been developed and implemented in order to determine signal reception via reflected propagation paths. A three stage specular reflection model specifically designed for use with large geometric datasets has been developed. Following application of the propagation models selected for use within a particular simulation, a numerical output file, showing all signal propagation results can be produced by the software toolkit. This is accompanied by a graphical output file that can be displayed on computers with appropriate VRML viewing software. Graphical verification of results has proven to be

invaluable, both during development and as a means to understanding the complex signal propagation. In addition to the principal problems tackled during this research, defined in brief as the accurate prediction of satellite availability and characterisation of signal degradation, a number of solutions have been developed for peripheral problems, particularly with respect to the rapid processing of large amounts of geometric data contained within the initial input file.

11.1.4 Test Methodologies

Testing and control measures were applied throughout this study. As far as possible, all elements of the simulator have been tested individually. This has been achieved via three types of procedure. One-off procedures have been performed following development of individual pieces of software code. Runtime procedures, where gross-error and threshold breach tests are performed, have taken place during data processing and simulation. Finally, subsequent procedures are performed following simulation, normally consisting of graphical examination of results. Satellite positions are determined using an SP3 precise orbit file and also a BRDC broadcast ephemeris file. A comparison of the two is made. By doing this, the chance of any significant error in computation of satellite position is minimal. In addition, periodic comparisons have been made between the satellite azimuth and elevation values produced by the software written for this study and two independent commercial pieces of software.

Other GNSS signal simulators have been acknowledged and reviewed in section 3.4. The review of existing simulator technologies revealed no other software simulators aimed at enhanced prediction of satellite availability and signal degradation (including detection of reflected only propagation), by using large VRML environment models. Due to the differences in applications for (and specifications of) the GNSS signal simulators that exist, any attempt to benchmark the simulator developed during this research with another, would be full of inconsistencies. Under such circumstances this was not considered a valuable addition to this research.

The ouputs of a comprehensive validation of one of the urban environment models [Chamberlin, 2006] used for this research has been made available to this project. Access to such information has allowed consideration of the quality of the input data. Analysis of the outputs of this validation has lead to the belief that such models are of appropriate quality for this work.

11.1.5 Test Areas and Results

Validation of each signal propagation model, individually, has been performed. This is the first project of its kind where so many separate signal propagation modes have been considered and simulated data has been compared with corresponding observed data. During such work every precaution must be taken to ensure that simulated data is not inadvertently seeded or contaminated by observed data. This would only occur through some sort of coding error within the software. However, the best way to truly guarantee that this cannot occur is to treat observed and simulated data in complete isolation. Therefore separate software has been developed/used to process observed data in isolation from the simulator software. For validation of the signal propagation models, three test sites were chosen. The three sites exist on two separate environment model datasets. One dataset being slightly more densely populated by buildings than the other, thereby testing performance in two different environment types. Observation data has been collected at each of the three sites. For each site, and collection time period, satellite availability simulations were then performed. Direct comparison between observed and simulated data could then be made. Furthermore, the performance of each propagation model could then be determined with reference to the observed (truth) data.

Following validation of the signal propagation models, results have been produced for spatially and temporally varied satellite availability. The output is a map of satellite availability for a defined area. The process accounts for the fact that satellite availability is a function of time, by averaging availability over a defined period. Maps can be produced for availability computed using different propagation modes. This research has presented spatially and temporally varied LOS and Fresnel availability. Considering a wide area and long time period means that to collect corresponding observation data is not feasible. This is not considered problematic, as the propagation models have already been validated. Validation of the specular reflection model, for the detection of reflected-only signals, has allowed confidence in the prediction of the presence and attributes of reflected signals. Computation of the range error that occurs as a result of the presence of reflected signals in addition to a LOS signal (multipath) is not possible, due to a lack of commercially sensitive information surrounding the signal processing inside a receiver. However, confidence in the ability to predict the presence of reflected signals has allowed the prediction of signal degradation over a defined area and averaged over time. In order to achieve this, a correlator model has been used to turn a collection of reflected signals (produced by the signal propagation simuations), with a

variety of associated attributes, into an estimate of the likely level of signal measurement disruption. It remains uncertain as to whether the outputs of the correlator model bare a strict comparison to the true range measurement error, and it is unfeasible to attempt any direct comparison, particularly as different receiver technology will respond in different ways to the presence of reflected signals. However, it is certain that this method produces a good map of signal degradation, as it applies a consistent process to the inputs that are determined by performing the signal propagation simulation. The method is thereby capable of mapping relative signal degradation over a defined space and this can be averaged over time to respect the fact that signal degradation is a function of time and position.

With the ultimate objective of applying such research to GNSS enabled mobile devices, an indication of the likely resource useage by such a simulator, is of interest. A strategy to test simulation time and memory useage has been employed to produce estimates of resource useage for individual processes performed by the simulator.

11.2 Research Contribution

The novel techniques presented within this methodology section have resulted in the following research contributions.

1. A technique has been developed that takes large models of geometrically complex environments expressed in computerised datasets and converts them to a form that can be used for signal based GNSS experiments. All data conversion retains initial geometrical measurement fidelity (tested in chapter 5). In this process a new file format for this area of work has been developed.

2. An algorithm for predicting the outward-pointing direction of surface normals from geometric datasets providing only index and coordinate data has been designed, implemented and tested during this research. Such an algorithm is required to determine potential reflecting surfaces in any environment.

3. A robust two-stage algorithm that rapidly processes large model datasets to produce LOS results is a key element in predicting signal behaviour. The applications for such an algorithm extend far beyond simple assessment of volumeless LOS vectors to determine potential satellite obstruction.

4. Acknowledgement that signal propagation does not occur over volumeless transmission lines is made through the use of Fresnel zone analysis. A technique to assess the percentage of obstruction of a transmission zone, by objects present in the urban environment, has been created.

5. Using facet based computerised models of urban environments necessitates that local environments for topics of interest be defined. For example, a local environment for reflection modelling consists only of those surfaces in an entire dataset that might cause a signal reflection that will affect a receiver at a defined location and point in time. A three-step technique to define a local environment for reflection and multipath modelling is presented in this thesis.

6. Diffracted signal propagation can be modelled using knowledge of objects near to the signal propagation path. A method of determining the points on building tops and sides that could give rise to diffracted propagation is an outcome of this research. This method can be employed for even the most intricate of structures despite the computationally intensive nature of performing such a problem.

7. The ability to assess the response of a receiver in the presence of disrupted signals, modelled by algorithms and techniques developed during this research, is provided by means of a code correlator model.

11.3 Conclusions

Seven research objectives were identified at the outset of this thesis (section 1.2). All of the stated objectives have been met. Additional achievements, such as the development of a simulator capable of producing availability and signal degradation visual mapping, have been made. In order to fully assess the achievement and surpassing of the stated

objectives, the following subsections concentrate on conclusions in the areas of environment models, processing large geometric datasets and signal propagation models.

11.3.1 Environment Models

The accuracy of the results of this study rely fundamentally upon the accuracy, in the dual senses of position and completeness of the environment model data utilized. Moreover, this aspect affects directly any future developments of the technology developed in the study. Knowledge gained during the acquisition of urban model data (from third party vendors) together with research into the topic, leaves no doubt that the future of computerised environment models is assured. Furthermore, an increase in diversity of emerging applications for such models is evident. The effect of this increased demand, is acting as a driver for the model producers to constantly increase the quality of environment models. The following five elements are relevant:

- The range of techniques for construction of such model datasets is becoming more advanced. Although outside the scope of this work, it has been noted that technologies for data acquisition are becoming more sophisticated. Automated model generation technologies are now commonplace in this field, and a great deal of work is being undertaken to solve the most severe remaining problem, the modelling of complex roofscape morphologies.

- Originally only the most densely populated areas were covered. A greater coverage (centred about city environments) is demanded by city model users (such as architects, town planners, computer game producers).

- Urban environments undergo change at a staggering pace. Construction and modification of existing structures is accompanied by the addition of street furniture. The need to remain current is being addressed by model producers, and data is being collected and then recollected at certain intervals.

- The accuracy with which structures are positioned and represented in model datasets is increasing thanks to better measurement technologies and better processing techniques.

- The level of detail inherent within models is increasing. It is understood that the entire model dataset production process is not yet fully automated, and in most cases some manual intervention is required. The level of detail contained within a model is, at the time of writing, a function of the human resources employed to produce the model.

11.3.2 Processing Large Geometric Datasets

It has been established during this research that, given the amount of geometric data typically present in urban environment models and the complexity of simulating signal propagation, it is necessary to employ techniques to process large data volumes very rapidly. Such techniques have been developed during this research. The cost of not employing such techniques are higher processing times and memory useage that may exceed that available.

For reasons provided in section 11.1.2, the chosen external format for this work is VRML. Whilst VRML as a standard is mature, highly respected and well defined, it has been found that it is not always well adhered to. This is apparent when a selection of VRML files with different originators, are examined. Any software reader of such a format must tolerate some deviation from the standard.

Urban model files (datasets) used during this research have all consisted of a collection of structures, which in turn consist of a number of planar facets. When applying the reflected propagation model, presented in section 4.8.2, all planar facets within a model must, in the first instance, be considered capable of reflecting a satellite signal. In order to rapidly cull surfaces that are incapable of causing a signal reflection that will be visible by the receiver, a three stage algorithm is employed. The first and second stages rely upon knowledge of the direction of the outward pointing normal of all surfaces. As such, it is important to establish the outward pointing normal of each surface, where outward pointing is defined as the direction that points away from the centre of the volume enclosed by a structure. A problem arises when we seek to determine the side of the planar facet that is external to the structure under consideration. This problem, referred to in this work as the *normal uncertaintly problem* has been solved by development of a set of algorithms employed during the environment model processing stage. The output of the algorithms is a conclusive or inclonclusive flag. Conclusive

indicates that the outward pointing normal has been successfully established. This can then be relied upon by subsequent processes such as the reflected propagation model. If the result is inconclusive, then the reflection algorithm can not cull the surface by relying on the direction of the outward pointing normal alone. For all geometries examined, this techniques has performed well. However, it is feasible that special case geometrical configurations may exist that would cause an erroneous result. This risk is mitigated by the use of a confidence flag, where any doubt as to the direction of the outward pointing normal will produce an inconclusive result. This area could be examined in further detail and could constitute a substantial piece of research by itself. The technique developed for this research proved adequate for employment in the reflected propagation model.

A technique to rapidly process an entire model dataset and determine the structures that might give rise to an obstruction between a satellite and a receiver can be applied before more intensive geometry processing. A technique that approximates all structures, no matter how complex, as simple cuboids is employed to great effect in this research. One example case demonstrated a 62% reduction in the number of surfaces to be tested for LOS obstruction, by employing such a strategy.

11.3.3 Signal Propagation Models

A number of signal propagation models have been implemented in order to better understand the nature of signal propagation in urban environments. In all cases, collected data has been compared to corresponding simulated data, and the outputs of each individual propagation model are compared with observation data.

A LOS propagation model was implemented to produce an initial estimate of satellite availability. This can be used to characterise rapidly the satellite availability. For a 30 satellite constellation, simulation time is typically below 0.9 seconds for a small section of dataset containing 10761 polygons. When compared to observation data, the LOS propagation model performs very poorly. Throughout observed data the signal habitually arrives before the corresponding simulated prediction. Observed signals are also present for some period of time after the corresponding simulated LOS has been obstructed. This clearly indicates that more complex propagation modes must be considered if accurate availability predictions are sought.

Analysis of the Fresnel zone between satellite and receiver was performed to provide more information as to the level of transmitter to receiver obstruction. This algorithm provides an estimate of the maximum obstruction of any cross section of the Fresnel zone. Typical processing time on a mid specification desktop PC varies between 0.5 seconds and 2.8 seconds for a dataset containing 10761 polygons. For this model, processing time is highly dependent on the configuration of the environment model presented to the simulator. By definition, this analysis partially characterises the diffracted propagation field, as the edges of structures, that could give rise to diffracted propagation, are determined. By considering the point at which the Fresnel zone is 100% obstructed, and taking this as the predicted point at which a signal will not be tracked by a receiver, a much better prediction of satellite availability is provided. Again, observed data and corresponding simulation data have been used to conclude this. A significant enhancement is provided over the use of an LOS propagation model alone.

A diffracted propagation model predicts events whereby it may be possible that signal energy is reradiated by edges of structures that are visible to both receiver and satellite by LOS. A simple diffracted propagation field is defined by setting a maximum angle through which signal diffraction may occur. This is a computationally intensive process and it is anticipated that the Fresnel zone analysis, which also characterises the diffraction field, is a better model if low resource devices are to be considered. The diffracted propagation model offers a considerable enhancement in the prediction of satellite availability over use of LOS alone. However, a single threshold value for the maximum angle through which a signal can be diffracted is required by this process. It is not expected that a single angle is applicable to all cases. Consequently, this type of model can offer an enhancement, but will only ever reach a certain level of performance.

A specular reflection model that considers single reflections only, has been implemented. By identifying cases in observed data where range measurements have been made on reflected signals in the absence of LOS signals, reflected-only observations have been found. These reflected-only observations have been used to validate the reflection model in two ways.

- The presence of the reflected only signal has been predicted by corresponding simulations.

- By processing the observation data, it has been possible to estimate the extra path length through which reflected signals have travelled. These estimates have been compared with corresponding simulation outputs detailing the simulated extra path length for reflected only signals.

11.3.4 Overall Conclusions

Software has been developed and tested that uses computerised models of urban environments to predict satellite availability via a range of complex signal propagation modes. The transmission models have been individually validated using observed data.

An effective technique for modelling reflected signals has been demonstrated. In addition to predicting the reflected-only signal reception, the reflection model can be used to determine signal degradation by estimating the presence and attributes of reflected signals that arrive in combination with an LOS signal. It has been determined that computerised models are applicable for this type of work. At the outset of this research, their applicability was unknown.

The situation whereby a signal arrives at a receiver via a reflected-only path has been demonstrated. By simulating the signals present at a receiver, reflected only signals can now be identified. Furthermore, as simulation can determine the extra path length travelled by the signal, pseudoranges can now be corrected appropriately. This alone will lead to more accurate point positioning within urban environments.

By performing spatially and temporally varied simulations, availability maps can be produced. Such maps are are of benefit to applications that take advantage of mission planning techniques. An example of this is the determination of appropriate locations for control stations within GNSS surveys in a deep urban environment.

By using a model of a receiver code correlator, and performing spatially and temporally varied simulations, it is possible to produce a map of signal degradation due to the presence of reflected signals. In this way, multipath can be characterised. Again, this is of real use to applications that benefit from mission planning.

11.4 Further Research

It is without doubt that this research has opened up an entire area with multiple channels for continuing research. The following is a non-exhaustive list of streams that are considered appropriate for continuing the research documented within this thesis.

- Enhancement of geometric processing for environment models that can be employed in low resource devices. This would include research into the acquitision of models, or sections of models over wireless communications networks. By orientating this work for low-resource devices, it would be applicable to high quality geodetic receiver technology as well. This would lead to real-time integration of computerised model environments with GNSS, for use in both high quality geodetic receivers and in low resource devices.

- It has been stated within this thesis that intensive electromagnetic computation is not applicable to this work. This is true for many reasons. Firstly, it is currently unachievable from a computational perspective, over a reasonably sized environment model. Perhaps more prohibitive is the current lack of material attributes within environment models. The VRML format can hold data that would lead to the ability to compute signal attenuation. However, the surface composition data (surface roughness and reflectivity coefficients) is not currently expressed over wide areas or at an appropriate resolution. It may be that future increases in processing resources, combined with models that will likely hold vast quantities of surface attribute data, will lead to enhanced propagation modelling. The processing engine developed during this research could be used in a controlled environment for which surface attribute data has been acquired.

- The work performed within this thesis has focussed upon novel techniques for successful processing of large amounts of environment model data, followed by implementation of signal propagation models that have subsequently been validated using real world observations. All results have been generated by performing static simulations. A logical extension to this work would be a thorough examination of the implications of performing simulations for dynamic applications. The software written for this reasearch could feasibly be adjusted to perform high frequency (in this case 1-5Hz would be considered high

frequency) simulations that would predict the signal availability and signal degradation for dynamic scenarios (e.g vehicle movement through a city).

11.5 Practical Implementation

A large component of practical work has been undertaken throughout the research described in this thesis. This has been necessary in order to establish the potential level of enhancement that the integration of environment models could offer to GNSS based positioning and navigation applications in the future. A software simulator, for the prediction of satellite availability and signal degradation, that makes use of computerised models of environments surrounding a receiver, has been developed. The design of this simulator is detailed within this thesis. The performance of individual elements of the simulator including environment model processing and signal propagation modelling, has been assessed and is also documented within this thesis. Throughout the thesis, practical applications for the work have been described. It now remains to summarise these applications and detail some of the issues that would stand between the work detailed in this thesis and the practical implementation of the research. It is likely that the implementation of this work will fall into three modes. The first of which is standalone PC based software. Here, further development of the software developed for this research and possibly the addition of outcomes from further research, could result in a software product for data processing on desktop PCs and laptop computers. In the second mode, the models and algorithms developed during this work could be optimised for insertion into hardware, particularly limited resource devices for applications that run on handheld computers (PDAs etc). The third mode of practical implementation is where the models and algorithms described within this thesis are integrated (either as a software module or as individual components) with existing software. These three approaches to practical implementation are now addressed with respect to likely applications.

Chapter 8 presents the idea of running multiple simulations that are varied in spatial and temporal domains. The stated applications include enhanced mission planning for GNSS survey work, especially applicable for areas where limited satellite availability is experienced. It is envisaged that such an application would be used to produce statistics regarding the best periods of a day and exact positions within a location that would yield the highest levels of satellite availability and lowest levels of signal degradation.

Consequently a higher success rate in obtaining absolute positions for GNSS based survey work in difficult locations, would be achieved. This would result in cost savings as less survey time (e.g. man hours and equipment hire etc) would be needed. The hardware platform for such an application would be a desktop PC or a laptop computer. As such, there is little that obstructs the practical implementation of such a tool. Minor modifications to the simulator would be required in order to generate more appropriate statistics. The use of visual heat maps is, from experience, a very satisfactory method for rapid assessment of ideal survey positions. In such a mode, whereby simulations are performed in advance, it would also be desireable to increase the speed at which the availability and signal degradation maps could be generated. This is a matter that could be addressed with some further software development.

Adoption of this work for use within GNSS receivers (especially in mobile devices) is more problematic, as this mode of implementation includes integration with hardware. Current levels of available processing power and memory mean that implementation on such platforms is impossible in the current simulator form. Such applications would include enhanced route planning for emergency vehicles, whereby routes with higher availability and lower signal degradation would be chosen, when multiple routes with similar travel times are at first computed. This would rely upon computation of availability and signal degradation in a similar fashion to that described for mission planning, but would need to be performed in near real-time. Perhaps the most important future application is the near real-time correction of range measurement observations within GNSS hardware. This research acts as a significant first step towards such an achievement. Such implementation involves the highest level of integration of software with hardware and an embedded software solution is envisaged. The models and algorithms presented in this thesis would need to be more mature before such implementation is performed. It is likely that further research, especially with respect to the use of material attributes (when available), will be required. Device resource limitations apply to both of the given example applications for this mode of practical implementation. In time, these limitations will be eliminated by advances in processing and memory capabilities. The afore mentioned near real-time computation, along with consideration of environment model data acquisition over mobile communications networks, are the predominant issues that cause obstruction to this mode of practical implementation.

The third mode is best illustrated by consideration of implementing the use of environment models (along with the propagation modelling and algorithms developed during this research), with hardware that generates simulated RF GNSS signals. Such simulators are produced by SPIRENT Communications. Collaboration with SPIRENT during this research has allowed the examination of how this would be possible. A sophisticated piece of software is used to control the hardware GNSS signal generators. The software essentially performs computations to determine the signals (with associated characteristics) that are subsequently produced by the hardware. It is within this software that components of this research could reside in order to inform the existing software of satellite availability and signal degradation. The predominant issue that currently acts as a barrier between the work detailed in this thesis and its adoption for such an application, is the generation of results in near real time. This issue is of critical importance. Again, the solution exists in the form of further software development work.

11.6 Discussion

An increasing dependency on GNSS for positioning and navigation is an inevitable consequence of its successful and rapid adoption by so many applications. The accessibility of the technology has ensured that its uses have far outstripped any initial expectations. As such, we find that as a technology, it becomes more and more prominent even to the extent that it replaces existing technologies that have for many years worked to our satisfaction. In light of such a profound effect, it is important that we seek to progress the technology. The parallel development of separate but related technologies with potential for integration with GNSS should be exploited in order that ever more progressive applications arrive. Advances in electronics provide ever more exciting opportunities for GNSS. Single integrated circuit GNSS receivers are one such example. Additionally, advances in available physical memory and the power of integrated circuits for processing, are fuelling the possible capabilities of future applications. With this in mind, it is certain that the types of simulations performed on desktop computers throughout this research will find their way into GNSS receivers. By developing simulation and modelling techniques it is possible to afford a receiver a level of intelligence. With reference to this research, that intelligence will take the form of knowledge of the environment surrounding a receiver. This is an extension of what we already see, in the form of map matching and other such techniques. It is considered

entirely achievable that future GNSS devices will be capable of applying corrections for range measurement errors that occur due to the presence of surrounding objects. This is a true enhancement, but considered to its extreme case, this research could have even further reaching effects. It is fair to say that the desired objective of seamless positioning in all environments will only be achieved by employing multiple positioning, navigation and sensing technologies. Indoor positioning by using high sensitivity GNSS receivers, localised radio networks, ultra-wide band, indoor pseudolites, or other related technologies, are all heavily subjected to influence by the objects in the environment that surround the positioning device. As such, positioning errors and poor availability will occur, for the same reasons that they occur in the urban environment. The output of this research is a prime candidate to alleviate such problems. It is also the case that continuation of this work will ensure that the developed techniques reach an appropriate level of maturity in time to be integrated in such positioning and navigation devices.

REFERENCES

Ames, A. L., Nadeau, D. R., and Moreland, J. L. (1997).
The VRML 2.0 sourcebook.
John Wiley & Sons, Inc.
ISBN 0471165077.

Batty, M. (2000).
Visualising the City: Communicating Urban Design to Planners and Decision-Makers.
Paper 26, CASA Working Paper Series, University College London.

Bell, G., Pairsi, A., and Pesce, M. (1995).
The Virtual Reality Modelling Language - Version 1.0 Specification.
Internet: http://www.web3d.org/x3d/specifications/vrml/VRML1.0/index.html.
(Retrieved: Aug 2008).

Bradbury, J., Ziebart, M., Cross, P., Boulton, P., and Read, A. (2007).
Code Multipath Modelling in the Urban Environment Using LArge Virtual Reality City Models: Determining the Local Environment.
The Journal of Navigation, Vol. 60, No. 1, 2007.
Cambridge University Press. doi:10.1017/S0373463307004079.

Byun, S. H., G. A. Hajj, and Young L. E. (2002).
Development and application of GPS signal multipath simulator.
Radio Science, 37(6), 1098, doi:10.1029/2001RS002549.

Cannon, M.E., Lachapelle, G., Qui, W., Frodge, S.L. and Remondi B. (1994).
Performance Analysis of a Narrow Correlator Spacing Receiver for Precise Static GPS Positioning.
Proceedings of the IEE PLANS94 conference, Las Vegas, 12-15 April 1994,
pp.355-360.

Cannon, M.E., Ray, J. K., Deschamps, J. (2000).
Attitude Determination Using Multipath Mitigation on Multiple Closely-Spaced Antennas.
Proceedings of the ION GPS 2000 conference, 19-22nd September 2000, Salt Lake City, UT, USA.
pp.2201-2208.

Carnegie Mellon University School of Computer Science. (2007).
Ray-Polygon and Ray-Quadratic Intersection Testing.
Notes 11, Computer Graphics 2, 15-463. Teaching material.
Internet: http://www.cs.cmu.edu/afs/cs.cmu.edu/academic/class/15462/web.98s/notes/rayinter.pdf. (Retrieved: July 2007).

Chamberlin, T. (2006) .
Validation and Error Analysis of the ZMapping Geometric Model of the City of London.
MSc Thesis, Department of Geomatic Engineering, University College London, 1st September, 2006.

Council of the European Union. (2007).
Council Conclusion on Launching the European Global Navigation Satellite System Programmes.
2835th Transport, Telecommunications and Energy Council meeting, Brussels, 29-30 November and 3 December 2007.

Ercek, R., De Doncker, Ph., Grenez, F. (2006).
Statistical determination of the PR error due to NLOS-Multipath in Urban Canyons.
Proceedings of the ION GNSS 2006 conference, Fort Worth, Texas, USA, Sept. 2006.
pp.1171-1177.

ErgoSpace (2007).
Ergospace® software simulator.
ErgoSpace Website: http://www.ergospace.fr/. (Retrieved: July 2007).

Felsen, L. B. and Marcuvitz, N. (1994).
Radiation and Scattering of Waves.
IEEE Press 1994. Wiley-IEEE Press (January 1, 1994).
ISBN: 0780310888.

Fenton, P. and Jones, J. (2005).
The Theory and Performance of Novatel Inc.'s Vision Correlator.
Proceedings of the ION GNSS 2005 conference, Long Beach, CA, USA, 2005.
pp.2178-2187.

Fisher, J., Simpson, S., and Welsh, T. (2002).
An Urban Canyon Multipath Model for Galileo.
Written to be presentated at the ENC 2002 conference, Copenhagen.
Internet: http://www.roke.co.uk/download/papers/An_Urban_Canyon_Multipath_
Model_for_Galileo.pdf (Retrieved: June 2007).

Fruh, C. and Zakhor, A. (2001).
Fast 3D Model Generation in Urban Environments.
IEEE Conference on Multisensor Fusion and Integration for Intelligent Systems, Baden-Baden, Germany, 2001.
pp.165-170.

Garrison, J. and Katzberg, S. (1998)
The application of reflected GPS signals to ocean and wetland remote sensing.
Proceedings of the Fifth International Conference on Remote Sensing for Marine and Coastal Environments, San Diego, CA, USA, 5-7 October 1998.
Vol. 1, pp.522-529.

Gouldsworthy, S. N., Groves, P. D., and Wells, M. (2002).
High-fidelity Model Development for Navigation Warfare Simulation Studies.
Proceedings of the ION GPS 2002 conference, Portland, Oregon, USA, 24-27 September, 2002.
pp.643-654.

Gruen, A. (1997).
Automation in Building reconstruction.
Proceedings of the Photogrammetric Week '97, University of Stuttgart, Institute for Photogrammetry.
pp.175-186.
Internet: http://www.ifp.uni-stuttgart.de/publications/phowo97/gruen.pdf.
(Retrieved: Aug 2007).

Gruen, A. and Wang, X. (1999).
Acquisition and Management of Urban 3-D Data.
Proceedings of the Photogrammetric Week'99, Instanbul, Turkey.

Gurtner, W.(2001).
RINEX: The Receiver Independent Exchange Format Version 2.10.
8-6-2001. University of Berne.
Available from: www.ngs.noaa.gov/CORS/Rinex2.html. (Retrieved: Aug 2008).

Hannah, B. M. (2001).
Modelling and simulation of GPS multipath Propagation.
PhD Thesis. Queensland University of Technology, Australia.

Hannah, B. M., Kubik, K., and Walker A. (1999).
Technical Reports (Report Number 1999.6).
University of Stuttgart – Department of Geodesy and Geoinformatics.
ISSN: 0933-2839 (October 1999).
pp. 137-150.

Hilla, S., Cline, M. (2002).
Evaluating Pseudorange Multipath Effects at Stations in the National CORS Network.
National Geodetic Survey, NOS/NOAA.
Poster paper presented at the Weikko A. Heiskanen Symposium in Geodesy at The Ohio State University, Columbus, Ohio.
1st – 4th October, 2002.

Hoffmann-Wellenhof, B., Lichtenegger, H., and Collins, J. (1997).
GPS Theory and Practice.
Springer; 4th Rev edition (May 1997).
ISBN: 3211828397.

Hoper, M., Boelow, T., and Hoffmann, H. (2001).
Detection of Multipath Influence at DGPS Reference Stations.
Proceedings of ION GPS 2001, Salt Lake City, UT.
pp.581-590.

Hubral, P., Schleicher, J., Tygel, M., and Hanitzsch, C. (1993).
Determination of Fresnel Zones from Traveltime Measurements.
Journal of Geophysics, Vol. 58, No. 5, 1993.
pp.703-712.

ICD-GPS-200. (1995).
ICD-GPS-200, Revision C, 1995 (IRN-200C-001).
Navstar GPS Space Segment/Navigation User Interfaces, Navtech Seminars & Navtech Book and Software Store.

James, G. L. (1986).
Geometrical Theory of Diffraction for Electromagnetic Waves.
Published by: Institution of Engineering and Technology (IEE),
3rd revised edition (1 Oct 1986).
ISBN: 0863410626.

Jones J., P. Fenton, and Smith, B. (2004).
Theory and performance of the pulse aperture correlator.
NovAtel, Calgary, Alberta, Canada, September 2004.
Internet: http://www.novatel.com/Documents/Papers/PAC.pdf. (Retrieved: Aug 2007).

Juang, C., Chen, Y. S., Tseng, C. L., and Shen, L. C. (2004).
On the Reception and Processing of GPS Reflective Signals.
Presented at GNSS 2004, The 2004 International Symposium on GNSS/GPS, Sydney, Australia, 6-8 December 2004.

Kaplan, E. D. (1996).
Understanding GPS, Principles and Applications.
Artech House Publishers (February 1996).
ISBN: 0890067937.

Kunysz, W. (1998).
Effect of Antenna Performance on the GPS Signal Accuracy.
Westin Long Beach Hotel, Long Beach, California, 21-23 January 1998.
http://www.novatel.com/Documents/Papers/effectofantenna.pdf.
(Retrieved: Aug 2008).

Lachapelle, G., Henriksen, J. & Melgard, T. (1994).
Seasonal Effect of Tree Foliage on GPS Signal Availability and Multipath for Vehicular Navigation.
Proceedings of the ION GPS-94 conference, Salt Lake City, USA, 21-23 September 1994.
pp.527-532.

Lee, Y.W., Shu, Y., and Shibasaki, R. (2006).
Simulation Based Estimation of Multipath Mitigation Using 3D-GIS and Spatial Statistics.
Proceedings of the ION GNSS 2006 conference, 26-29 September 2006 Fort Worth, Texas.
pp.1778-1783.

Leica Geosystems. (2005).
Geo Office. [version 2.0.0.0]. 2005.
Computer program.

Leick, A. (1995).
GPS Satellite Surveying.
2nd edition, January 23, 1995, Wiley Interscience.
ISBN: 0471306266.

Li, J., and Kuo, J. (1998).
Progressive Compression of 3D Graphic Models.
Proceedings of IEEE, Vol. 86, June 1998.
pp.1052-1063.

Liang, G. and Bertoni, H. L. (1998).
A New Approach to 3-D Ray Tracing for Propagation Prediction in Cities.
IEEE Transactions on Antennas and Propagation, Vol. 46, No. 6, 1998.

Ma C., Jee G., MacGougan G., Lachapelle G., Bloebaum S., Cox G., Garin L., and Shewfelt J. (2001).
GPS signal degradation modeling.
Proceedings of the ION GPS 2001 conference, September 2001.
pp.882–893.

Melgard, T. E., Lachapelle, G., and Gehue, H. (1994).
GPS Signal Availability in an Urban Area - Receiver Perfomrance Analysis.
IEEE PLANS '94 conference, Las Vegas, 17th-15th April 1994.

Microsoft. (1994).
MS Visual Studio 6. [Version 6.0].
Computer program.

Microsoft. (2005).
MS Visual Studio 2005 - Professional Edition. [Version 8.0.5].
Computer program.

Microsoft. (2003).
MS Excel 2003 [Version 11].
Computer program.

Misra, P. and Enge, P. (2004).
Global Positioning System - Signals, Measurements, and Performance.
Ganga-Jamuna Press (2004).
ISBN: 0970954409.

Mott, H. (1992).
Antennas for Radar and Communications: A Polarimetric Approach.
Wiley-Interscience, 1st Edition (October 16, 1992) .
ISBN: 0471575380.

Navstar. (2007).
Navstar GPS Constellation Status (06-12-06).
Internet: http://gge.unb.ca/Resources/GPSConstellationStatus.txt.
(Retrieved: Dec 2007).

Nelson, L. M., Axelrad, P., and Etter, D. M. (1997).
Adaptive Detection of Code Delay and Multipath in a Simplified GPS Signal Model.
Proceedings of the ION GPS-97 conference, Kansas City, September 1997.
pp.569-581.

NOVATEL. (1997).
Novatel's Narrow Correlator Tracking Technology.
Technical Note: APN-001 Rev 1 (12th November 1997).
Internet: http://www.novatel.com/Documents/Bulletins/apn001.pdf.
(Retrieved: July 2007).

NOVATEL. (2000).
Discussions on RF Signal Propagation and Multipath.
Technical Note: APN-008 Rev 1 (3rd February 2000).
Internet: http://www.novatel.com/Documents/Bulletins/apn008.pdf.
(Retrieved: July 2007).

Ordnance Survey. (2002).
A Guide to Coordinate Systems in Great Britain.
Version 1.7. May 2002. Crown Copyright 2002.

Ordnance Survey. (2004)
Grid Inquest. [6.6.0 Build 1313]. 2004.
Quest Geo Solutions Ltd Passfield Business Centre,
Lynchborough Road, Passfield, Hampshire, GU30 7SB, UK.
Computer program.

Parallel Graphics. (2007).
Cortona VRML Client. [5.1]. 2007.
Internet: http://www.parallelgraphics.com/products/cortona/.
(Retrieved: Aug 2008).
Computer program.

Platinum Technology. (2007).
Cosmo VRML Viewer. [2.1.1]. 2007.
Internet: http://www.cic.nist.gov/vrml/cosmoplayer.html.
(Retrieved: Aug 2008).
Computer program.

Pomaska, G. (2003).
Implementation of Web 3D Tools for Creating Interactive Walkthrough Environments from Building Documentations.
Proceedings of the ISPRS WG V/4 and IC WG III International Workshop on Vision Techniques for Digital Architectural and Archaeological Archives 2003. Ancona, Italy.

Rakkolainen, I., Kupila, H., Majahalme, T., and Salmenpera, H. (2001).
Improving GPS Accuracy for a Mobile 3D City Info.
Proceedings of The 4th International Symposium on Multi-Dimensional Mobile Communications (MDMC'01), Tampere University of Technology, Pori School of Technology and Economics, Pori, Finland.

Ray, J.K., and M.E. Cannon (1999).
Characterization of Carrier Phase Multipath.
Proceedings of the ION National Technical Meeting, San Diego, January 25-27.
pp.343-352.

Ray, J. K., Cannon M. E., and Fenton, P. (1999).
Code Range and Carrier Phase Multipath Mitigation Using SNR, Range and Phase Measurements in a Multi-Antenna System.
Proceedings of the ION GPS-99 conference, Nashville, Tennesse, 14th-18th September 1999.

Rlinami, M., Morikawa, H., Aoyama, T.
An adaptive multipath mitigation technique for GPS signal reception.
Proceedings of theVehicular Technology Conference, 2000 (VTC 2000), Spring 2000, Tokyo.
IEEE 51st Volume 2, Issue , 2000.
pp.1625–1629.

Rizos, C., Higgins, M. B., Hewitson, S. (2005).
New GNSS Developments and their Impact on Survey Service Providers and Surveyors.
Proceedings of SSC2005 Spatial Intelligence, Innovation and Praxis: The national biennial Conference of the Spatial Sciences Institute, September 2005.
Melbourne: Spatial Sciences Institute.
ISBN 0958136629.

Robert McNeel and Associates. (2001).
Rhinoceros NURBS Modelling for Windows. [2.0].
28th December 2001.
Computer program.

Sadek, Ali and Kadzim. (2007).
The Design and Development of a Virtual 3D City Model.
Internet: www.hitl.washington.edu/people/bdc/virtualcities.pdf. (Retrieved: Aug 2008).

Schneider, P. J. and Eberly, D. H. (2002).
Geometric Tools for Computer Graphics.
Morgan Kaufmann (26th September 2002).
ISBN: 1558605940.

Schwartz, R. (2007).
An Introduction to Linear Recursive Sequences in Spread Spectrum Systems.
SIGTEK Inc.
Internet: http://www.sss-mag.com/pdf/aps_ss.pdf. (Retrieved: Aug 2001).

Shiode, N. (2001).
3D Urban Models: Recent Developments in the Digital Modelling of Urban Environments in Three-Dimensions.
GeoJournal, Vol. 52, No. 3, 2001.
pp.263-269.

Snay, R.A., Soler, T. (2000).
Modern Terrestrial Reference Systems (Part 3) – WGS 84 and ITRS.
Professional Surveyor.
March 2000.

SiRF. (2007).
Location-Based Services: Amplifying ARPU for Carriers.
Internet: http://www.sirf.com/sirfamplifyingLBS.pdf. (Retrieved: Aug 2008).
Sleewaegen, J.- M. and Boon, F. (2001).
Mitigating short-delay multipath: a promising new technique.
Proceedings of the ION GPS 2001 conference, Salt Lake City, UT.
pp.204-213.

Spetzler, J. and Snieder, R. (2004).
The Fresnel Volume and Transmitted Waves.
Geophysics, Vol. 69, No. 3, (May-June 2004).
pp.653-663.

Spilker Jr, J. J. (1996).
Global Positioning System: Theory and Applications Volume 1.
Edited by; Parkinson, B. W., Spilker Jr, J. J., Axelrad, P., and Enge, P.,
American Institute of Aeronautics and Astronautics (AIAA), Inc. 15th January1996.
ISBN: 156347106X.

Spilker Jr, J. J. (1996).
Global Positioning System: Theory and Applications Volume 2.
Edited by; Parkinson, B. W., Spilker Jr, J. J., Axelrad, P., and Enge, P.
American Institute of Aeronautics and Astronautics (AIAA), Inc.
ISBN: 1563471078.

SPIRENT Communications. (2004).
SimGEN. [2.46 SR04].
Computer program.

Steed, A. (2005).
GPS Satellite Visualisation.
Satellite Viewer Demo v0.3., 9th August 2005.
Computer program.

Steed, A. (2004).
Supporting Mobile Applications with Real-Time Visualisation of GPS Availability.
Lecture Notes in Computer Science, 3160 series. Lecture Notes in Computer Science, 3160 series. Springer 373-377.

Steingass, A. and Lehner, A. (2003).
Land Mobile Satellite Navigation - Characteristics of the Multipath Channel.
Proceedings of the ION GPS/GNSS 2003 conference, Portland, Oregon, USA.
pp.1016-1022.

Steingass, A. and Lehner, A. (2004).
Measuring the Navigation Multipath Channel – A Statistical Analysis.
Proceedings of the ION GNSS 2004 conference, 21st-24th September 2004, Long Beach, California USA.
pp.1157-1164.

Suh, Y., Konishi, Y., Hakamata, T., Manandhar, D., Shibasaki, R., and Kubo, N. (2004).
Evaluation of Multipath Error and Signal Propagation in Complex 3D Urban Environments for GPS Multipath Identification.
Proceedings of the ION 2004 conference, 2004.
pp.1147-1156.

Takase, Y., Sho, N., Sone, A., and Shimya, K. (2004).
Automatic Generation of 3D City Models and Related Applications.
The International Archives of the Photogrammetry, Remote Sensing and Spatial Information Sciences, Vol.XXXIV, Part 5/W10, 2004.

Taubin G., Horn W., Lazarus F., Rossignac J. (1998).
Geometry coding and VRML.
Proceedings of IEEE 96, 6th Jun 1998.
pp.1228–1243.
.

Taylor, G. (1994).
Point In Polygon Test.
Survey Review, 1994.

Taylor, G., Li, J., Kidner, D., and Ware, M.(2005).
Surface Modelling for GPS Satellite Visibility.
Proceedings of the W2GIS conference, 2005.
pp.281-295.

Townsend, B. R., Fenton P. C., Van Dierendonck, A. J., Van Nee, R.D.J. (1995).
L1 Carrier Phase Multipath Error Reduction Using MEDLL Technology.
Proceedings of the ION GPS-95 conference, Palm Springs,
12th-15th September 1995.
pp.1539-1544.

Trimble Navigation Ltd. (2002).
Trimble Office - Planning. [2.7].
Internet: http://www.trimble.com/planningsoftware_ts.asp. (Retrieved: July 2007).
Computer program.

Van Dierendonck, A. J., Fenton P., Ford, T. (1992).
Theory and Performance of Narrow Correlator Spacing in a GPS Receiver. Navigation:
Journal of the Institute of Navigation, Vol. 39, No. 3, Fall 1992.
pp.265-283.

Viterbi, A. J. (1995).
CDMA: Principles of Spread Spectrum Communication.
Addison-Wesley Wireless Communications, Prentice Hall PTR, 27th April, 1995.
ISBN: 0201633744.

Vrhovski, D. (2003).
Satellite Visibility in Simulating Urban Satellite Positioning-Based Road User Charging (SPRUC).
Proceedings of the ION GPS/GNSS 2003 conference, 8th-9th September 2003.
Portland, Oregon, USA.
pp.199-205.

Walker, R. A. and Kubik, K. (1996).
Numerical Modelling of GPS Signal Propagation.
Proceedings of the ION GPS-96 conference, Kansas City, 1996.
pp.709-717.

Web3D. (2007).
Web3D: A forum for the creation of 3D Standards.
Internet: http://www.web3D.org. (Retrieved: Aug 2008).

Weiss, Jan P., Axelrad P., Anderson S. (2006).
Assessment of Digital Terrain Models for Multipath Prediction at Geodetic GNSS Installations.
Proceedings of the ION GNSS 2006 conference, Fort Worth, TX, USA, 26th-29th September 2006.
pp.2815-2823.

Wolf, P. R. (1983).
Elements of Photogrammetry.
McGraw Hill Higher Education; 2Rev Ed edition (Mar 1983).
ISBN: 0070713456.
pp.576-602.

Yan, Z., Kumar, S., and Kuo, J. (2001).
Error Resilient Coding of 3D Graphics Models via Adaptive Mesh Segmentation. IEEE Transactions on Circuits and Systems for Video Technology, Vol. 11, No. 7, 2001.

Yang, Y., Hatch, R. R., Sharpe, R. T. (2004).
GPS multipath mitigation in measurement domain and its applications for high accuracy navigation.
Proceedings of the ION GNSS 2004 conference, 21st-24th September 2004, Long Beach, California USA.
pp.1124-1130.

ZMapping Ltd. (2005).
Fenchurch St area, London (as at 2005).
Internet: http://www.zmapping.com/ (Retrieved: Aug 2008).
Computerised model datasets.

APPENDIX A Typical GPS Survey Within an Urban Canyon

Below is a RINEX observation file extract from a survey within an urban canyon.

```
     2              OBSERVATION DATA    G                   RINEX VERSION / TYPE
LEICA GEO OFFICE 2.0                     17-4-7 18:55        PGM / RUN BY / DATE
                                                             OBSERVER / AGENCY
is307                                                        MARKER NAME
is307                                                        MARKER NUMBER
133482              LEICA SR530          4.20                REC # / TYPE / VERS
                    LEIAT502                                 ANT # / TYPE
  3977821.0814    -5366.0653  4969090.4970                   APPROX POSITION XYZ
       1.5450        0.0000        0.0000                   ANTENNA: DELTA H/E/N
L1PhaOff:   0.0683  L2PhaOff:   0.0712                       COMMENT
     1     1                                                 WAVELENGTH FACT L1/2
     4    C1    L1    P2    L2                             # / TYPES OF OBSERV
  2007     1    31    15    25   55.000000                  TIME OF FIRST OBS
  2007     1    31    15    39   52.000000                  TIME OF LAST OBS
    14                                                       LEAP SECONDS
     8                                                       # OF SATELLITES
         C1    P1    L1    D1    P2    L2    D2            COMMENT
   G 1  533     0   533     0   513   513     0            PRN / # OF OBS
   G 2    0     0     0     0     0     0     0            PRN / # OF OBS
   G 3    0     0     0     0     0     0     0            PRN / # OF OBS
   G 4    0     0     0     0     0     0     0            PRN / # OF OBS
   G 5    0     0     0     0     0     0     0            PRN / # OF OBS
   G 6    0     0     0     0     0     0     0            PRN / # OF OBS
   G 7    0     0     0     0     0     0     0            PRN / # OF OBS
   G 8    0     0     0     0     0     0     0            PRN / # OF OBS
   G 9    0     0     0     0     0     0     0            PRN / # OF OBS
   G10    0     0     0     0     0     0     0            PRN / # OF OBS
   G11  587     0   587     0   585   585     0            PRN / # OF OBS
   G12    0     0     0     0     0     0     0            PRN / # OF OBS
   G13    0     0     0     0     0     0     0            PRN / # OF OBS
   G14   65     0    65     0    57    57     0            PRN / # OF OBS
   G15    0     0     0     0     0     0     0            PRN / # OF OBS
   G16    0     0     0     0     0     0     0            PRN / # OF OBS
   G17  107     0   107     0     0     0     0            PRN / # OF OBS
   G18    0     0     0     0     0     0     0            PRN / # OF OBS
   G19  540     0   540     0   301   301     0            PRN / # OF OBS
   G20  154     0   154     0   131   131     0            PRN / # OF OBS
   G21    0     0     0     0     0     0     0            PRN / # OF OBS
   G22    0     0     0     0     0     0     0            PRN / # OF OBS
   G23   58     0    58     0    39    39     0            PRN / # OF OBS
   G24    0     0     0     0     0     0     0            PRN / # OF OBS
   G25    0     0     0     0     0     0     0            PRN / # OF OBS
   G26    0     0     0     0     0     0     0            PRN / # OF OBS
   G27    0     0     0     0     0     0     0            PRN / # OF OBS
   G28   74     0    74     0    62    62     0            PRN / # OF OBS
                                                            END OF HEADER
.
.
.
  7  1 31 15 28 14.0000000  0  2G11G19
  20231867.282   106319178.31848  20231864.024    82846101.47949
  23922309.029   125712569.31345  23922305.429    97957839.95446
  7  1 31 15 28 15.0000000  0  3G11G19G23
  20231979.305   106319767.09948  20231976.054    82846560.28649
  23923010.909   125716257.65345  23923007.350    97960713.92046
  25237434.967   132623617.13954         0.000           0.00040
  7  1 31 15 28 16.0000000  0  2G11G19
  20232090.648   106320352.17548  20232087.403    82847016.17849
  23923711.946   125719941.59744  23923708.410    97963584.45745
  7  1 31 15 28 17.0000000  0  1G11
  20232230.585   106321087.48848  20232227.354    82847589.12849
  7  1 31 15 28 21.0000000  0  3G11G19G23
  20232665.740   106323374.30648  20232662.496    82849371.08849
  23927237.056   125738469.89253         0.000           0.00040
  25233002.007   132600314.77455         0.000           0.00040
  7  1 31 15 28 22.0000000  0  3G11G19G23
  20232772.773   106323936.70548  20232769.516    82849809.31549
  23927933.158   125742129.31244         0.000           0.00040
  25232255.778   132596392.19244         0.000           0.00040
```

APPENDIX B Determination of Fresnel Zone Radius

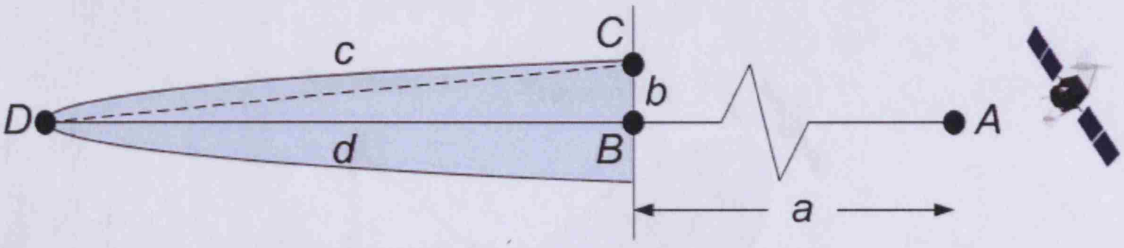

Appendix B Figure 1: Fresnel transmission zone

The radius of the first Fresnel zone at point B is determined by performing the following calculations.

As distance AB is many thousands of times greater than distance DB, then AC is modelled as equal to AB.

For the first Fresnel zone; ACD = AD + (λ/2) [see section 3.1.2]. Therefore CD = BD + (λ/2). The Fresnel zone radius at point B is thereby calculated as follows:

$$\vec{c} = \sqrt{\vec{d}^2 + \vec{b}^2}$$

and $$\vec{c}^2 = \vec{d}^2 + \vec{b}^2$$

and $$\vec{b}^2 = \vec{c}^2 - \vec{d}^2 \qquad \text{(eqn. B-1)}$$

From the definition of the Fresnel zone:

$$\vec{c} = \vec{d} + \left(\frac{\lambda}{2}\right) \qquad \text{(eqn. B-2)}$$

Substituting equation B-2 into equation B-1:

$$\vec{b}^2 = \left(\vec{d} + \left(\frac{\lambda}{2}\right)\right)^2 - \vec{d}^2 \qquad \text{(eqn. B-3)}$$

Expanding equation B-3 gives:

$$\vec{b}^2 = \vec{d}^2 + 2\vec{d}\left(\frac{\lambda}{2}\right) + \left(\frac{\lambda^2}{4}\right) - \vec{d}^2$$

$$\vec{b}^2 = \vec{d}\lambda + \left(\frac{\lambda^2}{4}\right) \qquad \text{(eqn. B-4)}$$

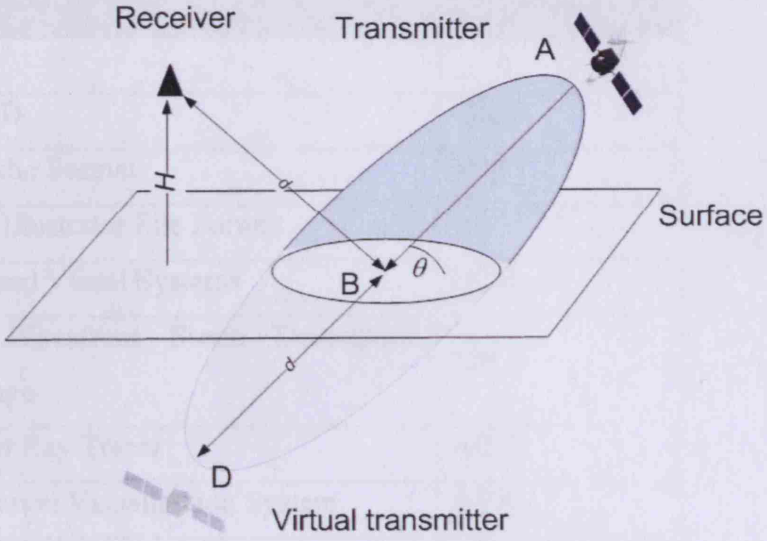

Appendix B Figure 2: Fresnel zone radius calculation at distance *d* from a receiver

From Appendix B Figure 2, distance d is calculated as follows:

$$\vec{d} = \frac{H}{Sin\theta} \qquad \text{(eqn. B-5)}$$

The $\frac{\lambda^2}{4}$ term is negligible for frequencies in GHz and is therefore omitted. Substituting equation B-5 into equation B-4 yields:

$$\vec{b} = \sqrt{\lambda \frac{H}{Sin\theta}} \qquad \text{(eqn B-6)}$$

APPENDIX C Data Formats

	Data Format	Acronym/ Extension
1	3D CAD	CAD
2	3D Studio Format	3DS
3	Adobe Illustrator File Format	AI
4	Advanced Visual Systems	UCD
5	Alias Wavefront Scene Description Language	SDL
6	Another Ray Tracer	ART
7	Application Visualization System	AVS
8	Atari ST Graphics File Formats	AST
9	AutoCAD ASCII	ASE
10	Autodesk 3D Studio	3DS
11	Autodesk drawing	DWG
12	Autodesk Drawing eXchange Format	DXF
13	Ballistic Research Laboratory CAD	BRL
14	Brender	BRender
15	Brigham Young University	BYU
16	CADKey CADL Language	CDL
17	Calgari trueSpace2 File Format	COB
18	Carnegie Mellon University Formats	CMU
19	CCITT Group 3 and Group 4 Encoding	CCITT
20	ColoRIX Image File	RIX
21	Computer Aided Acquisition and Logistics Support Raster Format	CALS
22	Computer Graphics Metafile	CGM
23	Criterion RenderWare	RWX
24	Cyberspace Description Format	CDF
25	Data Exchange Format	DXF

26	Digital Elevation Models	DEM
27	Digital Line Graph	DLG
28	Digital Moving Picture Exchange	DPX
29	DKB Trace	DKB
	Digital Terrain Map	DTM
30	Electronic Arts Interchange File Format	IFF
31	Encapsulated PostScript	EPS
32	Extended Neutral File Format	ENFF
33	FIG	FIG
34	File Format for the Interchange of Virtual Worlds	FFIVW
35	Flexable Image Transport System	FITS
	Formal Data Structure	FDS
36	Fuzzy Bitmap	FBM
37	GLC	GLC
38	Graphical System for Presentation	GRASP
39	Graphicon 2000 Interactive Real Time PHIGS	IRTP
40	Graphics Interchange Format	GIF
41	Graphics Kernel System	GKS
42	Haines Neutral File Format	NFF
43	Hewlett Packard Graphics Language	HPGL
44	Hierachical Data Format	HDF
45	Hierarchical Data Format	HDF
46	Hierarchical Data System	HDS
47	Hitachi Raster Format	HRF
48	Image JPEG	IMJ
49	Imagine Object File Format	TDDD
50	Initial Graphics Exchange Specification	IGES

51	Initial Graphics Exchange Specification	IGES
52	InnovMetric Software Polygon Models Format	POL
53	Inset Pix	PIX
54	Intergraph Raster File Format	INGR
55	Inventor VRML Format	IV
56	Joint Bilevel Image Group	JBIG
57	JPEG File Interchange Format	JFIF
58	LeadView	CMP
59	Lightscape Technologies ASCII and Binary	LSA/LSB
60	Lightwave 3D Layered Object	LWLO
61	Lightwave 3D Object	LWOB
62	Lightwave 3D Scene	LWSC
63	Lightwave Object Format	LWOB
64	Lotus PIC Graphics Format	PIC
65	Macintosh Picture	PICT
66	Magick Image File Format	MIFF
67	Manchester Scene Description Language	MSDL
68	Material Library Format	MLI
69	Materials and Geometry Format	MGF
70	MAZ	MAZ
71	McDonnell	GDS
72	MEME Shape File	RWX
73	Micrografx Designer/Draw Plus Format	DRW
74	Micrografx Draw! Graphics Format	PIC
75	Microsoft Enhanced Metafile	EMF
76	Microsoft Resource Interchange File Format	RIFF
77	Microstation?	DGN ?

78	MultiGen Flight	FLT
79	MultiGen Openflight	FLT
80	Multiple Network Graphics	MNG
81	National Imagery Transmission Format	NITF
82	Network Common Data Format	netCDF
83	Neutral File Format	NFF
84	Neutral File Format (Extended)	ENFF
85	Object Description Language	ODL
86	Object File Format	OFF
87	Object Oriented Graphics Library	OOGL
88	Open Document Interchange Format	ODIF
89	Open Inventor File Format	IV?
90	Pegasus Imaging Corporation Format	PIC
91	Performer	IM
92	Performer Terrain Utilities	PTU
93	Persistence of Vision	POV
94	Photoshop RAW	RAW
95	Planetary Data System Format	PDS
96	Polygon	PLG
97	PolyHedra Database	PHD
98	Portable Bitmap	PBM
99	Portable Greymap	PGM
100	Portable Network Graphics	PNG
101	Portable Pixmap	PPM
102	QuickDraw 3D	QD3D
103	QuickDraw 3D Metafile	3DMF
104	QuickTime	QT
105	Radience	RAD
106	Rayshade	RAY
107	Renderman Interface Bytestream	RIB
108	RenderMorphics	XOF
109	Scene File Format	SFF
110	SCeNe RTrace	SCN

111	Segmented Hyper Graphic	SHG
112	SGI Inventor	IV
113	SGI Powerflip	BIN
114	SGI Radiosity	GFO
115	Silicon Graphics Image File Format	SGI
116	SoftImage	SI
117	Spacial Data Modelling Language	SDML
118	Spatial Archive Interchange Format	SAIF
119	Spatial Data Transfer Standard	SDTS
120	StereoLithography	STL
121	StereoLithography ASCII	STLA
122	Stereolithography Interface Format	STL
123	StereoLthography Binary	STLB
124	Still Picture Interchange File Format	SPIFF
125	Sun Rasterfile	RAS
126	Tag Image File Format	TIFF
127	Tiled Raster Interchange Format	TRIF
128	TrueType Font	TTF
129	Truevision (Targa) File Format	TGA
130	Turbo DDD	TDDD
131	Utah Raster Toolkit	URT
132	V3D	V3D
133	Vector Map Data Format	CBD
134	Vector Product Format	VPF
135	Video Image Communication and Retrieval	VICAR
136	Video Show Graphics Format	PIC
137	Virtual Geometry Interchange	VIZ/VGI
138	Virtual Reality Modelling Language	VRML
139	Visualization Image File Format	VIFF
140	VLA	VLA
141	Wavefront	MTL

142	Wavefront Object	OBJ
143	Wavefront Object Files	OBJ/WOF
144	Wavelet packet Scalar Quantization Format	WSQ
145	Web Object Oriented Graphics Library	WebOOGL
146	Windows Bitmap Format	BMP
147	Windows Meta File	WMF
148	WLD	WLD
149	WorldToolKit Neutral File Format	NFF
150	X BitMap	XBM
151	X PixMap	XPM
152	X Window Dump	XWD
153	x3d and xdart Formats	X3D
154	XGL	XGL
	Extended VRML with Lattice	XVL
155	Zenographics Mirage Graphics File Format	IMA
156	ZipPack	PLY
157	ZSoft Paint	PCX
158		DWG

APPENDIX D City Models

	Country	City	Organisation	URL
	Austalia			
1		Sydney	Planet 9 Studios	http://www.planet9.com/earth/sydney/index.htm
	Austria			
2		Graz (Austria)	Grazer Congress	http://www.grazercongress.co.at/vrml/welcome.htm
	Canada			
3		Ottawa	Wizard Solutions	http://www.intoronto.com/wizard.html
4		Toronto	Wizard Solutions	http://www.intoronto.com/wizard.html
5		Vancouver	S.Wang (University of British Columbia)	
	Finland			
6		Helsinki	Helsinki Telephone Company	http://www.helsinkiarena2000.fi/maailmat/wrl/stocka_y.wrl

7		Tampere	Tampere University	http://juna.dmi.tut.fi/tred/3d.html
	France			
8		Strasbourg	Francis Felix	http://www.3dvr.org/vrstrasbourg/
	Germany			
9		Tubingen	Max Planc Institute	http://www.kyb.tuebingen.mpg.de/bu/projects/vrtueb/final/markt/vrml/markt.wrl
10		Berlin	Art+Com	
11		Hamburg	Graphisoft	http://www.graphisoft.com/company/press_zone/Hamburg3D.html
	Ireland			
12		Dublin	Dublin Institute of Technology	http://www.dmc.dit.ie/guests/eirenet/eirenet/eirenet/thic.htm
	Japan			
13		Tokyo	Planet 9 Studios	http://www.planet9.com/earth/tokyo/index.html
	Poland			
14		Warsaw	M. Jacek Szamrej - University of Warsaw	http://andante.iss.uw.edu.pl/cgi-bin/modzel

	UK			
15		Bath	University of Bath	http://fos.bath.ac.uk/projects/bath/bath.html
16		London	University of Bath	http://www.bath.ac.uk/casa//london/
17		London	CASA UCL	http://www.CASA.ucl.ac.uk
18		Glasgow	Virtual Reality Glasgow	http://www.vrglasgow.co.uk
	USA			
19		Atlanta	Planet 9 Studios	http://www.planet9.com/earth/atlanta/index.htm
20		Austin	Planet 9 Studios	http://www.planet9.com/earth/austin/index.htm
			Planet 9 Studios	http://www.planet9.com/earth/boston/index.htm
21		Boston	Earth Data	http://www.earthdata.com/
22		Chicago	Earth Data	http://www.earthdata.com/
23		Dallas	Earth Data	http://www.earthdata.com/
			Planet 9 Studios	http://www.planet9.com/earth/denver/index.htm
24		Denver	Earth Data	http://www.earthdata.com/
25		Houston	Earth Data	http://www.earthdata.com/
26		Las Vegas	Planet 9 Studios	http://www.planet9.com/earth/lasvegas/index.htm
27		Los Vegas	Earth Data	http://www.earthdata.com/
28		New Orleans	Planet 9 Studios	http://www.planet9.com/earth/neworleans/index.htm

29		New York	Planet 9 Studios	http://www.planet9.com/earth/newyork/index.htm
30		Portland	Planet 9 Studios	http://www.planet9.com/earth/portland/index.htm
31		Salt Lake City	Earth Data	http://www.earthdata.com/
32		San Diego	Planet 9 Studios	http://www.planet9.com/earth/sandiego/index.htm
33		San Francisco	Planet 9 Studios Earth Data	http://www.planet9.com/earth/sanfrancisco/index.htm http://www.earthdata.com/
34		Washington	Earth Data	http://www.earthdata.com/

APPENDIX E Example Simulation Settings File (Annotated)

Example Settings file with description given below. Comments in italic print.

```
////////////////////////////////////////////////////////////////////////////////

FILES

        CM FILENAME:    zMappingSIM3.txt        Model filename
        NAV FILENAME:   brdc0310.txt            RINEX Nav or RINEX BRDC filename
        SP3 FILENAME:   igs14123.txt            SP3 filename
        OBS FILENAME:   *                       RINEX Observation filename [optional] or *
        ANT FILENAME:   *                       Ant gain pattern filename [optional] or *
        GEO FILENAME:   L2S2MP.geo              GEO output filename
        VRML FILENAME:  L2S2MP.wrl              VRML output filename
        SIM FILENAME:   L2S2MP.cmo              Text output filename

SIMULATION SETTINGS

        BE/SP3:                         S                       B = BE (Nav/BRDC) S = SP3
        SIM EPOCH INC:                  3600                    Time increments (seconds)
        SIM X Y Z INC:                  1                       Spatial increments (m)
        SIMULATIONS[T,Px,Py,Pz]:        1 2 2 2                 Time at X and Y and Z
        USER X:                         166.437                 Initial X
        USER Y:                         70.405                  Initial Y
        USER Z:                         18.146                  Initial Z
        SIM TIME:                       2007 01 31 10 33 25     Initial timetag
        MIN ELEVATION:                  0                       Availability mask
        MAX RANGE:                      500                     Range culling
        VRML REP:                       A a M                   See below
        NORMAL CHECK:                   N                       Y or N

SIGNAL PROPAGATION MODELS

        AVAILABILITY TYPE:    SIMPLE    SIMPLE/FRESNEL [Max obstruction %][PRN, 0 = all]
        MULTIPATH:                       N 0 3   Y/N [Min footprint %][PRN or 0 for all]
        REFLECTION PHASE SHIFT:          0       0 or 180 - determines correlator +/-
        REFLECTION ATTENUATION FACTOR:   0.3     0-1 Factor applied to all reflections
        DIFFRACTION:                     N 3 0   Y or N [Max diffraction][PRN, 0 = all]
        DIFFRACTION PHASE SHIFT:         0       0 or 180 - determines correlator +/-
        DIFFRACTION ATTENUATION FACTOR:  0.5     0-1 Factor applied to all diffractions

RECEIVER SPECIFICATION

        CORRELATOR SPACING:             1       1 for Standard 0.1 for Narrow
        PRE CORRELATOR BdW:             2       Affects polynomial. 2 or 8 generally used
        CORRELATOR RES:                 0.001   X axis resolution
        POLYNOMIAL FIT:                 N       Y/N
        ANT ELEVATION MASK:             -90     Signals below this angle are completely
supressed

REFERENCE FRAME TRANSFORM - CORRESPONDING COORDINATES       WGS-84 and Model Equivalent

        P1:     R1X     R1Y     R1Z     M1X     M1Y     M1Z
        P2:     R2X     R2Y     R2Z     M2X     M2Y     M2Z
        P3:     R3X     R3Y     R3Z     M3X     M3Y     M3Z
        P4:     R4X     R4Y     R4Z     M4X     M4Y     M4Z
        P5:     R5X     R5Y     R5Z     M5X     M5Y     M5Z
        P6:     R6X     R6Y     R6Z     M6X     M6Y     M6Z


        VRML REP assignments
                N or NONE for no output or one or a combination of the following...
                                A = Availability Vectors
                                a = Surfaces and Structures
                                F = Fresnel floor for all PRNs (manually remove unwanted)
                                D = Diffraction Vectors
                                M = Multipath Vectors
                                m = Multipath Surfaces
                                R = Potential Reflectors (LE)
                                L = Labels (Buildings and Vectors)
                                O = Original Geometry

////////////////////////////////////////////////////////////////////////////////
```

APPENDIX F Example Antenna Gain Pattern File (XML)

```
<XML ID="XMLID">
      <az_res> 90.0000000e+000 </az_res>
      <elev_res> 0.25000000e+000 </elev_res>
      <aperture_angle> 1.0000000e+001 </aperture_angle>
      <data>
            -180.000,   -90.000,    0.000,      90.000,
90    ,     -5.054,     -5.054,     -5.054,     -5.054,
89.75 ,     -5.073,     -5.073,     -5.073,     -5.073,
89.5  ,     -5.093,     -5.093,     -5.093,     -5.093,
89.25 ,     -5.112,     -5.112,     -5.112,     -5.112,
89    ,     -5.132,     -5.132,     -5.132,     -5.132,
88.75 ,     -5.151,     -5.151,     -5.151,     -5.151,
.
.
.
-88.75,     -30.687,    -30.687,    -30.687,    -30.687,
-89   ,     -30.555,    -30.555,    -30.555,    -30.555,
-89.25,     -30.420,    -30.420,    -30.420,    -30.420,
-89.5 ,     -30.283,    -30.283,    -30.283,    -30.283,
-89.75,     -30.143,    -30.143,    -30.143,    -30.143,
-90   ,     -30.000,    -30.000,    -30.000,    -30.000,
</data>
</XML>
```

APPENDIX G Numerical Output File Examples

Both single and multiple simulation outputs state simulation time, date, and a list of the simulation settings. The format for single and multiple simulations differ from that point on.

```
OS time: 00:08:42        OS date: 06/18/07

SETTINGS

CM FILENAME:                          zMappingSIM3.txt
NAV FILENAME:                         brdc0940.txt
SP3 FILENAME:                         igr14213.txt
OBS FILENAME:                         *
ANT FILENAME:                         *
GEO FILENAME:                         SIM42.geo
VRML FILENAME:                        SIM42.wrl
SIM FILENAME:                         SIM42.cmo.txt
BE/SP3:                               S
SIM EPOCH INC:                        10
SIM X Y Z INC:                        0
SIMULATIONS[T,P]:                     1 1,1,1
USER X:                               161.492
USER Y:                               145.714
USER Z:                               16.161
SIM TIME:                             2007 4 4 10 50 0
MIN ELEVATION:                        0
MAX RANGE:                            500
VRML REP:                             ...
NORMAL CHECK:                         0
AVAILABILITY TYPE:                    FRESNEL 0
MULTIPATH:                            0
REFLECTION PHASE SHIFT:               0
REFLECTION ATTENUATION FACTOR:        1
DIFFRACTION:                          1 3
DIFFRACTION PHASE SHIFT:              0
DIFFRACTION ATTENUATION FACTOR:       1
CORRELATOR SPACING:                   1
PRE CORRELATOR BdW:                   2
CORRELATOR RES:                       0.001
POLYNOMIAL FIT:                       0
ANT ELEVATION MASK:                   -90
```

Single simulation output

```
-------------------------------------------------------------------
|            REFERENCE FRAME TRANSFORMATION PARAMETERS            |
-------------------------------------------------------------------
| Scale:                                      0.9998461525        |
| Translation X:                           -962.259 units         |
| Translation Y:                          20989.250 units         |
| Translation Z:                      -6364109.050 units          |
| Rotation about X (Omega):                   2.470 radians       |
| Rotation about Y (Phi):                     3.158 radians       |
| Rotation about Z (Kappa):                   1.593 radians       |
-------------------------------------------------------------------

-------------------------------------------------------------------
|            REFERENCE FRAME TRANSFORMATION RESIDUALS             |
-------------------------------------------------------------------
| XYZ | REF FRAME 1  | REF FRAME 2 | COMPUTED 2(m)| RESIDUAL(m) |
|-----|--------------|-------------|--------------|-------------|
|  X  | 3977685.176  |    -227.533 |    -227.534 |      -0.001 |
|  Y  |   -5804.628  |    -123.027 |    -123.026 |       0.001 |
|  Z  | 4969217.290  |      26.542 |      26.548 |       0.006 |
|  X  | 3977450.542  |     -77.658 |     -77.662 |      -0.004 |
|  Y  |   -5646.768  |     169.832 |     169.827 |      -0.005 |
|  Z  | 4969386.059  |      12.482 |      12.491 |       0.009 |
|  X  | 3977757.686  |    -231.908 |    -231.907 |       0.001 |
|  Y  |   -5809.871  |    -152.136 |    -152.141 |      -0.005 |
|  Z  | 4969261.913  |     106.603 |     106.595 |      -0.008 |
|  X  | 3977495.588  |    -116.408 |    -116.403 |       0.005 |
|  Y  |   -5684.605  |     206.692 |     206.701 |       0.009 |
|  Z  | 4969503.659  |     132.600 |     132.593 |      -0.007 |
-------------------------------------------------------------------
| Variance factor:                                    0.0000000   |
| Std dev for unweighted adjustment:                  0.0000048   |
-------------------------------------------------------------------

RESULTS

-------------------------------------------------------------------
|                          CONSTELLATION                          |
-------------------------------------------------------------------
| Constellation SVs:                                          32  |
| SVs below horizon:                                          21  |
| SVs 0 degrees -> Masking angle:                              0  |
| Possible visible SVs:                                       11  |
-------------------------------------------------------------------
| SV PRNs above elevation mask:                                   |
```

```
|   1   3   9  11  14  17  19  20  22  28  32                    |
| Elevation angle (deg):                                         |
|  42   1   0  85  35  21  28  49   4  24  42                   |
| Azimuth angle (deg):                                           |
| 119 155 355 240  59 313 158 226  54 271  58                    |
 ----------------------------------------------------------------

 ----------------------------------------------------------------
|                 COARSE AVAILABILITY MODELLING                  |
 ----------------------------------------------------------------
|  BUILDING  | USER-SV |  PLANE - VECTOR INTERSECTION COORDINATES  |
|------------|---------|-------------------------------------------|
|  #  | Face | Vector# |      x       |      y       |      z       |
|-----|------|---------|--------------|--------------|--------------|
|   79| X-Z  |   22    |     207.540  |     180.750  |      19.988  |
      .
      .
      .
| 2610| Y-Z  |    3    |     204.720  |      60.136  |      18.029  |
 ----------------------------------------------------------------
|                   COARSE AVAILABILITY SUMMARY                  |
 ----------------------------------------------------------------
| Affected Structures:                                        33 |
| Obstructed Vects:                                           11 |
| Available SVs:                                               0 |
 ----------------------------------------------------------------
| Available PRNs:                                                |
|                                                                |
 ----------------------------------------------------------------

 ------------------------------------------------------------------------------------------------
|                                DETAILED AVAILABILITY MODELLING                                 |
 ------------------------------------------------------------------------------------------------
|    BUILDING    | USER-SV |  PLANE - VECTOR INTERSECTION COORDINATES (3D)  |    SIGNAL FRONT     |
|----------------|---------|------------------------------------------------|---------------------|
|  #  |   Poly   | Vector# |      x       |      y       |      z       | 2D | Rad (m) | % Captured |
|-----|----------|---------|--------------|--------------|--------------|----|---------|------------|
|   79|        3 |   22    |          --- |          --- |          --- |  x |   6.750 |      0.323 |
      .
      .
      .
| 2589|       21 |    3    |     221.363  |      27.187  |      18.749  |  x |   5.273 |    100.000 |
 ------------------------------------------------------------------------------------------------
|                                 DETAILED AVAILABILITY SUMMARY                                  |
 ------------------------------------------------------------------------------------------------
| Affected Surfaces:                                                                         273 |
| Obstructed Vects:                                                                            5 |
| Available SVs:                                                                               6 |
| Fresnel available SVs:                                                                       0 |
 ------------------------------------------------------------------------------------------------
| Available PRNs:                                                                                |
|  1 11 14 19 20 32                                                                              |
 ------------------------------------------------------------------------------------------------

 ----------------------------------------------------------------------
|                        FRESNEL AVAILABILITY L1                       |
 ----------------------------------------------------------------------
|      |          % OBSCURRED FOR INDIVIDUAL CROSS SECTIONS            |
| PRN  |-----------------------------------------------------------------|
|      |   1  |   2  |   3  |   4  |   5  |   6  |   7  |   8  |   9  |  10  |
|------|------|------|------|------|------|------|------|------|------|------|
|   1  | 0.00 | 0.00 | 0.00 | 0.00 | 0.00 | 0.00 | 0.00 | 0.00 | 0.00 | 0.00 |
      .
      .
      .
|  32  | 0.00 | 0.00 | 0.00 | 0.00 | 0.00 | 0.00 | 0.00 | 0.00 | 0.00 | 0.00 |
 ----------------------------------------------------------------------

 ----------------------------------------------------------------------
|                        FRESNEL AVAILABILITY L2                       |
 ----------------------------------------------------------------------
|      |          % OBSCURRED FOR INDIVIDUAL CROSS SECTIONS            |
| PRN  |-----------------------------------------------------------------|
|      |   1  |   2  |   3  |   4  |   5  |   6  |   7  |   8  |   9  |  10  |
|------|------|------|------|------|------|------|------|------|------|------|
|   1  | 0.00 | 0.00 | 0.00 | 0.00 | 0.00 | 0.00 | 0.00 | 0.00 | 0.00 | 0.00 |
      .
      .
      .
|  32  | 0.00 | 0.00 | 0.00 | 0.00 | 0.00 | 0.00 | 0.00 | 0.00 | 0.00 | 0.00 |
 ----------------------------------------------------------------------

 ----------------------------------------------------------------------
|                           DIFFRACTION                                |
 ----------------------------------------------------------------------
| PRN  | DIFF ANGLE |  TOTAL PATH  | PATH DELTA |  ESTIMATED ATTENUATION  |
|------|------------|--------------|------------|-------------------------|
 ----------------------------------------------------------------------

 ------------------------------------------------------------------------------------------
|                              RECEIVED SIGNALS PREDICTION                                 |
 ------------------------------------------------------------------------------------------
| # | PRN | D/R | P LENGTH(m) | P DELTA(m) | CA Chip | P Chip | R COEFF | Azi(deg) | Ele(deg) |
|---|-----|-----|-------------|------------|---------|--------|---------|----------|----------|
| 1 |   1 |  D  | 22008123.99 |   0        |   0     |   0    |   0     |   119.22 |    41.67 |
      .
      .
      .
| 6 |  32 |  D  | 22252372.70 |   0        |   0     |   0    |   0     |    58.41 |    42.44 |
 ------------------------------------------------------------------------------------------
| RINEX Observations                                                                     0 |
 ------------------------------------------------------------------------------------------
```

PREDICTED RANGE ERRORS AND CORRECTIONS						
#	PRN	Dir Ref Com	CORRECTIONS(m) CA Code	CORRECTIONS(m) P Code	EXPECTED PSEUDORANGES(m) CA Code	EXPECTED PSEUDORANGES(m) P Code	P-Fit (r)
1	1	D	0.00	0.00	22008123.99	22008123.99	0.000
.							
.							
.							
6	32	D	0.00	0.00	22252372.70	22252372.70	0.000

PROCESSING SUMMARY	
City Model	
City model file size:	6659.042 KB
Filtering & Geometry file creation:	86.984 s (0.013 s/MB)
City model objects:	4953
City model surfaces:	78780
Availability	12.048 s
Coarse processing time:	1.454 s
Detailed processing time:	10.594 s
Multipath	0.000 s
Determining candidate surfaces:	0.000 s
Calculate intersections:	0.000 s
Assess l.o.s availability:	0.000 s

Multiple simulation output

```
TT;2007,4,3,13,17,15*POS;265.008,11.541,5.395*AM;1,4,5,11,12,13,17,20,
23,25,30,31*#AM;12*AMA;46.899,301.131,344.506,145.499,336.464,198.878,
245.959,74.877,172.630,127.015,5.969,50.739*AME;25.922,32.677,1.767,26
.090,4.178,32.788,40.143,63.921,61.969,23.330,0.731,21.237*LOS;1,13,20
,23,25,31*#LOS;6*FREL1;*FREL2;*MP;1,13,17,20,23,25,31*#MP;7*MPL;,23326
569.556,22511320.800,21942048.580,20616857.532,20806538.619,23359412.6
65,23735321.293*MPD;0.160,0.336,9.089,0.314,0.404,1.101,0.240*MPA;29.7
93,237.820,181.814,1.808,264.073,309.680,25.954*MPE;25.921,32.786,40.1
46,63.917,61.965,23.324,21.236*MPRR%;100.000,100.000,100.000,100.000,1
00.000,100.000,100.000*DIF;*#DIF;0*DIFL;*DIFA;*DIFE;*C/AorC1;0.000*PCO
DE;0.000*PPOS;255.451,15.159,2.078*EERR;9.459,3.868,7.473*EMAG;12.660*
PDOP;1.393*HDOP;1.203*VDOP;0.702*TS;86.947*TA;11.877*TC;0.203*TD;11.67
4*TF;0.000*TMP;3.297*TMPINT;6.876*TMPLOS;52.943*TD;0.000*TDLOS;0.000*M
CLOS;15492.000*MDLOS;-8716.000*MFAV;0.000*MMP;-
80348.000*MDIFF;0.000*SCB;635*SDS;3945*
```

TT;YYYY,MM,DD,HH,MM,SEC*	Timetag
POS;X,Y,Z*	Position
AM;,,,,…,*	Above Mask satellite PRNs
#AM;*	Number of above mask PRNs
AMA;,,,,…,*	Above Mask Azimuth (°)
AME;,,,,…,*	Above Mask Elevation (°)
LOS;,,,,…,*	LOS satellite PRNs
#LOS;*	Above Mask satellites
FREL1;,,,,…,*	Above Fresnel obstructions L1(%)
FREL2;,,,,…,*	Above Fresnel obstructions L2(%)
MP;,,,,…,*	Reflected signals PRNs
#MP;*	Number of reflected signals

MPL;,,,,…,*	Reflected signals total path lengths
MPD;,,,,…,*	Reflected signals - total path lengths
MPA;,,,,…,*	Reflected signal azimuths (°)
MPE;,,,,…,*	Reflected signal elevations (°)
MPRR%;,,,,…,*	Available area for re-radiation
DIF;,,,,…,*	Diffracted signal PRNs
#DIF;*	Number of diffracted signals
DIFL;,,,,…,*	Diffracted signal total lengths
DIFA;,,,,…,*	Diffracted signal azimuths
DIFE;,,,,…,*	Diffracted signal elevations
CAorC1;*	CA or C1 correlator error (range correction)
PCODE;*	P code correlator error (range correction)
PPOS;X,Y,Z*	Estimated position with disrupted signals
EERR;X,Y,Z*	Difference between estimated and true positions
EMAG;*	3D error vector magnitude
PDOP;*	Position DOP for visible satellites
HDOP;*	Horizontal DOP for visible satellites
VDOP;*	Vertical DOP for visible satellites
TS;*	Simulation time, total (sec)
TA;*	Simulation time LOS availability (sec)
TC;*	Simulation time LOS coarse algorithm (sec)
TD;*	Simulation time LOS detailed algorithm (sec)
TF;*	Simulation time Fresnel (sec)
TMP;*	Simulation time multipath stage 1 (sec)
TMINT;*	Simulation time multipath intersections stage (sec)
TMPLOS;*	Simulation time multipath LOS stage 1 (sec)
TD;*	Simulation time diffraction stage 1 (sec)
TDLOS;*	Simulation time diffraction LOS stage 1 (sec)
MCLOS;*	Simulation memory LOS coarse availability (kb)
MDLOS;*	Simulation memory LOS detailed availability (kb)
MFAV;*	Simulation memory Fresnel averaged (kb)
MMP;*	Simulation memory multipath (kb)
MDIFF;*	Simulation memory diffraction (kb)

APPENDIX H VRML Sample Object

```
Shape { # triangle mesh
      appearance Appearance {
            material Material {ambientIntensity 0.50196 diffuseColor 1
1 1 specularColor 0 0 0 emissiveColor 0 0 0 shininess 1 transparency
0}
      } # appearance
      geometry IndexedFaceSet { # triangle mesh
            ccw    TRUE
            convex TRUE
            solid  FALSE
            coordIndex [
0,1,2,-1,          ] # 1 triangles
            coord Coordinate { point [
-50.158 -242.18 63.332,-44.72 -252.53 69.066,-54.595 -246.21 63.332
            ] } # 3 coord points
            normal Normal { vector [
0.30473 -0.33497 -0.89159,0.30473 -0.33497 -0.89159,0.30473 -0.33497 -
0.89159
            ] } # 3 normal vectors
      } # geometry
} # triangle mesh
```

APPENDIX I Example '.GEO' File Object

```
-------------- Building # 2570 --------------
Building # 2570 coordinate index:
             0              1              2      96.033 -174.911 22.613
             1              3              2      97.640 -174.366 28.798
             2              3              4     103.622 -174.297 23.299
             3              5              4     103.813 -174.861 27.938
             4              5              6      97.966 -178.189 22.613
             5              7              6      96.358 -178.734 28.798
             6              7              8      90.377 -178.803 23.299
             7              9              8      90.187 -178.239 27.938
Building # 2570 coordinate points:
       89.7800     -177.0300        9.9996
       89.7800     -177.0300       36.7250
      103.0300     -172.5400        9.9996
      103.0300     -172.5400       36.7250
      104.2200     -176.0700        9.9996
      104.2200     -176.0700       36.7250
       90.9680     -180.5600        9.9996
       90.9680     -180.5600       36.7250
       89.7800     -177.0300        9.9996
       89.7800     -177.0300       36.7250
Building # 2570 normal vectors:
     -0.320941      0.947099      0.000000             C
     -0.320941      0.947099      0.000000             C
      0.947604      0.319447     -0.000000             C
      0.947604      0.319447      0.000000             C
      0.320898     -0.947114      0.000000             C
      0.320898     -0.947114      0.000000             C
     -0.947766     -0.318965      0.000000             C
     -0.947766     -0.318965     -0.000000             C
Building # 2570 geometric max and min:
         X max          Y max          Z max
        104.22       -172.54          36.73
         X min          Y min          Z min
         89.78       -180.56          10.00
```

END OF THESIS